



UNIVERSITAT DE  
BARCELONA

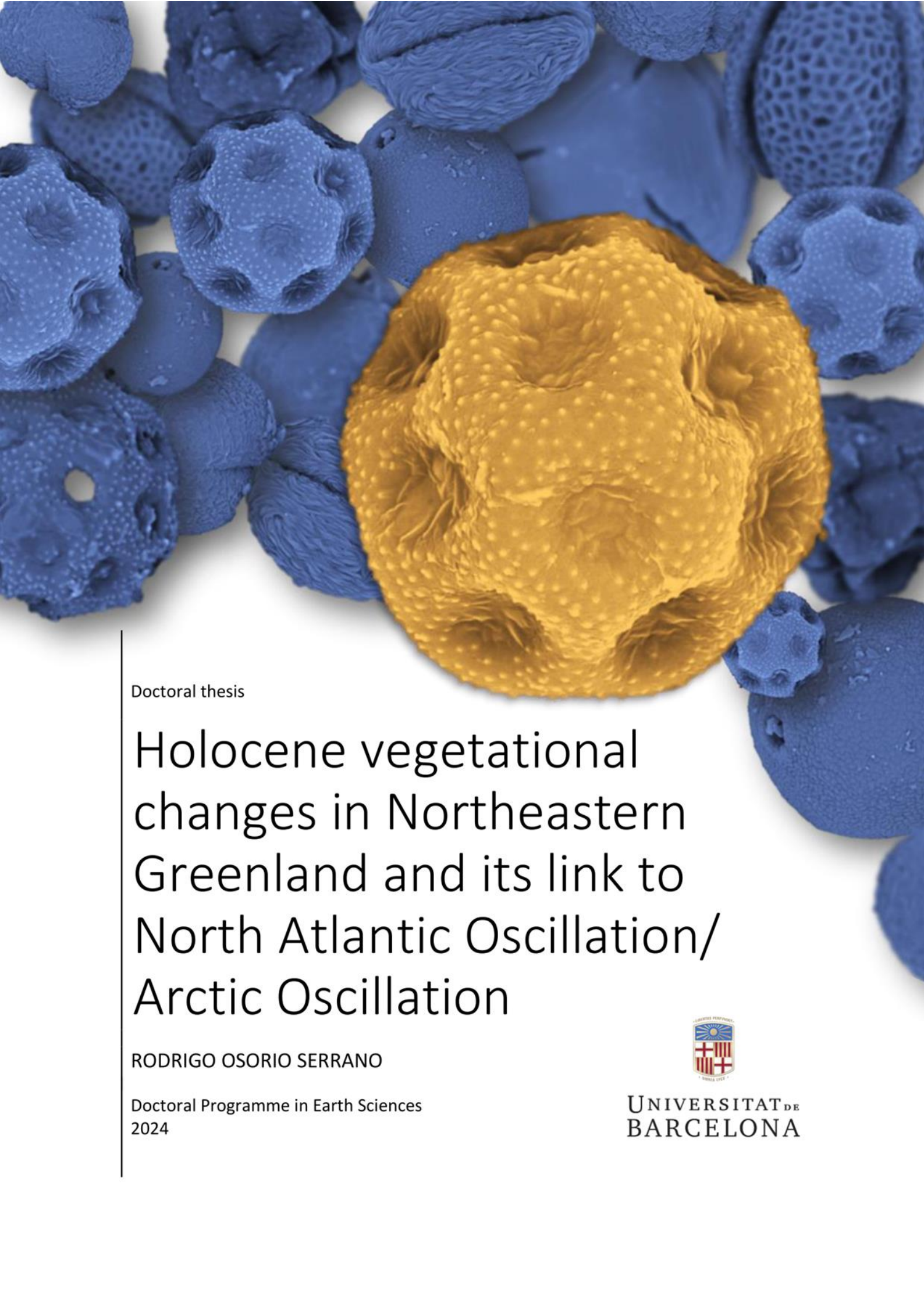
# Holocene vegetational changes in Northeastern Greenland and its link to North Atlantic Oscillation/Arctic Oscillation

Rodrigo Osorio Serrano

**ADVERTIMENT.** La consulta d'aquesta tesi queda condicionada a l'acceptació de les següents condicions d'ús: La difusió d'aquesta tesi per mitjà del servei TDX ([www.tdx.cat](http://www.tdx.cat)) i a través del Dipòsit Digital de la UB ([deposit.ub.edu](http://deposit.ub.edu)) ha estat autoritzada pels titulars dels drets de propietat intel·lectual únicament per a usos privats emmarcats en activitats d'investigació i docència. No s'autoriza la seva reproducció amb finalitats de lucre ni la seva difusió i posada a disposició des d'un lloc aliè al servei TDX ni al Dipòsit Digital de la UB. No s'autoriza la presentació del seu contingut en una finestra o marc aliè a TDX o al Dipòsit Digital de la UB (framing). Aquesta reserva de drets afecta tant al resum de presentació de la tesi com als seus continguts. En la utilització o cita de parts de la tesi és obligat indicar el nom de la persona autora.

**ADVERTENCIA.** La consulta de esta tesis queda condicionada a la aceptación de las siguientes condiciones de uso: La difusión de esta tesis por medio del servicio TDR ([www.tdx.cat](http://www.tdx.cat)) y a través del Repositorio Digital de la UB ([deposit.ub.edu](http://deposit.ub.edu)) ha sido autorizada por los titulares de los derechos de propiedad intelectual únicamente para usos privados enmarcados en actividades de investigación y docencia. No se autoriza su reproducción con finalidades de lucro ni su difusión y puesta a disposición desde un sitio ajeno al servicio TDR o al Repositorio Digital de la UB. No se autoriza la presentación de su contenido en una ventana o marco ajeno a TDR o al Repositorio Digital de la UB (framing). Esta reserva de derechos afecta tanto al resumen de presentación de la tesis como a sus contenidos. En la utilización o cita de partes de la tesis es obligado indicar el nombre de la persona autora.

**WARNING.** On having consulted this thesis you're accepting the following use conditions: Spreading this thesis by the TDX ([www.tdx.cat](http://www.tdx.cat)) service and by the UB Digital Repository ([deposit.ub.edu](http://deposit.ub.edu)) has been authorized by the titular of the intellectual property rights only for private uses placed in investigation and teaching activities. Reproduction with lucrative aims is not authorized nor its spreading and availability from a site foreign to the TDX service or to the UB Digital Repository. Introducing its content in a window or frame foreign to the TDX service or to the UB Digital Repository is not authorized (framing). Those rights affect to the presentation summary of the thesis as well as to its contents. In the using or citation of parts of the thesis it's obliged to indicate the name of the author.



Doctoral thesis

# Holocene vegetational changes in Northeastern Greenland and its link to North Atlantic Oscillation/ Arctic Oscillation

RODRIGO OSORIO SERRANO

Doctoral Programme in Earth Sciences  
2024



UNIVERSITAT DE  
BARCELONA



UNIVERSITAT DE  
BARCELONA

# Holocene vegetational changes in Northeastern Greenland and its link to North Atlantic Oscillation/Arctic Oscillation

Canvis vegetatius de l'Holocè al nord-est de Groenlàndia i el seu vincle  
amb l'oscil·lació de l'Atlàntic Nord/Oscil·lació àrtica

Memòria de tesi presentada per **Rodrigo Eduardo Osorio Serrano** per optar al grau de Doctor. Aquesta tesi s'ha escrit dins del programa de Doctorat de Ciències de la Terra (HDK09) de la Universitat de Barcelona sota direcció del **Dr. Alberto Sáez Ruiz** (Universitat de Barcelona) i el **Dr. Santiago Giralt Romeu** (Institut de Geociències Barcelona – GEO3BCN-CSIC).

## Acknowledgments

I want to thank my mother for always being a fundamental pillar in my development both as a human being and as a researcher.

Thanks Dr. Alberto Sáez and Dr. Santiago Giralt for allowing me to come to Barcelona as I dreamed and for all the guidance and good energy. I'm proud of what this research has become after all these years of work, and it wouldn't be the same without your advice. Thanks for allowing me to work at my own pace, that was priceless.

Special thanks to the researchers that directly helped me with the research. Dr. Alejandro Gallardo, head of the Paleontology lab of the University of Barcelona for his help and kindness when I was processing pollen samples, Dr. Jacob Nabe-Nielsen for hosting and helping me when I went to Denmark, and GEO3BCN's Dra. Encarnación Montoya and Dra. Núria Cañellas for their help with modern pollen work at the institute. I'd also like to thank Dr. Mario Pino for his immense help to fulfill this project.

Finally, I'd like to thank the National Agency of Research and Development (ANID) of the Ministry of Science, Technology, Knowledge, and Innovation of Chile for allowing me to make this journey funding my stay as a recipient of the 'Becas Chile – Doctorado en el extranjero' scholarship, and to projects PALEOGREEN (CTM2017-87976-P) and NEOCLIM (PID2020-113798GB-C33) funded by the Ministry of Science and Innovation of Spain for allowing this research to happen.

## Table of contents

	page
List of figures	i
List of tables	iv
List of abbreviations	v
List of units	vii
List of chemical elements	viii
Abstract	Ix
Resum	xiii
Resumen	xvii
1. Introduction	1
1.1. Motivation	1
1.2. Greenland in the context of the Arctic system	2
1.3. North Atlantic Oscillation (NAO)/Arctic Oscillation (AO) and Atlantic Meridional Overturning Circulation (AMOC) as the regional main climate driving forcings	7
1.4. Late Quaternary evolution of East Greenland climate	14
1.5. Palynology as a key tool to track environmental changes in the Arctic	20
1.6. Study area	24
1.6.1. Climate of the Zackenberg region	25
1.6.2. Geology of the Zackenberg region	25
1.6.3. Flora of Zackenberg	26
1.6.4. Characteristics of lakes in the Zackenberg area	30
1.7. Objectives	31
2. Material and methods	33
2.1. Pollen key and reference collection	33
2.2. Sedimentary records	34
2.2.1. Coring	34
2.2.2. Sedimentary facies description	35
2.2.3. Chronology	36
2.2.4. Mineralogical analysis	37
2.2.5. Geochemical analysis	37
2.2.6. Diatom analysis	37
2.2.7. Pollen analysis	38

2.2.8. Alpha and beta diversity	39
2.3. Quantitative climate reconstruction	40
2.3.1. Pollen-climate calibration set	40
2.3.2. Transfer function	41
3. Results	42
3.1. Pollen morphology of Zackenberg key plants	42
3.2. The ZAC Lake record	45
3.2.1. Sedimentary facies and units	45
3.2.2. Age-depth model	48
3.2.3. Mineralogical data	49
3.2.4. Geochemical data	50
3.2.5. Sedimentological multivariate analysis	51
3.2.6. Pollen stratigraphy	56
3.2.7. ZAC pollen-based diversity index	58
3.3. The Lomsø Lake record	62
3.3.1. Sedimentary facies and units	62
3.3.2. Age-depth model	64
3.3.3. Geochemical data	65
3.3.4. Pollen stratigraphy	68
3.3.5. Lomsø pollen-based diversity index	70
3.4. The Aucella Lake Record	74
3.4.1. Chronology	74
3.4.2. Stratigraphy and sediment characteristics	79
3.4.3. Multivariate analysis	80
4. Discussion	84
4.1. Pollen morphology study	84
4.2. Modern pollen-climate relationships in the Arctic	85
4.3. Transfer function-based temperature reconstruction	88
4.3.1. Performance of the quantitative climate model	91
4.4. Zackenberg fossil pollen assemblages as an ecological indicator	94
4.5. Holocene environmental history of the Zackenberg area	103
4.5.1. Glacial to warm Early to Middle Holocene (12,000 – 7,200 cal yrs BP)	104
4.5.2. Warm Middle Holocene (7,200 – 3,800 cal yrs BP)	110
4.5.3. Colder Late Holocene, establishment of tundra environments	114

	(3,800 – 2,400 cal yrs BP)	
4.5.4.	Roman Warm Period (2,400 – 1,600 cal yrs BP)	115
4.5.5.	Dark Ages Cold Period (1,600 – 1,100 cal yrs BP)	118
4.5.6.	Medieval Climate Anomaly (1,100 – 700 cal yrs BP)	118
4.5.7.	The Little Ice Age (700 – 200 cal yrs BP)	119
4.5.8.	Industrial Era and recent Global Warming (200 cal yrs BP – present)	119
4.6.	Paleoclimatic implications	120
4.7.	Importance for high-arctic conservation and management	126
4.8.	Challenges in enhancing quantitative climate reconstructions in the Arctic	129
5.	Conclusions	131
6.	References	134
7.	Appendix	154

## List of figures

	page
Figure 1. The Arctic region and the variety of boundaries of climatic/ vegetational zones proposed	3
Figure 2. Diagram of the main components of the Arctic climatic and geological system	4
Figure 3. Bioclimatic division of Greenland	6
Figure 4. Synoptic map for the positive and negative phases of the NAO occurs and its effects on surrounding areas during winter months	9
Figure 5. Summary diagram of the effect of AO and NAO phases	10
Figure 6. Satellite image of Greenland and the main ocean currents composing the AMOC	12
Figure 7. Distribution of superficial sea temperature in the North Atlantic	13
Figure 8. Mean annual solar insolation at 80°N	14
Figure 9. Reconstruction of NAO climatic modes for last 5,000 years, using continental Holocene records	17
Figure 10. Diagram of the effects of sea-ice cover on the continental climate conditions of the Arctic	19
Figure 11. Theoretical model of the standard pollen analysis based on lacustrine records	21
Figure 12. Diagram of the theory behind pollen-based quantitative climate reconstructions	23
Figure 13. Location of the study area	24
Figure 14. Geological map of the study area	26
Figure 15. Distribution of the main plant communities along a gradient in the Zackenberg area	27
Figure 16. Land cover map of the study area	30
Figure 17. Satellite image of the study is indicating location of studied lakes and main geographical elements	31
Figure 18. PALEOGREEN project team coring over a frozen lake in the 2019 campaign.	35
Figure 19. Distribution of sites included in the pollen-climate calibration set	40
Figure 20. Sedimentary facies and units' description and paleoenvironmental interpretation of core ZAC19_06_02	47

Figure 21.	Age-depth model for the ZAC19_06_02 core	48
Figure 22.	Stratigraphical mineral content plot of core ZAC19_06_02	49
Figure 23.	Stratigraphical plot of the geochemical content of core ZAC19_06_02	51
Figure 24.	RDA plot based on the ZAC19_06_02 mineralogical and geochemical content	52
Figure 25.	Broken stick test plot for the ZAC19_06_02 XRF based PCA	53
Figure 26.	PCA plot based on the ZAC19_06_02 geochemical record	54
Figure 27.	Stratigraphical PC1 and PC2 scores plot based on the ZAC19_06_02 XRF data	55
Figure 28.	Pollen stratigraphy of the ZAC19_06_02 record	57
Figure 29.	DCA plot based on the ZAC19_06_02 pollen record	58
Figure 30.	Stratigraphical DCA1 and DCA2 scores plot based on the ZAC19_06_02 pollen data	60
Figure 31.	Stratigraphical $\alpha$ and $\beta$ diversity plot based on the ZAC19_06_02 pollen record	61
Figure 32.	Facies and sedimentary units' description and paleoenvironmental interpretation of core LOM18_02 sediments	63
Figure 33.	Age-depth model for core LOM18_02	64
Figure 34.	XRF-based geochemical content of the LOM18_02 sediment core	65
Figure 35.	Broken stick test plot for the LOM18_02 XRF-based PCA	66
Figure 36.	PCA plot based on the LOM18_02 XRF data	67
Figure 37.	Stratigraphical PC1 and PC2 scores plot based on the LOM18_02 XRF data	68
Figure 38.	Pollen stratigraphy of Unit B of the LOM18_02 record	69
Figure 39.	DCA plot based on the LOM18_02 pollen record	71
Figure 40.	Stratigraphical DCA1 and DCA2 scores plot based on the LOM18_02 pollen record	72
Figure 41.	Stratigraphical $\alpha$ and $\beta$ diversity plot based on the LOM18_02 pollen record	73
Figure 42.	Multi-proxy data from the AUC18_02 sediment core	75
Figure 43.	Diatom diagram for the AUC18_02 core	78
Figure 44.	Age-depth model for sediment core AUC18_02	80
Figure 45.	DCA plot based on the AUC18_02 diatom record	81
Figure 46.	DCA plot based on the XRF and TOC content of the AUC18_02 record	82
Figure 47.	AUC18_02 RDA plots	83

Figure 48.	Pollen diagram of the pollen-climate calibration set	86
Figure 49.	RDA plot of climatic and pollen data from the calibration set	88
Figure 50.	Diagram based on the bootstrapping cross-validation of the selected transfer function	89
Figure 51.	Summer temperature ( $Ths$ ) since 9,000 cal yrs BP based on the ZAC19_06_02 and LOM18_02 pollen records	90
Figure 52.	Summer temperature ( $Ths$ ) since 1,800 cal yrs BP based on the ZAC19_06_02 and LOM18_02 pollen records	91
Figure 53.	Cluster plot based on both Lomsø and ZAC fossil pollen records	95
Figure 54.	DCA plot based on both Lomsø and ZAC fossil pollen records	97
Figure 55.	Broken stick test plot for the unified pollen based PCA	98
Figure 56.	PCA plot based on both Lomsø and ZAC fossil pollen records	99
Figure 57.	Stratigraphical DCA1 plot based on both Lomsø and ZAC pollen records	100
Figure 58.	Stratigraphical ecological change plot based on both Lomsø and ZAC fossil pollen records	101
Figure 59.	Stratigraphical rate of ecological change plot based on both Lomsø and ZAC fossil pollen records	102
Figure 60.	Stratigraphical plot depicting the ecological distance towards present-day pollen assemblages based on both Lomsø and ZAC fossil pollen records	103
Figure 61.	Stratigraphical plot of sediment core ZAC19_06_02 multi-proxy data	105
Figure 62.	Stratigraphical plot of sediment core LOM18_02 multi-proxy data	106
Figure 63.	Hypothetical altitudinal profile based on the environmental reconstruction of the Zackenberg area between 9,000 and 7,200 cal yrs BP	109
Figure 64.	Hypothetical altitudinal profile based on the environmental reconstruction of the Zackenberg area between 7,200 and 3,800 cal yrs BP	113
Figure 65.	Hypothetical altitudinal profile based on the environmental reconstruction of the Zackenberg area since 3,800 cal yrs BP	116
Figure 66.	Model of a thermokarst lake inception	117
Figure 67.	Distribution of the climate reconstructions discussed in this section	121
Figure 68.	Comparison of ZAC19_06_02 $Ths$ record with other regional records for the last 9,000 cal yrs BP	122
Figure 69.	Comparison of this study $Ths$ record with other regional records since 2,000 cal yrs BP	125

## List of tables

	page	
Table 1.	Key plant species selected for the reference collection	33
Table 2.	Samples processed for $^{14}\text{C}$ AMS dating	36
Table 3.	Worldclim based climatic variables used in this study	41
Table 4.	Summary of pollen types and their main measures in equatorial view	44
Table 5.	Statistical values for the first five constrained components of the ZAC19_06_02 XRD and XRF based RDA	51
Table 6.	Statistical values for the first five axis of the ZAC19_06_02 XRF based PCA	52
Table 7.	Statistical values for the ZAC19_06_02 pollen based DCA analysis	58
Table 8.	Statistical values for the first five axis of the LOM18_02 XRF based PCA	66
Table 9.	Statistical values for the LOM18_02 pollen based DCA	70
Table 10.	Explanatory power of each climate variable of the set	87
Table 11.	WA-PLS based transfer function statistics	88
Table 12.	Comparison with other northern high latitude temperature transfer functions	92
Table 13.	Statistical values for the unified fossil pollen based DCA	96
Table 14.	Statistical values for the first five axis of the unified fossil pollen based PCA	97

## List of abbreviations

<i>Abbreviation</i>	<i>Meaning</i>
N	North
S	South
E	East
W	West
NE	Northeast
SW	Southwest
SLP	Sea-level pressure
NAO	North Atlantic Oscillation
AO	Arctic Oscillation
NAM	Northern Annular Mode
AMOC	Atlantic Meridional Overturning Circulation
NADW	North Atlantic Deep Water
EGC	East Greenland Current
NAC	North Atlantic Current
IC	Irminger Current
WGC	West Greenland Current
LC	Labrador Current
LGM	Last Glacial Maximum
HCO	Holocene Climatic Optimum
RWP	Roman Warm Period
DACP	Dark Ages Cool Period
MCA	Medieval Climate Anomaly
LIA	Little Ice Age
IE	Industrial Era
MAT	Modern Analogue Technique
WA	Weighted Average
WA-PLS	Weighted Average Partials Less Squares
ZERO	Zackenberg Ecological Research Operations
LM	Light Microscope
SEM	Scanning Electron Microscope
XRD	X-Ray Diffraction
XRF	X-Ray Fluorescence

CONISS	Stratigraphically Constrained Cluster Analysis
PCA	Principal Component Analysis
DCA	Detrended Correspondence Analysis
$\alpha$	Alpha diversity
$\beta$	Beta diversity
ANOVA	Analysis of Variance
RDA	Redundancy Analysis
RMSE	Rooted Mean Squared Error
TOC	Total organic carbon
TN	Total nitrogen
<i>Ths/JJA T</i>	Temperature of the warmest quarter / Summer temperature
<i>Ta</i>	Annual temperature
<i>Tmin</i>	Minimum temperature

## List of units

<i>Abbreviation</i>	<i>Meaning</i>
°C	Degree Celsius
°	Degree (angle)
cal yrs BP	Calibrated years before present
m	Meter
cm	Centimeter
cm <sup>2</sup>	Squared centimeter
cm <sup>3</sup>	Cubic centimeter
mm	Millimeter
µm	Micrometer
W	Watt
asl	Above sea level
kV	Kilovolt
cps	Count per second
SD	Standard deviation

## List of chemical elements

<i>Abbreviation</i>	<i>Meaning</i>
H	Hydrogen
O	Oxygen
Si	Silicon
K	Potassium
V	Vanadium
Ca	Calcium
Ti	Titanium
Mn	Manganese
Fe	Iron
Sr	Strontium
Cl	Chlorine
Br	Bromine
S	Sulfur
Rb	Rubidium
Sr	Strontium
Zr	Zirconium
<sup>14</sup> C	Carbon-14
$\delta^{13}\text{C}$	(delta) Carbon.13
$\delta^{15}\text{N}$	(delta) Nitrogen-15

## Abstract

Rapid climate change and its pronounced effect over the Arctic has become a hot topic for both the scientific community and the public, raising concerns about the future of its ecosystems. In this context, Greenland, with its minimal human influence serves as a natural archive of past climate. This island's climate is strongly influenced by large-scale atmospheric and oceanic interactions, particularly the North Atlantic Oscillation/Arctic Oscillation (NAO/AO) and the Atlantic Meridional Overturning Current (AMOC). These patterns influence temperature and precipitation, with NAO<sup>+</sup> phases bringing colder and drier conditions and NAO<sup>-</sup> phases bringing warmer and moister conditions. AMOC, a key component of global heat distribution, also plays a role by influencing sea-ice cover along Greenland's eastern coast.

This study was conducted on the Zackenberg valley and its surroundings, in NE Greenland (74°N, 20°W). The main aim of this study is to quantitatively reconstruct the climate evolution of NE Greenland based on modern pollen-climate relationships. Our specific goals are to: (1) establish a reference collection of modern pollen from the Zackenberg area, (2) identify the key environmental and ecological factors influencing pollen assemblages in the sediment record, (3) reconstruct past vegetation changes throughout the Holocene epoch in Zackenberg, and (4) establish linkages between these reconstructed vegetation changes and past climate variations, including those associated with the NAO/AO. To achieve these objectives, a quantitative approach based on modern pollen-climate relationships was executed.

In first place, custom Pollen Key and Reference Collection for NE Greenland were made. On the other hand, the multi-proxy paleolimnological study was performed over three sediment cores obtained from different selected lakes: Core LOM18\_02 (30.5 cm long) was obtained from lake Lomsø and core AUC18\_02 (83.6 cm long) was obtained from the Aucella Lake during the 2018 field trip, while core ZAC19\_06\_02 (77.5 cm long) was obtained from lake ZAC. Sedimentary facies were described for each sediment core, as well as custom chronologies and geochemical analyses based on XRF data. XRD-based mineralogical analysis was performed on the Aucella and ZAC

records. As of biological proxies, diatom analysis was performed on the Aucella record while pollen analysis was executed on the ZAC and Lomsø records. Pollen data was also employed to generate alpha and beta diversity reconstructions, and a WA-PLS quantitative climate reconstruction based on the modern pollen-climate relationships in the Arctic.

When it comes to the modern-pollen related results, the morphological study of modern pollen allowed the detailed description and photography of 11 key NE Greenland pollen types. Additionally, the study of modern pollen-climate relationships within the Arctic pollen data set unveiled the influence of *Ths* (summer temperature; 18.93% of the variance explained,  $\lambda_1/\lambda_2$  ratio of 1.01 and ANOVA-derived p-value of 0.001) as the main driver of the distribution of pollen data. Based on this, a 2-component WA-PLS transfer function (RMSE: 2.11°C;  $r^2$ : 0.66; max bias: 8.19°C; skill: 65.63) was selected to apply on the fossil pollen records.

The ZAC record covers the past 12,000 years and displays four sedimentary units, showing the transition from glacial rock flour deposits to lacustrine conditions with seasonal ice cover ca. 9,600 cal yrs BP. Decreasing organic matter contents and runoff are followed by the on-set of pollen sedimentation in the lake, showing a scarce vegetation dominated by pioneer polar tundra elements such as Poaceae, Cyperaceae, *Oxyria/Rumex* and Papaveraceae (*Ths*: 0.09°C). An initial cooling trend that peaked around the 8.2k cold event (*Ths*: -3.26°C) was reversed paving the way for Holocene Climate Optimum (HCO) conditions since ca. 7,200 cal yrs BP, presenting sustained summers with temperatures higher than 5°C, allowing the colonization by woody elements and later the domination of southern mild elements such as *Betula* marking a pronounced moment of change ca. 6,800 cal yrs BP accompanied by decreasing soil moisture. Warm conditions prevailed until ca. 5,000 cal yrs BP marking the deterioration of climate and Low Arctic *Betula* reign in the region (with *Ths* reaching near present values), and the subsequent expansion of wet tundra elements such as *Luzula/Juncus* during the Late Holocene accompanied by oscillating temperatures.  $\beta$  diversity indicates that peak magnitude of ecological change during the Holocene has been reached during the Industrial Era (IE).

The Lomsø record contains the last 4,200 cal yrs BP and is divided into two main units, showing the transition of a high-energy abandoned deltaic deposit characterized by low organic content and sandy texture to a permafrost-related thermokarst shallow lake ca. 1,900 cal yrs BP. The lacustrine sequence displayed subtle changes trending towards more anoxic conditions. The first sample dated at the end of the Roman Warm Period (RWP) displays  $Ths$  ca. 1.22°C. The pollen record shows the dominance of wet tundra elements as *Luzula/Juncus* and snowbed representation with *Salix*, recording an expansion of fens and grassland ca. 1,000 cal yrs BP ( $Ths$ : 1.76°C). Increased plant activity manifested as influx peak happened between 700 and 400 cal yrs BP during the Little Ice Age (LIA) with oscillating  $Ths$  (0.93 – 2.15°C). The most recent samples display the expansion of Ericaceae shrubs, indicating the moment of maximum ecological change leading to an eventual change in vegetal composition during the IE in concordance with recent global warming bringing summers up to 3.39°C.

The Aucella record was sampled for pollen analysis, but the extremely low content did not allow the execution of pollen analysis. The high-mountain lake records 5,000 years of climatic history with a Middle Holocene characterized by low but constant terrigenous input indicating warm conditions that allowed the lake to become completely ice free during summer. The period between 3,800 and 3,400 represented the most abrupt change in all proxies studied, marking strengthened ice-cover and increased precipitation causing more runoff and sediment input into the lake, affecting the penetration of light to the water column. This pattern was constant during the Late Holocene with the intermittence of “warm” periods with limited ice-cover during summers (3,400 – 2,400 cal yrs BP; 2,000 – 1,100 cal yrs BP and 300 – 0 cal yrs BP) with cool periods of little to no ice thaw and reduced light penetration (2,400 – 2,000 cal yrs BP; 1,100 – 300 cal yrs BP).

The combined analysis of the three lacustrine records allowed to successfully reconstruct the climatic and vegetational history of the Zackenberg area, describing latitudinal and altitudinal movement of vegetation types in concordance with climatic fluctuations. The interpretation of the pollen record and the application of the transfer

function allowed us to link the environmental changes with regional climate modes. The Early Holocene presented NAO<sup>+</sup> and weak AMOC conditions, with overall cool conditions. AMOC stabilization at the beginning of the HCO and a shift to NAO<sup>-</sup> brought warm temperatures and reduced sea-ice cover. The return on NAO<sup>+</sup> conditions and weak AMOC during the Late Holocene caused cold, dry conditions with likely permanent sea-ice. Finally, a reversal back to NAO<sup>-</sup> is related to warming temperatures during the IE.

Based on the global interpretation, the importance of paleoecological data for Arctic biome conservation is discussed, highlighting the utility of this studies to understand the response of past ecosystems towards natural climate change. Aditionally, several challenges were identified for the confection of quantitative climate reconstructions based on pollen in the Arctic. Limited modern reference data, lack of knowledge on past ecological dynamics hindering the identification of regional forcings and potential biases in the fossil record are among the challenges listed.

**Key words:** Palynology, Northeastern Greenland, Quantitative climate reconstruction, North Atlantic Oscillation/Arctic Oscillation, Holocene.

## Resum

El canvi climàtic i el seu fort efecte sobre l'Àrtic s'ha convertit en un tema rellevant tant per a la comunitat científica com per al públic general, despertant una gran preocupació sobre el futur dels seus ecosistemes. En aquest context, Groenlàndia, amb la seva mínima influència humana, serveix com un arxiu natural del clima del passat. El clima d'aquesta illa està fortement influenciat per diverses interaccions atmosfèriques i oceàniques a gran escala, particularment l'Oscil·lació de l'Atlàctic Nord/Oscil·lació Àrtica (NAO/AO) i la Circulació de Retorn Meridional de l'Atlàtic (AMOC). Aquests patrons influeixen tant a la temperatura com a les precipitacions: les fases NAO<sup>+</sup> generen condicions més fredes i seques mentre que les fases NAO<sup>-</sup> generen condicions més càlides i humides. La AMOC, un component clau de la distribució global de la calor, també exerceix un paper en influir en el gruix de la capa de gel marí al llarg de la costa oriental de Groenlàndia.

Aquest estudi es va desenvolupar a la vall de Zackenberg i els seus voltants, en el NE de Groenlàndia (74°N, 20°O). L'objectiu principal del estudi és reconstruir quantitativament l'evolució climàtica del nord-est de Groenlàndia basant-se en les relacions modernes entre el pol·len i el clima. Els objectius específics són: (1) establir una col·lecció de referència de pol·len modern de l'àrea de Zackenberg, (2) identificar els factors ambientals i ecològics clau que influeixen en les associacions de pol·len en el registre de sediments, (3) reconstruir els canvis en la vegetació al llarg de l'època de l'Holocè en Zackenberg, i (4) establir els vincles entre els canvis de vegetació reconstruïts i les variacions climàtiques passades, incloses aquelles associades amb la NAO/AO. Per a aconseguir aquests objectius, es va executar un enfocament quantitatiu basat en les relacions modernes entre pol·len i clima.

En primer lloc, es van crear les claus i col·lecció de referència personalitzades de pol·len del NE de Groenlàndia. D'altra banda, l'estudi paleolimnològic multi-proxy es va realitzar sobre tres testimonis de sediments obtinguts de diferents llacs seleccionats: el testimoni LOM18\_02 (30,5 cm de llarg) es va obtenir del llac Lomsø, el testimoni AUC18\_02 (83,6 cm de llarg) es va obtenir del llac Aucella i el testimoni

ZAC19\_06\_02 (77,5 cm de llarg) es va obtenir del llac ZAC. Es van descriure les fàcies sedimentàries per a cada testimoni de sediment, així com cronologies personalitzades i ànàlisis geoquímiques basades en dades de XRF. Es va realitzar una ànàlisi mineralògica basada en XRD en els registres de Aucella i ZAC. L'ànàlisi de diatomees es va realitzar en el registre de Aucella mentre que l'ànàlisi de pol·len es va executar en els registres de ZAC i Lomsø. També es van emprar dades de pol·len per a generar reconstruccions de diversitat alfa i beta, i una reconstrucció climàtica quantitativa de tipus WA-PLS basada en les relacions modernes entre pol·len i clima a l'Àrtic.

Pel que fa als resultats relacionats amb el pol·len modern, l'estudi morfològic del pol·len actual va permetre la descripció detallada i la fotografia d'onze tipus clau de pol·len del nord-est de Groenlàndia. A més, l'estudi de les relacions modernes entre el pol·len i el clima dins del conjunt de dades de pol·len de l'Àrtic va revelar la influència de  $Ths$  (temperatura d'estiu; 18,93% de la variància explicada, relació  $\lambda_1/\lambda_2$  de 1,01 i p-value derivat del ANOVA de 0,001) com a principal impulsor de la distribució de dades de pol·len. Sobre aquesta base, es va seleccionar una funció de transferència WA-PLS de dos components (RMSE: 2,11°C;  $r^2$ : 0,66; biaix màxim: 8,19°C; skill: 65,63) per a aplicar-la en els registres de pol·len fòssil.

El registre ZAC cobreix els darrers 12.000 anys i mostra quatre unitats sedimentàries, que mostren la transició de dipòsits de “farina” glacial a condicions lacustres amb una coberta de gel estacional 9.600 anys cal AP. A la disminució del contingut de matèria orgànica i l'escorrentia li segueix l'inici de la sedimentació de pol·len en el llac, mostrant una escassa vegetació dominada per elements pioners de la tundra polar com Poaceae, Cyperaceae, *Oxyria/Rumex* i Papaveraceae ( $Ths$ : 0,09°C). Una tendència de refredament inicial que va aconseguir el seu punt màxim al voltant de l'esdeveniment fred “8,2k” ( $Ths$ : -3,26°C) es va revertir donant pas a les condicions característiques de l'Òptim Climàtic de l'Holocè (HCO) fa uns 7.200 anys, presentant estius amb temperatures superiors als 5°C de forma sostinguda, permetent la colonització per elements llenyosos i posteriorment el domini d'elements càlids del sud com *Betula* marcant un pronunciat moment de canvi fa 6.800 anys acompanyat d'una disminució de la humitat del sòl. Les condicions càlides van prevaldre fins a 5.000 anys cal AP, la qual

cosa marca la deterioració del clima i del regnat de *Betula* a la regió (amb *Ths* aconseguint valors pròxims als actuals), i la posterior expansió d'elements de la tundra humida com *Luzula/Juncus* durant l'Holocè Tardà, acompanyada de temperatures oscil·lants. La diversitat  $\beta$  indica que la magnitud màxima del canvi ecològic durant l'Holocè es va aconseguir durant l'Era Industrial (IE).

El registre de Lomsø conté els darrers 4.200 anys i es divideix en dues unitats principals, que mostren la transició d'un dipòsit de delta abandonat d'alta energia caracteritzat per un baix contingut orgànic i textura arenosa a un llac tipus thermokarst poc profund relacionat amb el permafrost de fa 1.900 anys. La successió lacustre mostra canvis subtils tendents a condicions més anòxiques. La primera mostra, datada a la fi del Període Càlid Romà (RWP), mostra *Ths* d'uns 1,22°C. El registre de pol·len mostra el predomini d'elements de la tundra humida com *Luzula/Juncus* i la presència de llits de neu amb *Salix*, registrant una expansió de pantans i prats fa uns 1.000 anys (*Ths*: 1,76°C). L'augment de l'activitat de les plantes manifestat com un pic d'influx va ocórrer entre 700 i 400 anys cal AP durant la Petita Edat del Gel (LIA) amb *Ths* oscil·lants (0,93 – 2,15°C). Les mostres més recents mostren l'expansió dels arbustos de Ericaceae, indicant el moment de màxim canvi ecològic que va conduir a un eventual canvi en la composició vegetal durant l'Era Industrial en concordança amb l'escalfament global recent que ha portat estius amb temperatures de fins a 3,39°C.

Es van prendre mostres del registre de Aucella per a realitzar l'anàlisi de pol·len, però el contingut extremadament baix no va permetre la seva execució. Aquest llac d'alta muntanya registra 5.000 anys d'història climàtica amb un Holocè Mitjà caracteritzat per una aportació terrígena baixa però constant que indica unes condicions càlides que van permetre que el llac quedés completament lliure de gel durant l'estiu. El període entre 3.800 i 3.400 anys va contemplar el canvi més abrupte en tots els indicadors estudiats, la qual cosa va marcar la formació d'una capa de gel enfortida i un augment de les precipitacions que van provocar més escorrentia i l'entrada de sediments en el llac, la qual cosa va afectar la penetració de la llum en la columna d'aigua. Aquest patró va ser constant durant l'Holocè tardà amb la intermitència de períodes “calids” amb una capa de gel limitada durant els estius (3.400 – 2.400 anys cal AP; 2.000 – 1.100 anys cal AP i

300 – 0 anys cal AP) amb períodes fredes de poca intensitat a no descongelar el gel i reduir la penetració de la llum (2.400 – 2.000 anys cal AP; 1.100 – 300 anys cal AP).

L'anàlisi combinada dels tres registres lacustres va permetre reconstruir amb èxit la història climàtica i vegetativa de l'àrea de Zackenberg, descriuint el desplaçament latitudinal i altitudinal dels tipus de vegetació en concordança amb les fluctuacions climàtiques. La interpretació del registre pol·línic i l'aplicació de la funció de transferència va permetre vincular els canvis ambientals amb els modes climàtics regionals. L'Holocè primerenc va presentar condicions NAO<sup>+</sup> i AMOC febles, amb condicions generals fredes. L'estabilització de l'AMOC al començament de l'Òptim Climàtic de l'Holocè i un canvi a NAO<sup>-</sup> van portar temperatures càlides i van reduir la capa de gel marí. El retorn de les condicions NAO<sup>+</sup> i la AMOC afeblida durant l'Holocè Tardà van provocar condicions fredes i seques amb gel marí permanent. Finalment, una reversió a NAO<sup>-</sup> està relacionada amb l'augment de les temperatures durant l'Era Industrial.

Finalment es discuteix la importància de les dades paleoecològiques per a la conservació del bioma àrtic, destacant la utilitat d'aquests estudis per a comprendre la resposta dels ecosistemes del passat al canvi climàtic. A més, es van identificar diverses dificultats per a la confecció de reconstruccions climàtiques quantitatives basades en pol·len a l'Àrtic. Entre aquestes dificultats es troben la escassetat de dades de referència moderns, la falta de coneixement sobre dinàmiques ecològiques passades que dificulten la identificació de forçaments regionals i possibles biaixos en el registre fòssil.

**Paraules clau:** Palinologia, Nord-est de Groenlàndia, Reconstrucció climàtica quantitativa, Oscil·lació de l'Atlàntic Nord/Oscil·lació de l'àrtic, Holocè.

## Resumen

El acelerado cambio climático y su pronunciado efecto sobre el Ártico se ha convertido en un tema relevante tanto para la comunidad científica como para el público general, despertando preocupación sobre el futuro de sus ecosistemas. En este contexto, Groenlandia, con su mínima influencia humana, sirve como un archivo natural del clima pasado. El clima de esta isla está fuertemente influenciado por interacciones atmosféricas y oceánicas a gran escala, particularmente la Oscilación del Atlántico Norte/Oscilación Ártica (NAO/AO) y la Circulación de vuelco meridional del Atlántico (AMOC). Estos patrones influyen tanto en la temperatura como en las precipitaciones: las fases NAO<sup>+</sup> generan condiciones más frías y secas y las fases NAO<sup>-</sup> generan condiciones más cálidas y húmedas. La AMOC, un componente clave de la distribución global del calor, también desempeña un papel al influir en la capa de hielo marino a lo largo de la costa oriental de Groenlandia.

Este estudio se realizó en el valle de Zackenberg y sus alrededores, en el NE de Groenlandia (74°N, 20°O). El objetivo principal de este estudio es reconstruir cuantitativamente la evolución climática del noreste de Groenlandia basándose en las relaciones modernas entre el polen y el clima. Los objetivos específicos son: (1) establecer una colección de referencia de polen moderno del área de Zackenberg, (2) identificar los factores ambientales y ecológicos clave que influyen en las asociaciones de polen en el registro de sedimentos, (3) reconstruir los cambios pasados en la vegetación a lo largo de la época del Holoceno en Zackenberg, y (4) establecer vínculos entre estos cambios de vegetación reconstruidos y variaciones climáticas pasadas, incluidas aquellas asociadas con la NAO/AO. Para lograr estos objetivos, se ejecutó un enfoque cuantitativo basado en las relaciones modernas entre polen y clima.

En primer lugar, se crearon claves y colecciones de referencia personalizadas de polen del NE de Groenlandia. Por otro lado, el estudio paleolimnológico multi-proxy se realizó sobre tres testigos de sedimentos obtenidos de diferentes lagos seleccionados: el testigo LOM18\_02 (30,5 cm de largo) se obtuvo del lago Lomsø y el testigo AUC18\_02 (83,6 cm de largo) se obtuvo del lago Aucella durante en el viaje de campo de 2018,

mientras que el testigo ZAC19\_06\_02 (77,5 cm de largo) se obtuvo del lago ZAC. Se describieron facies sedimentarias para cada testigo de sedimento, así como cronologías personalizadas y análisis geoquímicos basados en datos de XRF. Se realizó un análisis mineralógico basado en XRD en los registros de Aucella y ZAC. En cuanto a los proxies biológicos, el análisis de diatomeas se realizó en el registro de Aucella mientras que el análisis de polen se ejecutó en los registros de ZAC y Lomsø. También se emplearon datos de polen para generar reconstrucciones de diversidad alfa y beta, y una reconstrucción climática cuantitativa de tipo WA-PLS basada en las relaciones modernas entre polen y clima en el Ártico.

En lo que respecta a los resultados relacionados con el polen moderno, el estudio morfológico del polen actual permitió la descripción detallada y la fotografía de 11 tipos clave de polen del noreste de Groenlandia. Además, el estudio de las relaciones modernas entre el polen y el clima dentro del conjunto de datos de polen del Ártico reveló la influencia de *Ths* (temperatura de verano; 18,93% de la varianza explicada, relación  $\lambda_1/\lambda_2$  de 1,01 y p-value derivado del ANOVA de 0,001) como principal impulsor de la distribución de datos de polen. En base a esto, se seleccionó una función de transferencia WA-PLS de dos componentes (RMSE: 2,11°C;  $r^2$ : 0,66; sesgo máximo: 8,19°C; skill: 65,63) para aplicarla en los registros de polen fósil.

El registro ZAC cubre los últimos 12.000 años y muestra cuatro unidades sedimentarias, que muestran la transición de depósitos de harina glacial a condiciones lacustres con una capa de hielo estacional cerca de 9.600 años cal AP. La disminución del contenido de materia orgánica y la escorrentía son seguidos por el inicio de la sedimentación de polen en el lago, mostrando una escasa vegetación dominada por elementos pioneros de la tundra polar como Poaceae, Cyperaceae, *Oxyria/Rumex* y Papaveraceae (*Ths*: 0,09°C). Una tendencia de enfriamiento inicial que alcanzó su punto máximo alrededor del evento frío “8,2k” (*Ths*: -3,26°C) se revirtió dando paso a las condiciones características del Óptimo Climático del Holoceno (HCO) unos 7.200 años cal AP, presentando veranos con temperaturas superiores a los 5°C de forma sostenida, permitiendo la colonización por elementos leñosos y posteriormente el dominio de elementos cálidos del sur como *Betula* marcando un pronunciado momento de cambio

6.800 años cal AP acompañado de una disminución de la humedad del suelo. Las condiciones cálidas prevalecieron hasta 5.000 años cal AP, lo que marca el deterioro del clima y del reinado de la *Betula* en la región (con *Ths* alcanzando valores cercanos a los actuales), y la posterior expansión de elementos de la tundra húmeda como *Luzula/Juncus* durante el Holoceno Tardío, acompañada de temperaturas oscilantes. La diversidad  $\beta$  indica que la magnitud máxima del cambio ecológico durante el Holoceno se alcanzó durante la Era Industrial (IE).

El registro de Lomsø contiene los últimos 4.200 años cal AP y se divide en dos unidades principales, que muestran la transición de un depósito deltaico abandonado de alta energía caracterizado por un bajo contenido orgánico y textura arenosa a un lago tipo thermokarst poco profundo relacionado con el permafrost 1.900 años cal AP. La secuencia lacustre mostró cambios sutiles tendientes a condiciones más anóxicas. La primera muestra, fechada a finales del Período Cálido Romano (RWP), muestra *Ths* de unos 1,22°C. El registro de polen muestra el predominio de elementos de la tundra húmeda como *Luzula/Juncus* y la representación de lechos de nieve con *Salix*, registrando una expansión de pantanos y pastizales unos 1.000 años cal AP (*Ths*: 1,76°C). El aumento de la actividad de las plantas manifestado como un pico de influjo ocurrió entre 700 y 400 años cal AP durante la Pequeña Edad del Hielo (LIA) con *Ths* oscilantes (0,93 – 2,15°C). Las muestras más recientes muestran la expansión de los arbustos de Ericaceae, indicando el momento de máximo cambio ecológico que condujo a un eventual cambio en la composición vegetal durante la Era Industrial en concordancia con el calentamiento global reciente que ha traído veranos de hasta 3,39°C.

Se tomaron muestras del registro de Aucella para realizar el análisis de polen, pero el contenido extremadamente bajo no permitió su ejecución. El lago de alta montaña registra 5.000 años de historia climática con un Holoceno Medio caracterizado por un aporte terrígeno bajo pero constante que indica condiciones cálidas que permitieron que el lago quedara completamente libre de hielo durante el verano. El período entre 3.800 y 3.400 años cal AP representó el cambio más abrupto en todos los indicadores estudiados, lo que marcó una capa de hielo fortalecida y un aumento de las

precipitaciones que provocaron más escorrentía y entrada de sedimentos en el lago, lo que afectó la penetración de la luz en la columna de agua. Este patrón fue constante durante el Holoceno tardío con la intermitencia de períodos “cálidos” con una capa de hielo limitada durante los veranos (3.400 – 2.400 años cal AP; 2.000 – 1.100 años cal AP y 300 – 0 años cal AP) con períodos fríos de poca intensidad. a no descongelar el hielo y reducir la penetración de la luz (2.400 – 2.000 años cal AP; 1.100 – 300 años cal AP).

El análisis combinado de los tres registros lacustres permitió reconstruir con éxito la historia climática y vegetativa del área de Zackenberg, describiendo el movimiento latitudinal y altitudinal de los tipos de vegetación en concordancia con las fluctuaciones climáticas. La interpretación del registro polínico y la aplicación de la función de transferencia nos permitieron vincular los cambios ambientales con los modos climáticos regionales. El Holoceno temprano presentó condiciones NAO<sup>+</sup> y AMOC débiles, con condiciones generales frías. La estabilización de AMOC al comienzo del Óptimo Climático del Holoceno y un cambio a NAO<sup>-</sup> trajeron temperaturas cálidas y redujeron la capa de hielo marino. El retorno de las condiciones NAO<sup>+</sup> y la AMOC debilitada durante el Holoceno Tardío provocaron condiciones frías y secas con hielo marino permanente. Finalmente, una reversión a NAO<sup>-</sup> está relacionada con el aumento de las temperaturas durante la Era Industrial.

Finalmente se discute la importancia de los datos paleoecológicos para la conservación del bioma ártico, destacando la utilidad de estos estudios para comprender la respuesta de los ecosistemas del pasado al cambio climático de origen natural. Además, se identificaron varios desafíos para la confección de reconstrucciones climáticas cuantitativas basadas en polen en el Ártico. Entre los desafíos enumerados se encuentran datos de referencia modernos limitados, falta de conocimiento sobre dinámicas ecológicas pasadas que dificultan la identificación de forzantes regionales y posibles sesgos en el registro fósil.

**Palabras clave:** Palinología, Noreste de Groenlandia, Reconstrucción climática cuantitativa, Oscilación del Atlántico Norte/Oscilación del ártico, Holoceno.

# 1. Introduction

## 1.1. Motivation

The high vulnerability of Arctic regions to the current global warming linked to anthropogenic greenhouse gas emissions has inspired researchers during the last decades to study the relationships between Arctic flora and climate to better understanding of these ecosystems' stability and how Arctic biodiversity might evolve in this new climate paradigm (Coyne & Kelley, 1974; Oberbauer et al., 1996). Based on the varied physiological responses of Arctic plants related to climate conditions change, the rising temperatures are expected to cause different responses on each plant community, that could be manifested through short- and long-term changes in community structure and the range of species distribution (Elberling et al., 2008; Grogan & Chapin, 2000; Oberbauer et al., 1996).

Greenland's paleoclimatic research has become a key referent location, thanks to the study of ice cores, which have been widely used to reconstruct past temperatures based on changing oxygen isotopes of the ice (Grootes & Stuiver, 1997; Johnsen et al., 1995; Stuiver et al., 1995). However, even when Greenland ice cores present an annual temporal resolution, they describe a relatively homogeneous climate during the Holocene while other evidence displays significant climate oscillations as well as flora and fauna composition (Bennike, 1999). For that reason, it is essential to characterize the paleoclimate and paleoenvironmental evolution of these high latitudes using other natural archives such as lake sediment cores. Even if Greenland lacustrine records studied to date do not have a temporal resolution like the ice records, they provide complementary insight by allowing studies on biological and geochemical proxies. Consequently, using a variety of techniques to study past climatic and environmental conditions that can't be employed in ice cores (Briner et al., 2016; Willemse & Törnqvist, 1999)

In this context, we propose to study the paleoclimate and paleoenvironmental Holocene evolution using lacustrine sedimentary records to complement the already existing

Greenland research on the sensitivity of the Arctic and its biota to climate change. This knowledge will allow us to eventually evaluate and validate current climate change models for the area and its ecological meaning for a future sustainable management of these ecosystems.

## 1.2. Greenland in the context of the Arctic climate

The Earth global climate system operates within a dynamic framework governed by interconnected factors. Orbital forcing, which influences the planet's axial tilt, orbit shape, and precession, plays a pivotal role in determining the distribution of solar energy, creating an energy gradient across latitudes, and establishing climatic zones.

The Arctic, as the northern polar component of the global climate system, experiences distinct seasonal variations. In winter, the Arctic experiences little to no solar irradiation while in summer, solar radiation is almost permanent. This fact results in a mean annual temperature below 0°C in most regions but with huge seasonal oscillations. Key Arctic features, such as sea ice, permafrost, and glaciers, are influenced by the distribution of irradiation (ACIA, 2005). Geographically, the Arctic is defined as the land and sea north of the Arctic Circle found at 66.5°N (Meltofte & Rasch, 2008). Unlike Antarctica, a continent surrounded by an ocean, the Arctic features an ocean surrounded by land, with the Arctic Ocean at its center, encircled by the northernmost reaches of Europe, Asia, and North America. This unique geographical arrangement profoundly influences the Arctic's climate, ecology, and human interactions, as it interacts with regions further south via the atmosphere, oceans, and cryosphere. Climate models suggest a potential decrease in Arctic Sea Level Pressure (SLP) in winter, potentially shifting towards the positive phase of the North Atlantic Oscillation (NAO)/Antarctic Oscillation (AO) (Stendel et al., 2008).

Arctic bioclimatic zones are categorized into High Arctic and Low Arctic based on a mean of 6°C for the warmest month as the boundary from one another (Meltofte & Rasch, 2008). The Low Arctic zone, named tundra, has more lush vegetation compared

to the High Arctic, where large lowland areas may lack vegetation. The subarctic, part of the Boreal zone, is not considered part of the Arctic system. These zones extend southward as subalpine, low-alpine, and high-alpine zones in mountainous areas (Meltofte & Rasch, 2008; Raynolds et al., 2019) (fig. 1).

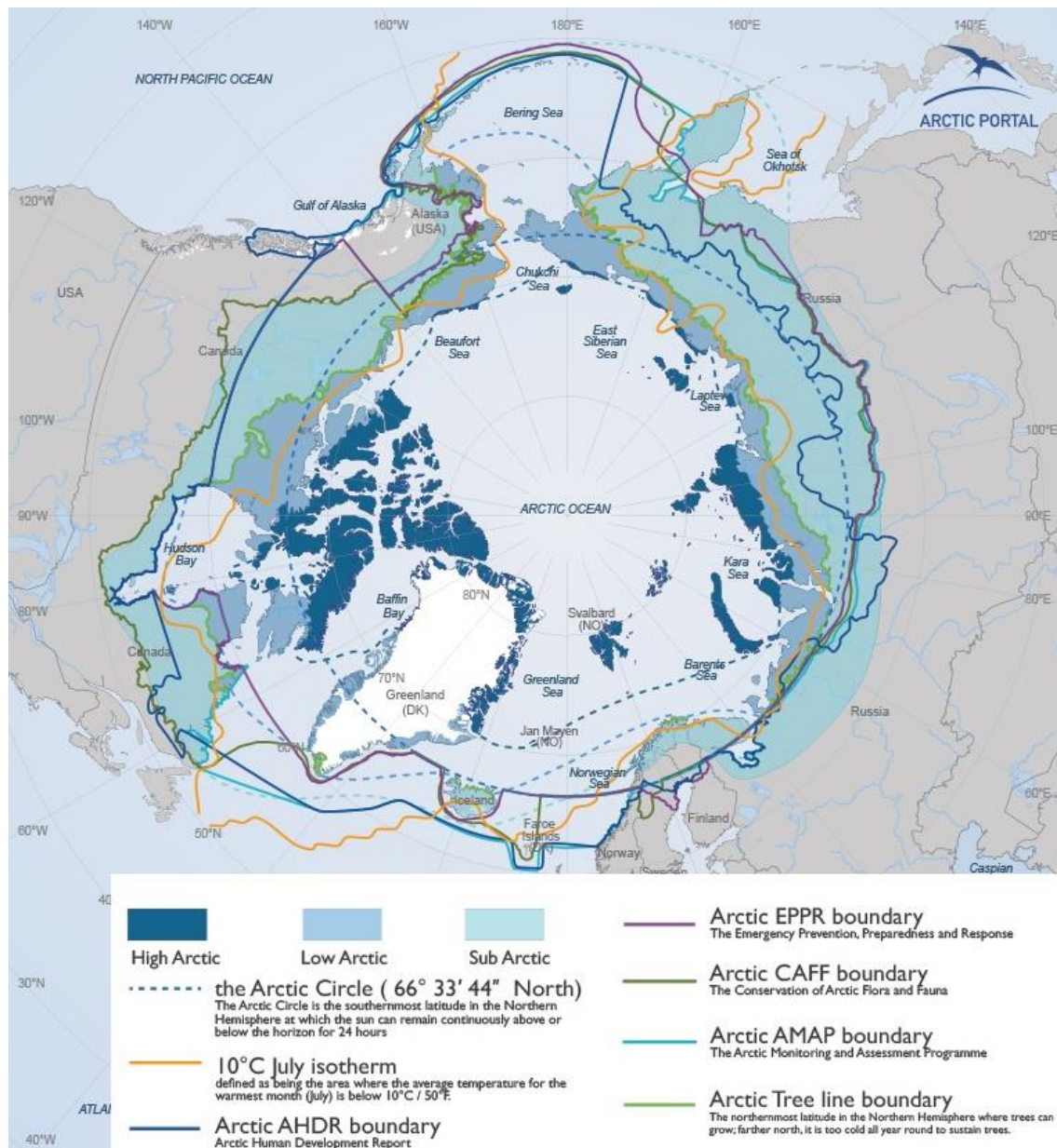


**Figure 1.** The Arctic region and the variety of boundaries of climatic/vegetational zones proposed. Modified from <http://arcticportal.org>.

The present day Arctic climate is characterized by extreme cold temperatures, low precipitation rates, and distinct seasonal variations (Stendel et al., 2008). Prolonged and

harsh winters witness temperatures well below freezing, while summers bring a burst of biological activity as ice cover recedes. Arctic sea ice, a dynamic entity, undergoes significant transformations, influencing energy absorption and reflection (Hewitt et al., 2015). The interplay between sea ice, ocean currents, and atmospheric conditions shapes Arctic habitats and animal migration patterns, impacting global climate patterns and sea level dynamics. Permafrost, defined as ground with temperatures not exceeding 0°C for at least 2 consecutive years, is particularly susceptible to climate changes, especially at its top layer also known as active layer (Westermann et al., 2015). In other words, rising temperatures associated with climate change pose a threat to permafrost stability (Christiansen et al., 2008) (fig. 2).

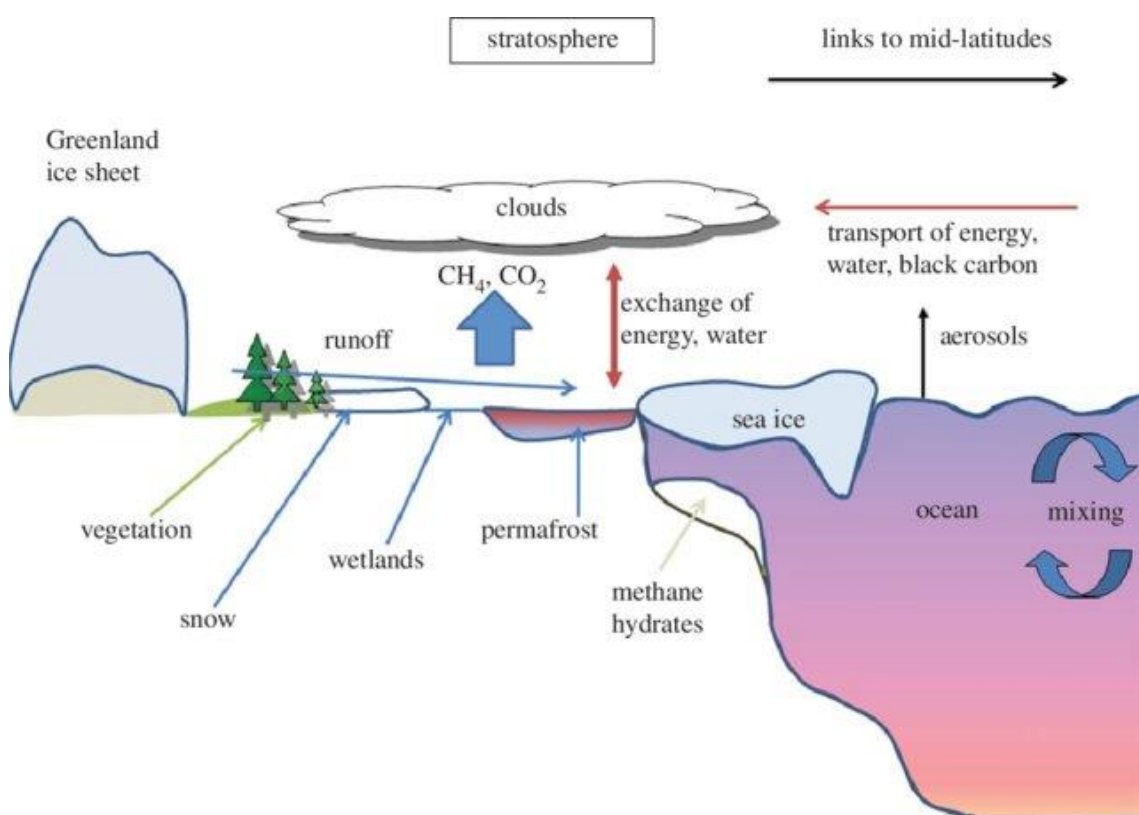


**Figure 2.** Diagram of the main components of the Arctic climatic and geological system. Source: Hewitt et al. (2015).

Summer temperatures in the Arctic during recent decades have been higher than at any time in the past 2,000 years, and the Arctic is warming three to four times as fast as the rest of the world (Meltófte et al., 2008). This phenomenon is referred to as Arctic

amplification, marked by the accelerated warming of the Arctic region compared to the global average during the Industrial Era (IE) (Serreze & Barry, 2011). This enhanced sensitivity to temperature changes is driven by several interconnected factors. One primary contributor is the ice-albedo feedback mechanism: as Arctic sea ice melts due to rising temperatures, the ocean surface absorbs more solar radiation, further warming the atmosphere and perpetuating the cycle of ice loss. Following the same pattern, the thawing of permafrost releases trapped greenhouse gases like methane and carbon dioxide, amplifying the greenhouse effect and contributing to further warming (Serreze and Barry, 2011; Serreze & Francis, 2006). The consequences of Arctic amplification are far-reaching and profound, with significant implications for the climate and ecosystems as rapidly melting sea ice alters regional climate patterns, leading to increased temperatures, altered precipitation regimes, and changes in the distribution and intensity of storms (Stendel et al., 2008).

The ecological definition of the Arctic includes all territories situated north of the 10°C isotherm, that is the northern latitudinal tree limit (Rochardson & Friedland, 2007). This means that Arctic vegetation consists of plants shorter than 2 m, most of them being herbaceous with a variety of characteristic dwarf shrubs, analogous to high mountain ecosystems above the altitudinal tree line. Solar radiation and temperature are key factors determining the distribution of vegetation types throughout the Arctic. While clear patterns in Family association exist, there is also regional endemism evident at a specific level within the Arctic flora (Stewart et al., 2016).

Greenland, the world's largest island situated in the North Atlantic between latitudes 60° to 83°N, exhibits a pronounced climatic gradient influenced by thermohaline circulation and the NAO/AO (Briner et al., 2016; Engels & Helmens, 2010; Hurrell et al., 2003). This unique geographical position and climatic influence make Greenland a key player in shaping the environmental dynamics of the Arctic region (fig. 3).



**Figure 3.** Bioclimatic division of Greenland. Localities correspond to the main settlements and scientific research station's location. Source: (Meltofte & Rasch, 2008).

The island's vast expanse is characterized by significant geological features, including expansive ice sheets and intricate fjord systems. These geological attributes, coupled with Greenland's climatic sensitivity, render it a crucial area for scientific exploration, particularly in understanding the broader context of Earth's climate history. The island's role extends beyond its geological significance, playing a vital part in the broader Arctic ecosystem and serving as a valuable focal point for research into the complexities of climate and environmental changes.

Numerous shallow and deep lakes are located in near-coastal areas in Greenland (Christoffersen et al., 2008). Greenlandic lakes and ponds are typically covered in ice for 8 – 10 months, freezing solid in late winter and spring, with a maximum ice thickness of approximately 2.5 m. Nutrient concentration is low in Greenlandic lakes due to inflowing water from melting ice and snow, resulting in limited species richness and relatively low biomass compared to temperate regions (Vincent & Hobbie, 2000).

### 1.3. North Atlantic Oscillation (NAO)/Arctic Oscillation (AO) and Atlantic Meridional Overturning Circulation (AMOC) as the regional main climate driving forcings

Large-scale inter-annual dynamics of pressure and ocean-atmosphere circulation anomalies exhibit statistically strong relationships with weather conditions, reflecting extensive space-time changes in climate (Forchhammer et al., 2008; Stenseth et al., 2003). Various factors, including the state of the Greenland Ice Sheet (GrIS), cloud cover, and volcanism in adjacent regions, influence the island's climate over different time scales (Hansen et al., 2008a). However, the NAO/AO and the extent of sea ice, regulated by the Atlantic Meridional Overturning Circulation (AMOC), play a determining role in modulating the climatic conditions in the coastal areas of Northeastern (NE) Greenland (Hinkler et al., 2008).

The NAO stands out as the most important climate mode in the northern hemisphere. It explains a significant portion of inter-annual variability in atmospheric circulation and

climate conditions in the medium and high latitudes of the North Atlantic (Clark and Feldstein, 2020; Hurrell et al., 2003). The NAO is associated with the redistribution of atmospheric mass between the Arctic and the subtropical Atlantic. Defined as the normalized difference in atmospheric pressure between the high-pressure center of action found over Iceland ( $50 - 70^{\circ}$  N) and the low-pressure center of action located on the Azores ( $20 - 40^{\circ}$  N), the NAO controls the strength and direction of westerly winds, the jet stream, and storm tracks crossing the Atlantic from west to east (Hurrell et al., 2003). It significantly influences precipitation abundance during winter months in regions surrounding the North Atlantic, exhibiting periodicities of 3 – 6 years and 8 – 10 years, with unpredictable long-term evolution and varied effects, distinctly impacting North America/Greenland and Europe (Hurrell et al., 2003; Stendel et al., 2008).

At present, two phases of the NAO determine distinct climatic conditions on Greenland, especially between the W and E sectors. In the positive NAO phase (NAO+), characterized by a strengthened Azores high and a deeper Iceland low, the pressure gradient over the North Atlantic strengthens. This results in a more zonal flow regime with stronger westerlies, enabling storms to follow a more northerly track across the Atlantic (Hurrell et al., 2003). Positive NAO phase (NAO+) is associated with warmer and wetter conditions in Northern and Central Europe, while S Europe experiences drier conditions. During periods of a dominant positive sign of NAO, frequent low-pressure centers determine dry and cold conditions, along with more sea ice, during winters in West (W) Greenland (Hansen et al., 2008a). Conversely, in a negative NAO phase (NAO-), the Azores high weakens, and the Iceland low becomes less intense, leading to a reduced pressure gradient on the North Atlantic. This allows weaker westerlies and the Jetstream to take a more southerly path across the Atlantic. NAO- results in unpredictable wetter conditions in Southern Europe and drier, colder conditions in Northern Europe (Hurrell et al., 2003). Changes in its phase are responsible for the direction and orientation of Atlantic Ocean winds, influencing the frequency and intensity of storms, as well as affecting the distribution of sea ice and precipitation patterns (Hurrell et al., 2003; Johannessen et al., 2004). A blocking high may persist, causing stable weather conditions over Central Europe. At broad scale, when NAO is

negative Greenland tends to be warm, wet, and displays less sea ice conditions in winter (Hansen et al., 2008a) (fig. 4).

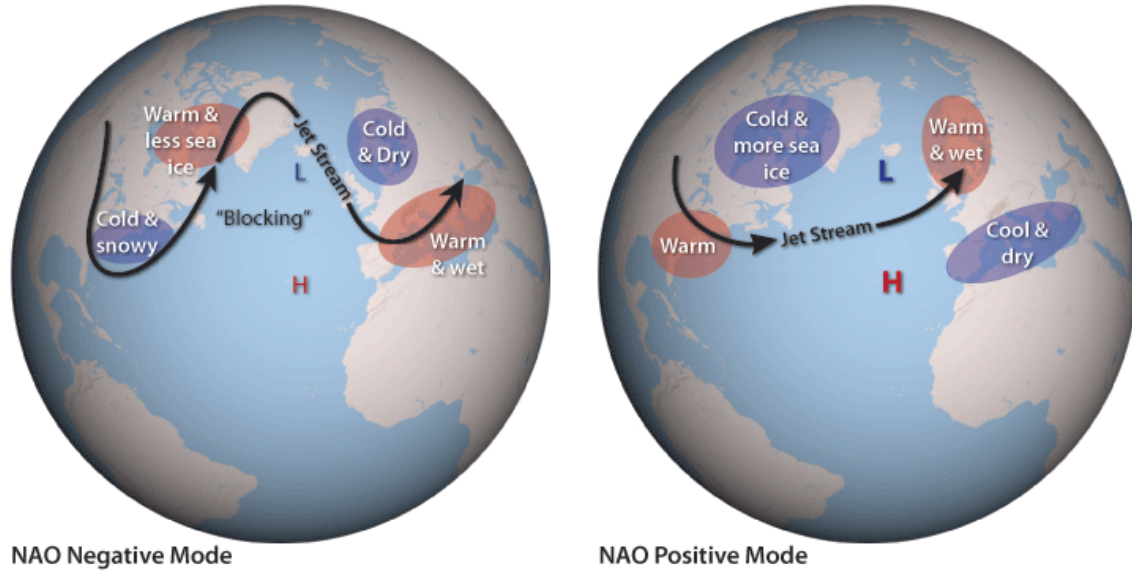


**Figure 4.** Synoptic map for the positive and negative phases of the NAO occurs and its effects on surrounding areas during winter months. Source: NOAA (2009).

Several reconstructions of the NAO have been conducted using continental Holocene records. The most extensive reconstruction was undertaken by Olsen et al., (2012), who reconstructed NAO for the last 5,200 years using geochemical indicators of periods of oxygenation/anoxia in sediments in a Greenland lake, although there are other paleo NAO reconstructions also based on multiple Greenland records, among others (Ortega et al., 2015).

In this context, even though it is proposed that the link between NAO and NE Greenland climate conditions is not linear (due to the E Greenland margin lying right on the limit between the two main regions affected by NAO), there are studies that propose that the variation of interannual snow cover in the study area is strongly controlled by NAO, and the influence of this climate mode on regional flora is evident (Forchhammer et al., 2008; Hansen et al., 2008a; Hinkel et al., 2008; Stendel et al., 2008). Actually, the last 35 years of inter-annual variability in snow onset, snowmelt, and snow-free days in NE Greenland are related to changes in North Atlantic atmospheric and oceanic

circulation patterns, mainly NAO/AO and the East Greenland current (EGC) (Hansen et al., 2008b; Hinkler et al., 2008; Stendel et al., 2008).

The AO, also referred to as the Northern Annular Mode (NAM), is characterized as the amplitude of the pattern delineated by the first empirical orthogonal function of monthly mean winter sea-level pressure anomalies north of 20°N (Thompson and Wallace, 1998, 2000).

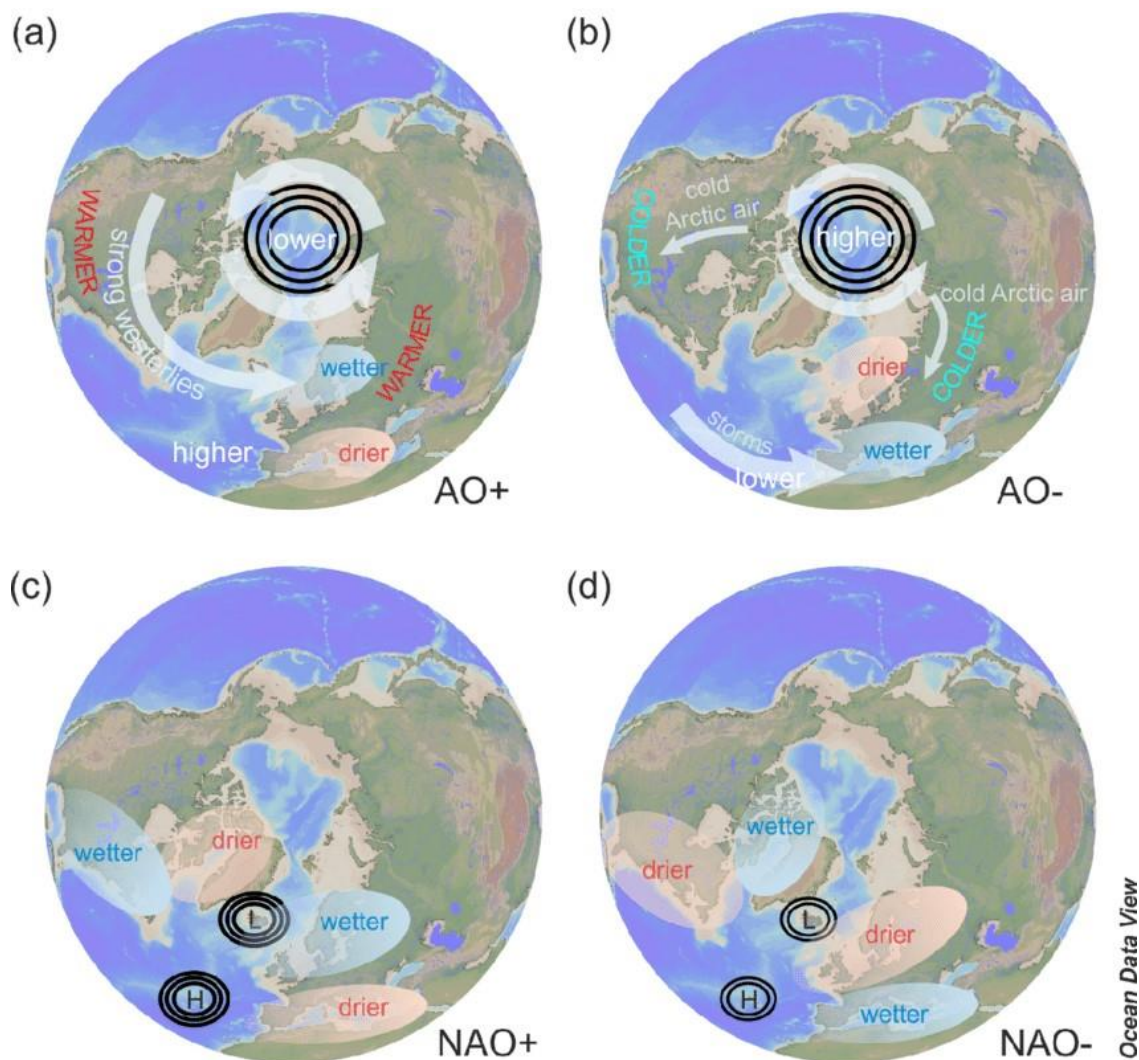


**Figure 5.** Summary diagram of the effect of AO and NAO phases. (a) and (b) represent AO modes while (c) and (d) show the features of both NAO modes. Source: Bartels, (2017).

While the physical relevance between the NAO and the AO over Eastern Greenland is not crystal-clear, both exhibit a close association, particularly during winter months (December to March), showcasing their most robust signatures and explaining a considerable portion of sea-level pressure variance (Stendel et al., 2008). As exhibited in figure 5, during the positive phase of the AO, characterized by a strong polar vortex and lower pressure over the Arctic, the NAO often assumes a positive phase as well. This configuration typically leads to milder temperatures and reduced sea ice extent over Greenland due to enhanced poleward advection of warm air masses (Stendel et al., 2008). Conversely, during the negative phase of the AO, which corresponds to a weaker polar vortex and higher pressure over the Arctic, the NAO may exhibit a negative phase. This configuration tends to bring colder temperatures and increased sea ice extent to Greenland as cold air masses extend further southward (Rogers & McHugh, 2002; Thompson & Wallace, 1998).

The AMOC plays a crucial role in heat transfer across the equator, involving the northward movement of warm, salty water in the upper Atlantic ocean and the southward flow of the transformed cold, fresh North Atlantic Deep Water (NADW) in the deep Atlantic (Zhang et al., 2019). At its core, AMOC functions as a large-scale circulation pattern, with surface currents carrying warm water northward, releasing heat to the atmosphere. As this water cools, becomes denser, and accumulates salt, it eventually sinks to deeper ocean layers, initiating a return flow southward at depth (Rahmstorf, 1995). This continuous circulation loop influences climate patterns, including temperature and precipitation, making AMOC a key driver of regional and global climate variability, characterized by a flow of warm, low-salinity surface waters northward (represented by the red lines in fig. 6) and a flow of colder, saltier deep waters southward (represented by the blue lines in fig. 6) (Vermassen, 2019).

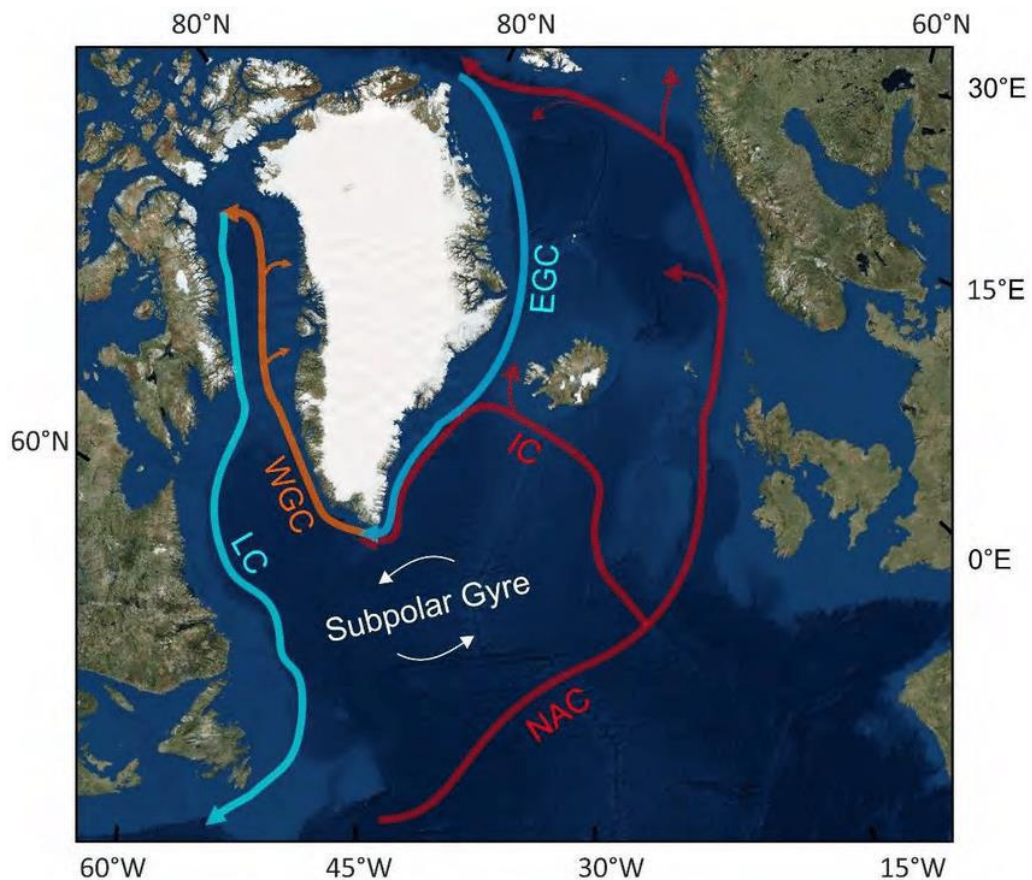


**Figure 6.** Satellite image of Greenland and the main ocean currents composing the AMOC. NAC = North Atlantic Current, IC = Irminger Current, EGC = East Greenland Current, WGC = West Greenland Current, LC = Labrador Current. Source: Vermassen (2019).

According to Buckley & Marshall (2016), the net northward heat transport in the Atlantic conducted by AMOC is responsible for the relative warmth of the Northern Hemisphere, serving as a key mechanism by which heat anomalies are captured in the ocean and, therefore, influencing the trajectory of climate change. In this context, the sea surface temperature around Greenland follows a N – S distribution. This latitudinal condition influences the difference in atmospheric temperatures experienced on the island (fig. 7).

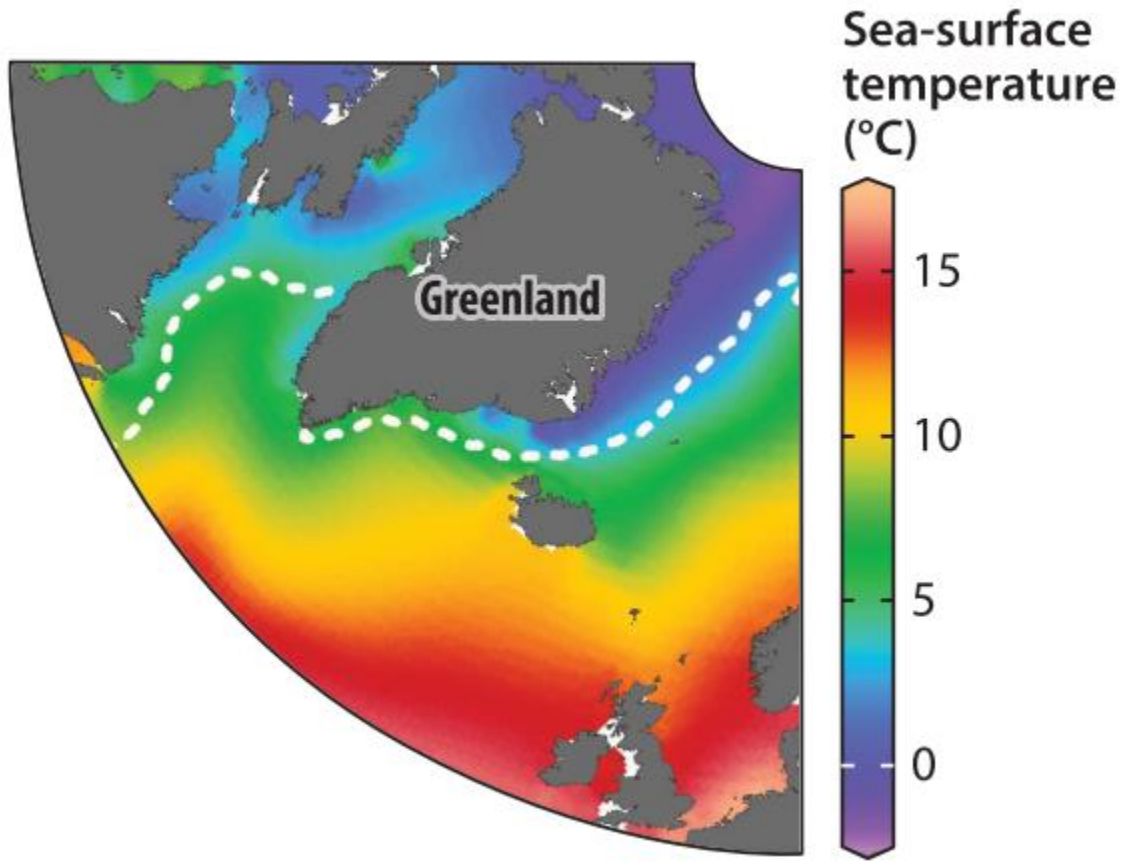


**Figure 7.** Distribution of superficial sea temperature in the North Atlantic. Modified from Axford et al. (2021).

In relationship with East Greenland, strengthened AMOC, marked by a more efficient flow of Atlantic water enhance the northward transport of warm Atlantic Water, bringing stratified conditions in the NE Greenland shelf, forming extensive sea-ice cover thanks to the strengthened cold EGC (Pados-Dibattista et al., 2022). On the other hand, increased freshwater input from the EGC weakens the AMOC (Wanamaker et al., 2012), resulting in reduced transport of Atlantic Water, sabotaging the formation of perennial sea-ice due to mixing of salt and fresh water causing less stratified waters as a result of weakened polar water influx through the EGC. Accordingly, (Gong et al., 2015) modelling data point to increased GrIS topography enhancing wind activity over the North Atlantic, causing intensified AMOC. On the contrary, less ice volume would be related to weak AMOC.

#### 1.4. Late Quaternary evolution of East Greenland climate

The current climate configuration of E Greenland reflects pronounced changes during the later part of the Quaternary period. Paleoecological research in the region was pioneered by Iversen's (1953) pollen study based on lacustrine sediments in Greenland, proposing that plants adapted to the harshest climate conditions had survived on the island during the last glaciation. Funder (1978) supported this theory through the first pollen analysis of E Greenland, documenting extensive unglaciated lowland areas that served as refugia.

Around 21,500 cal yrs BP, during the Last Glacial Maximum (LGM), Greenland's ice cap faced a significant cooling, reaching temperatures approximately 25°C lower than present-day values, contributing to the preservation of the expansive ice sheet (Johnsen et al., 1995). The subsequent retreat of glacier and the onset of the Holocene epoch were strongly influenced by orbital forcings such as solar insolation, a factor that played a key role in driving the thermal evolution in Greenland and surrounding areas (Axford et al., 2021) (fig. 8).

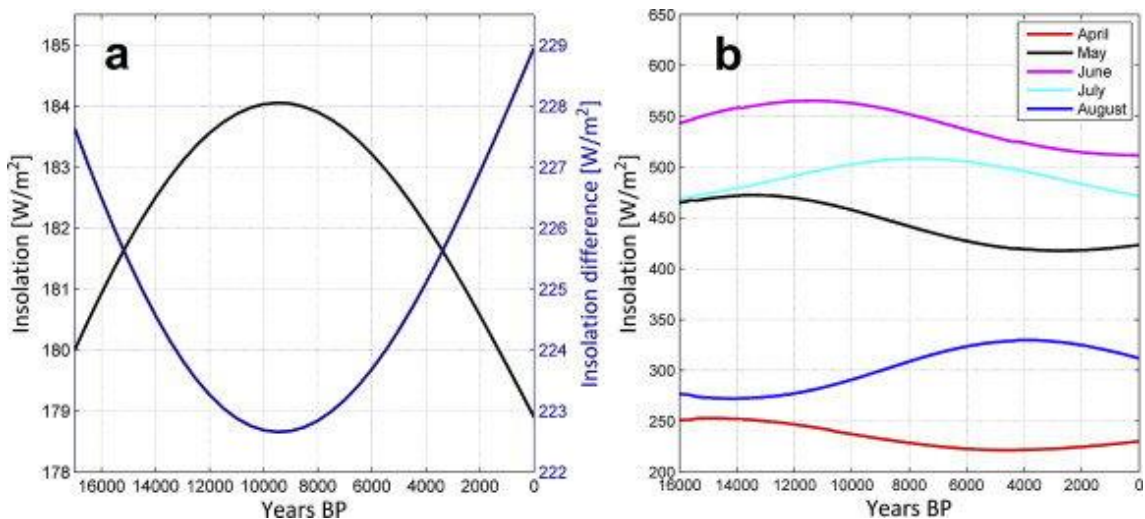


**Figure 8.** Mean annual solar insolation at 80°N. Source: Stranne et al. (2014).

During the Early Holocene, Greenland and adjacent regions exhibit increased biological activity, plant migration, and lake productivity, leading to the establishment of open water conditions in the fjords during summer complex reactions, influenced by

atmospheric, oceanic, and ice sheet dynamics, which varied due to regional factors, albedo feedback and the oceanic impact of freshwater input from ice melt (Marienfeld, 1992; Vasskog et al., 2015). Overall weak AMOC during this period brought highly stratified conditions in the NE Greenland sea presenting abundant sea-ice cover coupled with increased warm Atlantic sub-superficial water transport (Blaschek et al., 2015; Pados-Dibattista et al., 2022). Many of the authors agree that the main forcing behind this peak biological activity period was insolation (Briner et al., 2016; Laskar et al., 2004; Stranne et al., 2014 to name a few).

The timing of Holocene warming appears to have varied across Greenland, geomorphological data indicates that certain regions, particularly in the S and SW, recorded summer temperatures exceeding those of the 20<sup>th</sup> century, several thousand years later than other parts of the island, despite that, all the records experience this warm maximum during the Early or Middle Holocene (Axford et al., 2021; Briner et al., 2016; Larocca et al., 2020). Notably, the SE region of Tasiilaq experienced a peak warm period between 11,200 and 9,700 cal yrs BP, surpassing other Greenlandic sites within the same time. However, interpretations of this period remain uncertain (Jakobsen et al., 2008). The retreat of the NE Greenland ice shelf through Nioghalvfjerdsfjorden (79°N) coincided with a sustained period of thermal forcing. This period was characterized by atmospheric and ocean temperatures that were over 2°C warmer than present-day conditions, persisting for at least a millennium prior to the ice shelf's collapse and retreat (Smith et al., 2023). Even when the establishment of modern oceanographic circulation patterns in the region ca. 10,300 cal yrs BP, the early Holocene saw an increase in the inflow of warm Atlantic water and a rise in subsurface ocean temperatures. Despite these changes, a heavy sea-ice cover likely persisted at the surface, indicating a strong stratification of the water column, possibly driven by the influx of meltwater (Lloyd et al., 2023; Sha et al., 2022).

By around 10,200 cal yrs BP, July temperatures averaged approximately 4°C in the Western Canadian Arctic (Peros & Gajewski, 2008), allowing the generalized onset of biological activity ca. 10,000 cal yrs BP (Wagner, 2000). Subsequently, between 9,700 and 8,700 cal yrs BP, July temperatures stabilized between 6°C and 6.7°C in the Arctic

in general (Gajewski, 2015a). However, this stability was regionally interrupted by a cooling pulse, usually referred to as the 8.2k event, caused by an alteration in oceanic patterns, in particular by the input of fresh meltwater to the North Atlantic due to the partial collapse of the Laurentide ice sheet (Alley & Ágústsdóttir, 2005; Barber et al., 1999; Clarke et al., 2003).

Following the 8.2k cold event, the HCO brought significant warmth to NE Greenland, though with some regional variations (Briner et al., 2016). Along the coastal areas near NE GrIS ( $79^{\circ}\text{N}$ ), from 9,000 to 7,000 cal yrs BP, subsurface ocean temperatures reached their warmest recorded levels. However, surface conditions remained harsh, characterized by heavy sea-ice cover, indicating persistent stratification (Lloyd et al., 2023). This period also brought the highest summer sea surface temperature in the North Iceland sea (Sha et al., 2022). At Basaltsø ( $72^{\circ}\text{N}$ , NE Greenland), geochemical, pollen, and diatom data indicate the HCO spanning from 9,000 to 6,500 years BP (Wagner, 2000), while in Hochstetter Forland ( $75^{\circ}\text{N}$ , NE Greenland), Dodis Sø, Peters Bugt Sø, and Ailsa Sø pollen assemblages obtained from the sediment records of these lakes indicate higher than present summer temperatures between 8,800 and 5,600 cal yrs BP (Björck et al., 1994). In the Scoresby Sund region ( $70^{\circ}\text{N}$ , NE Greenland), the thermal maximum was dated between 8,800 to 5,800 years BP (Funder, 1978). Germania Havn Sø lake sediments in Sabine Ø indicate that the warmest period occurred at 7,600 – 6,600 years BP (Bennike & Wagner, 2012). Around 7,500 cal yrs BP, the EGC weakened, causing at least two months of open water conditions far from the coast during summer, as shown by an enrichment of lake sediments in Raffles So, associated with sea-bird colonies arriving in the basin (Wagner, 2000). This complex pattern of warming, with cold surface conditions and a potential shift in the EGC, suggests interplay between increased summer insolation, changes in atmospheric circulation and diminished transport of polar waters through the EGC (Pados-Dibattista et al., 2022).

Since 7,000 cal yrs BP summer surface temperatures in N Iceland started a constant decreasing trend, while subsurface ocean temperatures in the NE Greenland Sea followed the same pattern , marking a transition from relatively heavy to seasonal sea-

ice cover driven by a reduction in EGC and a weakening of the AMOC (Lloyd et al., 2023; Sha et al., 2022). While the HCO dated around 8,000 cal yrs BP in Greenland Ice cores, it lasted between 8,300 and 7,300 cal yrs BP in the Zackenberg Valley (Bennike et al., 2008; Vinther et al., 2009). Bennike & Wagner (2012) reported the HCO lasting until 6,600 cal yrs BP in the Wollaston Forland ( $74^{\circ}\text{N}$ , NE Greenland) region.

Paleooceanographic reconstructions from the Greenland Sea, 500 km east from Zackenberg, show that modern circulation patterns were established around 6,000 years BP (Hebbeln et al., 1998). Extended sea-ice conditions were present in the region since 5,200 cal yrs BP (Kolling et al., 2017). Olsen et al. (2012) NAO reconstruction based on Greenland lake sediments dates to this period and describes positive NAO values between 5,200 and 4,500 cal yrs BP. Subsequently, cooler conditions prevailed from the later part of the Middle Holocene onwards, with evidence of extended sea ice phases and a definitive transition to cooler climates around 5,000 years BP (fig. 9).

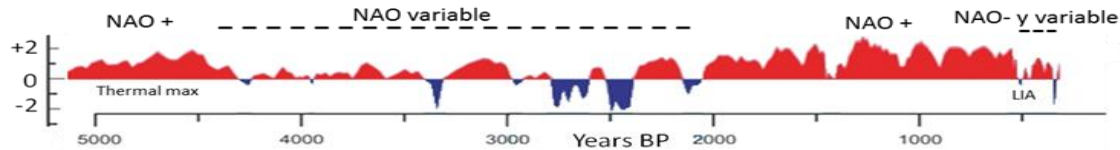


**Figure 9.** Reconstruction of NAO climatic modes for last 5,000 years, using continental Holocene records. Source: (Olsen et al., 2012).

Decreases in *Betula* pollen since 5,000 cal yrs BP is interpreted as the onset of a cooling trend that was recently reversed (Wagner & Melles, 2002). This cooling can also be verified on the GRIP ice record, that shows a decrease of  $3^{\circ}\text{C}$  between 5,000 – 2,000 cal yrs BP (Johnsen et al., 1995). Dynocist data from the E Greenland Sea around 4,500 cal yrs BP indicates low salinity due to freshwater discharge from the GrIS (Briner et al., 2016; Solignac et al., 2006). Diatom data obtained ca. 400 km east-southeast from Zackenberg shows increased sea-ice cover since 4,500 cal yrs BP (Koç et al., 1993). Posterior to this, from 4,400 to 4,000 cal yrs BP, the NE Greenland ice shelf underwent partial reformation, yet the spatial details of this process remain uncertain (Smith et al., 2023).

The late Holocene in the region was marked by glacier advances and overall cold conditions (Briner et al., 2016; Gajewski, 2015b; Vinther et al., 2009). Increased sea-ice cover conditions have been evident in E Greenland since at least 3,500 cal yrs BP (Briner et al., 2016; Solignac et al., 2006). Cold and dry conditions remained between 3,000 – 1,000 cal yrs BP, synchronous with a strengthening of the EGC, leading to increased sea-ice cover and a decline in the sea bird population in the area (Wagner, 2000). These conditions are attributed to the influence by both regional dynamics and orbital-driven summer cooling (McKay et al., 2018). Due to its high latitude location, changes in the seasonal variation of insolation related to Earth's axial tilt have had a significant influence on Greenland climate over the past 4,000 years (Laskar et al., 2004). The onset of neoglacial climatic conditions around this time is attributed to the cooling of surface water masses on the E Greenland Shelf (Perner et al., 2015). The term "Neoglacial" refers to a period of enhanced glacial activity or advancing glaciers that occurred during the late Holocene epoch, particularly from around 5,500 to 500 years ago (Axford et al., 2021; McKay et al., 2018; Werner et al., 2013). This period contrasts with the warmer conditions that characterized the early to mid-Holocene period, marked by glacial retreat and overall milder temperatures. The Neoglacial period is characterized by a general cooling trend, which saw fluctuations between warmer and colder intervals known as climatic optima and climatic minima, respectively (McKay et al., 2018). The warm and cold events during the Late Holocene are closely related to variability in sea-ice extent (Kolling et al., 2017). Neoglacial period introduced variability in sea ice extent, impacting the Arctic's climate, in this context, coastal regions sustained cold and dry conditions during this period, affecting vegetation and contributing to late Holocene glacial advances (Wagner, 2000).

The generalized paleoclimatological stages used to describe the climatic history of the Northern Hemisphere during the past couple of millennia has been widely studied and the bipolar trend of warming and cooling phases has been divided into warm phases, including events such as the Roman Warm Period (2,400 – 1,600 cal yrs BP) and the Medieval Climate Anomaly (1,100 – 700 cal yrs BP, as well as periods of cooling like the Dark Ages Cold Period (1,600 – 1,100) and the Little Ice Age (700 – 200 cal yrs

BP). The RWP characterized by warmer climates, occurred in the region from ca 2,200 to 1,600 years BP (Easterbrook, 2016). This warm interval, marked by a rise in temperature of approximately 2°C above current levels, was succeeded by a reduced sea ice phase between 2,200 and 1,300 cal yrs BP (Kolling et al., 2017). The interactions between sea-ice interactions and terrestrial environmental conditions are illustrated in fig. 10.

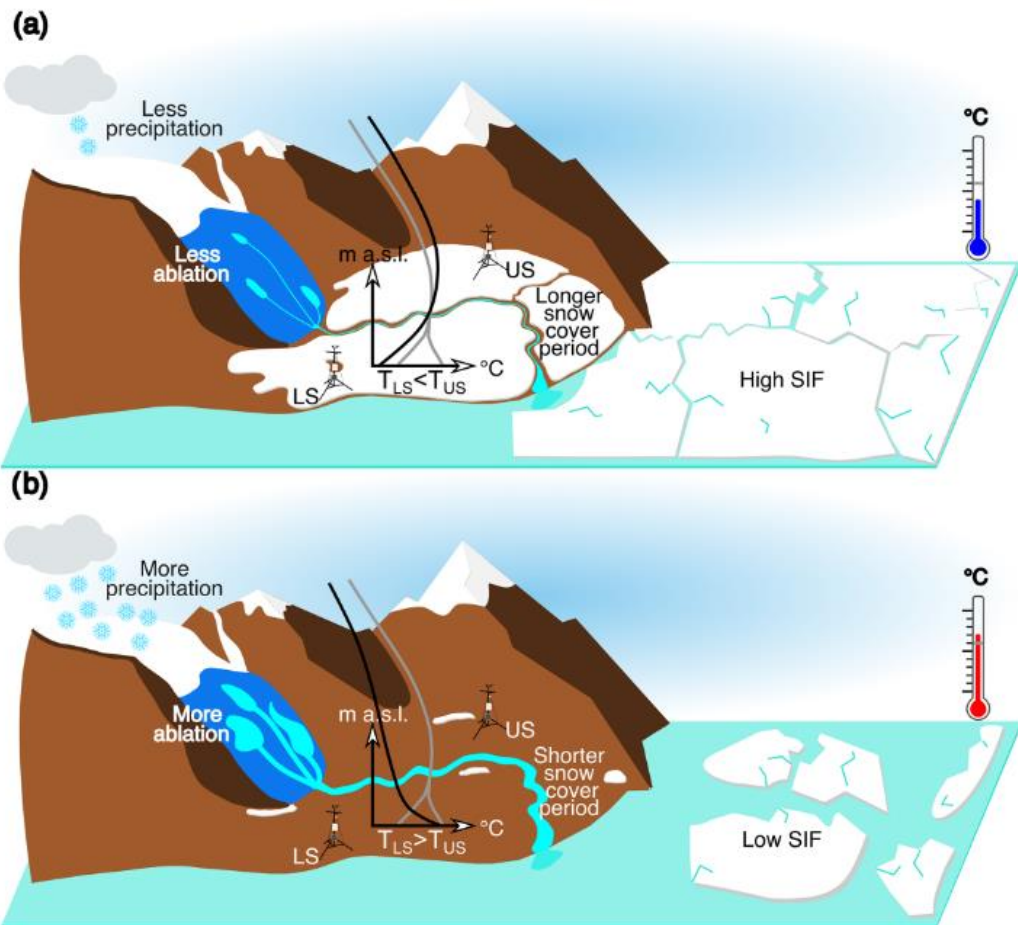


**Figure 10.** Diagram of the effects of sea-ice cover on the continental climate conditions of the Arctic. Source: Shahi et al. (2023).

Positive NAO conditions prevailed in the region from 2,000 to 650 cal yrs BP in Kangerlussuaq (67°N, SW Greenland) bringing colder and more arid conditions (Olsen et al., 2012). Raffles Sø experienced ice-free summer conditions from the Early Holocene to 1,800 years BP (Cremer et al., 2001). Subsequently, temperatures in Greenland dropped by 2.75°C after the RWP, with a cold event occurring 1460 years BP, marked by late tree growth, diminished sunlight, temperature drops in various

regions, unripe fruit, and summer snowfall, representing the peak of the DACP (Easterbrook, 2016).

A layer of thick sediments overlying an organic layer at 1,300 years BP in the Zackenberg valley suggest a mechanism akin to the HCO but possibly associated with the MCA (Cable et al., 2018). Around 1,000 years BP, a slight warming trend was associated with the medieval period, followed by strong cooling during the LIA, and a conspicuous warming in the last century (Jakobsen et al., 2008; Wagner, 2000). A brief warming period around 1,000 – 500 cal yrs BP gave way to a cooling phase until ca. 200 cal yrs BP, as indicated by reduced organic content and cold vegetation around the lakes (Wagner, 2000). The LIA was followed by the IE (200 cal yrs BP – present) bringing accelerated climate warming on Greenland during recent times, attributed to human-induced global warming (IPCC, 2023).

## 1.5. Palynology as a key tool to track environmental changes in the Arctic

Ice-core based studies conducted on the GrIS have been a useful tool to understand global and regional past climate (Johnsen et al., 1995; Stuiver et al., 1995). However, the main limitation of these key paleoclimate records is their geographical location. These ice cores are typically located in the interior of the GrIS, which limits their sensitivity to small, but crucial environmental changes. In this regard, non-glaciated coastal Greenland paleorecords are often overlooked although these areas are extremely sensitive to climate and environmental fluctuations. Pollen emerges as a particularly useful proxy for providing paleoecological and paleoclimatic information in these non-glaciated areas, of the Arctic (Gajewski, 2006). Since the mid-20<sup>th</sup> century, when paleoecological research was boosted to the present level, scientists have used fossils contained in lacustrine sediments to reconstruct past environmental conditions at local and regional scales (Birks et al., 2012a). Pollen and spores of plants are the most abundant plant remains on the fossil record, thanks to their sporopollenin wall (exine) that gives them high preservation potential, making palynological studies useful to

reconstruct changes in plant distribution patterns at various timescales (Traverse, 2007). Studies focusing on aerobiology claim that pollen productivity and regional community composition are effectively captured by pollen assemblages and influx (Chevalier et al., 2020). However, it is crucial to have in mind that even if pollen diagrams document changes in pollen over time, the corresponding vegetation must be inferred. Figure 11 illustrates the theoretical framework of pollen analysis.

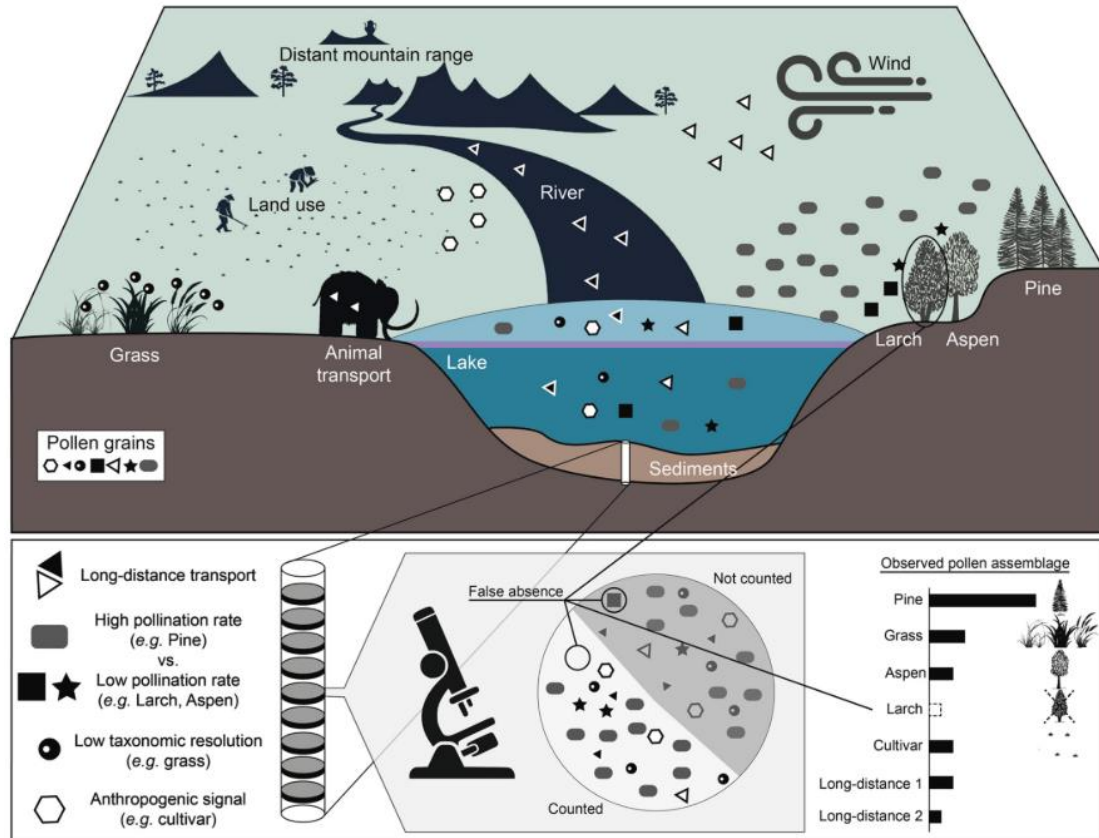


**Figure 11.** Theoretical model of the standard pollen analysis based on lacustrine records (Chevalier et al., 2020).

Arctic palynology represents a refined paleoecological tool, since just like in every other region, pollen found in sediments accurately reflects the pollen emitted by plants with minimal delay (Chevalier et al., 2020; Gajewski, 2006). This statement is in fact proposed due to the Greenland paleopalynological studies carried out by Fredskild, 2000, 1995, 1967, among others, which are feasible examples of meticulous taxonomic efforts allowing enhancing the reconstruction of the island's vegetation. However, achieving refined taxonomic resolution requires comprehensive pollen atlases, keys and reference collections (Gajewski, 2006). Additionally, one of the main challenges to face

in Arctic palynology lies in facing with low pollen concentrations stemming from factors such as low plant productivity, sparse vegetation cover, extreme climate conditions, phenological factors, as well as taphonomical conditions, among others (Gajewski, 2006).

On the last few decades, quantitative reconstructions of climatic parameters based on pollen assemblages contained on sediment cores have been developed, usually related to warmest month temperature and annual precipitation (Birks & Birks, 2006). Assuming a connection between contemporary pollen taxa distribution and climatic conditions (and this relationship has not changed through time), and later applying this observed relationship to fossil pollen records, it is possible to reconstruct the climatic conditions that surrounded past vegetations under presence/absence parameters or relative abundance on the record (Brewer et al., 2007). To formulate a transfer function, it is crucial to establish the numerical relationship between pollen deposition and climatic variable (Birks et al., 2012b; Juggins, 2013; ter Braak & Juggins, 1993). This transfer function (fig. 12) is generated using multivariate techniques on a calibration set of present-day (modern pollen) to estimate the environmental parameters (Telford & Birks, 2009). Every quantitative climate reconstruction based on a transfer function is proposed under several assumptions: (i) modern pollen assemblages are reflective of the present-day environmental conditions; (ii) the climatic variable being reconstructed defines taxa abundance, or is directly related with another defining factor; (iii) the ecological response to this climate variable remains constant over the time; and (iv) variations in the modern calibration set are not influenced by environmental factors different from those being reconstructed ones (Birks & Birks, 2006; ter Braak & Juggins, 1993) (fig. 12).

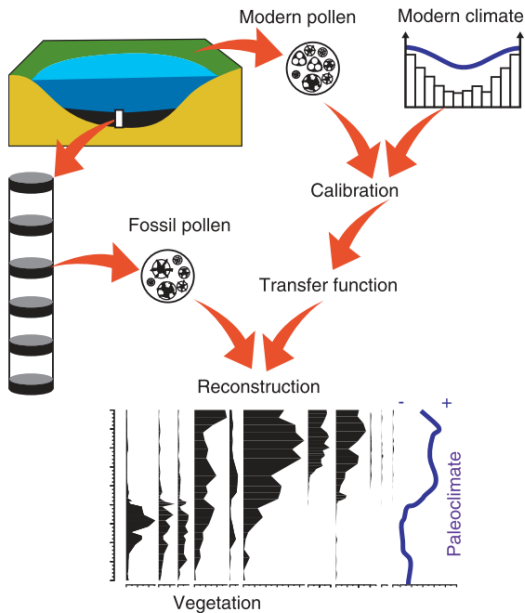


**Figure 12.** Diagram of the theory behind pollen-based quantitative climate reconstructions. Source: Brewer et al. (2007).

Quantitative paleoclimate reconstructions generated using modern analogue technique (MAT) don't assume any response model for the proxies, nor consider numerical relationships related to optimum or stress levels (Birks et al., 2010). However, the main weakness of MAT becomes known when fossil assemblages that respond in a unique way to given environmental gradient are included, causing prediction errors. These errors are particularly important when they are based on assemblages that don't have a modern analogue or have more than one (Birks et al., 2010; Cao et al., 2017). Taking this into account, and in order to avoid potential problems in reconstructions, multivariate calibrated methods that assume unimodal responses from organisms are proposed, such as weighted average (WA) or weighted average partial least squares (WA-PLS) (Birks et al., 2010; Juggins, 2013; ter Braak & Juggins, 1993). This technique is based on the assumption that if a taxon shows a unimodal response towards a certain environmental gradient, its abundance tends to increase as long as it reaches niche values and decrease as long as values augment or diminish, however, its main limitation is its sensitivity to site distribution, so it tends to co-relate (Birks et al., 2010; Birks & Seppä, 2004). Also, WA lacks precision when it comes to the ends of the gradient, underestimating low values and overestimating high values (Birks et al., 2010; Birks & Seppä, 2004). WA-PLS represents a more sophisticated, robust, yet simple

method that performs well, allowing to generate transfer functions with fewer errors and biases than WA, WA-PLS provides more precise estimates at the ends of the environmental gradient. This method was designed to work with ecological datasets with high number of taxa, lots of zeros (absence), and the assumption of unimodal responses to a gradient (ter Braak and Juggins, 1993). WA-PLS performs way better than MAT when fossil assemblages are not that similar to modern assemblages or when the calibration sets have fewer samples (Cao et al., 2017; ter Braak & Juggins, 1993).

## 1.6. Study area

This research was executed on the NE area of Greenland, which is the world's biggest island located in the North Atlantic (60 – 83°N). For years NE Greenland was poorly studied, however, since the onset of the Zackenberg Ecological Research Operations (ZERO) station, the valley – located in the Northeast Greenland National Park, the biggest protected area in the world – has become a key site for research on Greenland's high-Arctic ecosystems and the Arctic in general (Meltofte & Rasch, 2008) (fig. 13).

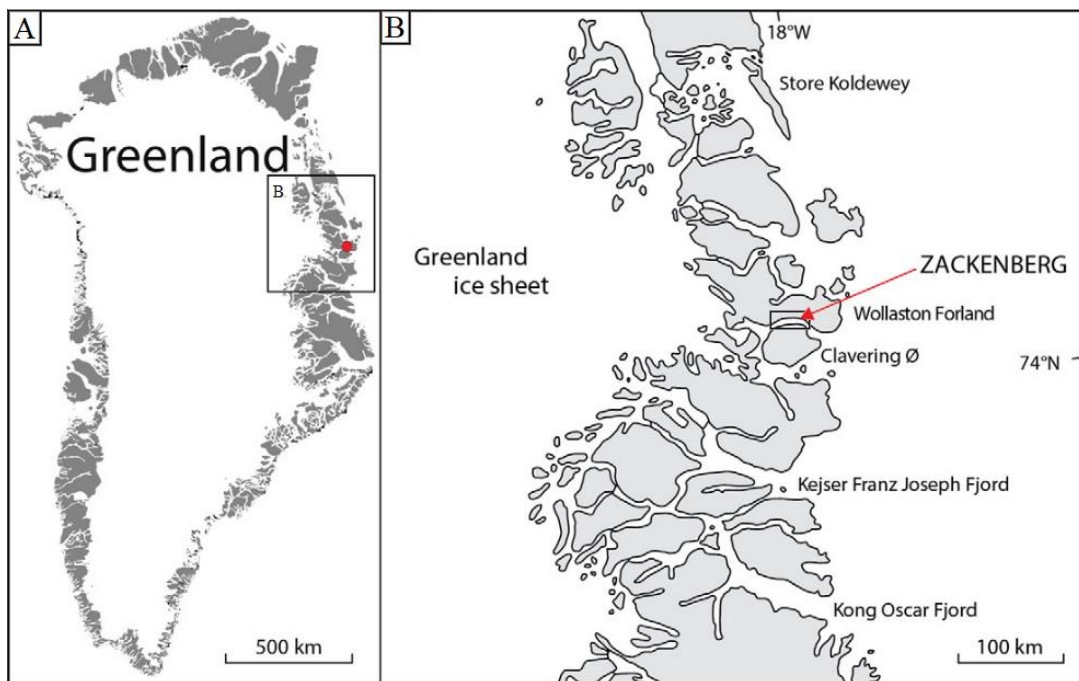


**Figure 13.** Location of the study area. Map A exhibits Greenland, with the NE region marked by the black square. Map B correspond to the studied area of Zackenberg.

which also corresponds to map area in figures 13, 15 and 16. Source: Cable et al. (2018).

#### 1.6.1. Climate of the Zackenberg region

The climate of the Zackenberg region is high Arctic type, characterized by mean annual temperatures of -9°C and mean annual precipitation of 211 mm, most part falling as snow (Hansen et al., 2008a). As in most E Greenland fiord areas, temperature increase from the cold coast towards the inland areas, from mountains towards lowlands and from flat and wind-exposed areas toward wind-protected areas (Karlsen & Elvebakk, 2003). The presence of glaciers is determined by the prevailing dry conditions, leading to their location primarily on mountainous terrain. Seasonal and perennial snow patches control most geomorphological processes on periglacial areas of the valley (Christiansen, 1998). Mountain tops are blown by the winds and are exposed to low to no snow accumulation during the year, while water presence increases downslope. Prevailing winds come from the north, supplying the S oriented slopes with big snow patches and providing superficial and underground water during most of the growing season (Cable et al., 2018).

#### 1.6.2. Geology of the Zackenberg region

The Zackenberg valley runs through a geological fault zone oriented N to S. This conforms a landscape of contrast between the eastern and western part of the valley and in the transition from glacial to periglacial areas. While mountain tops are composed by old bedrock materials, the lower lands of the valley are filled by Quaternary sediments (Cable et al., 2018). Breccia, sandstones, and mudstones dated from the Jurassic to Cretaceous under Tertiary basalts conform the Aucellabjerg mountain (911 m asl) on the east, while the Precambrian orthogneiss-made Zackenberg mountain (1372 m asl) stands on the west (Koch & Haller, 1971). The eastern mountain slopes are changed constantly by cryogenic, nival, and other surficial processes that contribute to a transport of fine-grained sediments to the lowlands. In contrast, the western slopes are dominated by gravitational processes where coarser sediments are transported but not

necessarily reach the lowlands (Cable et al., 2018). In the lower part of the valley, landforms are partially covered by the emerged delta, next to the Zackenberg river, affected by Holocene sea-level changes and reaching up to 30 m asl (Christiansen et al., 2002) (fig. 14).

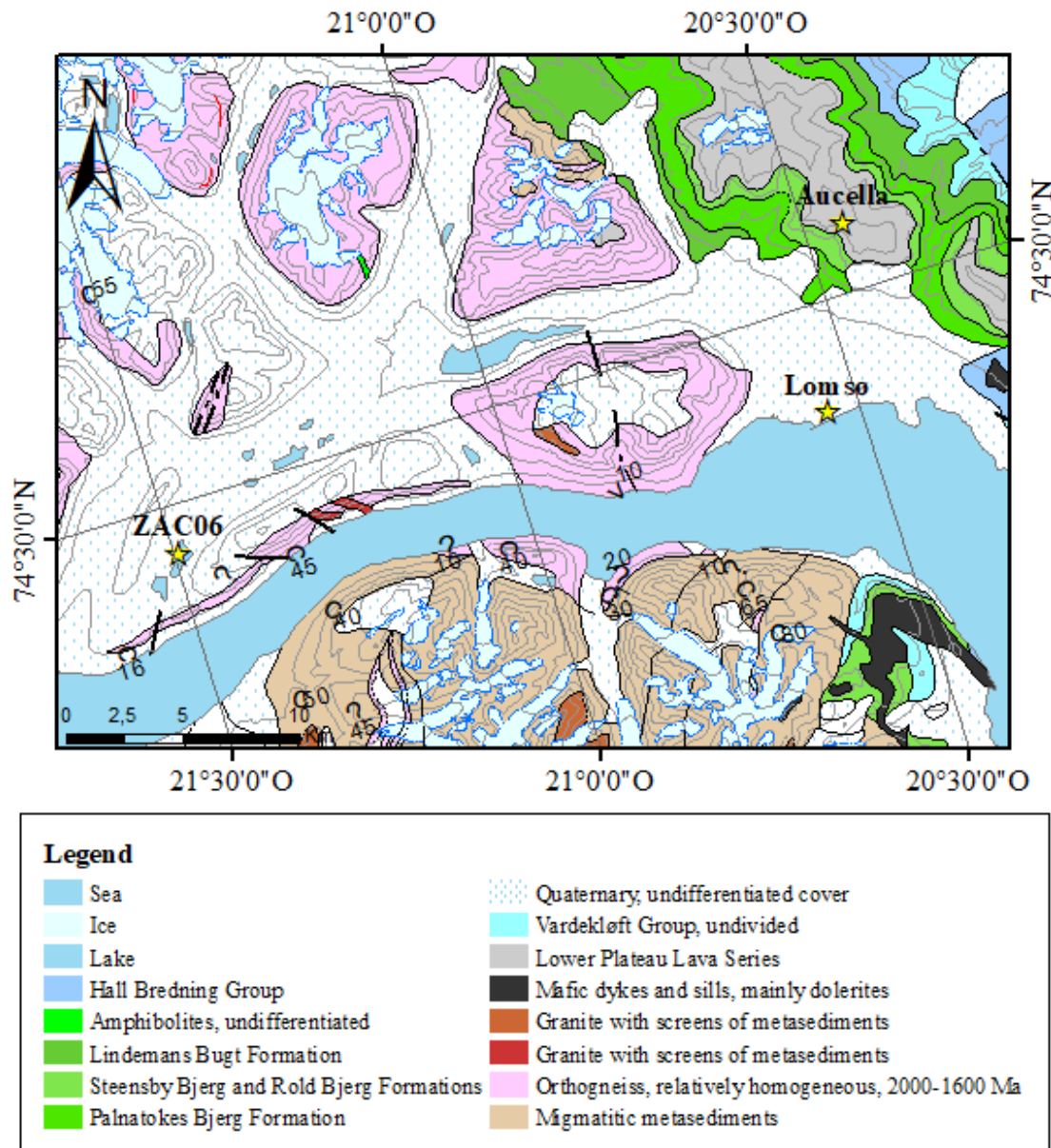


**Figure 14.** Geological map of the study area.

#### 1.6.3. Flora of Zackenberg region

Even when vegetational development in NE Greenland is mainly limited by the extreme climatic conditions and low soil formation, due to continuous permafrost, the high-

Arctic flora in Zackenberg area is considered as unusually rich and diverse for these latitudes, representing over 150 species of vascular plants that are distributed forming a mosaic rich in vegetal communities (Bay, 1998; Fredskild, 1998).

A distinct difference in composition is defined by the Zackenberg River as it flows through the valley from north to south (Elberling et al., 2008b). At the east of the river, lowlands are dominated by *Cassiope tetragona* heaths mixed with *Salix arctica* snow beds, while Herbs dominate the 50 – 100 m asl. area, while the 150 – 300 m asl. is dominated by open *Dryas* heaths, going more open until reaching fell field vegetation with scarce *Salix* and *Dryas*. The wet areas related to snow patches between 250 – 600 m asl. are colonized by species rich grasslands. To the west, *Vaccinium uliginosum* is more abundant on sparse rocks, and the fens show higher diversity (Elberling et al., 2008b). This distribution can be explained because the mountain tops are blown by the winds and are exposed to low to no snow accumulation during the year, while water content rises downslope. The dominant wind pattern supplies the S-orientated slopes with big snow patches, providing superficial and underground water during most of the growing season. (Elberling et al., 2008; fig. 15).

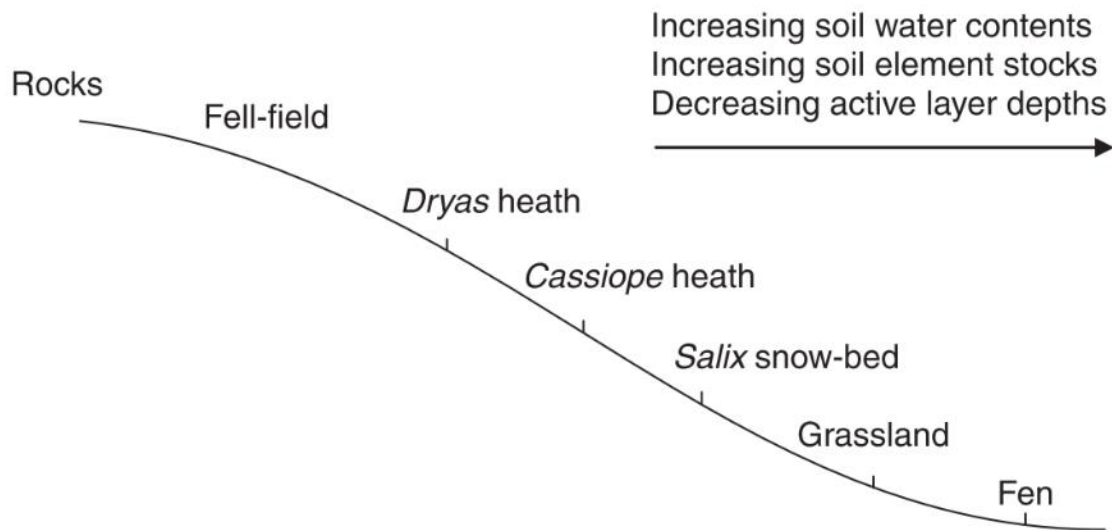


**Figure 15.** Distribution of the main plant communities along a gradient in the Zackenberg area. Modified from (Elberling et al., 2008b).

The lower area of the Zackenberg valley near the ZERO station is covered by fens dominated by *Dupontia pislansantha*, *Eriophorum scheuchzeri* and *Carex bigelowii* with

*Juncus triglumis*, *Luzula wahlenbergii* and *Pedicularis flammea* (Fredskild & Mogensen, 1997). Fens are related to hollow lowland terrains where soils retain water during the growing season, often associated to long lasting snow patches and water courses (Elberling et al., 2008b).

Grassland soils dry out during summer, which being the main difference between these vegetation type and fens. Most grasslands are dominated by *Carex bigelowii* with dry adapted species as *Eriophorum triste*, *C. capillaris* and *C. rupestris* (Fredskild & Mogensen, 1997). Elberling et al. (2008) also describes *Arctagrostis latifolia* and *Alopecurus alpinus* reigning on the unsaturated soil lowlands and slightly sloped terrain with high water availability early during the growing season.

Dwarf-shrub heaths in the area vary in species composition but *Salix arctica*, *Dryas* sp. and *Cassiope tetragona* are found in everywhere on the Zackenberg valley (Fredskild & Mogensen, 1997). The distribution of heath vegetation is defined by the extension and duration of snow patches (Christiansen et al., 2002). *C. tetragona* heaths develop only on humid and flat terrains at low elevations, under 50 m. *C. tetragona* dominates with *Luzula arctica* and *L. confusa*, with high bryophyte cover (Elberling et al., 2008b). *Vaccinium uliginosum* dominated heaths lie on S and W exposed slopes. While they are unusual at the east of the Zackenberg river, they are more abundant at the west part, where heaths are fragmented by eroded rock bottom (Elberling et al., 2008b). On Aucellabjerg slopes, *Vaccinium* heaths occur typically right below *Dryas* heaths and above *Salix* snow beds, with snow cover melting earlier than the snow beds (Elberling et al., 2008b). *Dryas* heaths with *Kobresia myosuroides*, *Carex rupestris* and *Poa glauca* dominate on wind exposed dry areas, while it is accompanied by *S. arctica*, *Silene acaulis* and occasional *Polygonum viviparum* in places that remain humid throughout all the growing season (Elberling et al., 2008b).

*Salix arctica* snow-patch heaths, or *Salix* snow beds are found on level ground or slopes with long-lasting snow cover, always distributed as a belt below the *Cassiope* heaths. *Pedicularis hirsuta*, *Luzula arctica* and *Hierochloe alpina* are companions in drier (early snow-melt) communities while *Eriophorum triste* and *Juncus biglumis* represent

the moister type (Fredskild & Mogensen, 1997). Elberling et al. (2008) additionally mentions *Alopecurus alpinus*, *Stellaria crassipes*, *Luzula* sp. and *Poa arctica* as secondary elements, stating that *Salix* snow beds occur on inclined areas with long lasting snow cover. Snowbed vegetation units lie on not too steep slopes, where the transition between snow-patch heaths and genuine snowbed vegetation is gradual, with absence of *Arctagrostis* sp., *Hierochloe* sp. and *Eriophorum* sp. (Fredskild & Mogensen, 1997). The typical late snow beds are dominated by *Phipsia algida* and *L. confusa*.

Herb-slopes are situated on the S slopes along moraines or on the frontal part of solifluction lobes, and are dominated by *Minuartia biflora*, *Polygonum* sp. and *Cerastium arcticum*, with *Oxyria digyna* and *Ranunculus pygmaeus* as important elements (Fredskild & Mogensen, 1997). On wet soil areas around 300 m asl. the landscape is dominated by open vegetation communities with variable snow cover dominated by *Dryas* sp., *Salix arctica* and *C. arcticum* (Elberling et al., 2008b). On abrasion plateaus the scarce vegetation is located in wind exposed areas as crests and moraine tops with little to no snow cover is dominated by *Kobresia myosuroides*, *Potentilla rubricaulis*, *P. hookeriana*, *Poa abbreviate* and *Carex nardina* (Elberling et al., 2008b)

Abrasions ridges in the lowland display low phanerogams cover. *Dryas* sp. and *Salix arctica* are the only woody plants that can be found here and there while *Poa glauca*, *Carex rupestris*, *Cerastium arcticum*, *Potentilla hookeriana* and *Melandrium trifolium* are often found (Fredskild & Mogensen, 1997).

Lakes and ponds frequently display *Pleuropogon sabinei* and *Ranunculus hyper-boreus* cover with *Hippuris vulgaris*. The borders of "geese-lakes" present local associations of *Carex subspathacea* with mosses *Aulacomnium turgidum*, *Aulacomnium palustre*, *Scorpidium tugescens* and *Drepanocladus exannulatus* (Fredskild & Mogensen, 1997)

A similar vegetation mosaic is described for the contiguous Store Sødal valley (Nabe-Nielsen et al., 2017) (fig. 16).

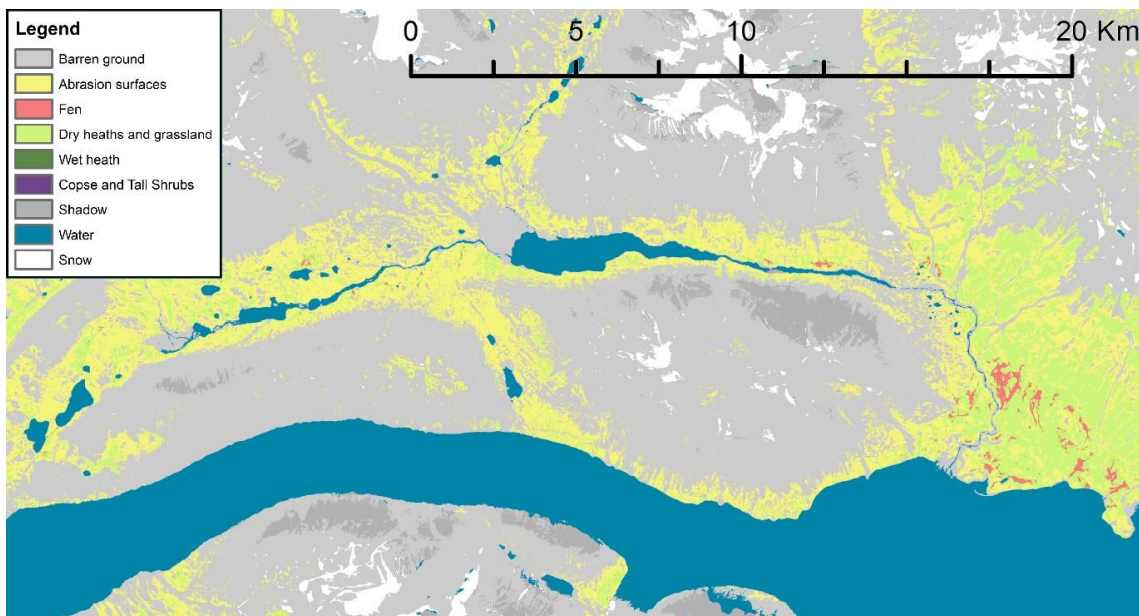


**Figure 16.** Land cover map of the study area. Modified from Rudd et al. (2021).

#### 1.6.4. Characteristics of lakes in the Zackenberg Area

The majority of the over twenty lakes in the Zackenberg area exhibit moss coverage in its bottom surface, while others have vascular plants like mare's tail *Hippuris vulgaris* and high-arctic buttercup *Ranunculus hyperboreus* in the littoral zone (Christoffersen et al., 2008). Ice in lakes starts melting nearshore in mid-June, but lakes are typically ice-free only from mid- or late July until the second half of September, similar to other investigated lakes (Christoffersen et al., 2008). Increased light influx in April – May initiates plant photosynthesis and a subsequent rise in phytoplankton biomass, indicating that light, not water temperature, limits primary production before ice-out (Christoffersen et al., 2008).

Three lakes have been selected: a) Lomsø ( $74^{\circ} 27' 33.4''$  N,  $20^{\circ} 33' 15.7''$  W; 550 m length; 100 m width; 2 m depth), a shallow lake located on the lower coastal part of the Zackenberg valley; b) Aucella Lake ( $74^{\circ} 31' 30.3''$  N,  $20^{\circ} 26' 31.4''$  W; 330 m length; 125 m width; 15 m depth) located near the top of the Aucellabjerg (Aucella mountain) at the eastern side of Zackenberg valley; and c) unnamed lake that we will refer to as “ZAC” ( $74^{\circ} 28' 54.54''$  N,  $21^{\circ} 29' 14.70''$  W; 1250 m length; 600 m width, 14 m depth) located 28 km to the west in the less studied Store Sødal valley (fig. 17).

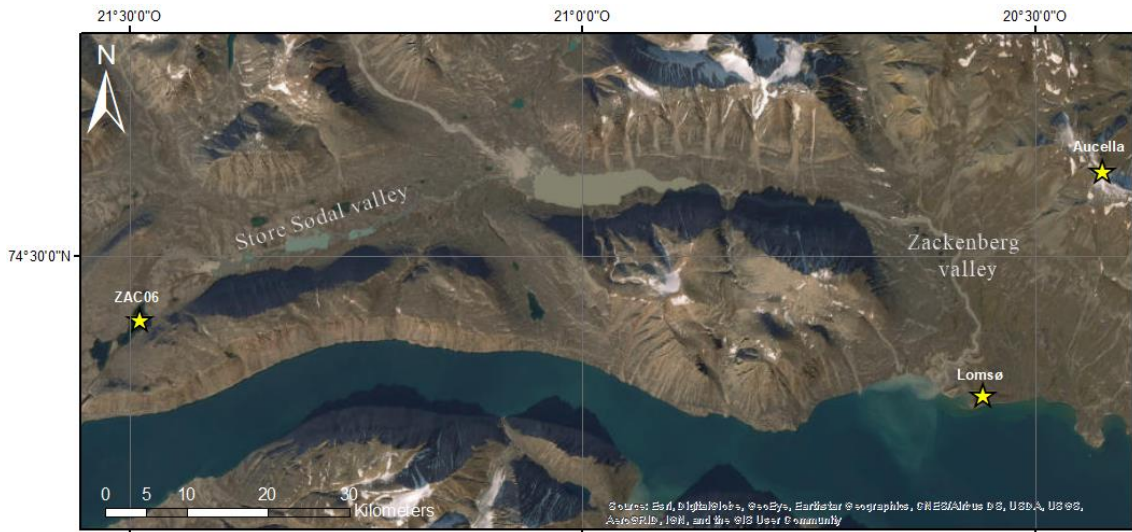


**Figure 17.** Satellite image of the Zackenberg area, indicating location of studied lakes and main geographical elements.

## 1.7. Objectives

Although plenty of palynological studies have been performed in Greenland since the pioneering research by Iversen (1953), the discussion tends to center in answering if currently extant plants remained in the island in ice-free refugia during the last glaciation or if they immigrated during the Holocene from surrounding areas (Bennike et al., 2008). This research aims to reconstruct past vegetational changes on NE Greenland during the Late-Holocene and establish their relationship with regional climate and other local processes using high-resolution palynological and sedimentary data.

Our hypothesis is that NAO fluctuation trigger sea-ice cover and precipitation in NE Greenland ruling short and long term plant composition in Zackenberg. Regarding climatic trends, we anticipate that the Middle Holocene will exhibit more optimal climate conditions that deteriorated through the Late Holocene. Lastly, we expect to discern signals of latitudinal changes in response to this temperature and/or precipitation oscillations.

The main aim of this study is to **quantitatively reconstruct the climate evolution of NE Greenland based on modern pollen-climate relationships.**

Specifically, our goals are to:

1. Generate a modern pollen reference collection for the Zackenberg area.
2. Characterize the main environmental and ecological factors driving changes in pollen stratigraphy.
3. Reconstruct vegetational changes in the Zackenberg area during the Holocene.
4. Establish their correlation with climate and NAO/AO changes.

## 2. Material and methods

### 2.1. Pollen key and reference collection

To accurately distinguish pollen grains, a comprehensive approach was employed, involving the creation of a pollen key and the establishment of a reference collection. The self-developed NE Greenland pollen key used in this study was based mostly from the key proposed by Moore et al. (1991) supplemented by additional pollen morphology data sourced from the high-Arctic North Atlantic (YAO et al., 2014, 2013), the Review of Paleobotany and Palynology series of Northwest European Pollen flora, as well as online pollen digital reference collections such as Global Pollen Project (<https://globalpollenproject.org/>) and PalDat (<https://www.paldat.org/>). (Appendix 1).

The reference collection realized in this research is the result of the doctoral stay developed in September 2021 at the Bioscience Department of the Aarhus University in Roskilde, Denmark. This pollen collection is made of 25 key plant species from the Zackenberg area selected based on Nabe-Nielsen et al. (2017) findings (table 1).

**Table 1.** Key plant species selected for the reference collection.

Species	Family
<i>Draba arctica</i>	Brassicaceae
<i>Cerastium articum</i>	Caryophyllaceae
<i>Carex capillaris</i>	Cyperaceae
<i>Eriophorum triste</i>	Cyperaceae
<i>Kobresia myosuroides</i>	Cyperaceae
<i>Cassiope tetragona</i>	Ericaceae
<i>Rhododendron lapponicum</i>	Ericaceae
<i>Vaccinium uliginosum</i>	Ericaceae
<i>Empetrum nigrum</i>	Ericaceae
<i>Juncus biglumis</i>	Juncaceae
<i>Luzula nivalis</i>	Juncaceae
<i>Luzula confusa</i>	Juncaceae
<i>Chamerion latifolium</i>	Onagraceae

<i>Euphrasia frigida</i>	Scrophulariaceae
<i>Pedicularis flammea</i>	Scrophulariaceae
<i>Arctagrostis latifolia</i>	Poaceae
<i>Hierochloe alpina</i>	Poaceae
<i>Poa glauca</i>	Poaceae
<i>Dupontia fisheri</i>	Poaceae
<i>Polygonum viviparum</i>	Polygonaceae
<i>Oxyria digina</i>	Polygonaceae
<i>Potentilla rubricaulis</i>	Rosaceae
<i>Dryas octopetala</i>	Rosaceae
<i>Salix arctica</i>	Salicaceae
<i>Saxifraga cernua</i>	Saxifragaceae

The 25 samples were obtained from herborized material contained in the Greenland Herbarium of the University of Copenhagen Herbarium. Anthers samples of each species were collected. Once in Barcelona, samples were treated with KOH and later acetolyzed. Half of the resulting sample was mounted on glycerin for observation under light microscope (LM) while the other half was transferred to stubs and sputtered with gold for further scanning electron microscope (SEM) observation. LM pictures were taken with a Nikon DS-Fi3 camera using a Nikon ECLIPSE Ci microscope. SEM observation and pictures were carried using a Hitachi TM4000 Plus microscope at the GEO3BCN institute.

## 2.2. Sedimentary records

### 2.2.1. Coring

We worked on three sediment cores (one for each studied lake) obtained by the project team using a 60 mm in diameter UWITEC gravity corer from a rubber boat in the case of lake Lomsø or on top of the lake ice cover when it was frozen in the case of the other two lakes (fig. 18). Core LOM18\_02 (30.5 cm long) was obtained from lake Lomsø and core AUC18\_02 (83.6 cm long) was obtained from the Aucella Lake during the 2018 field trip, while core ZAC19\_06\_02 (77.5 cm long) was obtained from lake ZAC during

the 2019 campaign. Each sediment core was sealed, transported, and stored at the GEO3BCN cold room at 4°C to preserve the organic matter until further analysis.



**Figure 18.** PALEOGREEN project team coring over a frozen lake in the 2019 campaign.

#### 2.2.2. Sedimentary facies characterization

High-resolution continuous pictures were taken for each sediment core at the CORELAB of the University of Barcelona to describe their sedimentary facies macroscopic features. For microscopic facies characterization smear slices were sampled every 5 cm and mounted on glass slides after dispersing the sediment with distilled water and covered using UV epoxy resin. Complementary samples of layers (such as laminated structure, or those who represented evident texture or color changes) were also taken. Smear slides were mounted and observed under 100x and 400x microscope lenses. Sedimentary facies and units were described and defined based on macrotextural and microscopic lithological features as proposed by (Schnurrenberger et al., 2003).

### 2.2.3. Chronology

A total of ten bulk sediment and seven moss samples were processed for  $^{14}\text{C}$  AMS dating at the Laboratoire de Radiochronologie at the Université Laval (Quebec, Canada). Specifically, four samples correspond to LOM18\_02 core, seven for the ZAC19\_06\_02 core and six for the AUC18\_02 core (table 2).

**Table 2.** Samples processed for  $^{14}\text{C}$  AMS dating.

Code	Depth (cm)	Sample type	Age ( $^{14}\text{C}$ yrs)
LOM1802-04	4	Bulk sediment	$870 \pm 15$
LOM1802-10	10	Bulk sediment	$1330 \pm 15$
LOM1802-16	16	Bulk sediment	$2240 \pm 15$
LOM1802-30	30	Moss	$4115 \pm 15$
ZAC1906-02	2	Bulk sediment	$650 \pm 15$
ZAC1906-12	12	Bulk sediment	$1315 \pm 15$
ZAC1906-22	22	Bulk sediment	$2505 \pm 15$
ZAC1906-32	32	Bulk sediment	$4495 \pm 20$
ZAC1906-42	42	Bulk sediment	$5685 \pm 20$
ZAC1906-52	52	Bulk sediment	$6445 \pm 20$
ZAC1906-74	74	Bulk sediment	$9690 \pm 25$
AUC1802-01	0.5	Moss	$1265 \pm 20$
AUC1802-11-12	11.5	Moss	$2425 \pm 15$
AUC1802-29-31	30	Moss	$3225 \pm 15$
AUC1802-56-57	56.5	Moss	$4390 \pm 15$
AUC1802-70-71	70.5	Moss	$4820 \pm 20$
AUC1802-78	78	Moss	$5430 \pm 20$

The age-depth models for LOM18\_02 and ZAC19\_06\_02 were defined running classical modelling techniques using the clam2.4 R package; while the AUC18\_02 core model was constructed using Bayesian methods via the bacon package in R due to a more complex nature of datations (Blaauw, 2010; R Team, 2013).

#### 2.2.4. Mineralogical analysis

Sediment samples were dried at 60°C for a duration of 48 hours and were manually pulverized utilizing an agate mill. Analysis of mineralogy was conducted through X-ray diffraction (XRD), employing a Bruker-AXS D5005 X-ray diffractometer under the specified conditions: wavelength of 1.5405, and an ultrafast PSD detector spanning the angles from 4° to 60° 2theta, at the GEO3BCN institute. The identification and quantification of mineralogical species within the crystalline fraction adhered to a standard procedure as outlined by Chung (1974). Results are expressed in percentage with respect of the crystalline fraction of the samples.

#### 2.2.5. Geochemical analysis

Geochemical data was obtained using X-ray fluorescence (XRF) with the AVAATECH XRF core scanner from the CORELAB laboratory of the University of Barcelona. The XRF measurements were performed every 2 mm at 10 kV and at 30 kV. Among the 32 chemical elements identified in both cores, only 14 elements (Si, K, V, Ca, Ti, Mn, Fe, Sr, Cl, Br, S, Rb, Sr and Zr) had average values higher than 300 cps to be considered statistically significant and included in the statistical analyses. All variables were standardized and transformed prior to statistical analysis.

Principal Component Analysis (PCA) was performed on XRF data to summarize geochemical variability of the sedimentary records. The mineralogical data of the ZAC19\_06\_02 and AUC18\_02 cores allowed us to perform a Redundancy Analysis (RDA) considering XRD data as explicative variables and XRF-derived data as responsive variables.

#### 2.2.6. Diatom analysis

*This analysis was carried only on the AUC18\_02 core by Dr. Sergi Pla-Rabés.* 40 sediment samples were collected at 2 cm intervals throughout the core for diatom analysis. Diatom samples underwent processing using a solution consisting of 33%

hydrogen peroxide ( $H_2O_2$ ) and HCl (1 M) following the methodology outlined in (Battarbee et al., 2001). A minimum of 300 valves were counted at 1,000x magnification using a LM, and the abundance of each taxon was expressed as a percentage of the total. Taxonomic identification primarily adhered to the criteria established by Krammer (1991a, 1991b, 1988, 1986), with basionyms updated to align with the current accepted nomenclature available at <https://www.algaebase.org/>.

Only diatom taxa representing >1% of the total diatom sum were used in statistical analyses, and those with >4% of the total diatom sum in at least one sample were plotted stratigraphically. Simpson's Index of diversity and PCA of the Hellinger-transformed diatom relative abundance data were used to summarize the main trends in diatom assemblages (Legendre & Gallagher, 2001; Legendre & Legendre, 2012).

#### 2.2.7. Pollen analysis

Pollen analysis was performed on sediment samples of 1 cm<sup>3</sup> each, taken every 1 cm depth. *Lycopodium clavatum* spores (n=18584) were added in each sample to calculate pollen concentration and influx (Stockmar, 1971). Samples were later processed using standard techniques involving the use of KOH, HF and acetolysis (Faegri & Iversen, 1989) at the Laboratory of Paleontology of the University of Barcelona. Slides were mounted using glycerin and sealed with candle wax. Each sample was observed under the optical microscope using 400x and 1,000x magnification. For every sample, we computed the total count of native terrestrial pollen, with a sample size of n=300 for the LOM18\_02 core. In the case of the ZAC19\_06\_02 core, the count was determined based on a single slide due to the exceptionally low concentration and limited sample quantity. The sums of aquatic, exotic and other palynomorphs were calculated separately. The pollen data was analyzed and plotted using TILIA 2.0.41 (Grimm, 2015). The identification of pollen zones was supported by a stratigraphy constrained CONISS analysis.

The fossil pollen dataset is based on the relative abundance data of both Lomsø and ZAC records. From the initial 41 pollen types across 82 samples, taxa with relative

abundance of under 2% and taxa that were not present on both records were deleted to avoid noise caused by rare or irrelevant species. This resulted in 21 pollen types for the analysis (appendix 2). Pollen types were treated as “samples” to group them based on the relative abundance trends across samples. A *ward.2* method Cluster analysis was created based on the Bray-Curtis dissimilarity index between pollen types, using the *vegan* package in R (Oksanen et al., 2019).

For the ordination purposes, pollen data was standardized using the square root transformation. Detrended correspondence analysis (DCA) was performed to plot the distribution of our pollen data. Based on an axis length smaller than 2 SD resulting of the DCA, PCA was performed using the *vegan* package in R.

#### 2.2.8. Alpha and beta diversity

Alpha ( $\alpha$ ) and Beta ( $\beta$ ) diversity were calculated for the available pollen and diatom records. Two distinct spreadsheets were generated for both the Lomsø and ZAC pollen record to analyze them separately. Pollen taxa with relative abundance over >2% and present in more than one sample were included in the datasets, resulting in 17 “observations” (pollen types) and 21 “sites” (samples) for the Lomsø dataset and 24 “observations” and 21 “sites” for the ZAC dataset.

$\alpha$ , a measure of species richness within a specific community, was quantified as the number of pollen types identified in each sediment core sample (Gosling et al., 2018). To delve into the compositional changes of the vegetation communities, DCA was performed on the square root-transformed pollen abundance data using the *vegan* package in R (Correa-Metrio et al., 2014; Oksanen et al., 2019). In this context DCA is known to summarize the underlying trends that better explain the variance of our data and the results are easy to interpret thanks to their units being in standard deviation (SD) so the scores of the first DCA axis (DCA1) were plotted against samples to see ecological turnover or  $\beta$  trends through time. Euclidean distances between ordination scores in the DCA1 axis for each sample were calculated. These distances served as a measure of dissimilarity in community composition among samples, so they were

interpreted as a proxy for "ecological change" a concept closely linked to beta diversity (Correa-Metrio et al., 2014). Rates of ecological change were calculated dividing the Euclidean distances by the years contained in each sample (Urrego et al., 2009). Euclidian distance of each sample towards the top samples were calculated to determine the dissimilarity between present-day pollen assemblages and past ones (Correa-Metrio et al., 2014).

### 2.3. Quantitative climate reconstruction

#### 2.3.1. Pollen-climate calibration set

The modern pollen-climate calibration set is based on modern pollen rain data sourced from the North American Pollen Database (<https://www.ngdc.noaa.gov/paleo/napd.html>), where sites located north of 66°N were selected (fig. 19).

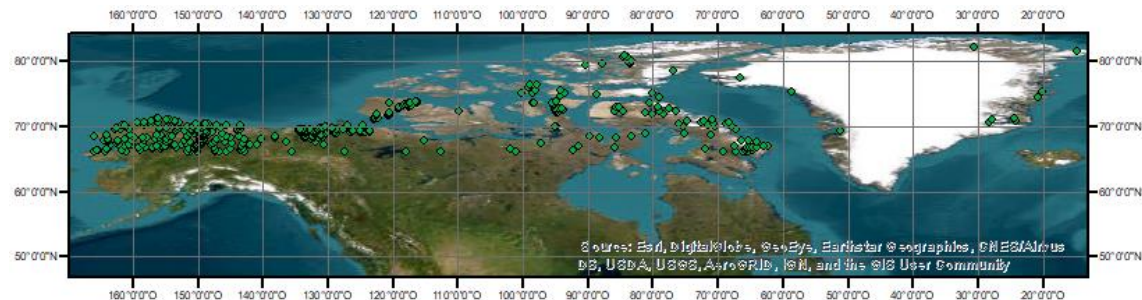


**Figure 19.** Distribution of sites included in the pollen-climate calibration set.

The initial matrix was made of 590 sites and 134 pollen types. Outlier sites and pollen types with concentrations lower than 2% were deleted, resulting in a definitive calibration set made of 577 sites, 51 pollen taxa and ten climatic variables obtained from the bioclimatic variable package of Worldclim (<https://worldclim.org/data/index.html>) (Fick & Hijmans, 2017) (table 3).

**Table 3.** Worldclim based climatic variables used in this study.

Climatic variable	Abbreviation (this study)
Mean annual temperature	<i>Ta</i>
Max temperature of the warmest month	<i>Tmax</i>
Min temperature of the coldest month	<i>Tmin</i>
Mean temperature of the warmest quarter	<i>Ths</i>
Mean temperature of the coldest quarter	<i>Tcs</i>
Annual precipitation	<i>Pa</i>
Precipitation of the wettest month	<i>Pmax</i>
Precipitation of the driest month	<i>Pmin</i>
Precipitation of the wettest quarter	<i>Pws</i>
Precipitation of the driest quarter	<i>Pds</i>

RDA with variance analysis (ANOVA) test was performed to track the links between the biological and climatic matrices, and therefore to determine if a given climatic variable that explains the most part of variance in the pollen matrix is directly related to the distribution of pollen types in the dataset,(Juggins, 2013)The explanatory power of the selected variable was determined by the relationship between the first constrained axis of the RDA and the first unconstrained axis ( $\lambda_1/\lambda_2$ ). A  $\lambda_1/\lambda_2$  value higher than 1.0 indicates that the variable represents a significant ecological gradient within the calibration dataset (ter Braak & Juggins, 1993). Based on this, the climatic variable chosen for quantitative reconstruction will be selected (Juggins, 2013; ter Braak & Juggins, 1993).

### 2.3.2. Transfer function

Transfer functions between pollen and the most statistically significative climatic variable were developed using the WA-PLS regression for the calibration set using the rioja package in R (Juggins, 2018; R Team, 2013; ter Braak & Juggins, 1993). To evaluate the predictive power of the model, the fit between observed and predicted values was evaluated with a cross-validation bootstrapping (or leave-one-out) test (ter Braak & Juggins, 1993). The WA-PLS function used for the reconstruction was selected

based on root mean square error (RMSE), higher fit of observed versus predicted values ( $r^2$ ), bias and number of components (ter Braak & Juggins, 1993).

### **3. Results**

#### **3.1. Pollen morphology of Zackenberg key plants**

From the originally 25 selected species, only the ones with enough material to be measured and photographed both in LM and SEM were taxonomically described, resulting in a group of 11 taxa (table 4).

The pollen morphology of the 11 studied plants exhibited remarkable diversity in terms of shape, aperture patterns, and exine ornamentation. Three distinct pollen shapes were identified based on the Polar/Equatorial (P/E) ratio: spheroidal, subprolate, and prolate. Additionally, a tetrad shape was defined by the presence of four united grains. Aperture types observed included monoporate, polypanthoporate, trizonocolpate, and trizonocolporate. The ornamentations observed on the pollen grains included scabrate, scabrate-perforate, striate, microechinate, psilate, and reticulate. Full description of each pollen type available at appendix 3.

**Table 4.** Summary of pollen types and their main measures in equatorial view.

Species	Polar Axis	Equatorial axis				Exine	
	length (μm)	length (μm)	P/E	Shape	Apertures	thickness	Ornamentation
<i>Draba arctica</i>	27.46 ± 2.35	25.31 ± 2.48	1.08	Spheroidal	Trizonocolporate	2.52 ± 0.41	Reticulate
<i>Cerastium arcticum</i>	43.47 ± 7.06	39.13 ± 6.78	1.11	Spheroidal	Polipantoporate	2.53 ± 1.08	Microechinate
<i>Cassiope tetragona</i>	26.93 ± 1.81	25.12 ± 1.73	1.07	Tetrad	Trizonocolporate	1.24 ± 0.20	Psilate
<i>Rhododendron lapponicum</i>	41.10 ± 5.36	38.78 ± 5.88	1.06	Tetrad	Trizonocolporate	1.85 ± 0.35	Psilate
<i>Vaccinium uliginosum</i>	32.11 ± 2.71	31.59 ± 3.44	1.02	Tetrad	Trizonocolporate	1.52 ± 0.12	Psilate
<i>Poa glauca</i>	30.39 ± 1.95	30.91 ± 2.01	0.98	Spheroidal	Monoporate	1.54 ± 0.17	Psilate
<i>Oxyria digina</i>	21.65 ± 1.31	22.62 ± 1.63	0.96	Spheroidal	Trizonocolporate	0.81 ± 0.11	Scabrate
<i>Dryas octopetala</i>	21.75 ± 1.82	19.41 ± 1.57	1.12	Subprolate	Trizonocolporate	1.59 ± 0.26	Striate
<i>Potentilla rubricaulis</i>	23.99 ± 2.04	22.57 ± 1.70	1.06	Spheroidal	Trizonocolporate	1.40 ± 0.17	Striate
<i>Salix arctica</i>	25.64 ± 2.00	21.67 ± 0.97	1.18	Subprolate	Trizonocolporate	1.58 ± 0.17	Reticulate
<i>Saxifraga cernua</i>	29.42 ± 2.86	25.35 ± 2.50	1.16	Subprolate	Trizonocolporate	1.42 ± 0.09	Scabrate

### 3.1. The ZAC Lake record

#### 3.1.1. Sedimentary facies and units

The ZAC19\_06\_02 core was divided into four sedimentary units that coincide with the same number and boundaries of sedimentary facies defined according to the biological, organic, and mineral content, and other lithological characteristics of the sediments (fig. 20):

Unit Z-A (77.5 – 71.5 cm): characterized by light-gray silt, rich in mineral content. Biological remains are scarce, with planktonic diatoms being the predominant type. Amorphous matter constitutes the main organic component of this unit. This unit has been interpreted as rock flour glacial deposits.

Unit Z-B (71.5 – 39 cm): consists of millimeter-thick layered silt with coloration varying from dark brown to brown. The thickness of the layers decreases upward ranging from 1.5 cm to less than 5 mm. Planktonic diatoms are abundant, and amorphous organic matter is the predominant type. There are few and mostly euhedral in shape mineral crystals. The facies of this unit are interpreted as deposited in a hemipelagic lake with seasonal ice cover.

Unit Z-C (39 – 2 cm): characterized by laminated silt, alternating very dark brown, organic-rich bands (0.5 – 0.8 cm) and brown bands (1 – 2.5 cm). Diatom abundance is high, with benthonic forms (e.g., *Eutonies* sp.) and cyst associated with acidic, high-energy environments dominating the light layers. Dark layers are characterized by a higher content of planktonic diatoms. Abundant particulate organic matter suggests a productive basin with oligotrophic conditions. Plant remains are few, and mineral fragments are scarce, mostly primary with varying degrees of rounding. These features indicate that sediments were deposited in lacustrine conditions, in a lake with seasonal ice cover and enhanced seasonality conditions, with changes in the duration of ice cover.

Unit Z-D (2 – 0 cm): consists of unconsolidated very soft and high water content reddish silt. Diatom remains are mainly planktonic, including *Cyclotellas* sp. Particulate organic matter and abundant amorphous organic matter are present. Mineral content is very low. Facies of this unit is interpreted as deposited in a well oxygenated lake with oligotrophic regime and seasonal ice cover.

Unit	Texture	Organic remains	Biological remains	Mineral content	Paleoenvironmental reconstruction
Unit Z-D	Laminated silt with organic rich layers	Abundant amorphous organic matter	Few vegetal remains. Diatoms abundant, mostly planktonic	Very low mineral content	<i>Oligotrophic, well-oxygenated lake</i>
Unit Z-C	Laminated grey silt	Abundant organic matter, most of it amorphous	High diatom abundance, benthonic dominating the light layers while the dark layers have higher planktonic components. Few plant remains.	Scarce mineral remains with varied levels of roundness.	<i>Lake with seasonal ice cover and enhanced seasonality</i>
Unit Z-B	Massive silt with less defined laminated pattern	High amorphous organic matter content	Few plant remains. High diatom content, going from planktonic dominated to a mixture with benthonic. Chironomid remains.	Few mineral remains, most of them euhedral shaped	<i>Lake with seasonal ice cover</i>
Unit Z-A	Massive light grey clay	Scarce amorphous organic matter	Very few biological remains Diatoms mostly planktonic	Very high mineral content	<i>Glacier flour deposits</i>

Depth (cm)

**Figure 20.** Sedimentary facies and units' description and paleoenvironmental interpretation of core ZAC19\_06\_02.

### 3.1.2. Age-depth model

The age-depth model for ZAC19\_06\_02 has been constructed using seven AMS  $^{14}\text{C}$  dates. According to this model, the bottom of the core would be dated at around 12,200 cal yrs BP, determining an average sedimentation rate of  $154 \text{ yrs cm}^{-1}$ . There seems to be three well differentiated states linked to sedimentation rates. There is an increasing sedimentation rates until 6,000 cal yrs BP, where sediment input seems to decrease until a new accelerated accumulation starts around 2,000 cal yrs BP (fig. 21).

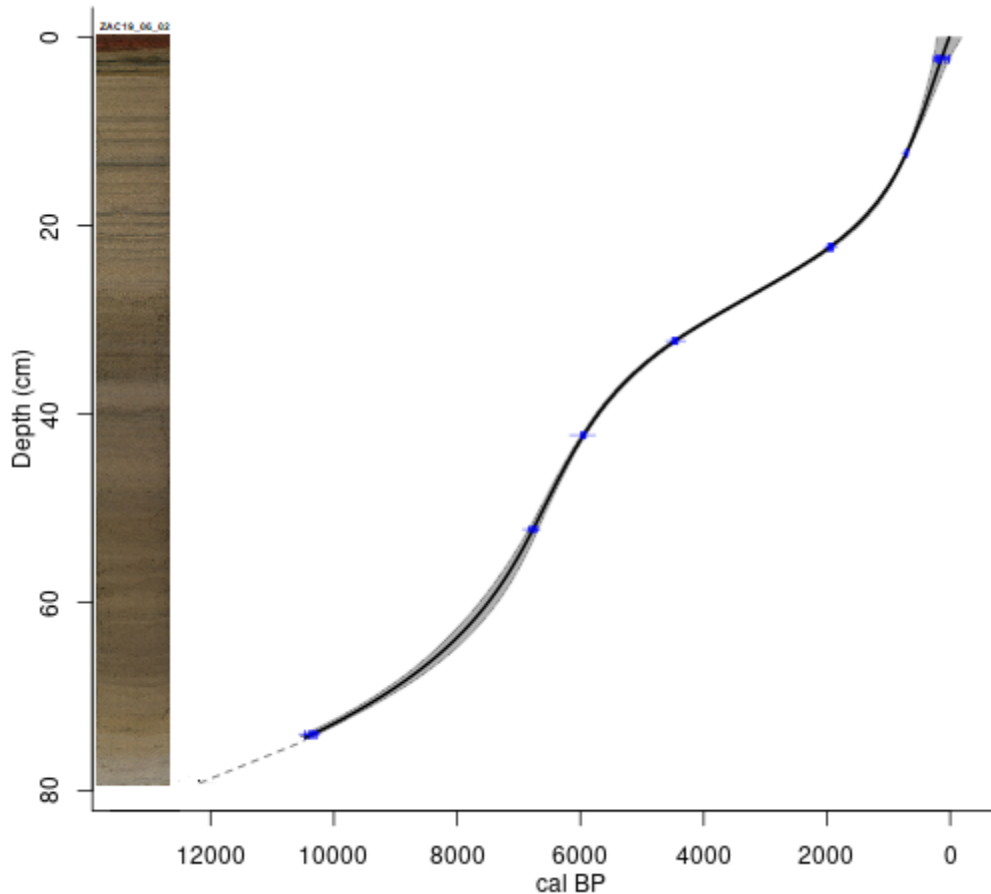


**Figure 21.** Age-depth model for the ZAC19\_06\_02 core. Unit A ages are represented as a dotted line since the ages are considered uncertain due to lack of dating samples at the bottom of the core, so the model assume lineal trajectory.

### 3.1.3. Mineralogical data

*Mineral content results are product of Ada Rodriguez's final Geology grade project.*

The XRD results revealed six mineral phases: chlorite, illite, riebeckite, quartz, plagioclase, and pyrite. These minerals are consistent with the lithology of the Precambrian gneissic bedrock on which the lake and its catchment are located. Overall, plagioclase and pyrite concentrations remain relatively constant throughout the core. Stratigraphically constrained cluster analysis of the mineralogical data identified four distinct zones within the core (fig. 22):

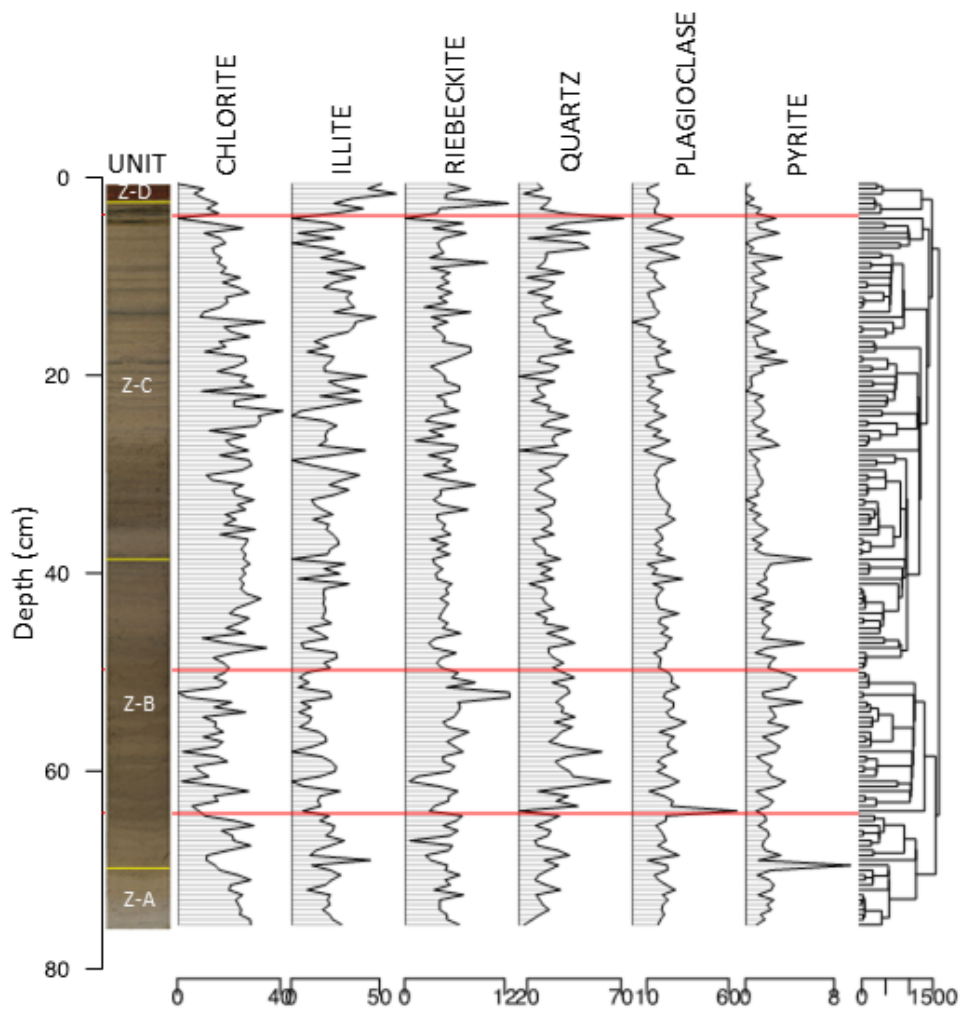


**Figure 22.** Stratigraphical mineral content plot of core ZAC19\_06\_02. Red lines mark the boundaries between clusters. Source: Ada Rodriguez final grade Project.

Zone 1 (77.5 – 64 cm): characterized by a high proportion of chlorite compared to riebeckite. It also exhibits the highest pyrite content of the entire core.

Zone 2 (64 – 50 cm): this zone exhibits a decrease in chlorite and illite contents while riebeckite and quartz percentages increase.

Zone 3 (50 – 5 cm): this zone shows an increase in chlorite and illite values while riebeckite, quartz, and plagioclase content diminishes.

Zone 4 (5 – 0 cm): this zone shows a decrease in chlorite, quartz, and plagioclase contents while illite and riebeckite percentage rise.

### 3.1.4. Geochemical data

*Geochemical content results are product of Ada Rodriguez's final Geology grade project.*

XRF-derived data shows varying concentration of chemical elements and was divided into four main zones based on a stratigraphic constrained cluster dissimilarity analysis (fig. 23).

Zone 1 (77.5 – 60 cm): all chemical elements show high initial values with a constant decreasing trend and a subsequent abrupt decline in most elements except Cl, Rb, Sr and Zr followed by an increase in all chemical elements

Zone 2 (60 – 47 cm): The lowest values of Al, Si, K, Ca, and Ti define this zone.

Zone 3 (47 – 2 cm): overall this zone displays oscillating values for all elements, with the upper part being defined by a sharp decrease in Al, Si, K, Ca, and Ti.

Zone 4 (2 – 0 cm): defined by a sharp increase in Mn and Fe accompanied by an abrupt Rb, Sr and Zr decrease.

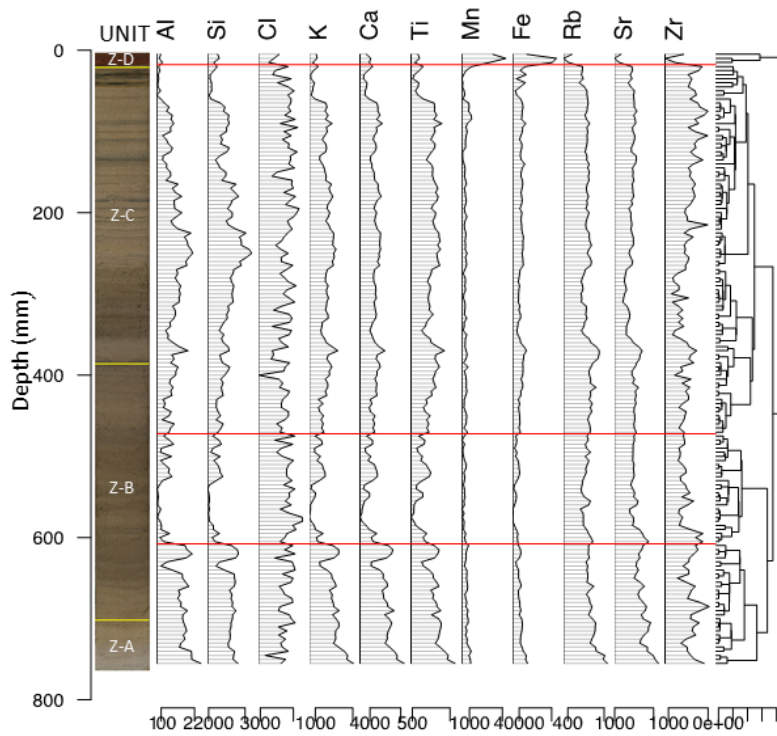


**Figure 23.** Stratigraphical plot of the geochemical content of core ZAC19\_06\_02. Red lines represent the boundaries between clusters. Source: Ada Rodriguez final grade project.

### 3.1.5. Sedimentological multivariate analysis

*Multivariate analysis results based on mineralogical and geochemical content are product of Ada Rodriguez's final Geology grade project.*

The relationships between mineralogical and geochemical data have been analyzed by a combination of RDA and PCA. While PCA was specifically used for XRF data, RDA was applied to both XRF and XRD data (table 5).

**Table 5.** Statistical values for the first five constrained components of the ZAC19\_06\_02 XRD and XRF based RDA.

	RDA1	RDA2	RDA3	RDA4	RDA5
Eigenvalues	1.0260	0.4790	0.0795	0.0324	0.0061
Proportion explained	0.6320	0.2949	0.0489	0.0199	0.0037
Cumulative	0.6320	0.9269	0.9758	0.9958	0.9995

The first RDA axis, accounting for 63% of the total data variance, revealed a strong association between chlorite and elements such as Ca, Si, K, Ti, and Al on the positive end of the axis. Conversely, riebeckite and Zr were negatively correlated with this axis. The second RDA axis, representing almost 30% of the variance, showed a positive association between illite and Mn and Fe, while quartz, plagioclase, pyrite, Cl, Sr and Rb were negatively correlated with this axis (fig. 24).

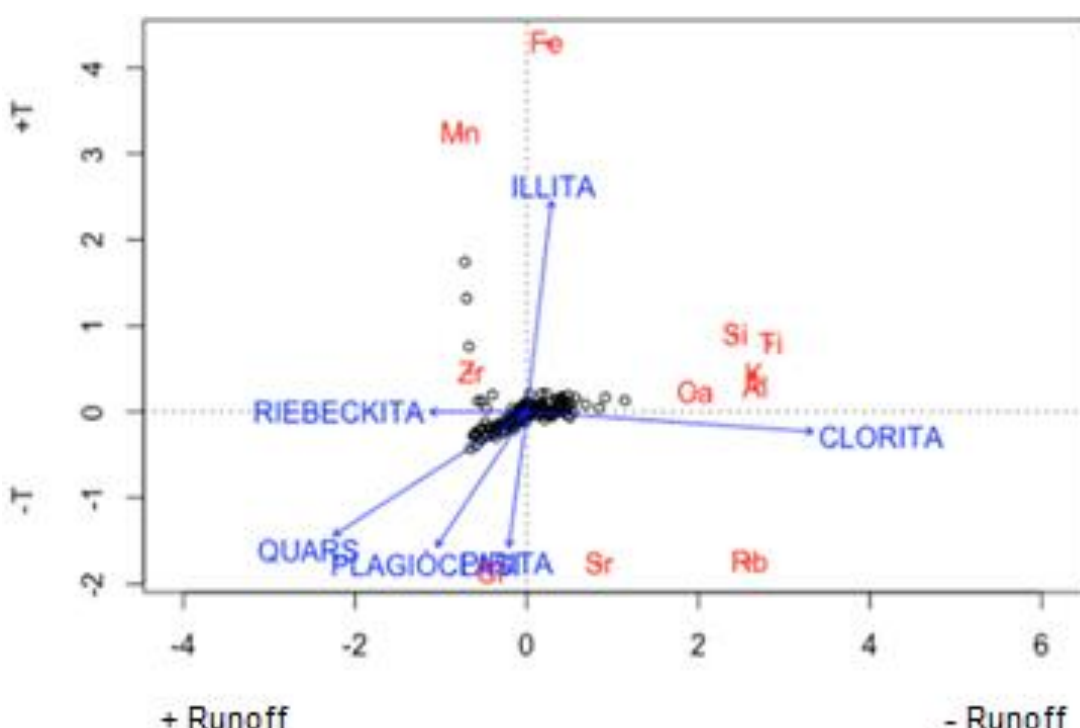


**Figure 24.** RDA plot based on the ZAC19\_06\_02 mineralogical and geochemical content. Black circles represent samples. Source: Ada Rodriguez final grade project.

PCA was performed over chemical elements data to summarize the main forces defining the development of the lake and interpret its changes over time (table 6). Broken stick test indicates the first two components are significant to explain the largest percentage of the data variance (fig. 25)

**Table 6.** Statistical values for the first five axis of the ZAC19\_06\_02 XRF based PCA.

	PC1	PC2	PC3	PC4	PC5
Eigenvalues	2,6153	1,2919	1,2017	1,0636	0,9478

Proportion explained	0,4886	0,1192	0,1032	0,0808	0,0642
Cumulative	0,4886	0,6078	0,7109	0,7917	0,8559

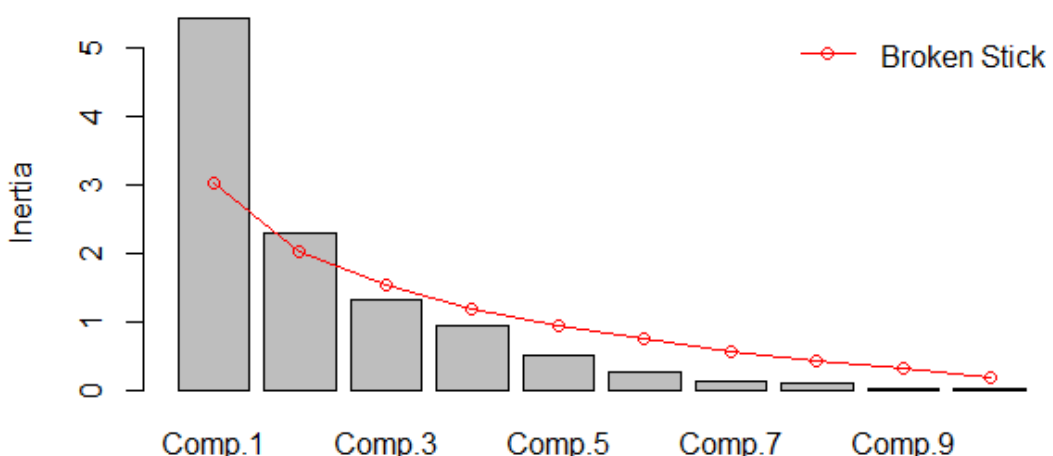


**Figure 25.** Broken stick test plot for the ZAC19\_06\_02 XRF based PCA.

The first PCA component (PC1) explains almost 49% of the variance and is related to clastic origin elements as Al, Sr, Si, Zr, K, Ca and Ti in the positive values and Cl, probably neoformed by diagenetic processes in the negative values. Based on this we interpret the PCA1 as a runoff signal, with exogenous elements on the positive end of the axis while allochthonous Cl was placed on the negative region. The second PCA component (PC2) explains 11.92% of the variance and is defined by S and Cl related to positive values and Fe and Mn related to negative ones. S and Cl are often associated with organic matter degradation and microbial activity in lake sediments. Higher concentrations of these elements could indicate warm conditions, allowing increased biological productivity and organic matter decomposition in the lake. Rising temperature may also promote the release of sulfur and chlorine from thawing permafrost, contributing to higher concentrations in the lake. Fe and Mn are commonly linked to redox processes in aquatic environments. Colder temperatures and prolonged ice and snow cover can lead to stratification of the water column, limiting oxygen exchange between the surface and bottom waters, allowing anoxic conditions at the lake bottom, favoring the preservation of reduced forms of Mn and Fe in the sediment (fig. 26).

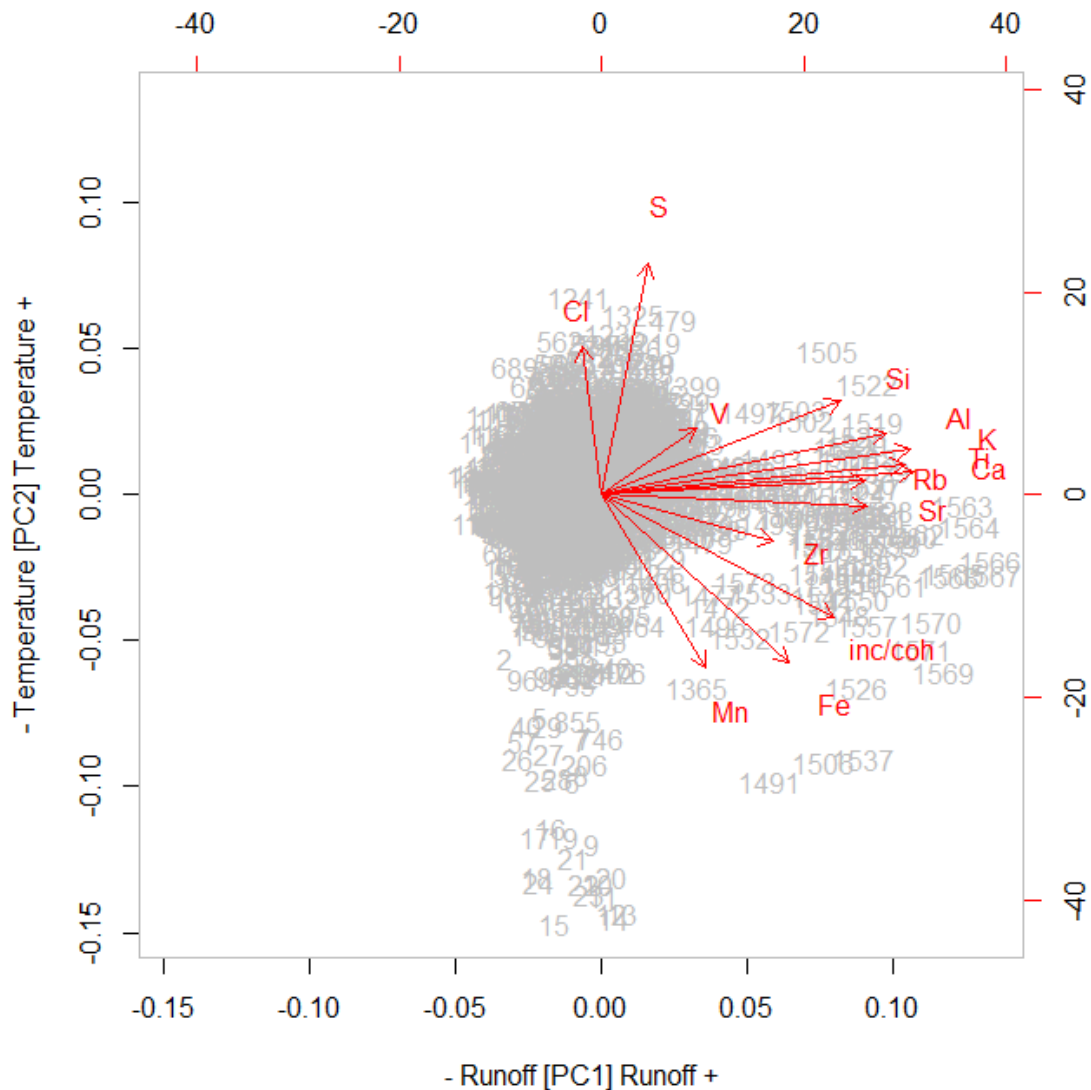


**Figure 26.** PCA plot based on the ZAC19\_06\_02 geochemical record. Grey numbers represent samples. Source: Ada Rodriguez final grade project.

Considering the relationship between both PCA axes, scores of each sample were plotted against depth to characterize changes in runoff and temperature in the ZAC lake stratigraphy. (fig. 27).

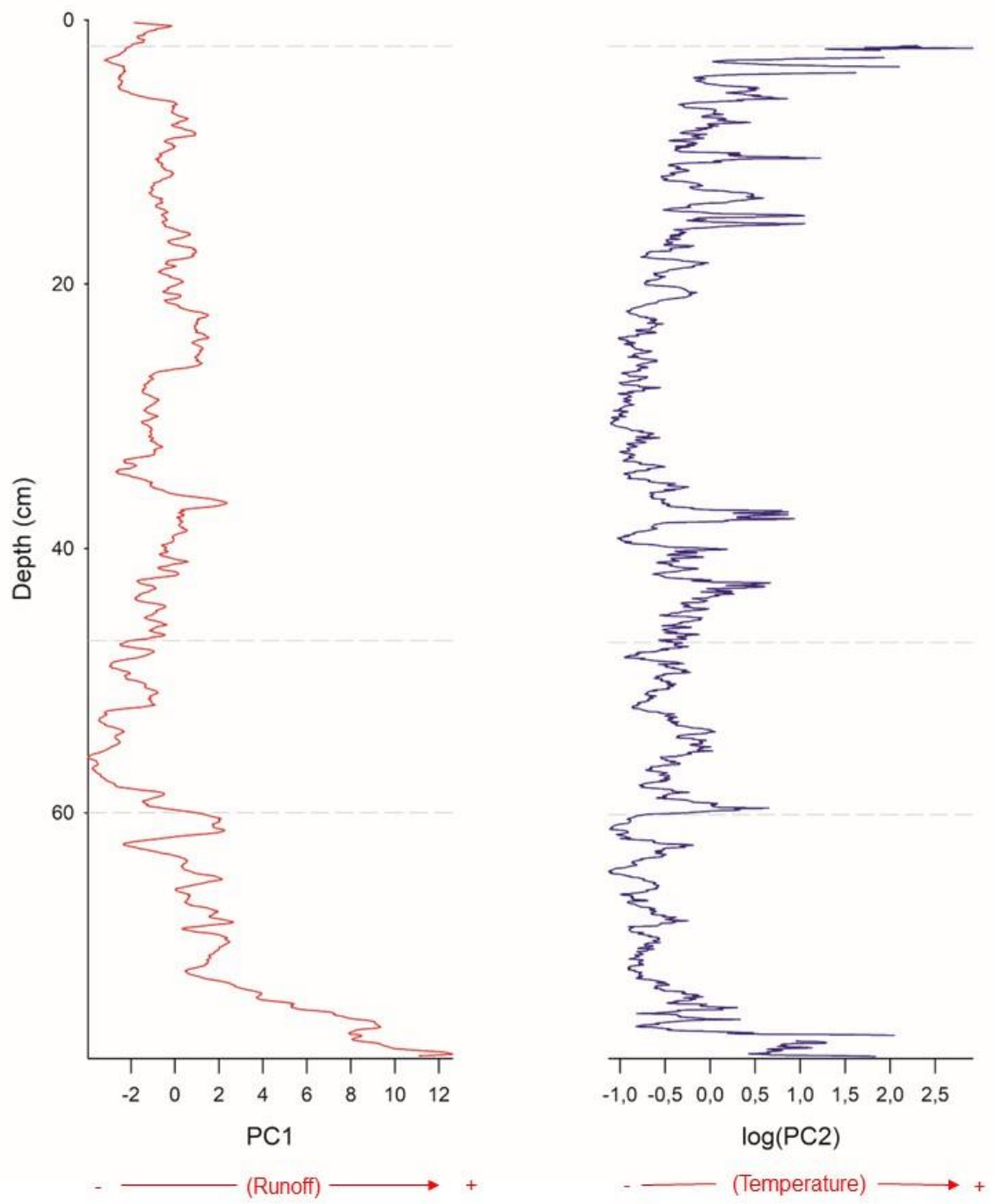


**Figure 27.** Stratigraphical PC1 and PC2 scores plot based on the ZAC19\_06\_02 XRF data. Dashed lines represent the boundaries between XRF zones.

PC1 scores show initial high runoff conditions indicating higher precipitation at the beginning of the record decreasing reaching less runoff between 60 – 47 cm, followed by slightly increasing runoff between 47 – 2 cm, interrupted ca. 37 cm and less precipitation on the top of the core. PC2 on the other hand shows initial high

temperature conditions that decreased abruptly ca. 70 cm of core depth, followed by subtle oscillations and a conspicuous increase towards the top of the core.

### 3.1.6. Pollen stratigraphy

The ZAC pollen diagram is restricted to units B, C and D owing to unit A is barren as already stated (fig. 28).

The record shows three pollen zones:

- Zone ZAC-I (69.5 – 58.5 cm): dominated by Poaceae (>20%), Cyperaceae summing up to 40% at the beginning of the record and *Oxyria/Rumex* reaching over 50% around 67 and 60 cm. The herbaceous component is dominant by far, with traces of woody elements increasing at the end of the zone. Pollen influx remained relatively low during this period.
- Zone ZAC-II (58.5 – 30.5 cm): Dominated by *Betula* reaching up to 70% of the pollen sum around 50 cm, with *Salix* (0 – 50%) and *Luzula/Juncus* (0 – 60%) as the most important taxa. The composition was oscillating between woody and herb dominated, with woody peaks at 48, 37 and 31 cm of the core depth. Pollen influx was on an increasing trend reaching its peak around 44 cm, leading to a subsequent decreasing trend.
- Zone ZAC-III (30.5 – 0 cm): Dominated by *Luzula/Juncus* (40 – 93%) with *Salix* (15%) and Cyperaceae (11%) as the most important taxa. The herbaceous component is dominant, with an increasing woody plant percentage throughout the zone, reaching up to 30% of terrestrial pollen around 7 cm, also marking peak woody influx on the record. Bryophyte *Hippuris* makes its only appearance in this zone while exotic taxa are barely present. Influx goes from record-lows at the beginning of the zone to record-peaks around 6 cm.

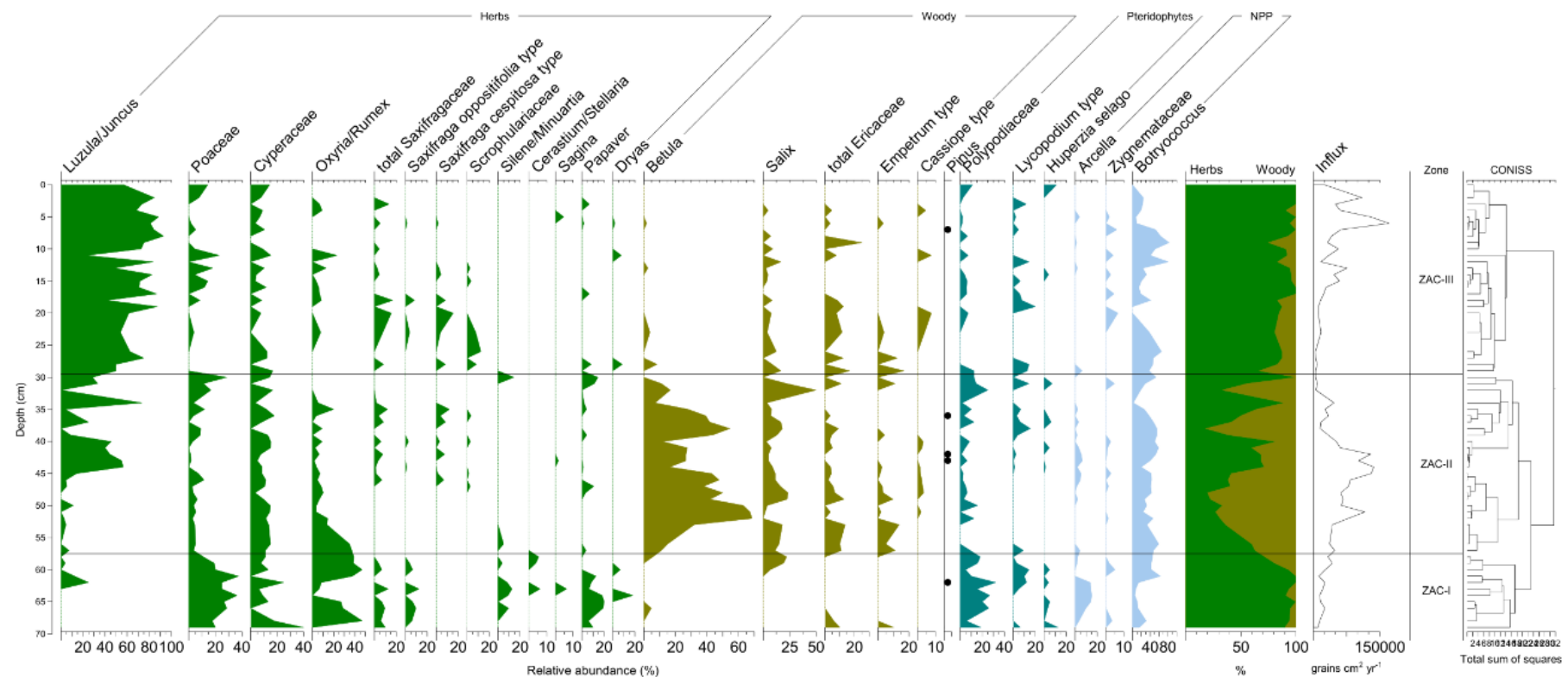


**Figure 28.** Pollen stratigraphy of the ZAC19\_06\_02 record.

### 3.1.7. ZAC pollen-based diversity index

The DCA analysis applied to the ZAC pollen record unveiled a substantial degree of variability within the pollen data, as evidenced by the maximum axis length of DCA1 reaching nearly 2.5 SD. This suggests significant community shifts throughout the record period, indicating dynamic environmental conditions in the surroundings of the lake, with species turnover exceeding 50% since the beginning of the record (table 7).

**Table 7.** Statistical values for the ZAC19\_06\_02 pollen based DCA analysis.

	DCA1	DCA2	DCA3	DCA4
Eigenvalues	0.325	0.193	0.165	0.142
Axis lengths	2.498	1.927	2.076	2.096

Taxa indicative of wet Arctic conditions, such as *Cerastium/Stellaria*, Saxifragaceae, and Ranunculaceae, were positioned towards the positive end of DCA1. Conversely, pollen taxa characteristic of dry conditions, such as *Sagina* and *Dryas*, exhibited negative DCA1 scores. Notably, all woody taxa were associated with negative DCA2. Abundant taxa in the record are clustered towards the center of the plot while rare species are positioned towards the extremes. At a broader scale, the first quadrant encompasses spores in the center and Arctic elements at the extremes; the second quadrant represents fell-field vegetation; the third quadrant groups heath elements; and the fourth quadrant is dominated by pioneer high- and low-Arctic taxa (fig. 29).

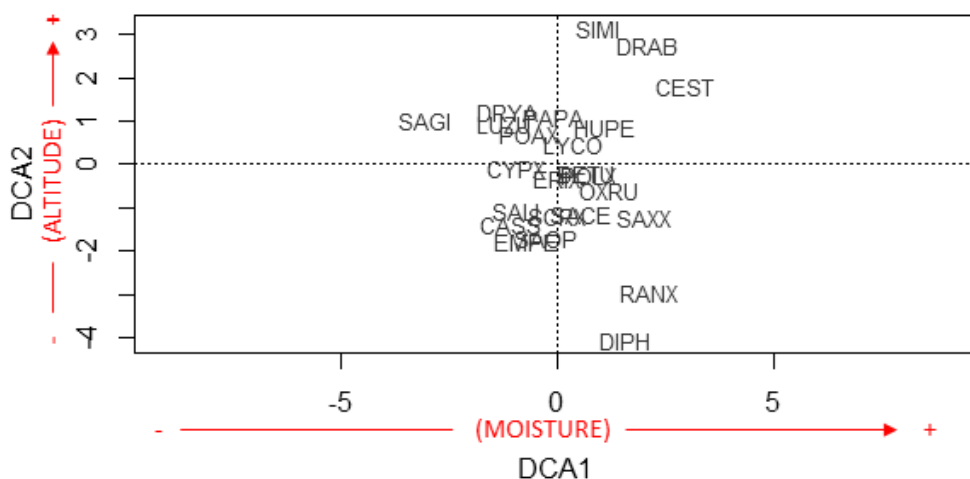


**Figure 29.** DCA plot based on the ZAC19\_06\_02 pollen record.

DCA of ZAC pollen taxa suggests that DCA1 represents a soil moisture gradient, with positive DCA1 scores indicative of greater moisture availability and negative scores reflecting drier conditions. DCA2, on the other hand, appears to be related to altitude, as evidenced by the clustering of low-Arctic, woody, and even aquatic taxa in the negative region of the axis, while open vegetation adapted to harsher climatic conditions occupies the positive values (fig. 29). This pattern suggests that axis 2 reflects an altitudinal gradient with higher scores indicating more open vegetation associated with harsher climatic conditions, while lower scores represent lowland vegetation characterized by higher diversity and more stable environmental conditions.

The ZAC DCA1 curve shows an evident change in soil moisture before and after 53 cm. At the beginning of the record, high soil moisture conditions remained somewhat stable. Following the record-peak moisture conditions of 59 cm, there was a subsequent decreasing trend, and the following 53 cm re-peak, moisture availability declined, showing negative values from that point onward. Oscillating moisture conditions oscillated for the remainder of the record, reaching the lowest values around 27 and 5 cm, with intensified variability on the core's top (fig. 30). The ZAC DCA2 curve describes an initial decreasing altitude peaking ca. 66 cm depth is reversed reaching an altitude peak ca. 53 cm then oscillating around 0 with a subtle increasing trend throughout the record.

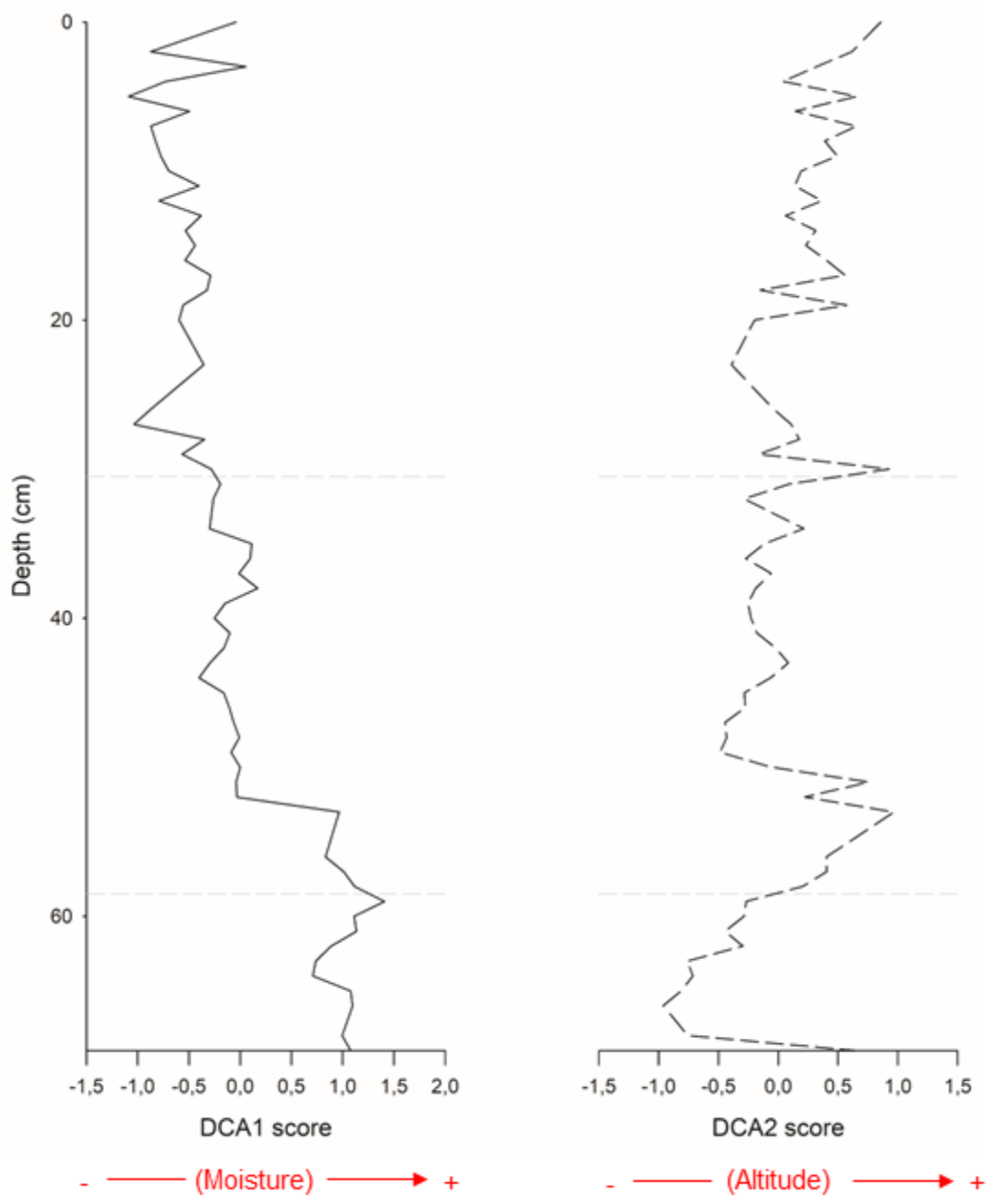


**Figure 30.** Stratigraphical DCA1 and DCA2 scores plot based on the ZAC19\_06\_02 pollen data. Dashed lines represent the boundaries between pollen zones.

The ZAC  $\alpha$  diversity record shows oscillations in number of species found in each sample (fig. 31, dotted line). The maximum number of species (13) is observed at 45 and 36 cm depth, while the lowest diversity (2 identified species) is noted around 9 cm.  $\beta$  shows that despite minor oscillations, the environment remained relatively stable. The

first peak in ecological change peak occurred at 52 cm of core depth, with other notable ecological changes observed at 27, 23, 5 and the top 3 cm of the core (fig. 31).

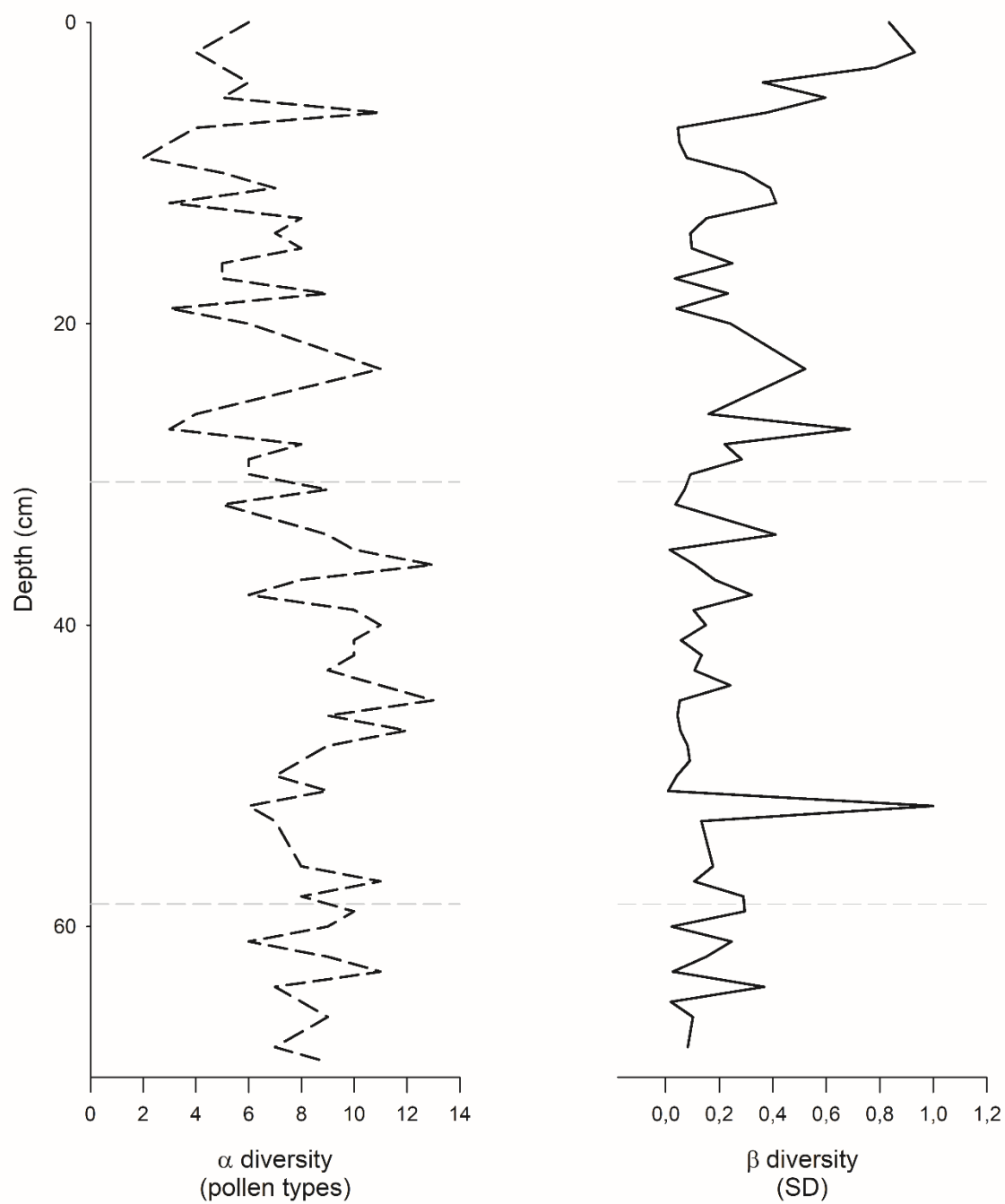


**Figure 31.** Stratigraphical  $\alpha$  and  $\beta$  diversity plot based on the ZAC19\_06\_02 pollen record. Gray dashed lines represent the boundaries between pollen zones.

## 3.2. The Lomsø Lake record

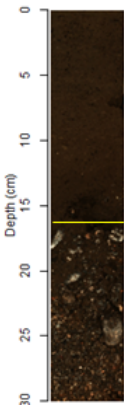
### 3.2.1. Sedimentary facies and units

Based on macro-and microscopical facies observations, sediment core LOM18\_02 was divided in two sedimentary units coincident with the same number of facies (fig. 32).

Unit A (31 – 17 cm): is mainly composed of a massive, unsorted gravel (pebble clast size) and sandy matrix. It exhibits very high mineral content and low organic remains. Sedimentary characteristics of this unit correspond to fluvial channel infill deposits almost devoid of pollen content.

Unit B (17 – 0 cm): consist of massive silt, with significant presence of amorphous material corresponding to organic matter generated by biological processes in the lake. The content of vegetal remains is high. There is a low skeletal diatom presence, with the majority consisting of planktonic and fragmented forms. The particulate mineral content is low. Sedimentary facies of this unit correspond to shallow lacustrine deposits, with the formation of a seasonal ice cover.

Unit	Texture	Organic remains	Biological remains	Mineral content	Paleoenvironmental reconstruction
Unit L-B	Massive silt rich in organic matter	Abundant amorphous organic matter	Diatoms scarce, mainly planktonic and fragmented. Abundant plant and <i>Botryococcus</i> remains	High primary mineral remains, mostly euhedral.	Shallow lake
Unit L-A	Massive sand to gravel with pebble presence.	Very scarce organic matter, which is amorphous	Very low biological content	Very high mineral content, mostly primary with different levels of roundness	Fluvio-deltaic deposits



Depth (cm)

**Figure 32.** Facies and sedimentary units' description and paleoenvironmental interpretation of core LOM18\_02 sediments.

### 3.2.2. Age-depth model

The age-depth model is based in four radiocarbon dated samples. The bottom of the core is dated at around 4,200 cal yrs BP, and the cores sequence shows an average sedimentation rate of 139 years/cm. The beginning of fine gran-size lacustrine sedimentation (Unit B) is abrupt and dates to 1,900 cal yrs BP and shows a continuous record towards the top, with increased sedimentation rate between 500 and 0 cal yrs BP. There are no signs of erosion episodes (hiatuses) or reworked sedimentary processes (fig. 33).

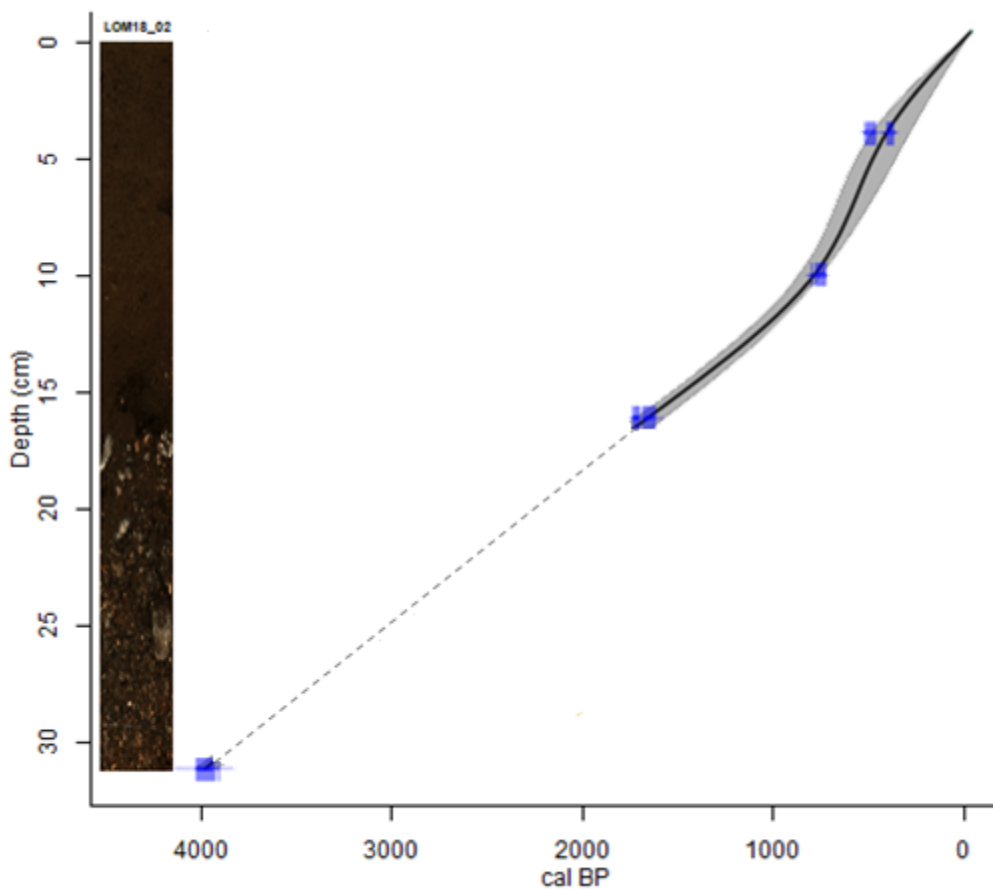


**Figure 33.** Age-depth model for core LOM18\_02. Unit A ages depicted as a dashed line since it is uncertain if this unit had a constant sedimentation rate as suggested by the model or if it was a deposit transported by a mass process.

### 3.2.3. Geochemical data

LOM18\_02 core XRF-derived geochemical content was plotted stratigraphically, and the cluster analysis shows three zones with distinct chemical composition (fig. 34).

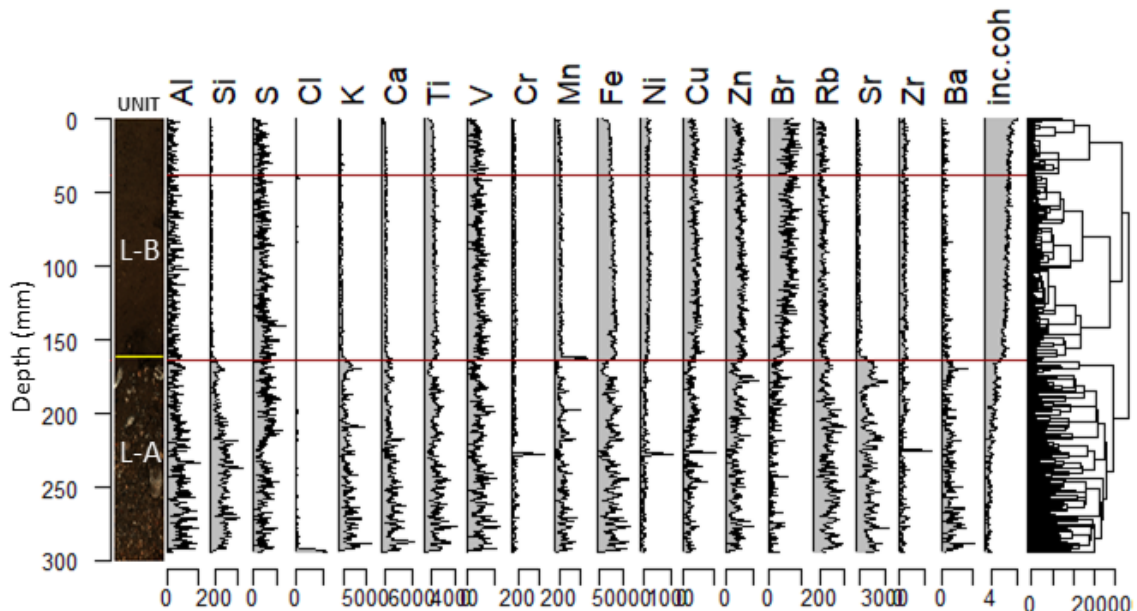


**Figure 34.** XRF-based geochemical content of the LOM18\_02 sediment core. Red lines stand for the boundaries between clusters.

Zone 1 (31.5 – 16.5 cm): corresponds with stratigraphical unit L-A. It is characterized by higher cps of chemical elements such as Al, Si and S, the first two chemical elements show a decreasing trend towards the top while the later rises towards the end of the zone. K, Ca, Rb and Sr show their highest values in this unit.

Zone 2 (16.5 – 4 cm): it is defined by sharp decreases in Si, K, and Sr, while elements such as Mn, Fe, Rb and S show a slight decreasing trend. The inc/coh ratio displays an evident increasing one.

Zone 3 (4 – 0 cm): similar in content to Zone 2, although a decreasing trend in S values and both Br an inc/coh ratio showing their highest content in this zone is seen.

PCA was performed over the Lomsø record XRF data (table 8). Broken stick test indicates the first two PCA axis are significant to explain the variance of our dataset (fig. 35).

**Table 8.** Statistical values for the first five axis of the LOM18\_02 XRF based PCA.

	PC1	PC2	PC3	PC4	PC5
Eigenvalues	2.7536	1.8094	1.1295	1.0555	0.9979
Proportion explained	0.3791	0.1637	0.0638	0.0557	0.0498
Cumulative	0.3791	0.5428	0.6066	0.6623	0.7121

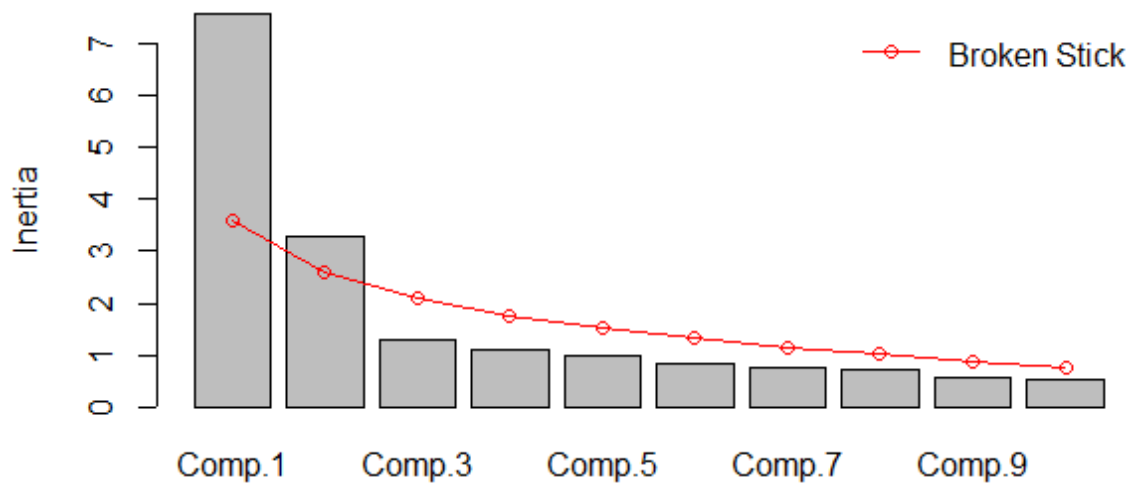


**Figure 35.** Broken stick test plot for the LOM18\_02 XRF-based PCA.

The first PCA component (PC1) explains almost 38% of the total variance and is related to inc/coh, Br, Ni, and Zr in the positive end of the axis and Si, Sr, K, Ba, Rb, Al in the negative one. The second PCA component (PC2) explains 16.36% of the variance and is defined by Cl related to the positive end of this component while Fe, Ti and Mn are present in the negative end of the PC2 (fig. 36).

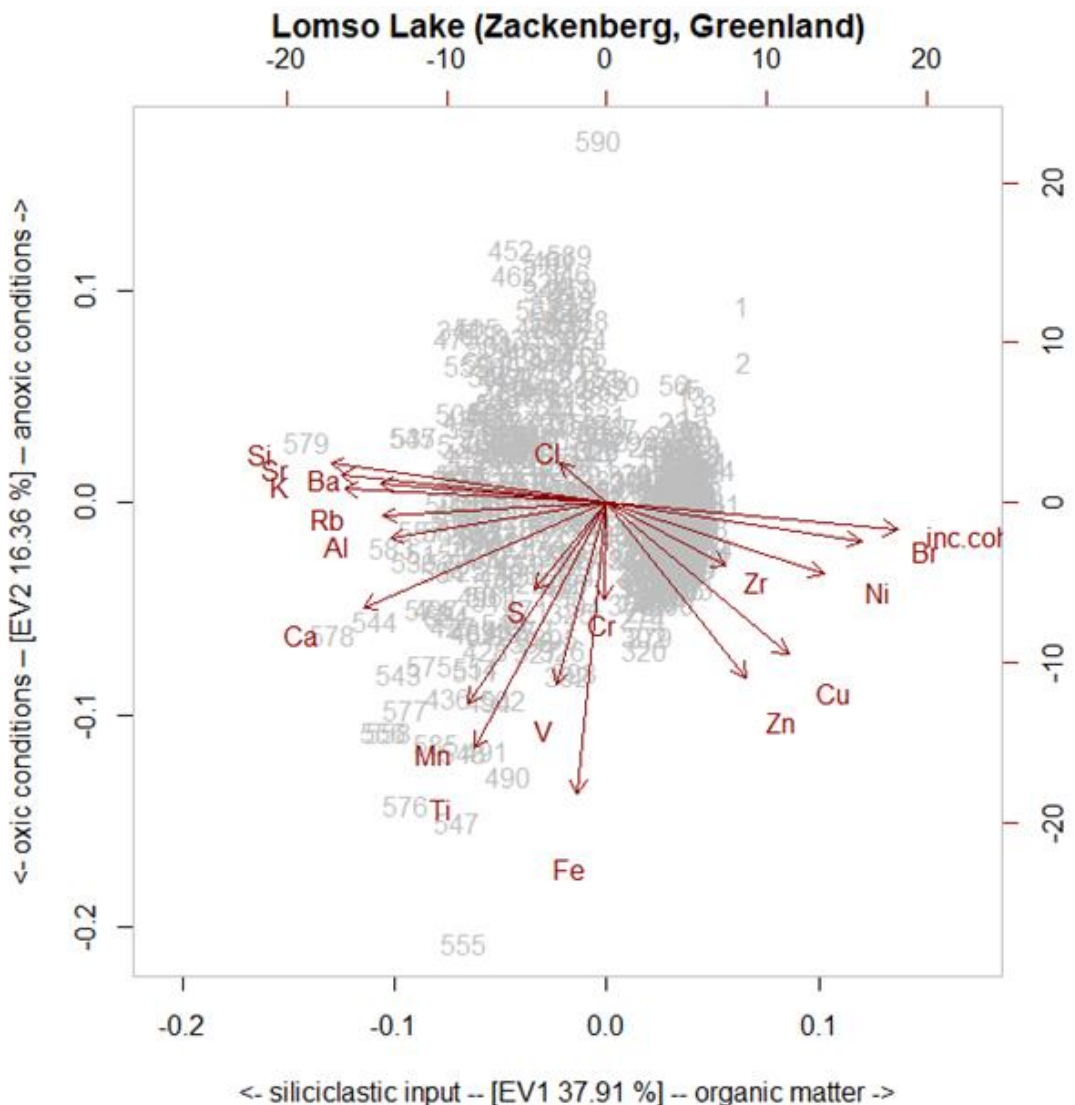


**Figure 36.** PCA plot based on the LOM18\_02 XRF data. Grey numbers represent samples.

Positive PC1 scores reflect high organic content whereas negative PC1 scores are related to siliciclastic deposits. On the other hand, PC2 scores reflect a gradient from anoxic conditions in the negative values and oxic conditions in the positive values of this second PCA axis. PCA scores were plotted to appreciate changes stratigraphically to characterize their evolution throughout the core (fig. 37).

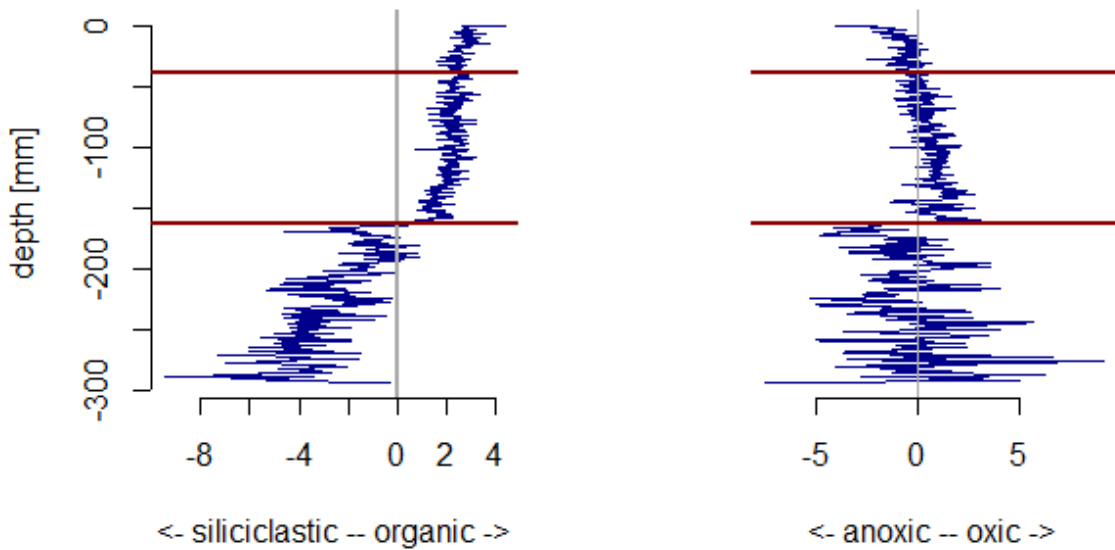


**Figure 37.** Stratigraphical PC1 and PC2 scores plot based on the LOM18\_02 XRF data. The left one illustrates PC1, related to organic composition while the right one plots PC2 scores related to oxic conditions.

Zone 1 presents higher siliciclastic composition and oscillating oxic and anoxic conditions while an abrupt change occurred around 17 cm. Both zone 2 and 3 shows steadily increasing organic and anoxic conditions.

### 3.2.4. Pollen stratigraphy

The palynological record is restricted to the upper unit B, ranging from 17 cm to the top of the core (fig. 38).

Unit B sediments shows two pollen zones:

- Zone LOM-I (16.5 – 11.5 cm): Dominated by *Luzula/Juncus* (25%) with *Salix* (15%) and *Cyperaceae* (11%) as the most significant taxa. The herbaceous component is dominant, with an increasing woody plant percentage throughout the zone, peaking at around 30% of terrestrial pollen ca. 12 cm. The aquatic bryophyte *Hippuris* makes its sole appearance in this zone, while exotic taxa such as *Pinus* are barely present.

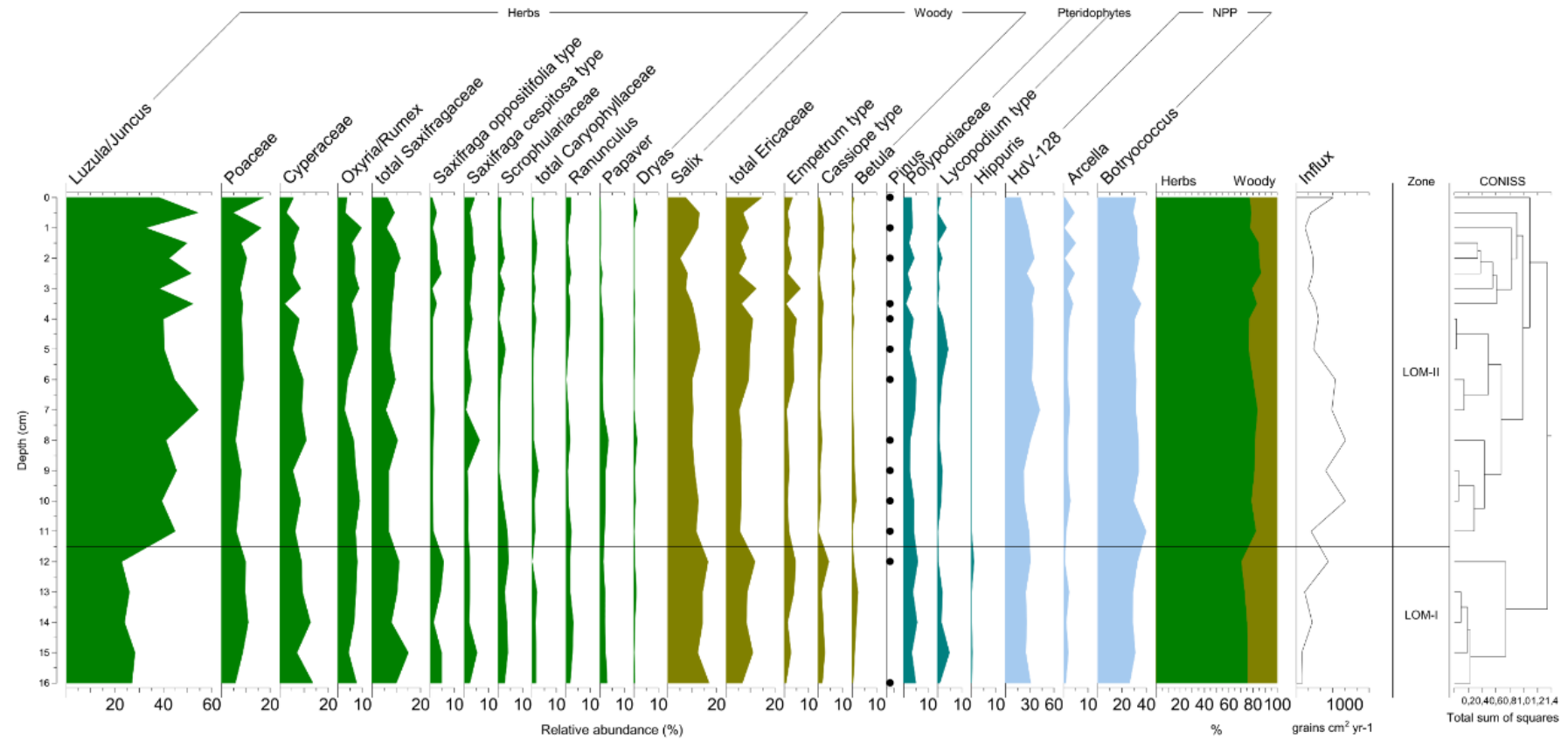


**Figure 38.** Pollen stratigraphy of Unit B of the LOM18\_02 record.

- Zone LOM-II (11.5 – 0 cm): Dominated by *Luzula/Juncus* (45%) accompanied by *Salix* (11%) and Cyperaceae (8%). The expansion of herbaceous vegetation (reaching up to 84%) is specially marked on fen taxa. Pollen influx reaches its peak of >900 grains/cm/yr at 10 and 8 cm, being specially marked on herbs with woody components achieving low pollen content of about 13% at 2.5 cm.

### 3.2.5. Lomsø pollen-based diversity index

DCA applied to the Lomsø pollen record revealed a limited variability in the pollen data, with a maximum axis length of 0.43 SD, indicative of minimal community changes throughout the record (table 9).

**Table 9.** Statistical values for the LOM18\_02 pollen based DCA.

	DCA1	DCA2	DCA3	DCA4
Eigenvalues	0.018	0.011	0.005	0.005
Axis lengths	0.426	0.509	0.323	0.283

The ecological space generated by the DCA suggests that the distribution of pollen taxa along axes 1 and 2 is associated with a combination of environmental factors. This implies that the observed pollen assemblages reflect relatively stable environmental conditions during the past 2300 years.

Pollen taxa indicative of low-Arctic environments, such as *Betula* and *Lycopodium*, were associated with positive DCA1 scores (fig. 39). In contrast, pollen taxa characteristic of high-Arctic regions, such as *Saxifraga* or *Oxyria/Rumex*, displayed low and negative DCA1 scores. Additionally, woody taxa related to various heath types, including *Salix*, *Cassiope*, *Betula*, *Empetrum* and Ericaceae, were positioned towards the positive end of axis 1. This suggests that DCA1 axis is related to the length of the snow-free period, with positive DCA1 scores representing longer snow-free periods while negative values indicate long term snow cover (fig. 39).

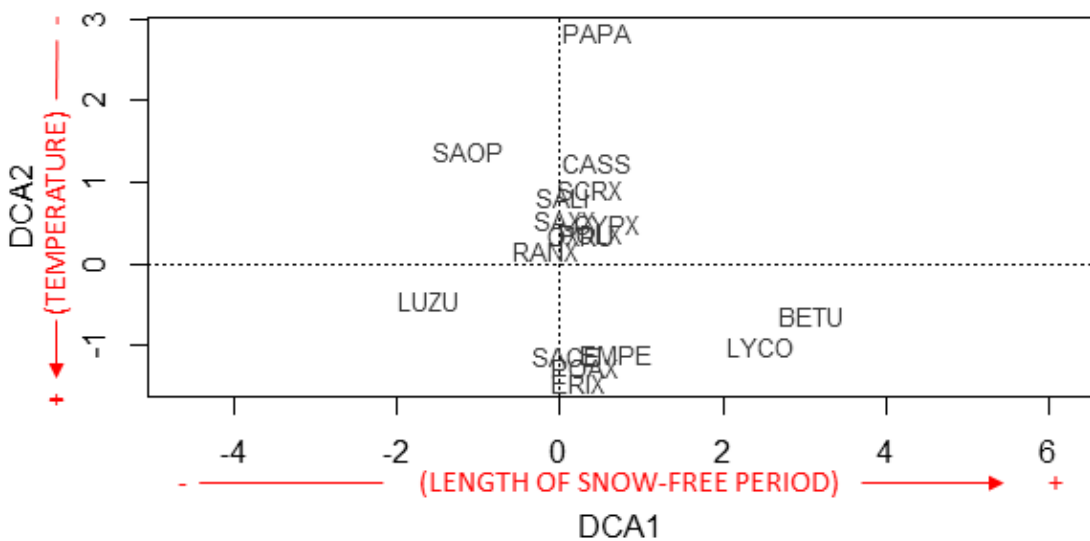


**Figure 39.** DCA plot based on the LOM18\_02 pollen record.

Axis 2 appears to be inversely related to temperature, as evidenced by the high DCA2 score of *Papaver*, a cold-tolerant species. Other cold-adapted taxa, such as *Saxifraga oppositifolia* and *Cassiope*, were also located towards the upper part of axis 2, while thermophilus elements such as Ericaceae and ferns exhibited negative scores. This pattern suggests that axis 2 reflects a temperature gradient, with higher scores indicating colder conditions and lower scores representing warmer periods.

Given the evident association between DCA axes and the ecological space represented by pollen data, a stratigraphic representation of axis scores can be employed to illustrate a simplified depiction of shift in the temporal length of the snow-free period. The Lomsø DCA1 curve describes an initial increasing in the length of snow-free period that peaked around 14 cm, followed by a decreasing trend peaking at 11 cm. The snow-free period became longer at 10 cm, underwent a reversal around 7 cm and re-peaked at 4 cm of core depth. From 4 cm until the top of the record, snow-free period length exhibited oscillations. The DCA2 curve on the other hand shows less oscillations but a constant warming trend that gets exaggerated towards the top of the record (fig. 40).

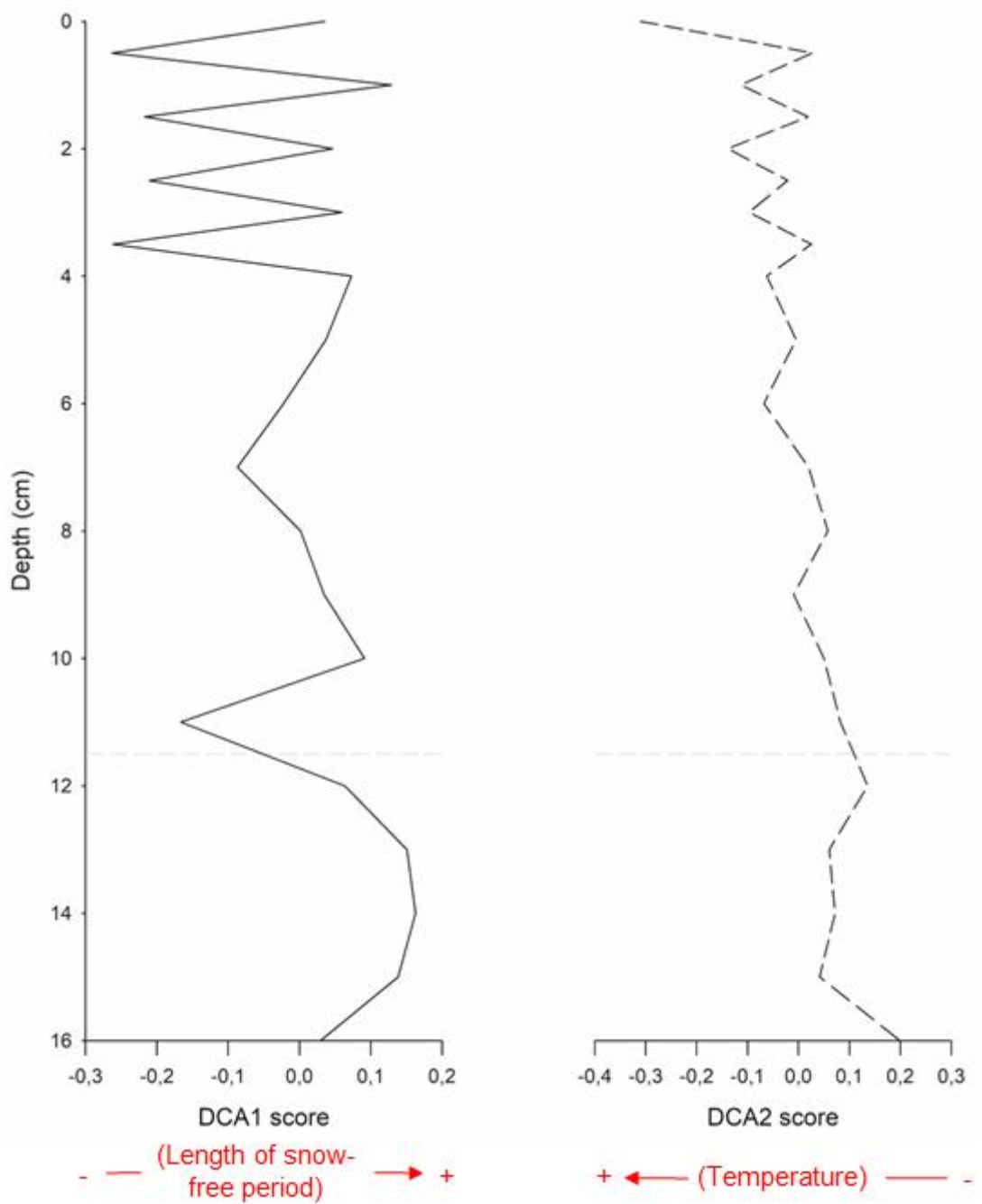


**Figure 40.** Stratigraphical DCA1 and DCA2 scores plot based on the LOM18\_02 pollen record. Grey dashed line represents the boundary between pollen zones.

The Lomsø  $\alpha$  diversity record shows an overall decreasing trend (fig. 41, dotted line). The maximum number of species (27) is present at the very bottom of the record while the lowest diversity (18 species) took place at 0.5 cm. On the other hand,  $\beta$  diversity shows a decreasing trend reaching record-low numbers indicating more ecological

stability between 14 and 12 cm. Ecological change increased until 10 cm and subsequently decreased, remaining stable between 9 and 4 cm. From 4 cm, the plant communities became more unstable, reaching peaks in ecological change around 3 and 1 cm depth (fig. 41).

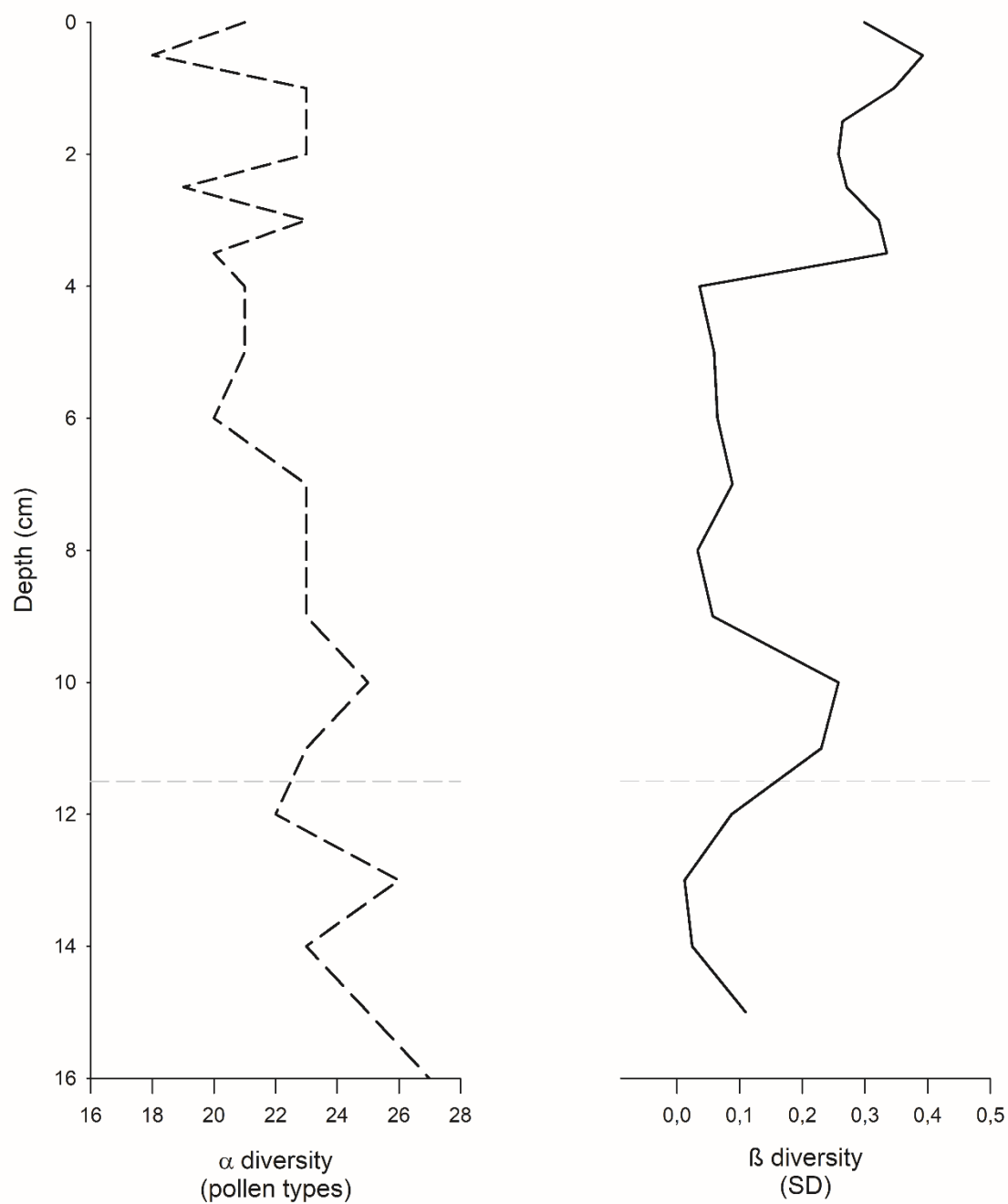


**Figure 41.** Stratigraphical  $\alpha$  and  $\beta$  diversity plot based on the LOM18\_02 pollen record. Grey dashed line represents the boundary between pollen zones.

### 3.3. The Aucella Lake record

In the Aucella lake record an insignificant pollen concentration in sediment samples is present. The AUC18\_02 core did not allow the development of pollen analysis, therefore no one of the pollen-related analysis on this record.

The results presented in this section were obtained as part of Julia García-Oteyza's PhD thesis and are partially presented in Garcia-Oteyza et al., (2024).

#### 3.3.1. Stratigraphy and sediment characteristics

The AUC18\_02 sediment core was subdivided into three primary sedimentary units: A, B, and C. Subzones within units B (B<sub>I</sub>, B<sub>II</sub>, B<sub>III</sub>, B<sub>IV</sub>) and C (C<sub>I</sub>, C<sub>II</sub>) were defined through facies visual examination (fig. 42).

Unit A (83.6 – 68 cm): the sediments of this unit were characterized by centimeter-thick laminations of light and dark brownish mud containing plant macrofossils. The clay-rich nature of these sediments was evident from their low grain size values and by the dominance of minerals such as kaolinite, biotite/muscovite, and, occasionally, montmorillonite. The presence of macrofossils, particularly mosses, was consistent with the high values of organic indicators, including TOC, TN, and chlorophyll. The diatom community in Unit A was characterized by the dominance of *Staurosira venter*, accompanied by *Pseudostaurosira pseudoconstruens*. Other frequently encountered species included *Staurosirella pinnata*, *Sellaphora seminulum*, *Sellaphora rectangularis*, *Rossithidium lineare* (although declining in abundance through the unit), and *Achnanthidium minutissimum* (fig. 43). The transition from Unit A to Unit B was distinctly visible both in physical observation and in the CT-scan image, marked by a change in sediment density from clay-rich to more sandy material.

Unit B (68 – 13 cm): the boundaries of Unit B were consistently identified across multiple proxy datasets, although the exact depths varied slightly. This unit was

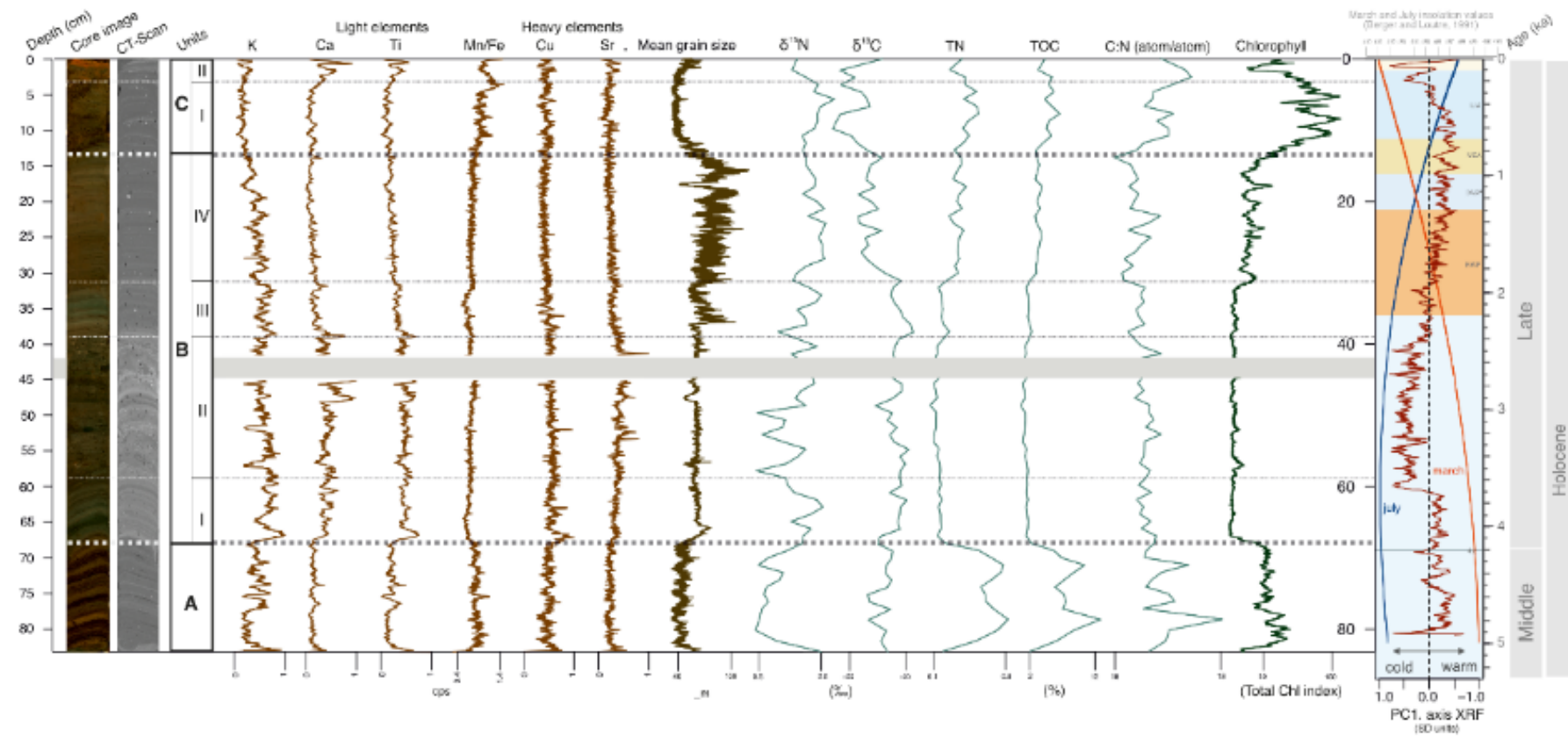


**Figure 42.** Multi-proxy data from the AUC18\_02 sediment core. Source: Garcia-Oteyza et al. (2024).

predominantly composed of silty mud and sands, and four distinct zones were identified within it:

Zone BI (68 – 59 cm depth): this zone's base was characterized by well-laminated green/gray silt. Geochemically, distinct peaks were observed in most chemical elements except for Sr, while Mn/Fe ratio showed a slight overall decrease and lower variability. The silty nature of the sediments was evident from an increase in grain size albeit with lower variability compared to the previous unit, and a sharp change in the CT-scan. Organic parameters TN, TOC, and chlorophyll values exhibited a marked decline. Diatom diversity and richness peaked, and diatom assemblages in this zone were characterized by increases in *Encyonema silesiacum*, accompanied by the appearance of *Encyonema procerum*, *Adlafia* sp. B, *Amphora copulata*, and *Naviculadicta* sp. A.

Zone BII (59 – 39 cm depth): this zone was generally characterized by massive brown silt sediment containing macrofossils although several centimeter-thick laminations were observed at ~47 cm and ~41 cm core depth. A mass movement event was identified between 42 and 45 cm depth based on visual evidence of disturbed sediment within a laminated unit and three anomalous radiocarbon ages within the zone. Consequently, these 3 cm were excluded from the record for both chronology construction and paleoecological interpretations. Biogeochemical proxies in zone BII exhibited trends like those in BI. Mineralogically, zone BII was characterized by a montmorillonite peak and the highest values of kaolinite and plagioclase. Diatom assemblages were dominated by *Staurosirella lapponica*, *S. pinnata*, *Pseudostaurosira pseudoconstruens*, and *Staurosira venter*.

Zone BIII (39 – 31 cm depth): Sediments in this zone were characterized by millimeter-thick orange/greenish laminations silty mud. All elements showed a decreasing trend except for K, which exhibited higher values than the zone below. Grain size showed an abrupt increase starting at around 37 cm of core

depth, followed by a gradual upward decline. Organic matter indicators did not exhibit significant changes compared to the underlying zone. Diatom assemblages were diverse, with no clearly dominant taxa, a marked decline in the relative abundance of *Staurosira venter*, and a peak in the abundance of *Adlafia sp. B* and in Simpson's index.

Zone BIV (31 – 13 cm depth): this zone was characterized by light and dark brown millimeter-thick silty mud laminations. Light chemical elements showed decreasing trends, with K exhibiting a more pronounced decline. In contrast, Mn/Fe ratio showed a slight increase in trend values, while other heavy elements remained relatively unchanged. Grain size increased gradually up to ~15 cm depth and then declined, although this trend was superimposed on significant variability, reflecting the unit's silty clay nature. Plagioclase, quartz, kaolinite, and biotite/muscovite displayed overall decreasing trends, while organic matter indicators and chlorophyll showed increased values and variability compared to the underlying unit BIII. Zone BIV was marked by the return to dominance of *Staurosira venter* and *Sellaphora seminulum*, accompanied by a decrease in *Pseudostaurosira pseudoconstruens* and the disappearance of *Staurosirella lapponica*.

#### Unit C (13 – 0 cm depth):

Zone CI (13 – 3 cm depth): CT-scan results revealed that this zone was mainly composed of millimeter-thick laminae, although they were not visually apparent and appeared as brown clayey mud containing macrofossils. Geochemical indicators showed no significant trends, except for Mn/Fe ratios values, which increased upwards and exhibited increased variability. Grain size decreased upwards in terms of both values and variability. The most prominent peaks of montmorillonite occurred in this zone, accompanied by the disappearance of nontronite and kaolinite and increases in the percentages of quartz and plagioclase. TN, TOC,  $\delta^{15}\text{N}$ , and chlorophyll showed increasing upward trends, while  $\delta^{13}\text{C}$  exhibited a decreasing trend. Diatom assemblages were strongly

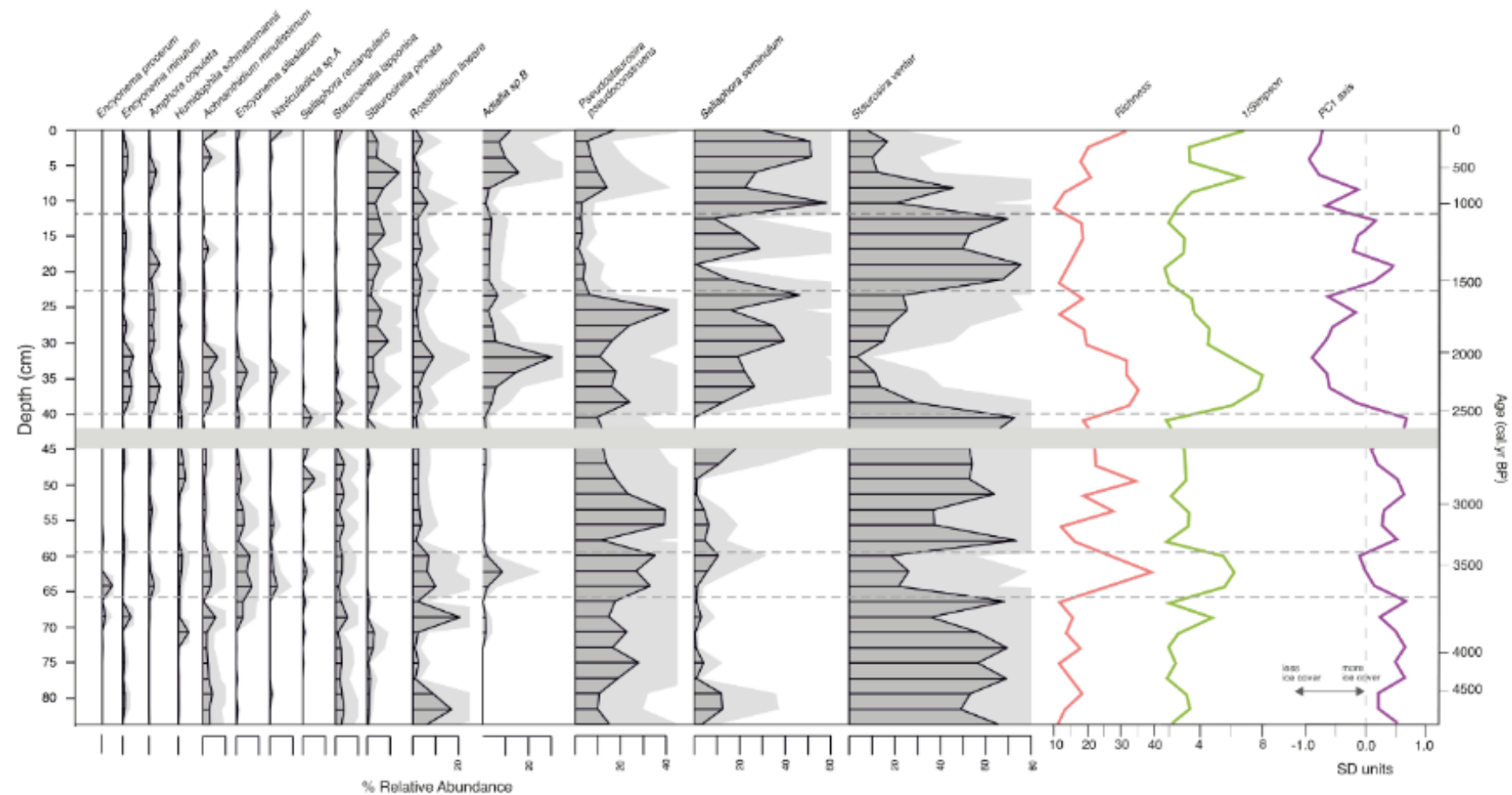


**Figure 43.** Diatom diagram for the AUC18\_02 core. Source: Garcia-Oteyza et al., (2024).

dominated by *Sellaphora seminulum*, with declines in most other taxa except for *Adlafia* sp. B and *Pseudostaurosira pseudoconstruens*.

Zone CII (3 – 0 cm depth): this zone exhibited abrupt changes, with a visually noticeable decline in the quantity of macrofossils and an orange hue in the upper centimeter. Elements including K, Ca, Ti, Cu, and Sr peaked in this zone, while the Mn/Fe ratio abruptly decreased. Mean grain size increased slightly, reflecting the silty mud nature of the sediments, and kaolinite reappeared along with a corresponding decrease in quartz.  $\delta^{15}\text{N}$ , TN, and TOC decreased, chlorophyll showed an abrupt decrease, and  $\delta^{13}\text{C}$  increased upwards to the sediment surface. No significant changes in diatom assemblages were observed, only minor increases in *Naviculadicta* sp. A, *Pseudostaurosira pseudoconstruens*, and *Staurosirella lapponica* (fig. 43).

### 3.3.2. Chronology

Radiocarbon dating of Aucella Lake sedimentary sequence revealed a largely continuous record of sedimentation, with a minor disruption caused by a sediment slump. The age-depth model, constructed using six radiocarbon dates, showed an average sedimentation rate of approximately 1 cm per 100 years, with limited variation throughout the core. An interval between 42 and 45 cm core depth showing sedimentary slump features has been excluded from the age model. This sedimentary sequence provides a valuable archive of paleoenvironmental changes over the past 5,000 years (fig. 44).

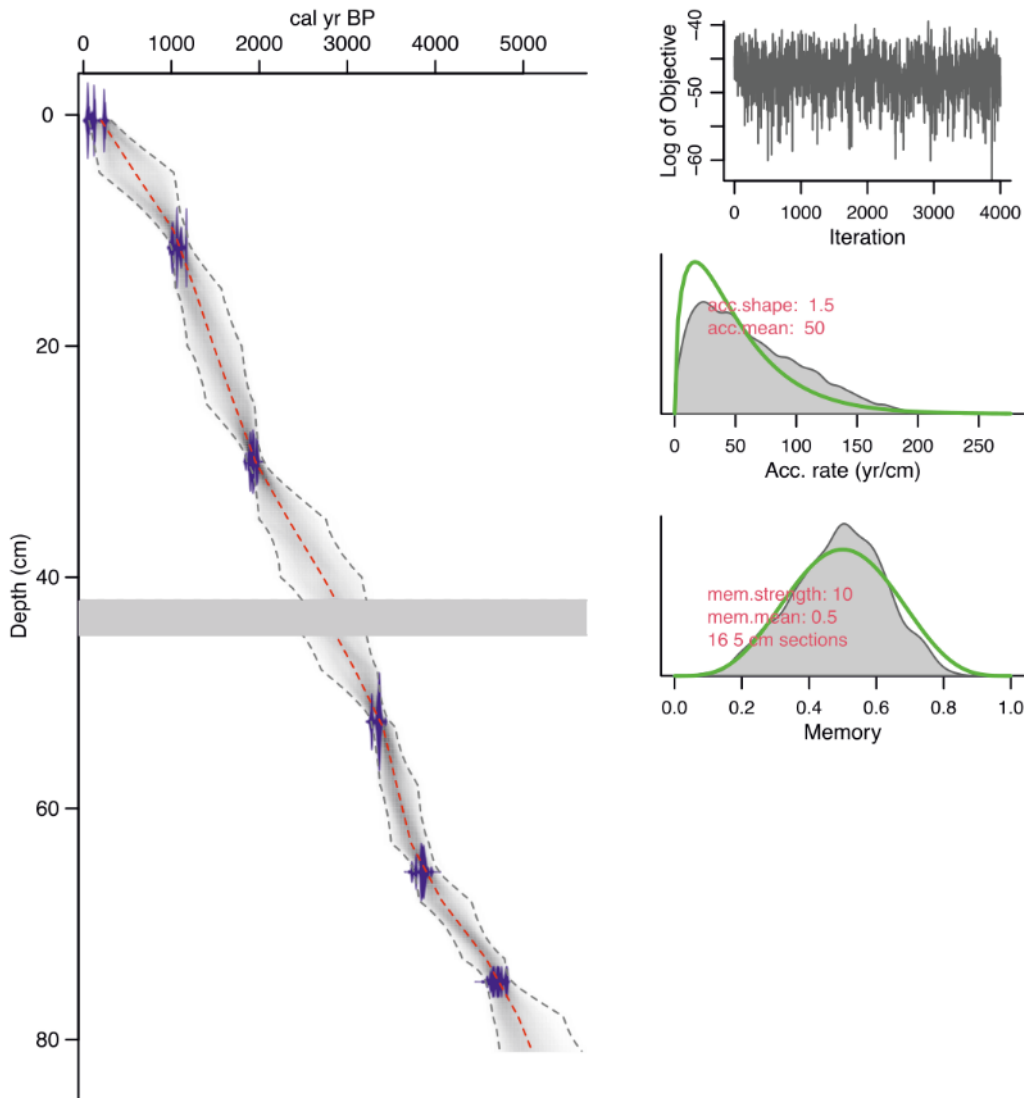


**Figure 44.** Age-depth model for sediment core AUC18\_02. Source: Garcia-Oteyza et al., (2024).

### 3.3.3. Multivariate analysis

Throughout the sediment core, three diatom species, *Staurosira venter*, *Sellaphora seminulum*, and *Pseudostaurosira pseudoconstruens*, exhibited dominance in terms of abundance. Fluctuations in these taxa delineated the primary diatom zones. PCA of diatom data revealed two significant axes, with the first axis accounting for 47.2% of the total variance and the second axis explaining 18.2%. *Sellaphora seminulum*, *Staurosira venter*, and *Adlafia* sp. B exerted the strongest influence on the first axis,

while *Pseudostaurosira pseudoconstruens*, *Staurosira venter*, and *Sellaphora seminulum* were the primary drivers of the second axis (fig. 45).

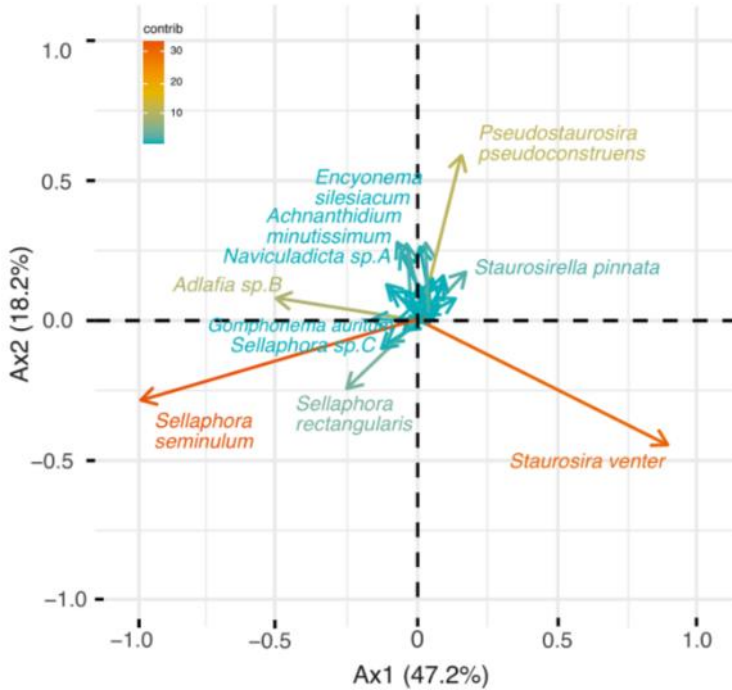


**Figure 45.** DCA plot based on the AUC18\_02 diatom record. Source: Garcia-Oteyza et al. (2024).

The PCA of XRF and organic matter data showed that the first axis explained 73.6% of the total variance and was negatively correlated with lighter elements, particularly Fe and Ti. RDA using mineralogical composition as the constraining matrix revealed the potential sources of light and heavy elements identified by XRF. The first axis of this RDA explained 87.8% of the total variance and indicated that Ca, Ti, Fe, Mn, Sr, Cu, and K were primarily associated with clays composed of muscovite/biotite, high  $\delta^{13}\text{C}$ , and kaolinite (fig. 46).

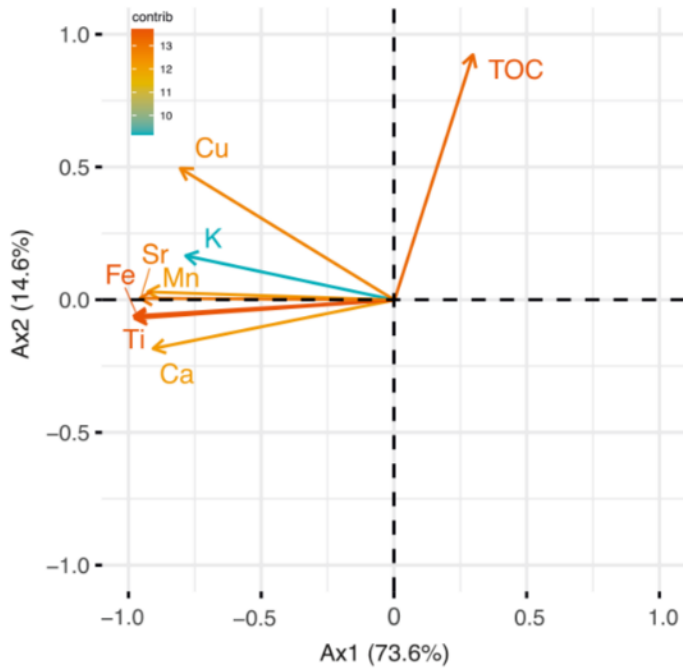


**Figure 46.** DCA plot based on the XRF and TOC content of the AUC18\_02 record.  
Source: Garcia-Oteyza et al. (2024).

RDA of diatom data constrained by the environmental dataset revealed that the first axis explained 34.8% of the total variance. The three lower diatom clusters were associated with terrigenous inputs and a dominance of *Staurosirella* taxa. In contrast, the genus *Sellaphora* exhibited a marked increase in the three upper clusters, where its interplay with *Staurosira venter* determined diatom zonation. High abundance values of *Sellaphora* taxa were more strongly correlated with elevated levels of internal ecosystem parameters such as  $\delta^{15}\text{N}$  (fig. 47).

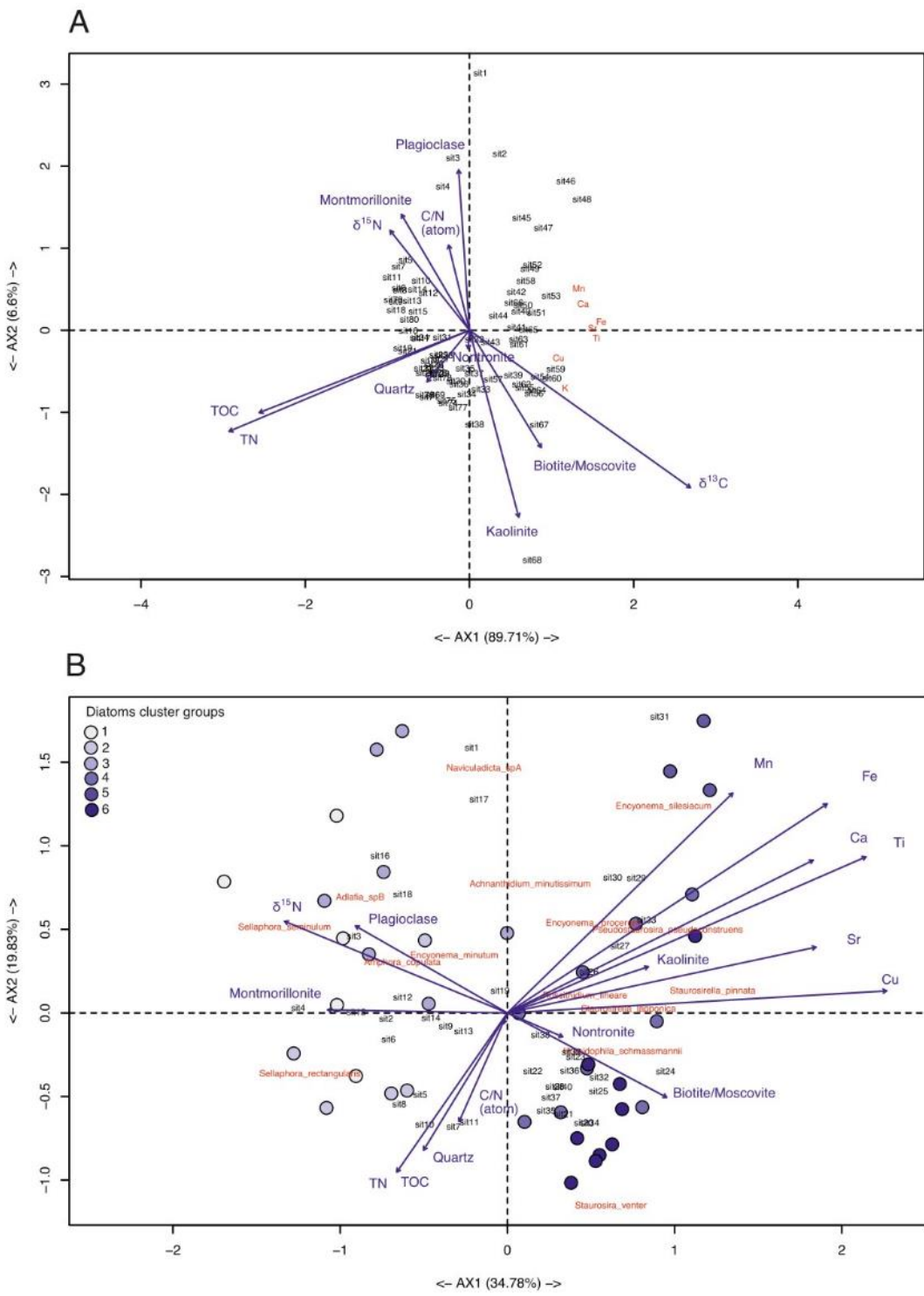


**Figure 47.** AUC18\_02 RDA plots. A) illustrates the relationship between mineralogical composition of the sediments (XRD) with organic parameters and the geochemical data (XRF). B) displays the relationship between diatom assemblages as a response variable to the environmental variables contained in the geochemical record and organic parameters. Source: Garcia-Oteyza et al. (2024).

## 4. Discussion

### 4.1. Pollen morphology study

The taxonomical study of the pollen grains of selected Zackenberg plants was useful considering the importance of pollen morphology in paleopalynology. The proper identification of fossil pollen is essential to achieve precise interpretations of past vegetation ecology (Chevalier et al., 2020). In NE Greenland, the identification of pollen grains at species or at least genus level would drastically be crucial to understanding of past Greenland flora and its long-term dynamics. Most studies are limited to identify pollen grains at family level because most of them are based on optical microscope observation, and resources to identify pollen grains of E Greenland are scarce.

Addressing methodological difficulties is essential to achieve these objectives. Creating reference collections involves accessing herbarium material or undertaking years of collection efforts, which from a logistical point of view, acquires extra difficulties in the Arctic. In this context, the fact that herbarium samples are often limited has to be considered (Gajewski, 2006). In this study we aimed to capture the morphological differences of the main taxa of each of the five main plant communities in the area and of climatically sensitive taxa. However, most of the samples lacked sufficient material for proper measurement and photography. It must be noted that the main genus of interest for this study, *Luzula* and *Juncus*, could not be described because no pollen grains remaining in the processed samples. The same happened with Cyperaceae, Onagraceae and Scrophulariaceae species. This issue may be related to pollen dispersal strategies, especially in the case of anemophilous plants that release their pollen into the atmosphere, leaving little to no grains left in the sampled flowers, or it could be attributed to sample preservation since herbaria conditions could harm pollen remains. The presence of Juncaceae pollen on other taxonomic artic pollen studies such as (YAO et al., 2013) supports the later hypothesis, as they worked with fresh material.

The results of this study support the idea that pollen morphology, particularly shape, size, and exine ornamentation, can be valuable tools for distinguishing palynomorphs at the species level. It is essential to acknowledge that the measurements for several pollen taxa were based on a limited number of grains: *Cerastium arcticum* (n=6), *Rhododendron lapponicum* (n=13), *Saxifraga cernua* (n=5), and *Vaccinium uliginosum* (n=15). Despite this limitation, these taxa were included in this study due to the availability of sufficient material for photographic documentation and description.

#### 4.2. Modern pollen-climate relationships in the Arctic

The selected sites from the calibration set were arranged longitudinally so they could be grouped in Arctic regions. This result in 472 sites grouped as Western Arctic (west of 100°W), 70 Central Arctic sites (between 100°W and 60°W) and 48 Greenland sites (east of 60°W). Subsequently, each group was further sorted by latitude to provide a clearly perspective on latitudinal patterns among regions.

The Western Arctic region displays clear latitudinal patterns with woody *Alnus*, *Betula* and *Picea* dominating on most low-latitude sites while herbaceous Poaceae and Cyperaceae reign at higher latitudes. Sphagnum also performs well on the southern areas. Brassicaceae, *Oxyria* and *Saxifraga oppositifolia* on the other hand are absent in the southern sites while its present in most high-latitude sites. Ericaceae flourishes both in high and low latitudes, Ericales type is more important in the middle range. *Salix* shows a pattern like Ericaceae. Cupressaceae was found only in this region.

The same pattern is observed in the central Arctic sites, with a strong latitudinal gradient of woody *Alnus crispa*, *Betula*, *Picea* and even Ericaceae dominating in the south and herbaceous Cyperaceae and Poaceae in the north. Brassicaceae, *Dryas*, *Oxyria* and *Saxifraga oppositifolia* are more important in the southern sites, whereas Sphagnum thrives at lower latitudes (fig. 48).

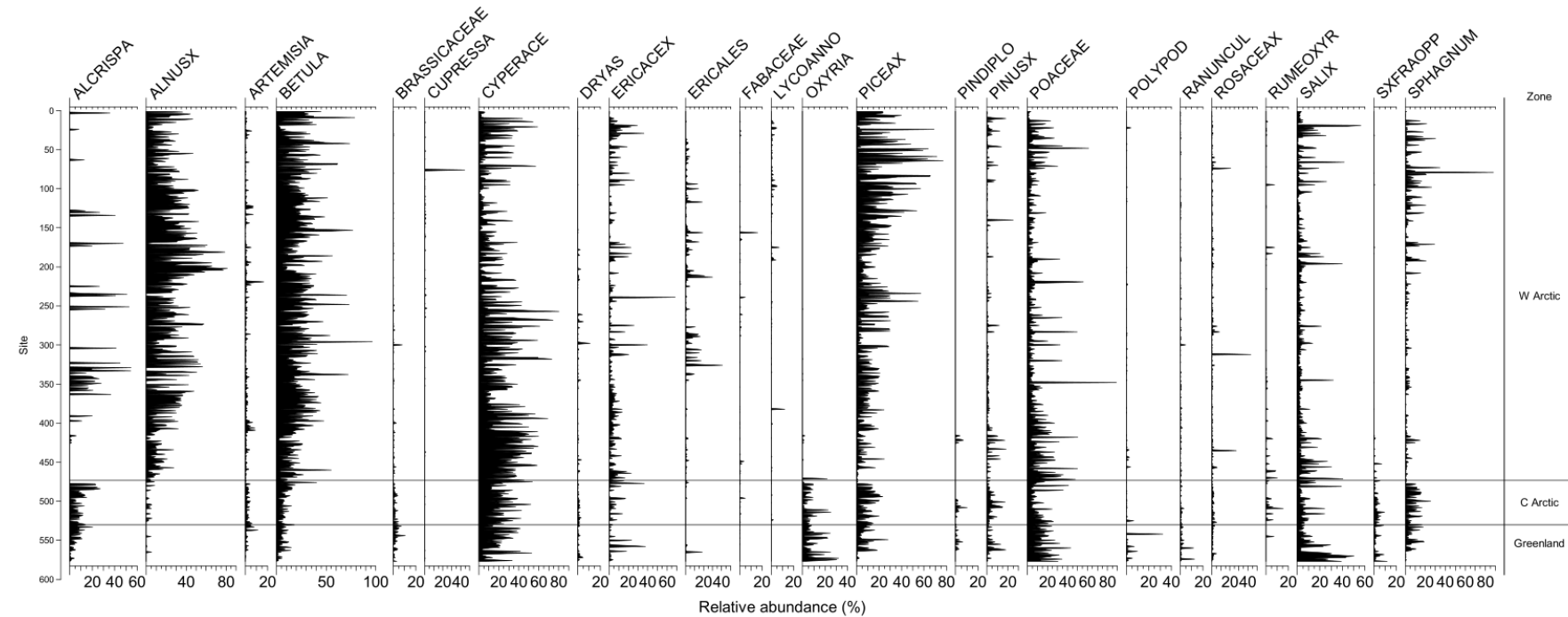


**Figure 48.** Pollen diagram of the pollen-climate calibration set.

Sites located in Greenland follow the same pattern. However, Cyperaceae triumphs on the southern part of the island and decreases in higher latitude sites, and *Salix* seems to do better in N Greenland. Ericaceae on the other hand flourishes in the middle parts of the island. Fabaceae and *Lycopodium annotinum* are completely absent.

Among the ten selected climatic variables, both *Ths* and *Ta* explain the most variance observed in the pollen across the calibration set. Specifically, accounts for 18.93% of the variance, with a  $\lambda_1/\lambda_2$  ratio of 1.01 and ANOVA-derived p-value of 0.001, indicating its significance as a relevant gradient within the dataset (table 10).

**Table 10.** Explanatory power of each climate variable of the set.

Variable	% Explained	$\lambda_1/\lambda_2$	p-value
Ta	18.58	0.92	0.001
Tmax	17.51	0.87	0.001
Tmin	5.79	0.18	0.001
<b>Ths</b>	<b>18.93</b>	<b>1.01</b>	<b>0.001</b>
Tcs	13.72	0.55	0.001
Pa	6.17	0.2	0.001
Pmax	7.68	0.26	0.001
Pmin	4.73	0.15	0.001
Pds	6.17	0.2	0.001
Pws	7.31	0.24	0.001

It's no surprise that temperature variables are stronger when explaining the variance of pollen data, after all the influence of temperature as the main forcing modelling plant distribution of Arctic plants is well documented (Elberling et al., 2008b; Grau et al., 2014; Stewart et al., 2016). Despite most WorldClim variables being co-related as they are based on modeled rather than instrumental data, *Ths* was confirmed to have greater weight both within the calibration set and among variables (appendix 11). In this context it must be noted that *Tmin* holds the less explanatory power among temperatures, which could be explained in part due to the narrow gradient but also that these temperatures are reached when plants are not experimenting biological activity during the boreal winter. The other temperatures on the other hand represent longer

gradients within the dataset with *Ths* being the most defining one when it comes to explain our pollen data distribution, showing the most variability – and sensitiveness – among sites. On the contrary, precipitation values, despite being considered as statistically significative variables, showed little relationship with the main defining factor among the calibration set (fig. 49).

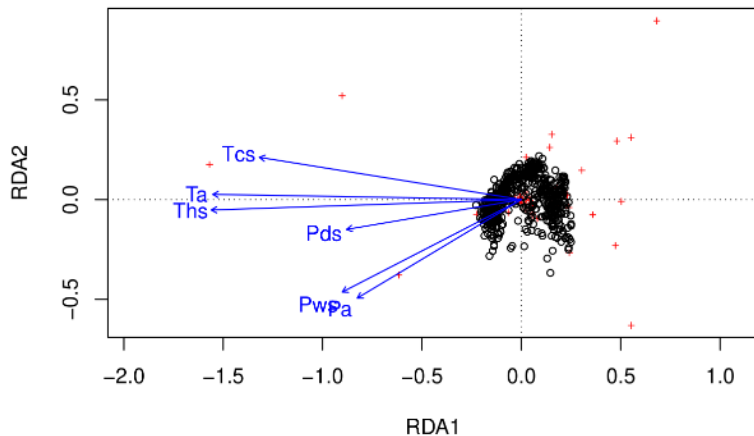


**Figure 49.** RDA plot of climatic and pollen data from the calibration set. Sites are plotted as black circles while and red crosses represent pollen types.

#### 4.3. Transfer function-based temperature reconstruction

Once *Ths* was selected as the variable to reconstruct, WA-PLS transfer functions based on it were generated. From the five functions considered, the two-component one was chosen due to its lower RMSE, higher  $r^2$ , narrow bias, and higher skill (table 11). (RMSE: 2.11°C,  $r^2$ : 0.66, max bias: 8.19°C, Skill: 65.63).

**Table 11.** WA-PLS based transfer function statistics.

Function	RMSE			Maximum bias		
	(°C)	$r^2$	Average bias (°C)	(°C)	Skill	
Comp01	2.21	0.62	-0.0067	7.54	61.71	
<b>Comp02</b>	<b>2.11</b>	<b>0.66</b>	<b>-0.0039</b>	<b>8.19</b>	<b>65.63</b>	
Comp03	2.13	0.66	-0.0048	8.35	65.79	
Comp04	2.16	0.66	-0.0146	8.81	65.54	
Comp05	2.19	0.65	-0.0171	8.97	65.21	

Transfer function performance test under the bootstrapping cross-validation method showed overall good fit between observed (X axis) and predicted (Y axis) mean *Ths*. However, inconsistencies were observed among temperatures under 2.5°C and between 5°C and 8°C, where the model tends to overestimate, while values above 12°C tend to be underestimated (fig. 50).

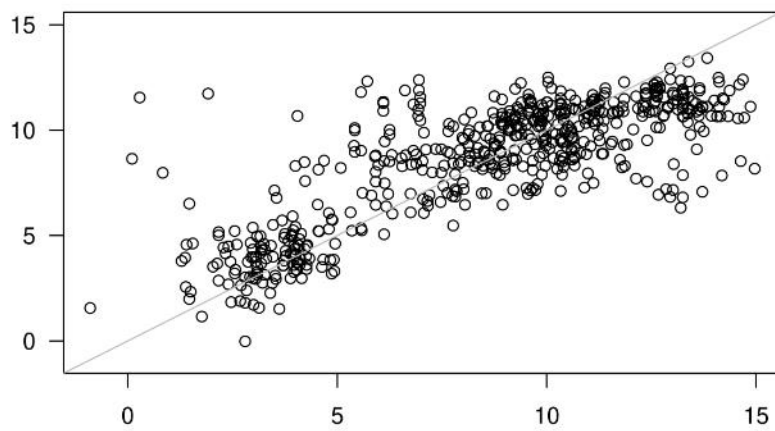


**Figure 50.** Diagram based on the bootstrapping cross-validation of the selected transfer function. The x axis represents observed values while the y axis corresponds to projected values. Black circles represent samples.

The ZAC06 temperature record has a range of oscillation ca. 12°C, being the maximum value 9°C and the minimum are almost -4°C. On the other hand, the Lomsø temperature record fluctuates between 0°C and 4°C. The ZAC pollen-based *Ths* record initial conditions were of 0.09°C at 9,000 cal yrs BP and described a cooling trend reaching -3.26°C at 8,300 cal yrs BP. The transition from the Early to Middle Holocene brought warming with temperatures reaching a first conspicuous peak at 7,500 cal yrs BP followed by a consistently warm period with *Ths* over 5°C between 7,000 and 5,100 cal yrs BP. Following the warm period, from 5,000 to 4,000 cal yrs BP temperatures seemed to stabilize around 3°C. The onset of the Late Holocene was accompanied by a sharp decrease in *Ths*, reaching -1.16°C ca 3,800 cal yrs BP, followed by a warming pulse reaching Mid-Holocene like values 2,900 cal yrs BP (fig. 51).

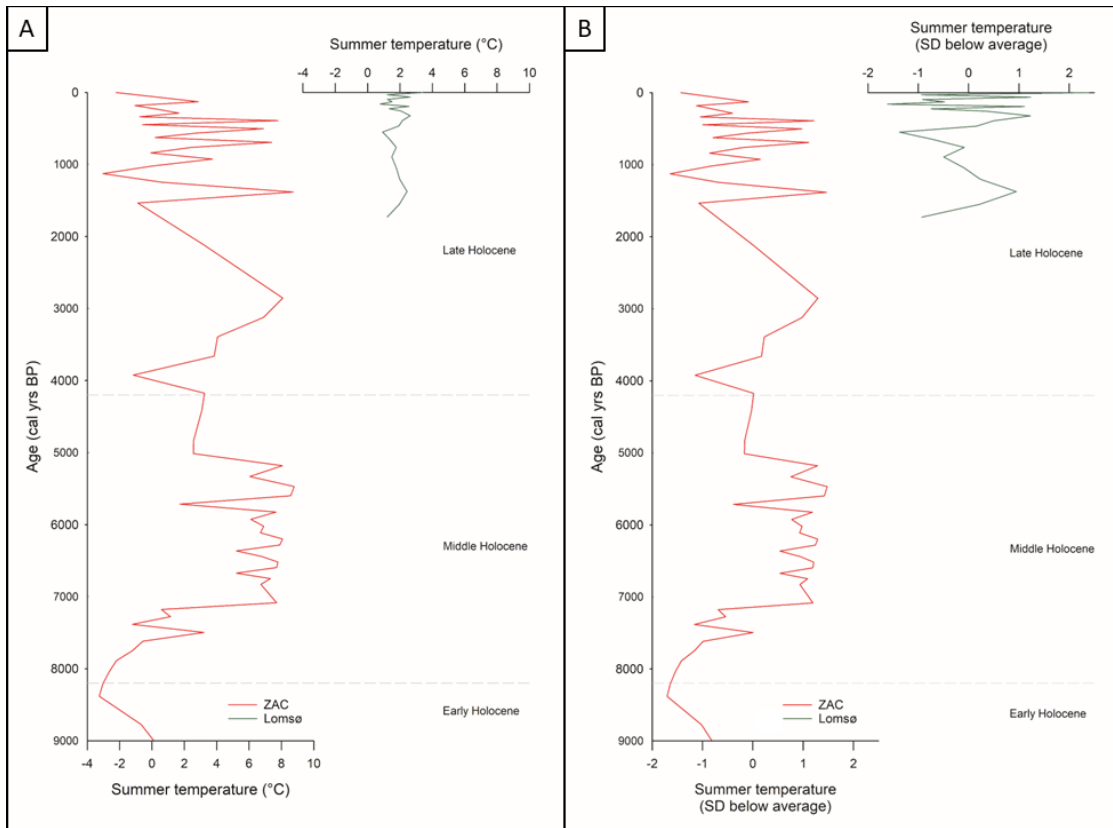


**Figure 51.** Summer temperature ( $Ths$ ) since 9,000 cal yrs BP based on the ZAC19\_06\_02 (black line) and LOM18\_02 (red line) pollen records. Results in plot A are the raw  $^{\circ}\text{C}$  values while those of plot B are standardized values.

Focusing on the last 1,800 years allow us to compare both pollen-based curves values and overall trends. At first sight, the ZAC record shows pronounced temperature changes during this period while the Lomsø temperature records show a more smoothed curve ranging from  $0.77^{\circ}\text{C}$  to  $3.39^{\circ}\text{C}$ . The only RWP sample from the ZAC record presented  $3.18^{\circ}\text{C}$ , while the one from the Lomsø record shows summers in lowland Zackenberg were ca.  $1.22^{\circ}\text{C}$ . The DACP was marked by a warming trend in both records, peaking ca. 1,400 cal yrs BP with modelled temperatures of  $8.73^{\circ}\text{C}$  in ZAC and  $2.44^{\circ}\text{C}$  in Lomsø. The MCA in the region was marked by an overall warming trend in ZAC, interrupted by a cool episode ca. 850 cal yrs BP ( $-0.07^{\circ}\text{C}$ ), and a subtle overall cooling in Lomsø. The LIA in ZAC was characterized by high oscillation with temperatures ranging between  $-0.75 - 7.79^{\circ}\text{C}$  while in Lomsø the cooling trend continued until 550 cal yrs BP although changes were not as evident with temperatures ranging from  $0.93^{\circ}\text{C}$  and  $2.62^{\circ}\text{C}$ . The LIA oscillating nature in

ZAC was followed by cooler conditions towards the present, with summers presenting  $-2.22^{\circ}\text{C}$ . In Lomsø on the other hand, the LIA cooling was followed by oscillating temperatures but an overall warming trend peaking in the top sample reaching near-present temperatures of ca.  $3.39^{\circ}\text{C}$  (fig. 52).

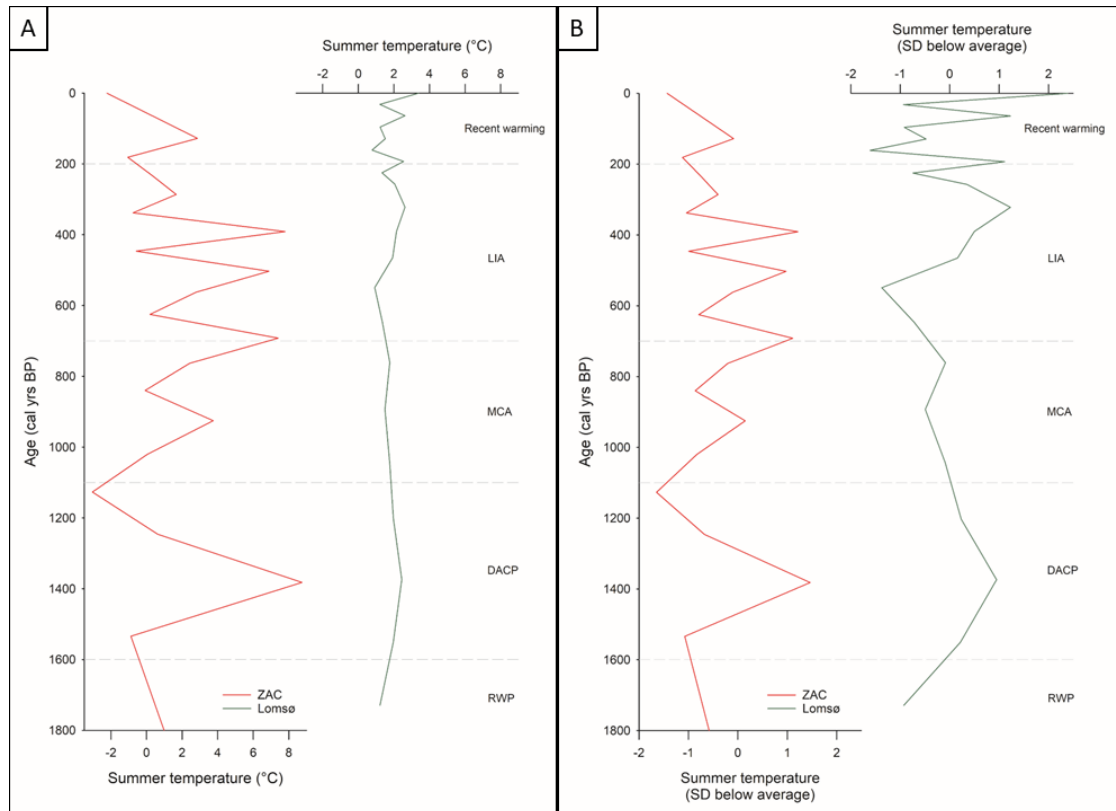


**Figure 52.** Summer temperature ( $Ths$ ) reconstruction since 1,800 cal yrs BP based on the ZAC19\_06\_02 (black line) and LOM18\_02 (red line) pollen records. Results in plot A are the raw  $^{\circ}\text{C}$  values while those of plot B are standardized values.

#### 4.3.1. Performance of the quantitative climate model

The climatic reconstruction statistics suggest that the calibration set effectively captures an important environmental gradient related to pollen distribution within the dataset. Other climatic variables were disregarded due to high correlation between them, so the most powerful variable was chosen. According to the RDA analysis, variable  $Ths$  explains 18.93% of the variance among the calibration set. The relation

between the first constrained axis (RDA1) and the first unconstrained axis (PCA1) is of 1.01, pointing that it is, or is directly related to, a defining factor on the distribution of pollen rain in the study area (ter Braak & Juggins, 1993). This makes sense considering that summer isotherm 10, therefore  $Ths$  values, is what defines Arctic vegetation broad scale.

When comparing the performance of our transfer function with other temperature transfer functions developed in the high latitudes, we can note that despite similar  $r^2$  with the  $T_{ju}$  models, our function exhibits higher RMSE and especially Maximum bias, suggesting an overall lower predictive capability (table 12).

**Table 12.** Comparison with other northern high latitude temperature transfer functions.

Reference	Function	RMSE (°C)	$r^2$	Max bias (°C)
Seppä & Birks (2001)	$T_{jul}$ (WA-PLS)	1	0.72	4.17
Klemm et al. (2013)	$T_{jul}$ (MAT)	1.57	0.61	4.75
<i>This study</i>	$Ths$ (WA-PLS)	2.11	0.66	8.19
Salonen et al. (2012)	$T_{mjja}$ (Bayesian)	0.8	0.93	1.18
Seppä et al. (2004)	$T_{ann}$ (WA-PLS)	0.89	0.88	2.13
Danesh et al. (2022)	$T_{ann}$ (MAT)	1.3	0.91	N/A

Despite the better statistics performance of the study by Salonen et al. (2012) study, the authors note clear biases on Bayesian-based temperature reconstructions. On the other hand, the MAT reconstructions of (Danesh et al., 2022; Klemm et al., 2013) on the other hand heavily depend on the existence of modern analogues, which in the case of Lomsø record, are nonexistent outside Zackenberg.

While the overall fit between observed and predicted values is satisfactory, this model, like many other WA-PLS based reconstructions, exhibits inherent biases that tend to overestimate low values and underestimate high values (Birks & Birks, 2006). This could be related to the broad taxonomic classification of the calibration set because pollen types that contain many diverse taxa that are affected in different ways by a

climatic gradient are less likely to have unimodal responses. Regarding the representativity of pollen rain and vegetation, the dataset successfully manages to cover both the low and high Arctic zones showing distinct distributions along the latitudinal gradient in the longitudinal division. The low Arctic is characterized by high abundances of *Ambrosia*, Brassicaceae and Poaceae across the three regions while *Equisetum*, Ranunculaceae and Saxifragaceae thrive on the high Arctic. Greenland sites are characterized by the absence of arboreal pollen, except for exotic, far-reaching *Pinus diploxyylon*. It should be noted that the *Luzula/Juncus* (Juncaceae) pollen type, dominant in Lomsø, is not included on the training set, so the reconstruction is based on secondary pollen types rather than the dominant vegetation.

Despite the statistical robustness of the calibration set, we consider that the pollen records used for applying the transfer function on LOM18\_02 and ZAC19\_06\_02 were not the most suitable for this methodology. In the case of Lomsø, there were few overall composition changes, and the pollen assemblages differ from those found in the central part of the gradient. Moreover, the only modern analogue for Lomsø is Lomsø itself, which exhibits low-*Ths* values (Birks & Birks, 2006; ter Braak & Juggins, 1993). This is particularly important because the reigning *Luzula/Juncus* led tundra vegetation of the last 1500 years seems to be more influenced by local conditions such as soil moisture than by microclimate (Nabe-Nielsen et al., 2017). In the case of ZAC, the low pollen concentration since pollen relative abundances are based in less than 300 pollen grains (the minimum for a sample to be statistically significant), leads to significant percentage changes due to insufficient sampling effort.

When discussing the representativeness of the pollen record, especially in the Arctic, it is crucial to consider the processes involved in pollen transport and lake sedimentation (Gajewski, 2006). Challenges related to the climatic reconstruction based on Arctic pollen data are the strong influence of latitude on plant phenology, the different levels of anthropic effects on Arctic vegetation, potential extra-local pollen transport that may also blur pollen signal, different kind of samples in the set (moss pollen traps capture a different signal than lake bottoms), and the impact of non-climatic factors

on vegetation, such as soil moisture availability (Birks & Seppä, 2004; Brewer et al., 2007; Li et al., 2014).

Klein et al. (2008) indicate that in the Zackenberg area the main pollen types found on pollinators are dwarf shrubs *Salix arctica*, *Cassiope tetragona* and *Dryas octopetala*. Meanwhile, the pollen dominating Juncaceae, Poaceae and Cyperaceae are wind pollinated, affecting the pollen signal codified at the lake bottom with an overrepresentation of anemophilous pollen types. Even if long-distance pollen transport seems to be a noise generator in most human-affected areas, in Greenland that does not represent a big problem thanks to its isolated location (Gajewski, 2006; Iversen, 1953). However, the over-representation of local plants like swampy pollen types such as *Luzula/Juncus* may be an artifact of the fen surrounding due to taphonomical factors (Lebreton et al., 2010). Pollen influx into the lake likely occurs through streams and sheet floods from melting snow-patches, melt-out from ice and snow over the lake, and airborne transport during the ice-free period. The complex relationship between these processes coupled with phenology and pollination factors makes difficult to reconstruct climatic changes based on pollen evidence only. Kobashi et al. (2013) proposed that most of the temperature changes in Greenland are explained by multi-decadal to centennial scale variability, so we recommend to step up the temporal resolution of pollen studies in the region. This enhancement would allow pollen diagrams and pollen-based climate reconstructions are able to capture this variability and its effects on Greenland plants at a finer scale.

#### 4.4. Zackenberg fossil pollen assemblages as an ecological indicator

To better understand the relationships among pollen taxa and their past abundance patterns, we conducted a cluster dissimilarity analysis on pollen data from both Lomsø and ZAC records. This analysis aimed to categorize pollen types based on their co-occurrence and abundance trends, potentially revealing ecological associations, and facilitating their utilization as an ecological proxy. The objective was to identify distinct clusters reflecting the preferred ecological parameters of the taxa such as climate or soil moisture conditions.

However, the cluster dendrogram derived from the pollen data does not fully capture these distinct groupings, suggesting that the overall dataset may not be enough sensitive to climate to reveal clear climatic-based sorting (fig. 53). Nevertheless, the analysis does reveal some meaningful patterns. Pollen types with higher abundance in the record are grouped in the left side of the cluster, with Poaceae and Cyperaceae forming the most closely related pair. This association aligns with their consistent presence in both records and their significance since the deglaciation of the area. *Salix* is closely linked to the Poaceae-Cyperaceae group, potentially representing the *Salix* snow bed vegetation.

On the other hand, the Polypodiaceae-other Saxifragaceae association seems to be related to *Oxyria/Rumex* content, which, in turn, is linked to woody *Betula* (fig. 53). This group likely corresponds to plants that dominated during the Early and Mid-Holocene conditions. *Luzula/Juncus*, while related to these two clusters, stands out as a distinct group due to its overwhelming dominance in both records, particularly in Lomsø. The right side of the cluster primarily encompasses heathland elements and is divided into two sub-clusters. The first subgroup includes rare species associated to cold heathlands, while the second one, with *Cassiope* and *Saxifraga oppositifolia*-type as the most related groups, represents *Cassiope* heath and is related to milder heathland elements (fig. 53).

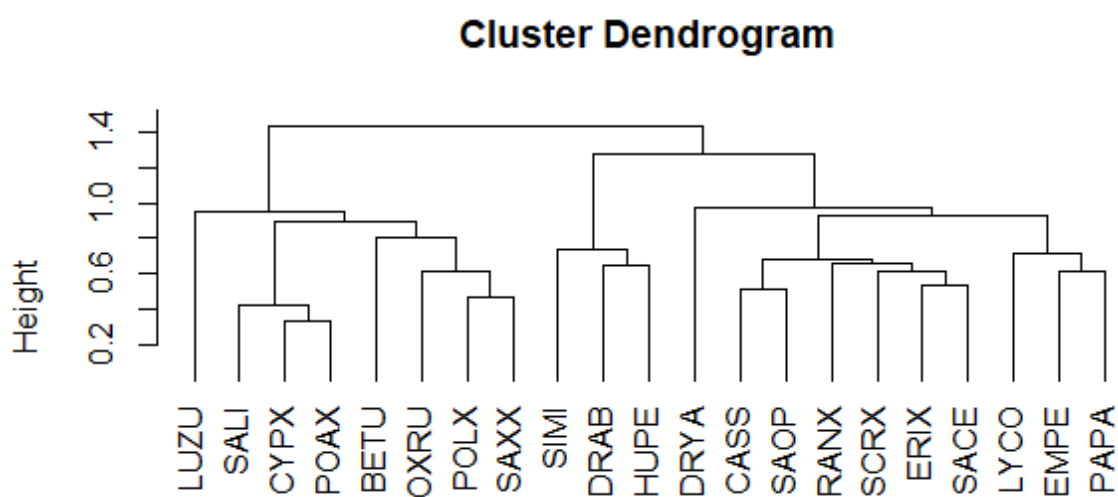


**Figure 53.** Cluster plot based on both Lomsø and ZAC fossil pollen records.

Since the cluster analysis does not provide a clear climatic or ecological sorting of pollen taxa, DCA was performed over the merged pollen data. DCA serves as a valuable tool in paleoecology enabling the exploration of relationships between pollen taxa and environmental gradients without assuming any theoretical distribution of data (Correa-Metrio et al., 2014). When performed on the unified pollen data DCA unveiled a narrow degree of variability within the pollen data as evidenced by the maximum axis length of DCA1 reaching nearly 1.5 SD (table 13).

**Table 13.** Statistical values for the unified fossil pollen based DCA.

	DCA1	DCA2	DCA3	DCA4
Eigenvalues	0.1945	0.121	0.0856	0.0601
Axis lengths	1.4987	1.467	2.0386	1.6304

The DCA distribution of plant communities in Zackenberg is influenced by a combination of environmental factors, primarily soil moisture, temperature, and nutrient availability. The DCA1 axis reflects a soil moisture gradient with plants like *Betula*, *Huperzia selago*, and Ranunculaceae positioned towards the positive end, indicating their preference for moist habitats. In contrast, *Luzula/Juncus* and *Dryas* occupy the negative end, suggesting their preference for harsh tundra environments. Notably, except for low-Arctic *Betula*, all Arctic woody elements cluster towards the negative DCA1 values. The DCA2 axis, while less related, appears to represent a temperature and nutrient gradients. Plants like Ranunculaceae, Saxifragaceae, and *Silene/Minuartia* cluster towards the positive end of DCA2 indicating their association with warmer temperatures and higher nutrient levels. Conversely, *Salix* and Cyperaceae occupy the negative end suggesting their preference for colder temperatures and lower nutrient environments (fig. 54).

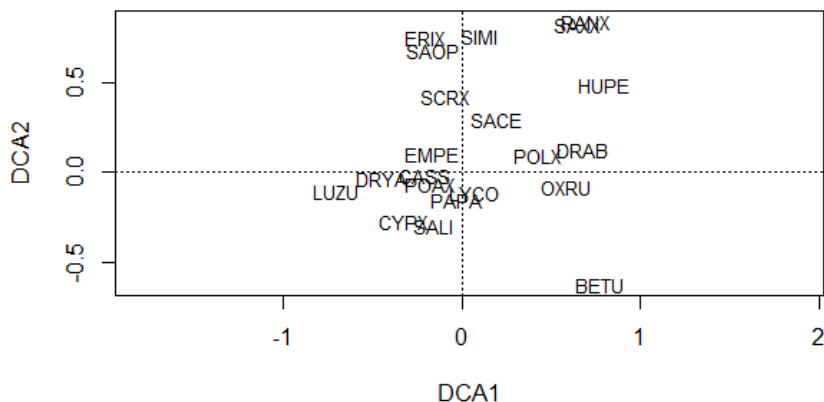


**Figure 54.** DCA plot based on both Lomsø and ZAC fossil pollen records.

Given the DCA1 axis length of almost 1.5 SD, we cannot assume that our data follows a normal distribution since the entire gradient is not captured in the dataset. In this scenario, PCA was employed on the unified pollen data since it is a useful tool for interpreting fossil pollen data helping researchers to uncover patterns and relationships among pollen types when assuming linear data distribution. Table 14 depicts the first five PCA axis. The first component (PC1) explains 51.17% of the variance within our dataset whereas he second component (PC2) captures 14.96% of the variance.

**Table 14.** Statistical values for the first five axis of the unified fossil pollen based PCA.

	PC1	PC2	PC3	PC4	PC5
Eigenvalues	140.4629	41.0661	21.4245	14.307	9.5705
Proportion explained	0.5117	0.1496	0.0781	0.0521	0.0349
Cumulative	0.5117	0.6613	0.7393	0.7915	0.8263

Broken stick test indicates only the first two components represent relevant factors defining our data variance (fig. 55).

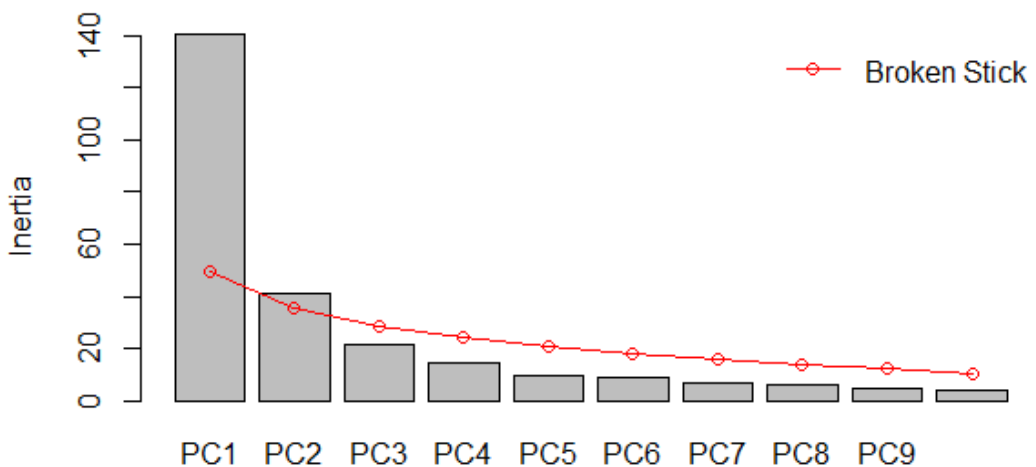


**Figure 55.** Broken stick test plot for the unified pollen-based PCA.

As in DCA, PC1 represents a moisture gradient, with pollen types like *Cassiope*, *Dryas*, and *Huperzia selago* positioned towards the positive end, indicating their preference for drier habitats. Conversely, *Luzula/Juncus* and Polypodiaceae occupy the negative end, suggesting their preference for moister environments. PC2, appears to represent a nutrient gradient. Pollen types such as *Betula* and *Oxyria/Rumex* cluster towards the positive end of this axis, indicating their association with higher nutrient levels. Conversely, *Cassiope*, *Dryas*, and *Saxifraga oppositifolia*-type occupy the negative end of PC2, suggesting their preference for lower nutrient environments. The PCA plot zonation is closely related to that of the cluster analysis and shows an interesting distribution with no pollen taxa placed on the first quadrant, while the second quadrant groups the most important elements during the Early to Middle Holocene. The third quadrant only contains *Luzula/Juncus* and the fourth quadrant groups most of the Arctic heath elements. Based on this, we can say that, even if graphically pollen taxa seem to be very concentrated and doesn't show much variance, soil moisture availability emerges as the primary driver of plant community distribution, as indicated by the strong gradient along the PC1 axis, while nutrient availability plays a secondary role, as suggested by the variation along the PC2 axis (fig. 56).

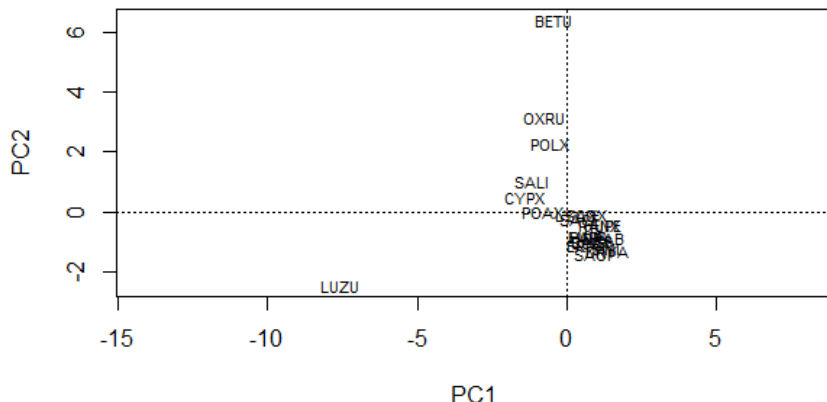


**Figure 56.** PCA plot based on both Lomsø and ZAC fossil pollen records.

When comparing the two independently-made DCA1 curves for the Lomsø and ZAC pollen records a remarkably similar pattern is evident between 1,700 – 200 cal yrs BP, this similarity demonstrates that the driving force behind ecological change operates in the same way and temporal sequence across both records. Lower values represent shorter snow-free periods and low moisture availability, while higher values represent longer snow-free periods and high soil moisture. The length of the snow-free period can be related to precipitation, since it is the main source of snow cover in the valley (Hansen et al., 2008a) and also to temperature, since warm conditions allow the fusion of previously deposited snow, while cold conditions cause the opposite effect. The soil moisture gradient is also influenced by both precipitation – since it is directly related to soil moisture availability – and to temperature since warm conditions are responsible for the redistribution of soil moisture in the valley thanks to snow and ice melt, active layer thawing, among other mechanisms. Based on this, positive DCA1 values are interpreted as a coupling of high precipitation and temperature conditions, allowing for a vast snow-cover to be melted, while negative scores represent more arid or cold conditions, where either precipitation was low so there wasn't much snow to melt, or temperatures were not warm enough to allow the snow to melt. Pollen data shows changes in soil moisture for the recorded period, indicating moister conditions before 7,000 cal yrs BP, with an abrupt decline ca. 6,700 cal yrs BP, paving the way for a more smoothed, oscillating pattern leading to the present, with higher variability observed during the last 500 years (fig. 57).

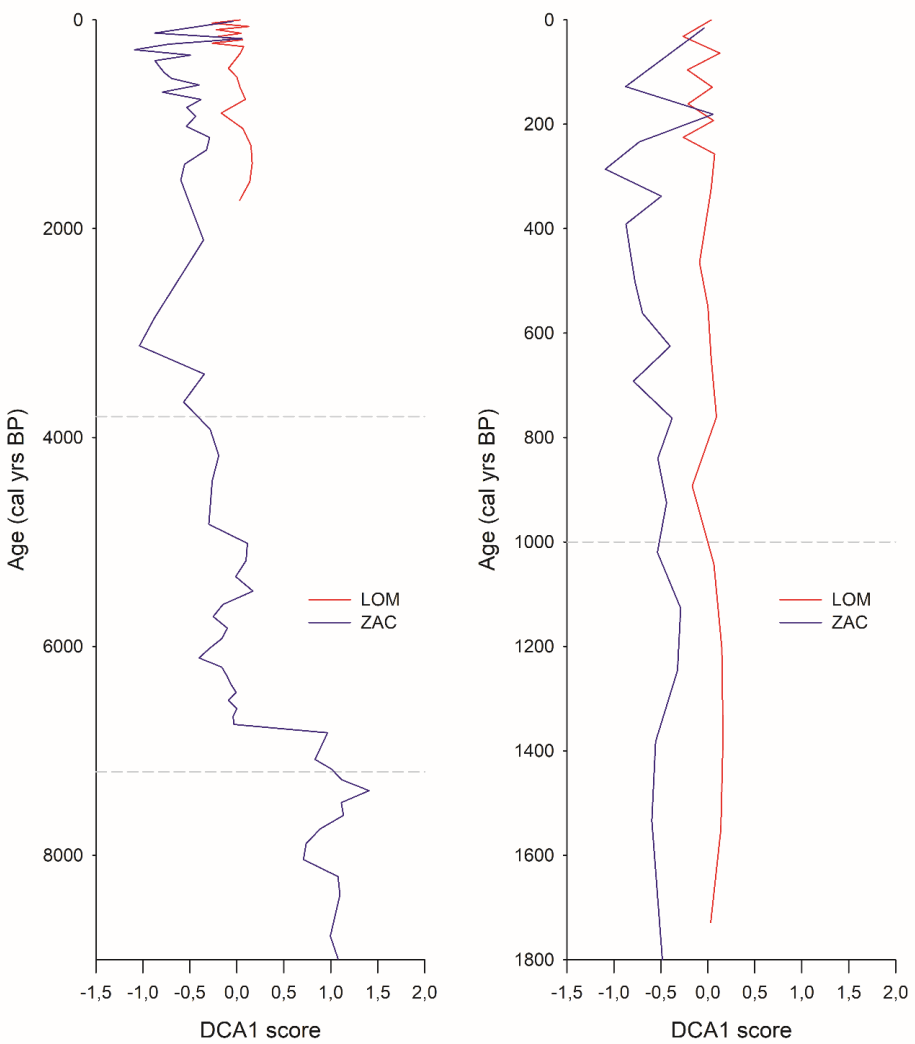


**Figure 57.** Stratigraphical DCA1 plot based on both Lomsø (red) and ZAC (blue) pollen records. The one in the left shows the record from 9,000 cal yrs BP while one in the right shows the record since 1,800 cal yrs BP. Grey dashed lines represent the boundaries between pollen zones.

Euclidian distance, understood as the dissimilarity between two stratigraphically contiguous samples, allow us to identify moments of high ecological change in the record, occurring when a community undergoes significant compositional shifts compared to an immediate early assemblage (Correa-Metrio et al., 2014). The ecological change record depicts a somewhat stable community with low, oscillating patterns. The more substantial ecological change occurred ca. 6,800 cal yrs BP, interpreted as a 25% species turnover. Other notable moments of change are observed around 3,100 and 2,100 cal yrs BP, and during the last 200 years. The Lomsø record

describes a similar pattern between 1,800 and 500 cal yrs BP period, characterized by overall low ecological change (fig. 58).

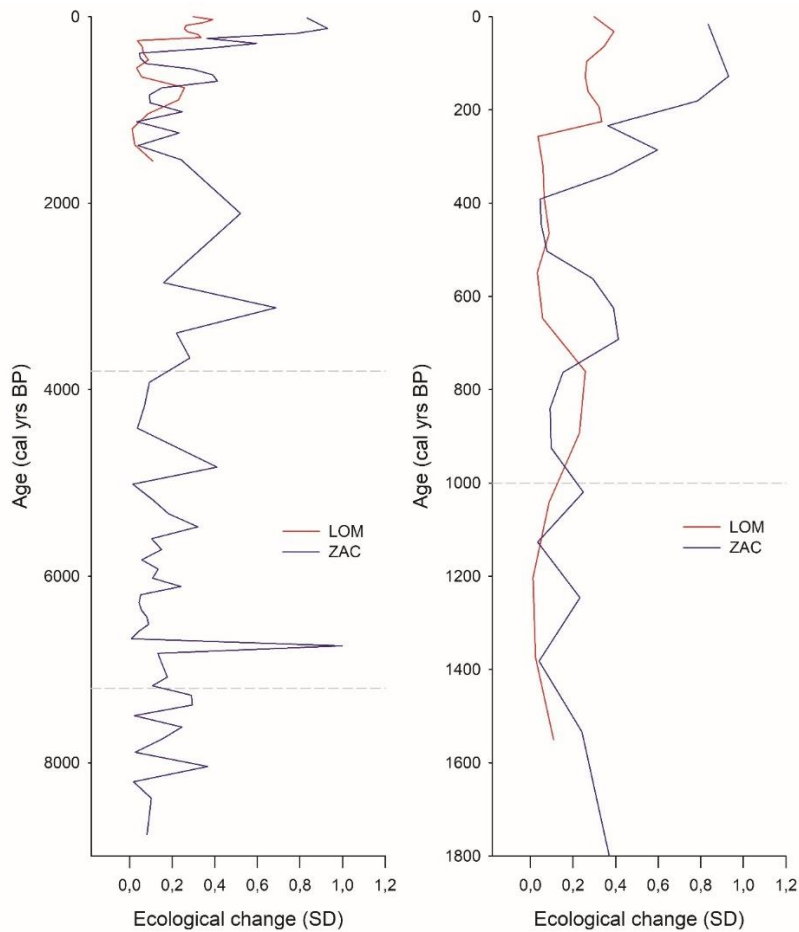


**Figure 58.** Stratigraphical ecological change ( $\beta$ ) plot based on both Lomsø (red) and ZAC (blue) fossil pollen records. The one in the left shows the record from 9,000 cal yrs BP while one in the right shows the record since 1,800 cal yrs BP. Grey dashed lines represent the boundaries between pollen zones.

To a better understanding of the magnitude of each ecological change-triggering event and considering the sedimentation rate, Euclidean distance was normalized by dividing it by the number of years contained in each centimeter. The rate of ecological change plot provides us a clearer picture of the magnitude and temporality of each triggering event. This analysis reveals one significant moment of change ca. 6,700 cal yrs BP, followed by relative ecological stability until ca. 750 cal yrs BP, when communities began experiencing strong ecological change, with a strengthened trend since 250 cal yrs BP. (fig. 59).

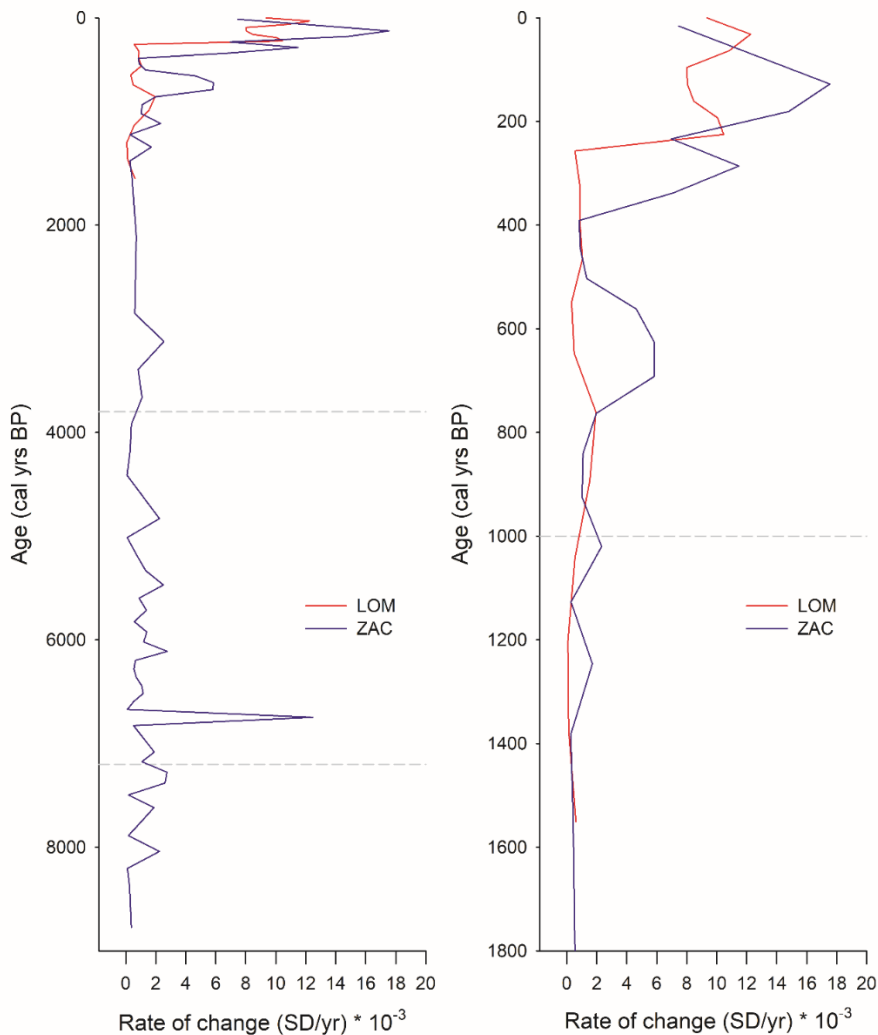


**Figure 59.** Stratigraphical rate of ecological change plot based on both Lomsø (red) and ZAC (blue) fossil pollen records. The one in the left shows the record from 9,000 cal yrs BP while one in the right shows the record since 1,800 cal yrs BP. Grey dashed lines represent the boundaries between pollen zones.

Euclidian distance between each sample and the most recent sample gives us a hint on how different each plant community composition of the past to that of the present was (or the most recent sample in the case of Lomsø). The ecological distance to present plot reveals that the initial vegetation surrounding ZAC lake differed by over 25% in composition from the most recent community captured in the record. This was a slightly greater similarity around 8,000 cal yrs BP followed by increased dissimilarity peaking around 7,400 cal yrs BP. Vegetation in the Zackenberg area became more like today's vegetation abruptly at 6,600 cal yrs BP, followed by a subtle increasing

dissimilarity trend peaking ca. 3,100 cal yrs BP. The Lomsø record shows more stability with Zackenberg's vegetation not variating significantly between 2,300 and 500 cal yrs BP, despite increased variability since 750 cal yrs BP. The ZAC record exhibits a similar trend of increased variability (fig. 60).

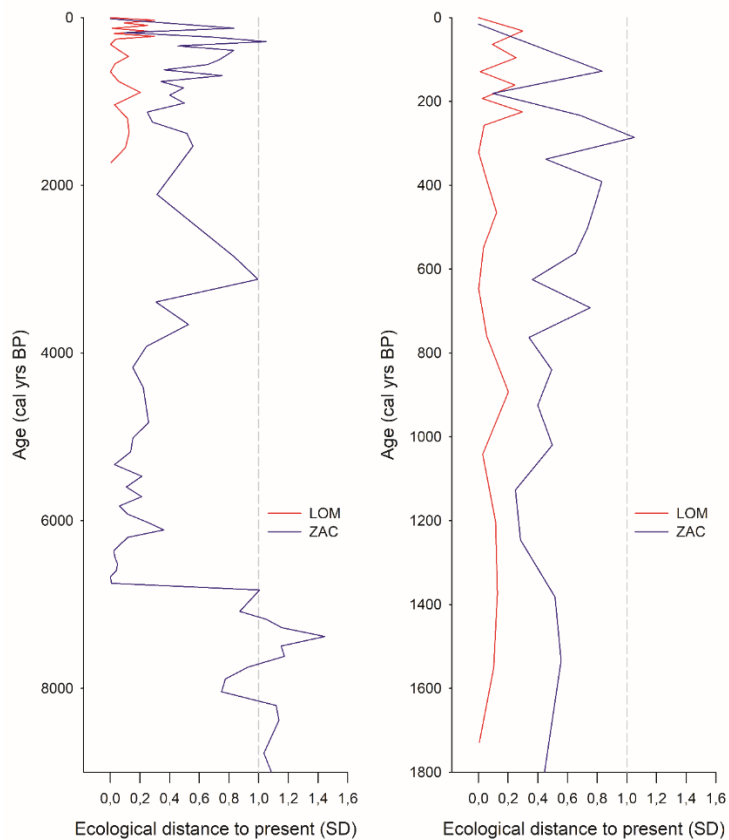


**Figure 60.** Stratigraphical plot depicting the ecological distance towards present-day pollen assemblages based on both Lomsø (red) and ZAC (blue) fossil pollen records. The one in the left shows the record from 9,000 cal yrs BP while one in the right shows the record since 1,800 cal yrs BP. Grey dashed lines represent 1 SD.

#### 4.5. Holocene environmental history of the Zackenberg area

The detailed Holocene history of the Store Sødal and Zackenberg valleys will be discussed based on the three lacustrine sediment records presented in chronological order. The records span different time and complementary. When merged, they show the environmental evolution from landscapes recently deglaciated, dominated by pioneer plants adapted to harsh climates. This phase is followed by the colonization by

low-Arctic components, represented by *Betula* (most probably dwarf birch *Betula nana*) under warmer conditions during the Mid-Holocene. The Late Holocene is characterized by a *Luzula/Juncus* tundra dominance, with increased variability observed during the last millennia (fig. 61 and 62).

#### 4.5.1. Glacial to warm Early to Middle Holocene (12,000 – 7,200 cal yrs BP)

During the Pleistocene-Holocene transition, the vegetation of Wollaston Forland was composed by few herbaceous species as *Oxyria digina* and *Papaver radicatum* (Bennike et al., 1999). The ZAC record begins around 12,200 calibrated years BP, extending back to the glacial origins of the lake basin. The grayish facies and geochemical data of Unit A indicate that a significant number of silty materials were transported to the recently formed lake by low-energy glacial meltwater stream currents, around 10,500 calibrated years BP. These glacial deposits suggest accumulation by decantation of suspended fine material formed from episodes of "milky" plumes into the lake during fluvial floods. These tardiglacial conditions gradually decreased to the Unit B, marked by abrupt decreases at 10,000 and 9,000 calibrated years BP, when pollen sedimentation became significant. Christiansen et al. (2002) proposed that in the outer portion of the Zackenberg valley, the Zackenberg delta began accumulating at 30 m asl around 9,500 years BP (Christiansen et al., 2002).

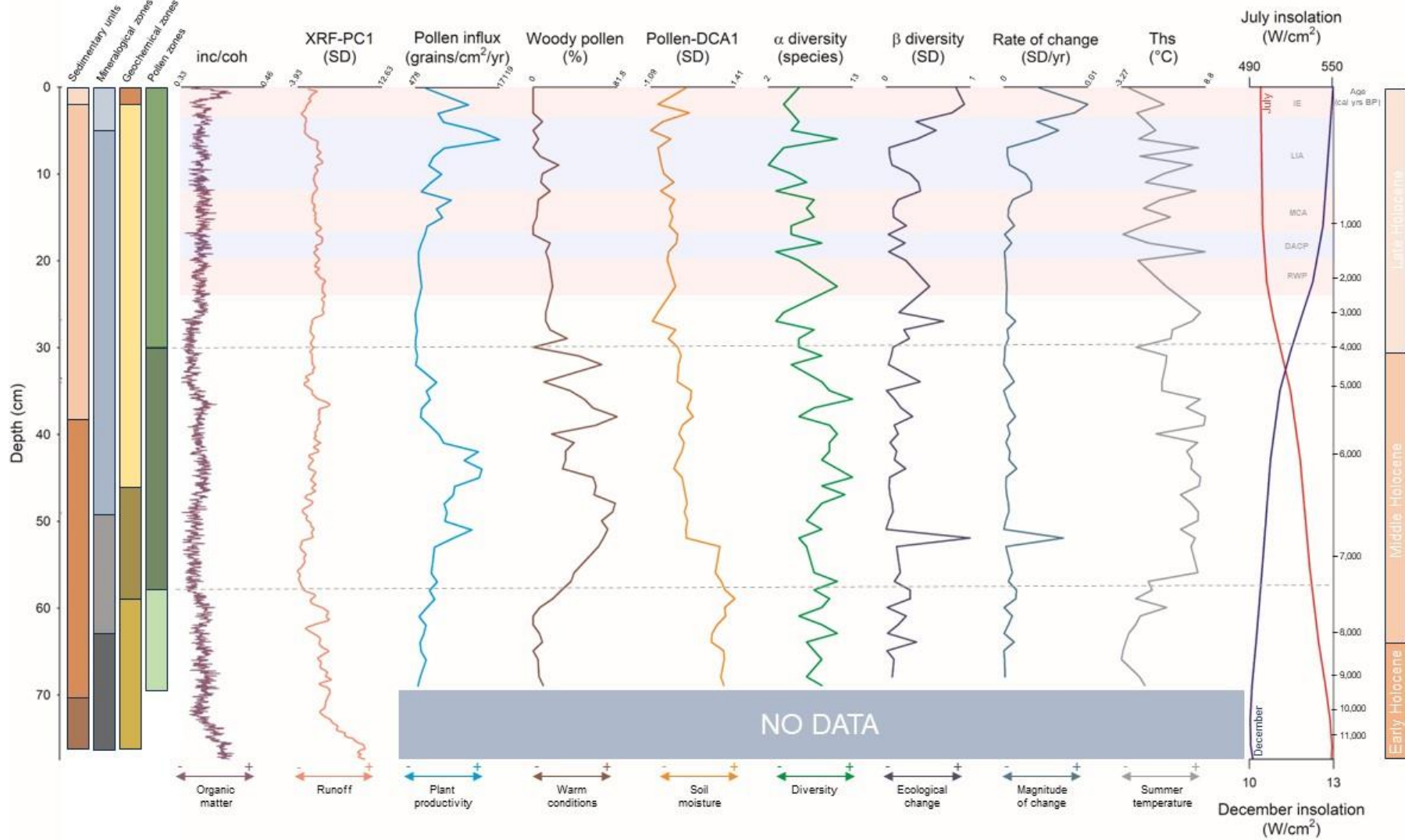


**Figure 61.** Stratigraphical plot of sediment core ZAC19\_06\_02 multi-proxy data. Dashed lines represent the boundaries between pollen zones.

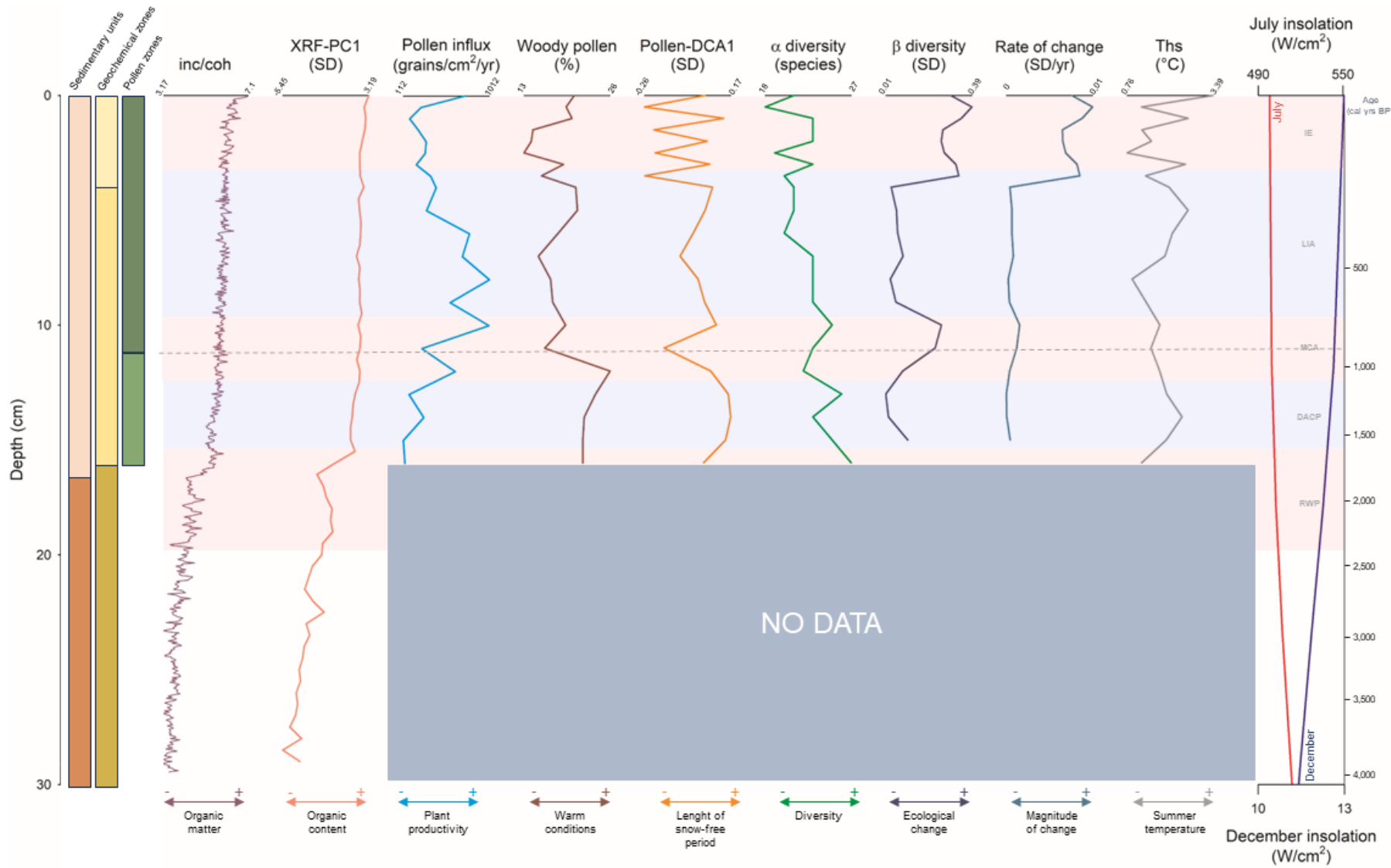


**Figure 62.** Stratigraphical plot of sediment core LOM18\_02 multi-proxy data. Dashed lines represent the boundaries between pollen zones.

The flora that surrounded lake ZAC 9,000 cal yrs BP was scarce as shown by the low pollen influx, and was dominated by herbs, mainly Cyperaceae, indicating the colonization of the basin by sedges under  $Ths$  about 0°C and high soil moisture, persistent for most of the period. Ericaceae pollen probably represents *Empetrum nigrum*, the first dwarf shrub to arrive to E Greenland and whose importance seemed higher in the Early Holocene than today is associated to warm summers (Bennike et al., 1999). A cooling trend was accompanied by increasing NPPs, decreasing spores and the irruption of high-Arctic pioneer elements such as *Oxyria/Rumex*, Poaceae, *Papaver* and Caryophyllaceae representing the scarce flora typical of recently deglaciated terrain with high nutrient availability. Between 9,000 – 8,300 cal yrs BP the inner area of the Zackenberg was characterized by pioneer open vegetation dominated by *Saxifraga oppositifolia*, also including *Oxyria*, *Silene*, *Minuartia* and *Ranunculus* among others (Bennike et al., 2008).

The decreasing trend in illite content from bottom to top indicates a progressive decrease in  $Ths$  reaching minimum of -3.26°C ca. 8,300 cal yrs BP, due to overall decrease in the weathering intensity and permafrost thawing, thus resulting in decreased sediment input to the lake. In the inner Zackenberg valley, this transition was determined by the first appearance of pollen from *Salix arctica* and *Salix herbacea*. Also new for this period are *Thalictrum alpinum*, *Tofieldia* sp and *Campanula* sp. (Bennike et al., 2008). Marked by a decrease in low-Arctic elements such as Cyperaceae and an increase in polar elements as *Papaver* linked to the 8.2k event. The vegetation succession that followed the 8.2k cooling event marks a deeper active layer, marking the end of the Greenlandian stage and the onset of the Middle Holocene (Cohen et al., 2013). The gradual temperature increase was accompanied by an increase in *Oxyria/Rumex*, a decline in pteridophytes and the appearance of *Salix* to the region around 7,500 cal yrs BP when  $Ths$  reached 3.21°C. It is proposed that these climate conditions allowed the development of *Salix* heaths in the area during the Early Holocene. Subsequently, a cooling pulse around 7,400 cal yrs BP induced significant vegetation changes, leading to the representation of woody species and the absence of high-Arctic tundra indicators such as Saxifragaceae – particularly *Saxifraga oppositifolia* – various Caryophyllaceae, *Dryas* and most pteridophytes.

The Zackenberg deltaic system was formed during the high stand eustatic phase of the Holocene interglacial period. However, the retreat of the glacier in Greenland around 10,500 yrs BP triggered a regional isostatic rebound, resulting in decreasing sea levels in the area during the Early Holocene. The presence of *Empetrum nigrum* macrofossils and Southern Greenland beetle assemblages in Zackenberg sediment confirm development of heathlands during the Early to Middle Holocene under climate conditions warmer than those observed today (Bennike et al., 2008, 1999). The deglaciation process led to the accumulation and the subsequent elevation of the Zackenberg delta, recording a transition from a salty marine deposit to fluvial sand and gravel deposits between 9,500 – 6,300 cal yrs BP (Christiansen et al., 2002). Fluvial channel sediments from the Zackenberg valley accumulated after the generation of low slopes during the Early Holocene's post glacial sea level fall, suggesting marine influence in the lower part of the valley between 8,500 and 8,100 cal yrs BP (Cable et al., 2018). Increased erosion related to active layer deepening occurred between 8,300 and 7,200 cal yrs BP in the region, with moisture progressively increasing through the Middle Holocene (Christiansen et al., 2002). Pioneer vegetation flourished on the valley floor until 7,300 years BP, under summers conditions warmer than today (Bennike et al., 2008). The abundance of plant macro remains discovered in the Zackenberg delta between 7,400 and 7,300 years BP indicates a period of exceptional plant growth (Christiansen et al., 2002). Bennike et al. (2008) document the occurrence of pioneer vegetation resembling that of Northern Greenland in the inner part of the Zackenberg valley until 7,300 cal yrs BP (fig. 63).

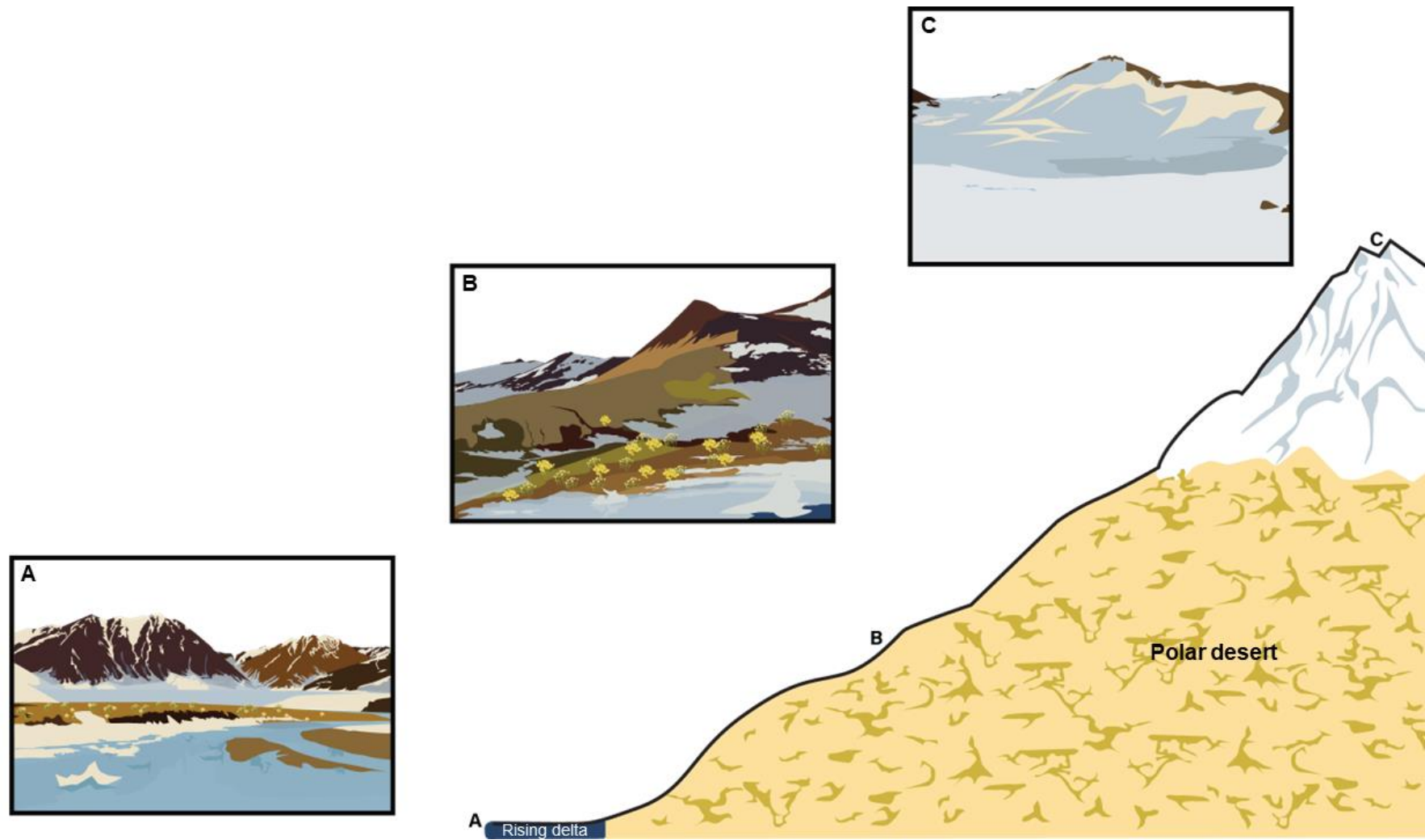


**Figure 63.** Hypothetical altitudinal profile based on the environmental reconstruction of the Zackenberg area between 9,000 and 7,200 cal yrs BP. A: Lomsø Lake, B: ZAC Lake, C: Aucella Lake.

#### 4.5.2. Warm Middle Holocene (7,200 – 3,800 cal yrs BP):

Middle Holocene deltaic deposits of the study area contained *Empetrum nigrum*, *Salix herbacea* and beetle *Phratora polaris*, accompanied by plenty of organic sediment reflecting a warming trend (Christiansen et al., 2002). During this period, the ZAC basin was productive, and the ZAC lake was in oligotrophic state, with low siliciclastic inputs from ca. 7,200 cal yrs BP, characterized by low Al, Si, K, Ca, and Ti content. River fan cryostratigraphy of the valley reveals that permafrost continuously aggraded in response to sedimentation. Warming events like the HCO are associated with increased precipitation, a deeper active layer, and the degradation of permafrost on ice-rich slopes, potentially leading to greater mass loss (Cable et al., 2018).

The replacement of high-Arctic from herbaceous flora in the valley to dwarf shrub heaths – especially low-Arctic *Betula* heaths – occurred under drier-than-before and warmer-than-today conditions. In this regard, palynological evidence indicates that *Betula nana* arrived to Greenland ca. 8,800 cal yrs BP, implying these conditions were present before the timing of pollen diagrams due to a lag in the arrival of indicator species to the valley (Bennike et al., 2008; Funder, 1978). *Ths* averaged 6.9°C between 7,000 and 5,000 cal yrs BP. Warmer summers during the Middle Holocene are also reported by Bennike et al. (2008, 1999) in the study area. The vegetation composed of up to 70% of woody taxa during two notable periods: 6,800 cal yrs BP, coinciding with the moment of maximum *Betula* expansion, and the second of highest ecological change event of the Holocene in the area, and 5,500 cal yrs BP, coinciding when the record-high *Ths* of 8.89°C were reached. Around 6,600 years BP a thickening in the active layer and increased rainfall occurred in the valley (Cable et al., 2018). The peak of pollen influx during the Mid-Holocene – interpreted as the highest vegetation productivity in the Store Sødal valley – occurred ca 6,000 cal yrs BP. This phase is characterized by the coexistence of herbaceous high-Arctic tundra with woody thermophilus low-Arctic elements. The warmer-than-today conditions are also supported by the presence of exotic *Pinus* grains. Those pollen grains are exogenous to NE Greenland and can only come from southern continental landmasses and brought

to the region by warm southern winds. The Boresø record in the inner part of the Zackenberg valley describes a cooling period started during the Middle Holocene, marked by a decline in summer temperatures and precipitation between 5,500 and 4,500 cal yrs BP (Bennike et al., 2008). These colder conditions are also present in our temperature reconstructions.

Previous studies have documented the presence of a persistent snowpack on Aucella Mountain since the Early to Mid-Holocene (Cable et al., 2018). The sensitivity of snow cover to changes in isotherm elevation is primarily influenced by summer temperatures, suggesting that the relationship between Aucella-derived geochemical PC1 and the July insolation curve reflects summer climate conditions (Garcia-Oteyza et al., 2024). Beginning around 5,000 cal yrs BP, the high-altitude Aucella record indicates relatively warm conditions with a low but consistent input of terrigenous material to the lake. This implies that the lacustrine system experienced seasonal ice-free periods. The prevailing oxidative conditions and high chlorophyll levels during this period, indicative of substantial biomass, imply that at least the littoral zone of the lake thawed, allowing nutrient influx into the system. The chlorophyll values suggest reduced snow accumulation on the lake ice cover, consistent with drier conditions during the Mid-Holocene. The deposition of recently formed clay, with its high biomass-related content, points to enhanced rates of organic matter productivity, likely attributed to the shorter ice-cover duration compared to other NE Greenland (Garcia-Oteyza et al., 2024). In Eastern Greenland, 4,500 yrs BP marks the most conspicuous change since the last glaciation, initiating the colder phase of the Holocene characterized by varying but permanent summer sea ice cover in the polar basin, strengthened influence of regional climate modes and neoglacial activity(Jakobsen et al., 2008; Jomelli et al., 2016). It also marks the arrival of the first humans to Zackenberg (Bennike et al., 2008). After the climatic optimum in the area at 5,000 cal yrs BP, the ZAC lake become shallower, runoff was reduced and *Ths* abruptly decreased to values lower than present, leading to a decrease in pollen influx and the collapse of *Betula* and species diversity. The declining *Betula* pollen trend is also described in the Boresø record, while *Cassiope*, *Salix arctica*, *Saxifraga oppositifolia* and *Oxyria digyna* increased, indicating the extent of snow beds and snow-protected

heathland. (Bennike et al., 2008). This favored the hegemony dominance? of the *Luzula/Juncus* in the ZAC record and the subsequent expansion of *Salix* snow beds along with Cyperaceae and ferns ca. 4,300 cal yrs BP followed by a cooling pulse ca. 4,000 cal yrs BP, marked by the decrease in heath elements and the expansion of Poaceae and *Papaver*, reaching 1.16°C in summer. Gilbert et al., (2017) indicates Zackenberg delta stabilization around 4,500 cal yrs BP, synchronous with the onset of fluvial sedimentation in the abandoned delta, marking the beginning of the Lomsø record (fig. 64).

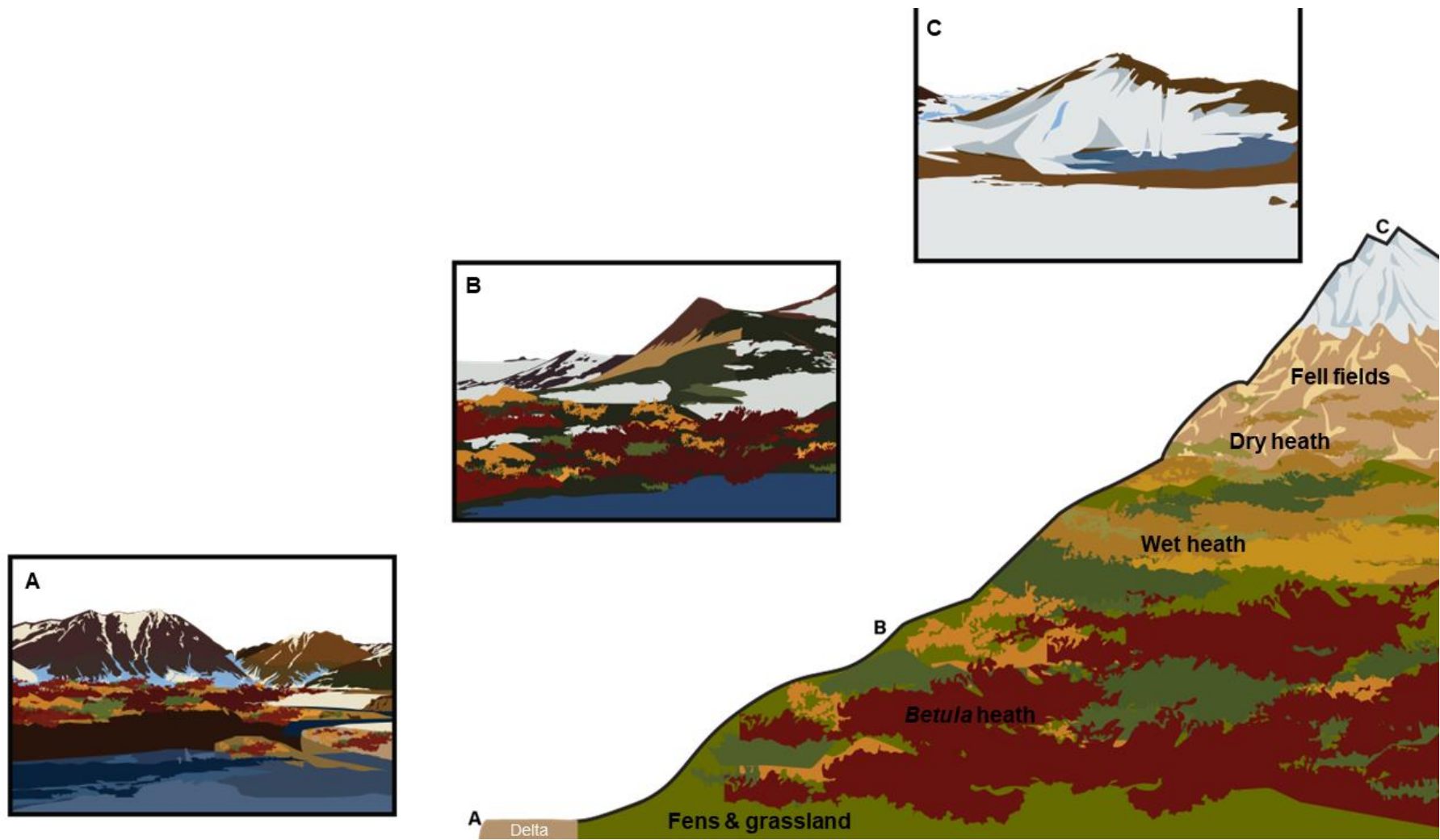


**Figure 64.** Hypothetical altitudinal profile based on the environmental reconstruction of the Zackenberg area between 7,200 and 3,800 cal yrs BP. A: Lomsø Lake, B: ZAC Lake, C: Aucella Lake.

#### 4.5.3. Colder Late Holocene, establishment of tundra environments (3,800 – 2,400 cal yrs BP):

Most high-Arctic Greenland pollen records don't go further on interpretation of Late Holocene vegetation, probably because of the general decrease on sedimentation rate during this period (Bennike et al., 2008; Fredskild, 2000, 1995; Funder, 1978; Wagner, 2000; Wagner et al., 2008; Wagner & Melles, 2002, 2001, among others). However, in vegetated areas, Late-Holocene high-Arctic tundra prevailed, displaying significant changes in pollen assemblages over the last 200 years. In the high-mountain Aucella record, the most abrupt transition took place between 3,800 and 3,400 cal yrs BP, marked by a surge in terrigenous sediment input suggesting a shift towards colder and moister conditions. This environmental change enhanced the transport of primary elements and chemically unaltered rock particles into the lake catchment, increasing turbidity and limiting light penetration, consequently affecting diatom diversity (Garcia-Oteyza et al., 2024).

At Zackenberg, summer air temperatures plummet further, wind processes intensify, and snow cover persists until 3,500 cal yrs BP, as reconstructed from lake sediments in Lake Boresø (Bennike et al., 2008). In contrast, between 3,400 and 2,400 cal yrs BP, the sedimentary record of Aucella indicates warming conditions accompanied by a sustained input of weathered terrigenous material. During this period, snow patches continued to dominate the landscape, with limited ice cover confined to specific areas of the lake. This partial snow cover allowed the entry of some material as evidenced by particles grain size analysis. However, the consistency of low chlorophyll content suggests that significant snow cover persisted, maintaining turbid conditions. The same warming trend is observed in the ZAC basin at an elevation over 200 m asl., where expansion of *Luzula/Juncus* and the disappearance Poaceae likely occurred under warming and slightly less moist conditions. An aridity peak ca. 3,100 cal yrs BP is evident and could be explained by increased Scrophullariaceae and the constant but variable presence of dwarf shrubs, reaching 8°C ca. 2,900 cal yrs BP. Extended nivation activity and covered podzol conditions on the Zackenberg delta began around 2,900 cal yrs BP showing strengthened northern winds during winter (Christiansen et

al., 2002). Supporting this, the climate in the Store Sødal valley turned colder as evidenced by a slight decrease in *Luzula/Juncus* -led grassland and fens and the expansion of cold and dry elements linked to *Cassiope tetragona* heaths, along with high-Arctic companions such as *Saxifraga cespitosa* as other Saxifragaceae ca. 1,500 cal yrs BP. On coastal lowland Zackenberg, fluvial deposition remained constant for approximately two millennia (Unit A) until 2,400 cal yrs BP when sea-ice level reached present-day values, as evidenced by nival deposit overlaying delta deposits in the lower part of the valley (Christiansen et al., 2002) (fig. 65).

#### 4.5.4. Roman Warm Period (2,400 – 1,600 cal yrs BP)

While the RWP, as its name suggest, is associated to warm conditions, it brought a decrease in diatom species diversity in Aucella, as reflected by the diatom index and multivariate analysis. Aucella-PCA trends during this period shifted towards negative values, indicating a transition to colder conditions due to thicker or longer ice cover until 2,000 cal yrs BP. However, between 2,000 and 1,100 cal yrs BP, a warming and drying trend predominated in the higher elevations. The recorded increase in temperature coincided with a decrease in grain size and terrigenous input, alongside higher chlorophyll content and greater diatom diversity. These changes suggest longer ice-free periods during the summer. In the Store Sødal valley, vegetation dominated by *Luzula/Juncus* remained resilient with herbaceous tundra elements under oscillating conditions marked by the expansion of fens and grasslands represented by Poaceae and Cyperaceae and dry *Dryas* and *Cassiope* heaths. The onset of fine-grained sedimentation in the Lomsø Lake started ca. 2,000 cal yrs BP. The presence of large-scale ice-wedge polygons and palsas in the lowlands of Zackenberg indicates a strong permafrost influence, allowing thermokarst-like sedimentation (Bouchard et al., 2020; Christensen et al., 2021; Gilbert et al., 2017). Thermokarst lakes have an overall important role in the hydrology, biogeochemistry, and geomorphology of Arctic deltas, formed by water ponding in topographic depressions, resulting by ice-wedge melting

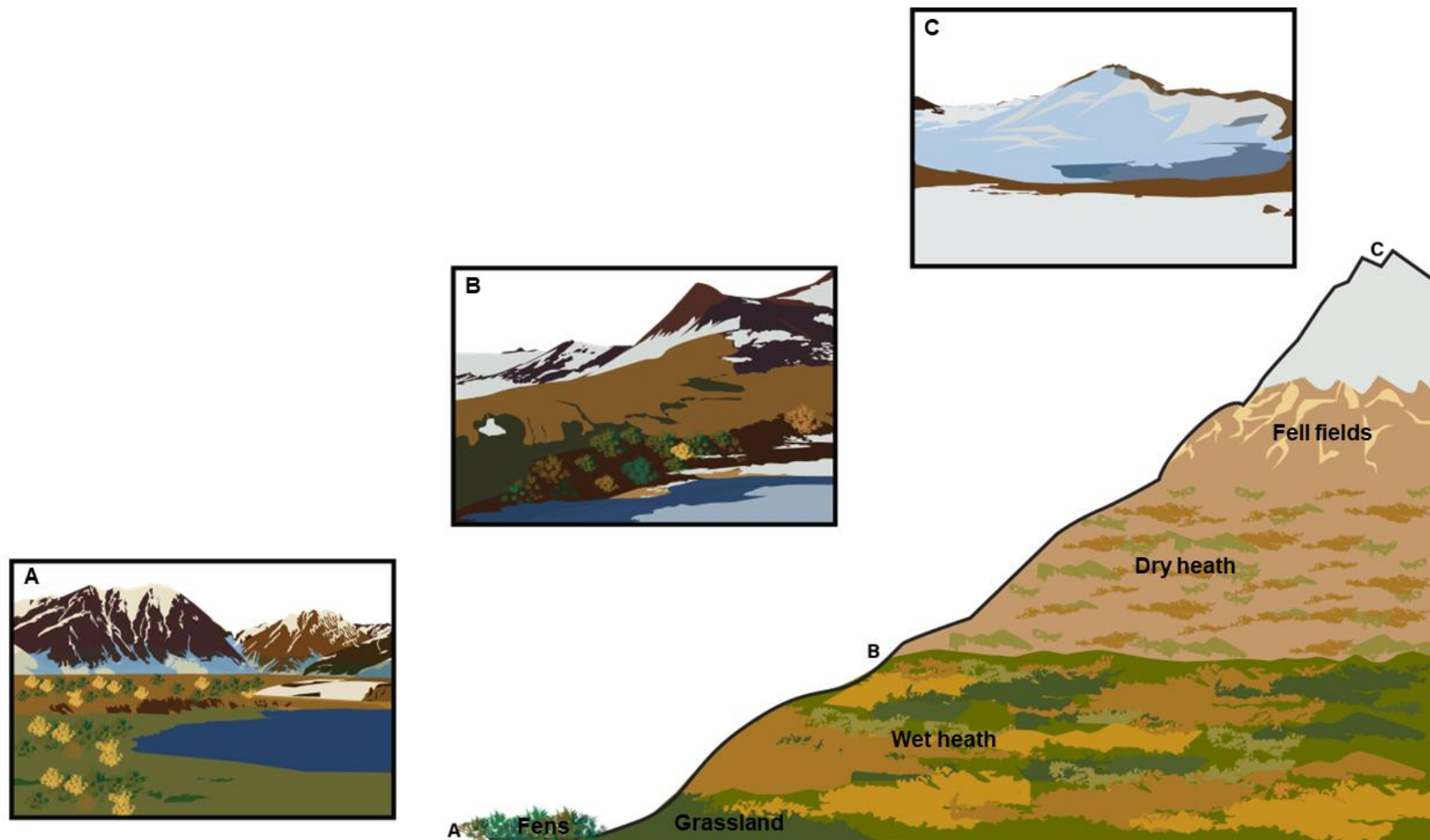


**Figure 65.** Hypothetical altitudinal profile based on the environmental reconstruction of the Zackenberg area since 3,800 cal yrs BP. A: Lomsø Lake, B: ZAC Lake, C: Aucella Lake.

(de Klerk et al., 2014; Overeem et al., 2022). Thaw subsidence resulted in sinking of the delta plain, enhancing thermokarst sedimentation and, consequently, lake development since 1,900 cal yrs BP. Figure 66 illustrates the inception and development of a theoretical thermokarst lake.

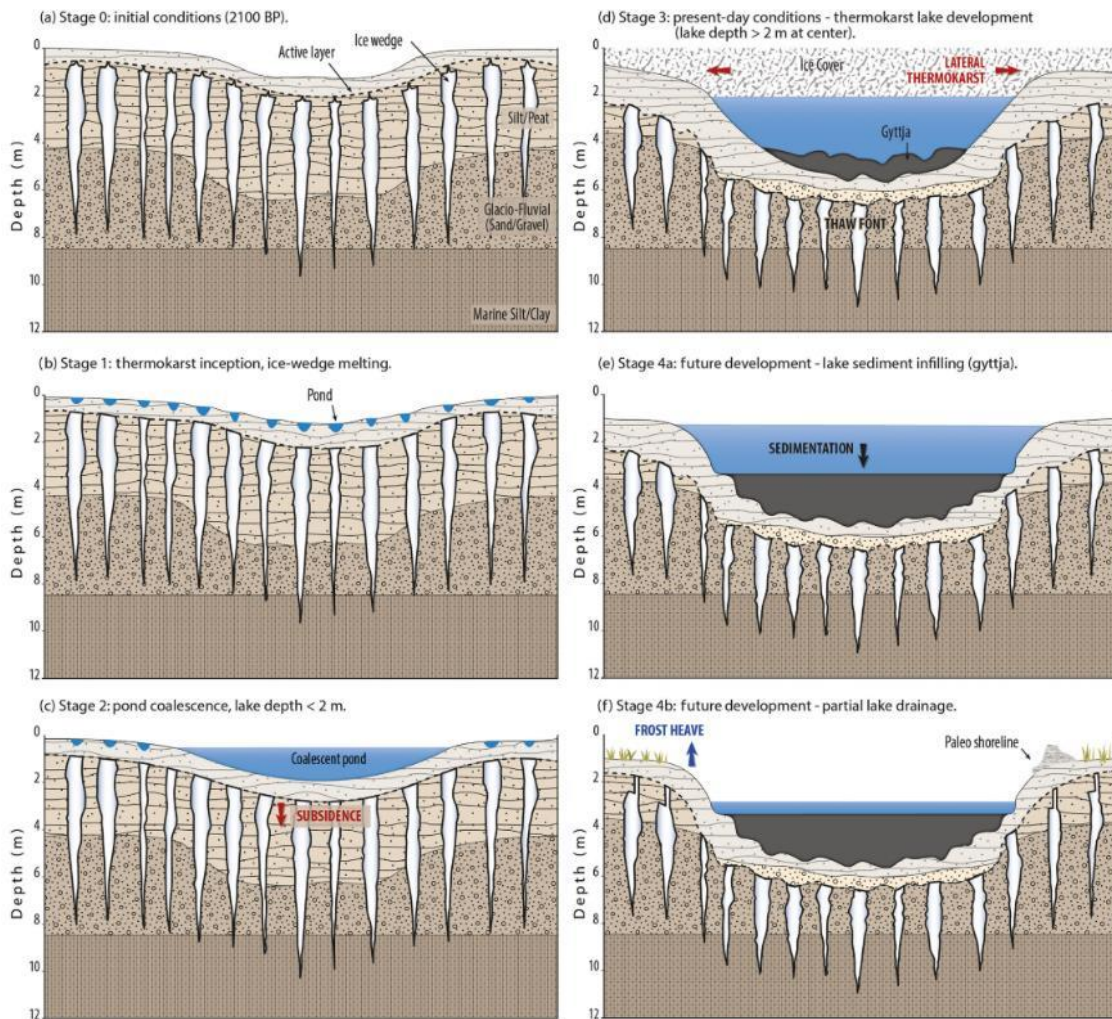


**Figure 66.** Model of a thermokarst lake inception. Source: (Bouchard et al., 2020).

The Lomsø pollen record begins ca. 1,800 cal yrs BP and shows the persistence of an already established high-Arctic tundra dominated by *Luzula/Juncus* and Cyperaceae. This is accompanied by woody elements as secondary components with constant concentrations of *Salix* and Ericaceae under moister conditions than present-day, and with initial temperatures lower than today ( $1.22^{\circ}\text{C}$ ) in the lower, outer areas of the Zackenberg valley.

#### 4.5.5. Dark Ages Cold Period (1,600 – 1,100 cal yrs BP)

The high mountain Aucella record describes the continuation of the warm period since 2,000 cal yrs BP while the ZAC pollen record shows low pollen influx and the expansion of *Luzula/Juncus* and *Saxifragaceae*, related to cold climate. In contrast, lowland Zackenberg, summers became warmer, reaching 2.44°C ca 1,400 cal yrs BP related to rise in *Poaceae* and *Cyperaceae* and a subsequent increase in woody elements synchronous with the rise in pollen influx until 1,000 cal yrs BP, when aquatic mosses disappear from the record. Therefore, a complex climate evolution took place with cold summers at medium altitude and highly fluctuating ones at low altitudes.

#### 4.5.6. Medieval Climate Anomaly (1,100 – 700 cal yrs BP)

The most notable shift in pollen stratigraphy at the end of zone LOM-I (1,000 cal yrs BP) may be associated with a change in wind/water pollen transport ratio (Jakobsen et al., 2008), favoring local *Luzula/Juncus* vegetation surrounding the lake. The disappearance of *Hippuris* – the sole aquatic taxa found on the record – from pollen records can be interpreted because of thicker ice cover eroding its habitats in shallow water, coinciding with decreasing summer temperatures and glacial readvance (Briner et al., 2016; Jakobsen et al., 2008). Following this point, *Luzula/Juncus* dominance was strengthened, with *Ths* around 1.5°C. From this moment, enhanced southern winds dominated this area based on the constant presence of exotic pollen, with the *Botryococcus* peak ca 900 cal yrs BP marking a dry event.

Despite generalized decrease in pollen influx after this period, *Luzula/Juncus* did not experiment influx decrease, on the contrary, it became by far the most dominant taxa for the rest of the record, indicating the expansion of herbaceous vegetation with thriving *Juncaceae*. The expansion of herbaceous fen vegetation and stable *Salix* abundance indicate humid conditions with snow-protected vegetation and saturated soils. The high sedimentation rate on zone LOM-II, reaching record peaks, is related to warmer *Ths* reaching record peaks, leading to more snowmelt, thermokarst

sedimentation, and consequently, sediment input (de Klerk et al., 2014; Jakobsen et al., 2008).

#### 4.5.7. The Little Ice Age (700 – 200 cal yrs BP)

Temperatures reached their minima during this period, and diatom assemblages exhibited low diversity, likely linked to the increased thickness and duration of ice cover. Both pollen records depict *Luzula/Juncus*-led tundra with changes in secondary elements, featuring pulses of expansion of heathlands and polar elements, exaggerated by the transfer function due to *Ths* values being based on other taxa different than the dominant one. Despite inaccuracies in magnitude and misalignment in sedimentation rates, this period shows increased variability in geochemical composition and diversity indices.

The ZAC pollen record shows the persistence of herbaceous vegetation under relatively dry and oscillating temperatures, describing an increasing trend in pollen influx towards the end of the period, coinciding with increased diversity. While Christiansen (1998) reports strengthened nival activity during the LIA in Zackenberg, the Lomsø record describes a warming trend starting ca. 500 cal yrs BP when temperatures rose from 0.93°C under the maximum expansion of reed lands, reaching 2.7°C ca 300 cal yrs BP. This was followed by a period of instability reflected in both pollen and diatom content, with significant ecological changes and thermal and moisture oscillations marked by the minimum concentration of low-Arctic plants ca. 300 cal yrs BP.

#### 4.5.8. Recent Global Warming (200 cal yrs BP – present):

This cooling trend during the LIA is reversed towards the present, showing an expansion of dwarf-shrub taxa, especially (unidentified) Ericaceae, decreasing cold elements such as *Saxifraga* or *Papaver*, and re-peaking influx due to warmer summers, reaching present-day values and shorter-lasting snow patches. A similar trend can be observed in several proxy based Holocene records from Eastern Greenland where several studies detect increased organic input and plant activity manifested as both

latitudinal (northwards) and altitudinal (upwards) expansion of woody vegetation (Klug et al., 2009; Schmidt et al., 2011; Wagner, 2000; Wagner et al., 2005, among others). And

The Aucella Lake sediment record concludes with an abrupt change, characterized by higher diatom diversity and warmer conditions featuring thin ice cover and longer ice-free periods. This abrupt temperature increase almost reached MCA values, accompanied by larger sediment grain size and higher chlorophyll content. These changes suggest a rise in temperatures and high turbidity environments, reflecting the recent climate warming observed at high latitudes (Garcia-Oteyza et al., 2024). Geochemical analysis revealed that ZAC had high content of Mn and Fe, indicating oxidative conditions in the lake water column where ice cover lasted short periods of time and the melting process was enhanced. The pollen record shows the highest ecological change in this period with an influx peaking ca. 300 and 200 cal yrs BP, coinciding with the maximum expansion of reed lands. Reedlands dominate present-day tundra vegetation along with Poaceae and Cyperaceae above 200 m asl. in the Store Sødal valley indicating cold climatic conditions and extensive snow-beds, in concordance with Late Holocene record of Boresø on the inner part of the Zackenberg valley (Bennike et al., 2008). The intermittent human settlements disappeared probably because of poor hunting conditions when the minimum *Ths* was recorded in Lomsø ca. 200 cal yrs BP (0.77°C). This event was followed by the highest *Ths* on the top sample of the record, surpassing 3°C, marking the maximum expansion of Ericaceae and Poaceae, representing the tundra mosaic currently developing in the Zackenberg valley.

#### 4.6. Paleoclimatic implications

This section aims to discuss the main paleoclimatic aspects of this research's environmental reconstruction and will center on the Holocene temperature evolution and NAO/AO inferences. Location of the quantitative climate reconstructions compared in this section is depicted in fig. 67.



**Figure 67.** Distribution of the climate reconstructions discussed in this section.

The ZAC *Ths* curve initiates at ca. 9,000 cal yrs BP and shows an initial cooling trend evident in most S and E Greenland temperature reconstructions as well as in the EastGRIP (Buizert et al., 2018; Gajewski, 2015a) (fig. 68).

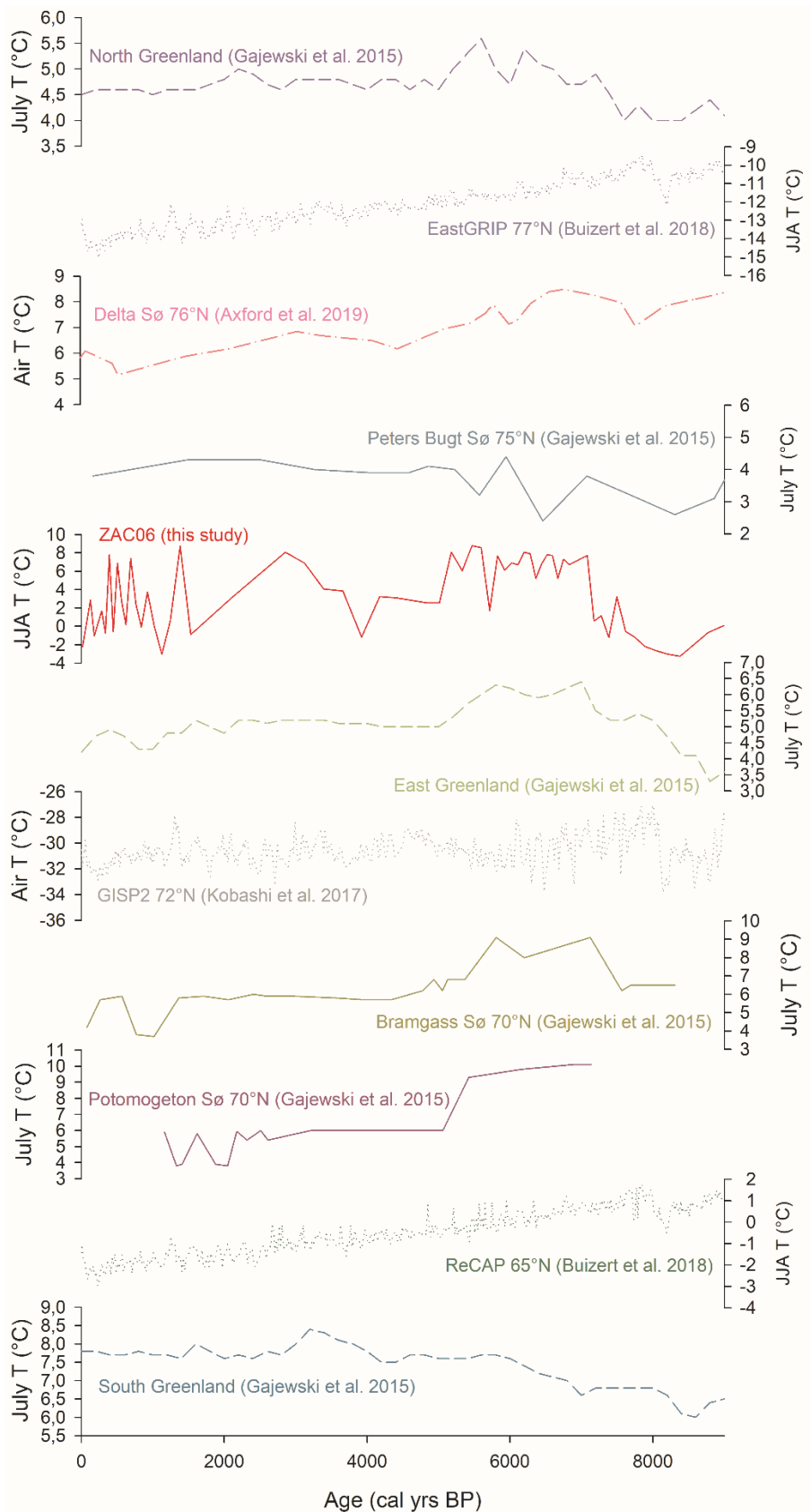


**Figure 68.** Comparison of ZAC19\_06\_02 *Ths* record with other regional records for the last 9,000 cal yrs BP.

This first zone is characterized by dry and cold conditions which are interpreted as NAO<sup>+</sup> conditions coupled with weak AMOC peaking around the 8.2k cold event . The presence of *Pinus* pollen ca. 7,800 cal yrs BP indicates the occurrence of NAO<sup>-</sup> pattern allowing the entrance of southerly winds transporting woody exotic pollen from forested areas. After this, the warming pulse recorded in ZAC ca. 7,500 cal yrs BP synchronizes with the formation of podzols in the Zackenberg valley, occurring under temperatures and precipitation higher than today (Christiansen et al., 2002). This marks the establishment of generalized NAO<sup>-</sup> conditions allowing the flourishing of *Betula* heaths.

Summer temperatures in the Wollaston Forland region remained higher than present values, allowing thermophilus low-Arctic elements to colonize the valleys at 74°N, indicating a local HCO between 7,000 – 5,000 cal yrs BP (Bennike et al., 2008). This contrast with other evidence and HCO dated around 8,000 cal yrs BP in Greenland Ice cores and lasting between 8,300 and 7,300 cal yrs BP in the Zackenberg Valley (Bennike et al., 2008; Vinther et al., 2009). Unified and independent temperature reconstructions for Eastern Greenland proposed by Gajewski (2015) record the highest July temperatures between 7,500 and 5,500 cal yrs BP. This period of generalized NAO<sup>-</sup> conditions that allowed warm southern winds to penetrate the region and weakened AMOC causing less sea-ice cover was interrupted by a dry event ca. 6,800 cal yrs BP, which symbolizes one of the sharpest moments of ecological change during the Holocene, and a cold event ca. 5,800 cal yrs BP.

The end of the HCO was marked by a cooling trend starting around 5,000 cal yrs BP marked by extended sea-ice cover and lower temperatures, explained by the irruption of a NAO<sup>+</sup> conditions suggested by our temperature reconstruction as well as the NAO proxy Late Holocene reconstructions (Olsen et al., 2012; Ortega et al., 2015). This period was characterized by the expansion of tundra elements. This overall positive NAO trend was interrupted by a warm pulse suggesting the transition towards NAO<sup>-</sup> conditions during a brief period ca. 3,000 cal yrs BP. When comparing the two temperature *Ths* records for the past 2,000 years, the Lomsø record seems to be smoothed, when a short NAO<sup>-</sup> phase marked by *Pinus* pollen influx erupted. In this

timeframe, the ZAC record displays marked fluctuations in temperature, whereas the Lomsø temperature records exhibits a more gradual curve, spanning from 0.77°C to 3.39°C. The ZAC-based *Ths* exhibited a decreasing trend of about -0.88°C peaking around 1,500 cal yrs BP. This cooling pulse coincided with a regional cooling event marked by late tree growth, dim sun, temperature drops in various regions, unripe fruit, and summer snowfall (Easterbrook, 2016). This temperature record difference could be related to the different altitude of both study sites. Higher altitudes would imply larger temperature fluctuations owing to closer proximity to the 0°C isotherm making the ZAC site more sensitive to temperature changes than Lomsø.

During the DACP (1,600 – 1,100 cal yrs BP) the Lomsø site showed an initial subtle cooling followed by a warming pulse and then another cooling event peaking at the end of the period, the ZAC record, despite differing in magnitude and temporality, exhibited a similar trend (fig 69). In the Zackenberg valley, a deposit of thick sediments overlying an organic layer at 1,300 years BP suggests a mechanism akin to the HCO (Cable et al., 2018) (fig. 69). The dominance of NAO<sup>+</sup> conditions during the DACP were interrupted by southern winds with exotic pollen suggesting a shift towards negative phase ca. 1,450 and 1,050 cal yrs BP at the beginning of the MCA, marking the beginning of a subtle warming trend during this period.

The LIA was characterized by oscillating temperature values in both studied records, ranging between 0.93°C and 2.62°C. in Lomsø and -0.75 - 7.79 °C in the ZAC record. The thermal variability of the LIA is projected towards the present in ZAC, estimating -2.22°C for the top sample. Lomsø on the other hand displayed pronounced warming towards the present reaching 3.39°C on the top sample. Accordingly with the proxy based NAO reconstructions, NAO phases were oscillating too, with intermittent pulses of NAO<sup>-</sup> conditions which led to southern woody exotic pollen between 900 and 500 cal yrs BP and a NAO<sup>+</sup> linked cool pulse ca. 300 cal yrs BP marking the beginning of the high ecological change stage related to the IE (Olsen et al., 2012; Ortega et al., 2015) (fig. 69). Finally, NAO<sup>-</sup> conditions have started to take over, giving way to warmer and moister climate during the past century.

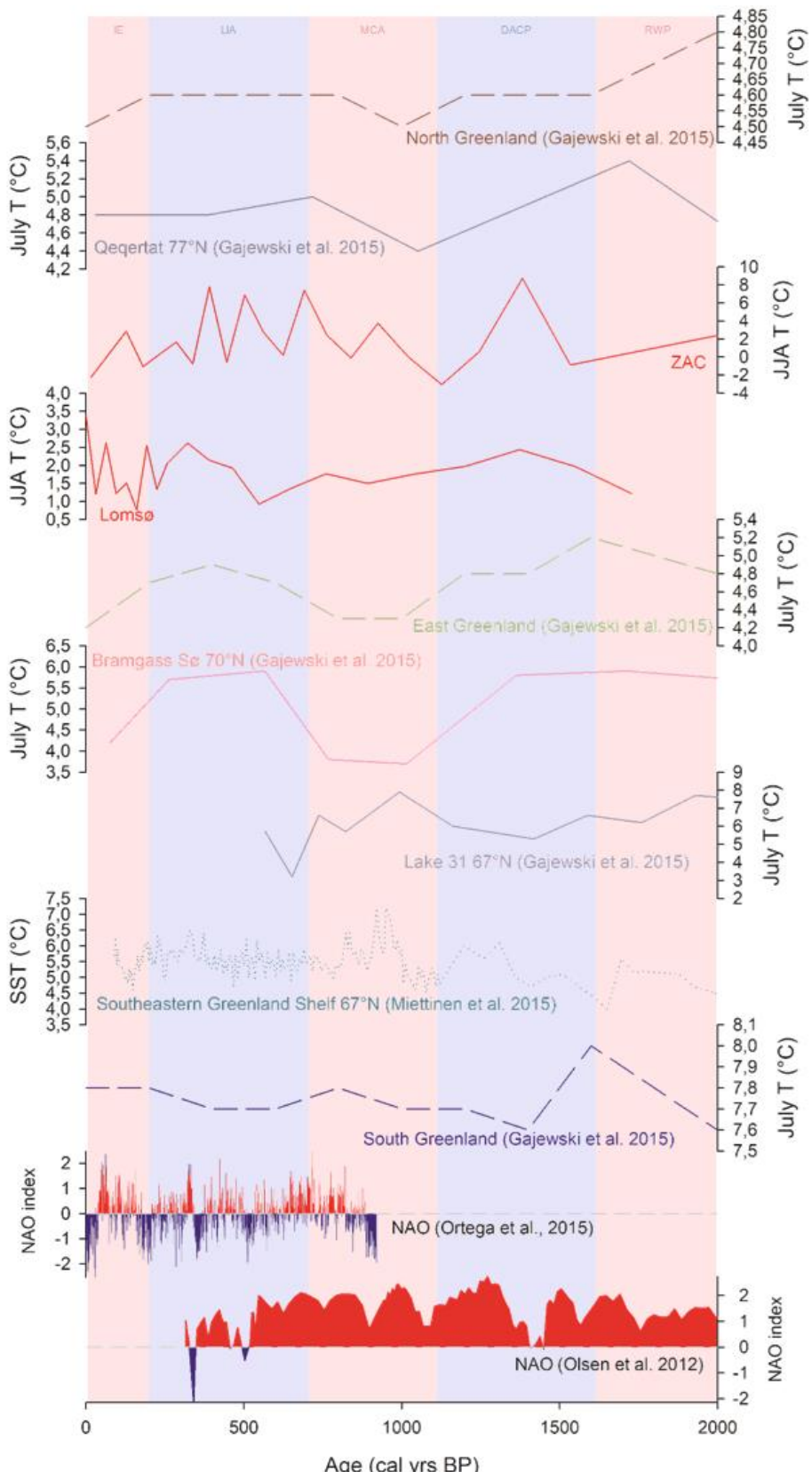


**Figure 69.** Comparison of this study *Ths* record with other regional records since 2,000 cal yrs BP.

#### 4.7. Importance for high-arctic conservation and management

The Holocene vegetation changes in the Arctic, particularly in the Zackenberg region, carry significant implications for plant conservation strategies in the context of ongoing climate shifts. The IPCC (2023) report highlight that human activities are directly implied in the retreat of glaciers, reductions in Arctic sea ice, decreased spring snow cover in the Northern Hemisphere, melting of the GrIS, and the acidification of ocean surface waters. This highlights the urgent need for climate action to mitigate these detrimental effects on the Arctic ecosystem since the impact of global warming, including the likelihood of sudden or irreversible shifts in the climate system rises as tipping points are approached (McKay et al., 2022). The Arctic regions are particularly vulnerable, with threats of species extinction and biodiversity loss increasing with global warming (Stendel et al., 2008). Sustained warming levels above 2°C may lead to the irreversible loss of the Greenland and W Antarctic ice sheets, resulting in significant sea-level rise over millennia and imminent impact various aspects of the ecosystem (IPCC, 2023). Considering the broader context of Arctic climate shifts, which include the loss of sea ice and the influence of large-scale climate modes like the NAO and the AMOC must be considered, as it is clear that the interconnectedness of the Arctic and global climate systems implies that changes in sea surface temperatures and climate variability strongly impacts Arctic ecosystems (Gillett et al., 2003; Wang et al., 2022).

Warming in NE Greenland is associated with decreased sea ice cover, altering precipitation patterns, snow-cover duration, soil moisture, and cloud cover (Stendel et al., 2008). Short summers limit flowering and pollination in the High Arctic, so climate warming therefore longer growing seasons is expected to expand the distribution of dwarf shrubs like *Salix* and *Betula* to new lands and higher elevations (Klein et al., 2008). Locally, climate change projections for Zackenberg support the expected warmer and more humid conditions, further complicating the dynamics of plant communities in the region (Stendel et al., 2008). The responses of plants to climate forcing and soil-plant interactions are expected to manifest in various ways, since changes in nutrient availability, weathering, nitrogen fixation, decomposition,

increased depth of the active layer, and growing season length collectively contribute to shifts in vegetation patterns (Robinson et al., 1997; Sørensen et al., 2006). In this context, paleoecological index hold crucial importance since they bring a light on how ecological communities coped with past climate changes, showing how pronounced climate change has spiked ecological change. As far as pollen data shows, the middle and lowlands of the study area have experienced the most abrupt changes during the IE, highlighting the abrupt effects that ongoing climate warming is having on Arctic ecosystems both inside and outside the lakes.

A critical challenge arises from the disappearance of snow patches in late July, traditionally vital for supplying meltwater to vegetation during the growing season, aligning with a decrease in the water table in swampy areas, directly impacting the plant community (Elberling et al., 2008b). Short-term observations highlight the vulnerability of certain vegetation types to warming, and higher summer temperatures leading to increased snowmelt, may decrease the water table levels in fens, making them more susceptible to changes. Visual observations suggest the gradual transformation of fen borders into grassland (Elberling et al., 2008a). In nutrient-limited communities, the potential for new, more resistant communities to colonize unvegetated areas emerges because of scarcer vegetation cover (Elberling et al., 2008a). Furthermore, under a warming trend, colonization by warm-adapted southern vegetation types is expected, indicating a potential broad transformation of the existing plant communities (Elberling et al., 2008a).

When it comes to the interpretation of the studied pollen stratigraphy, there's a clear pattern of "greening" of the area, as shown by the vegetal succession that followed sharp increases in temperature. During the HCO the NAO<sup>-</sup> predominance allowed the persistence of mild climate allowing the expansion of southern *Betula* heaths, displacing the native vegetation further north or higher by the mountain due to enhanced competition for resources, where tall woody plants are clearly advantaged. This is a phenomenon that is happening the arctic and supposes a complex ecological problem (Büntgen et al., 2015; Myers-Smith et al., 2020). The second and most recent warming pulse that has taken place since ca. 300 cal yrs BP has also caused important

change in the composition of pollen assemblages on the Lomsø record, characterized by the expansion of Ericaceae heaths, better adapted to High Arctic environments than *Betula*. On the other hand, past cooling trends have been manifested as expansion of High Arctic and Polar Tundra elements. Low pollen concentration aside, the fact that the ZAC record doesn't show the expansion of Ericaceae shrubs can be explained by the lack of soil moisture at higher elevations not allowing the development of shrub vegetation yet.

Additionally, the application of paleoecological data as an ecological proxy was useful for this purpose since it gives us valuable information about the mechanisms of how pollen assemblages, therefore plants, have responded to past climate change (Correa-Metrio et al., 2014; Lozano García et al., 2014). The application of Euclidean distance in this context allow us to track when an environmental change, like *Ths* fluctuations, is strong enough to cause a change in species composition, like the case of the events ca. 6,800, 300 and 100 cal yrs BP. It is of high importance to keep coupling the discovery of paleo data with conservation initiatives since as demonstrated here, we can identify trends of vegetation change, key species, key sites and can act beforehand.

As the Arctic undergoes widespread and substantial changes, plant conservation strategies must adapt to the intricate interplay between climate, water availability, and soil moisture conditions. Understanding the non-linear relationship between plant distribution and soil water content, as highlighted in the Young Sound area, is crucial for devising effective conservation measures (Nabe-Nielsen et al., 2017). In this dynamic scenario, where Arctic plants are adapted to low temperatures but face challenges from non-climatic factors, the preservation of biodiversity hinges on a comprehensive and adaptive approach that considers the nuanced interactions between climate, soil, and vegetation in the Arctic landscape.

#### 4.8. Challenges in enhancing Quantitative Climate Reconstructions in the Arctic Region

Despite the improvement of alternative climate indicators, like isotopes and biomarkers, fossil pollen stands out as the go-to for quantitative climate data in non-glaciated areas (Kaufman et al., 2020). The widespread and detailed coverage of pollen records throughout the Late Quaternary, coupled with their ability to unveil various paleoclimatic factors, established them as an indispensable tool in paleoclimatology. The main challenges in interpreting pollen data include: 1) the potential long-distance transport of pollen grains from their source plants, complicating the identification of local, regional, and external signals; 2) processes related to pollen transportation and deposition can impact the temporal resolution of pollen diagrams; and 3) pollen grains lack identification to the species level, thereby restricting ecological inferences. (Gajewski, 2006).

The precision of climate reconstructions using pollen relies on the pollen grain count. When it comes to provide climate insights based on pollen diagrams the standard suggestion is to count a minimum of 300 pollen grains in each fossil sample to obtain accurate readings of the dominant taxa percentages (Birks et al., 2010; Djamali & Cilleros, 2020). In the case of Lomsø, the pollen percentages are based on counting at least 300 terrestrial pollen grains, but the low pollen content of ZAC lake sediments made it unfeasible to achieve the 300-grain count per sample during this research, indicating the necessity to enhance the ZAC *Ths* curve for it to bring a more accurate estimate of temperature at middle altitude. Nevertheless, despite its limitations, the ZAC temperature curve agrees with the Lomsø one as well as with the main climate trends described by other climate reconstructions.

Overemphasis on certain high pollen-producing taxa, like *Luzula/Juncus*, coupled with the low pollen content, overshadowed the climatic signals preserved in past pollen assemblages. Another contributing factor to the challenge is the potential limitation in the representation of tundra plant species, influenced by factors like flowering and

overall production, as suggested by Rozema et al. (2006). Addressing these challenges is crucial for refining the accuracy of climate reconstructions and advancing our understanding of past climate and ecology in Arctic regions.

The taxonomical scale at which most grains are identified comprises a major challenge for Arctic palynology (Gajewski, 2006). The recent application of sedimentary DNA studies on the valley by Parisy et al. (2023) opens a door for the possibility of performing sedDNA analysis on lacustrine records, this would for sure upgrade the taxonomical resolution, allowing more precise interpretations. Another significant challenge is the time required for processing and counting pollen. However, recent advancements in processing methods have enabled an enhancement in the temporal resolution of pollen diagrams (Zabenskie & Gajewski, 2007). When it comes to lake setting, most of the lakes studied in Eastern Greenland are less than 10 m deep, most of them having less than 5 m, thus, sediment being more vulnerable to external factors as waves, ice cover, lake level fluctuations, among others, highlighting the need to revisit and upgrade past and present research dates (Wagner, 2000).

## 5. Conclusions

The study of lacustrine records from the Zackenberg area brings light to NE Greenland paleoecology and paleoclimatology, allowing to successfully generate a quantitative climate reconstruction and to describe significant changes in vegetation during the Holocene forced by climate changes:

- During the period between 9,000 and 7,200 cal yrs BP the Zackenberg area experienced glacier retreat and prominent environmental changes, witnessing the change from initial scarce high-Arctic polar desert-like vegetation on deglaciated areas. The ZAC Lake had seasonal ice cover and became partially thawed during summer. NAO<sup>+</sup> conditions reigned as the ZAC *Ths* curve described a cooling trend linked to the 8.2k cool event reaching -3.26°C. However, ca. 7,500 cal yrs BP the region became warmer than today conditions, bringing thickening of the permafrost active layer and formation of podzols allowing for important vegetational shifts at the end of this period. The lower lands of the Zackenberg valley were just emerging due to isostatic rebound, while the Aucella Mountain remained with a permanent snow hollow at the top.
- Between 7,200 and 3,800 cal yrs BP, under NAO<sup>-</sup> conditions dominance, vegetated areas of the region welcomed the intrusion of Low-arctic flora dominated by *Betula* heaths, as result of latitudinal and altitudinal migration brought by warmer than today conditions, over 6°C between 7,000 and 5,000 cal yrs BP. Glaciers reached their maximum retreat and permafrost reached peak-thawing. The Store Sodal valley exhibited high productivity, with the ZAC Lake showing a longer ice-free period. The lowland associated to the Zackenberg delta were emerging. The high mountain Aucella lake was well formed and showed a seasonal thawing regime with unvegetated surrounding areas. 5,000 cal yrs BP marks the climate deterioration manifested as a shift to NAO<sup>+</sup> conditions.

- The environmental conditions since 3,800 cal yrs BP were overall cooler and drier conditions allowing the replacement of *Betula* heaths on the lower altitudes of the region by *Luzula/Juncus* dominated tundra. The ZAC Lake acquired longer-lasting ice cover while the surrounding vegetation was turning more herbaceous. Permafrost dynamics on Zackenberg lowlands allowed the formation of thermokarst Lomsø lake ca. 1,900 cal yrs BP, recording the domination of snowbed vegetation. The Aucella Lake displayed oscillating ice and snow cover conditions regulating the entry of light and sediments into the system.
- During the past couple of centuries, the Zackenberg area witnessed a reversal of the cooling trend that peaked during the LIA. This warming trend is more evident in the low altitude records, where  $\alpha$  and  $\beta$  diversity indicate the biggest moment of ecological changes during the Holocene happening during this period, describing a shift in vegetation cover with dwarf-shrubs expanding and cold polar elements decreasing under NAO<sup>-</sup> conditions and weakened AMOC.

The employed methods, including palynology as part of a set of multiproxy analyses effectively helped to characterize the environmental history of the Zackenberg region. The combination of pollen, diatom, geochemical and mineralogical analyses offer a comprehensive view of past climatic conditions and vegetation changes and should be accordingly valued as such for their importance for future predictions of Arctic biomes. In this context, the usage of pollen assemblages as proxies to estimate  $\alpha$  and  $\beta$  diversity represent a novel technique in the Arctic so we encourage fellow researchers to include this approach to compare trends and probable causes.

While palynological studies provide valuable insights, several challenges unveil the complexity of reconstructing Arctic environmental history. Issues such as potential long-distance pollen transport, temporal resolution limitations, and the taxonomical scale for pollen identification pose challenges in accurately interpreting climatic signals. In this context, the confection of the reference collection was particularly useful to properly identify pollen grains, especially during the training period. The

necessity for higher pollen counts for accurate readings and the vulnerability of lakes to external factors such as ice and snow cover emphasize the ongoing challenges in enhancing the precision of quantitative climate reconstructions in Arctic regions. Addressing these challenges is crucial for advancing the reliability and accuracy of paleoclimatological interpretations in the Arctic.

In synthesis, palynological research, especially within a multiproxy framework, plays a vital role in unraveling the Arctic's environmental history. These kinds of investigations provide invaluable insights for understanding plant community responses to past climate fluctuations, ultimately aiding in predicting and managing the impacts of ongoing climate change in vulnerable Arctic regions.

## 6. References

- ACIA, 2005. Arctic Climate Impact Assessment. ACIA overview report, Cambridge University Press.
- Alley, R.B., Ágústsdóttir, A.M., 2005. The 8k event: Cause and consequences of a major Holocene abrupt climate change. *Quat. Sci. Rev.* 24, 1123–1149. <https://doi.org/10.1016/j.quascirev.2004.12.004>
- Axford, Y., De Vernal, A., Osterberg, E.C., 2021. Past warmth and its impacts during the holocene thermal maximum in greenland. *Annu. Rev. Earth Planet. Sci.* 49, 279–307. <https://doi.org/10.1146/annurev-earth-081420-063858>
- Barber, D.C., Dyke, A., Hillaire-Marcel, C., Jennings, A.E., Andrews, J.T., Kerwin, M.W., Bilodeau, G., McNeely, R., Southon, J., Morehead, M.D., Gagnon, J.M., 1999. Forcing of the cold event of 8,200 years ago by catastrophic drainage of Laurentide lakes. *Nature* 400, 344–348. <https://doi.org/10.1038/22504>
- Bartels, M., 2017. Atlantic Water advection and glacier responses at the margins of Svalbard since the deglaciation Atlantic Water advection and glacier responses at the margins of Svalbard since the deglaciation Dissertation 166.
- Battarbee, R.W., Carvalho, L., Jones, V.J., Flower, F.J., Cameron, N.G., Bennion, H., Juggins, S., 2001. Diatom analysis. *Track. Environ. Chang.* using lake sediments.
- Bay, C., 1998. Vegetation mapping of Zackenberg Valley, Northeast Greenland. Danish Polar Cent. Bot. Museum, Univ. Copenhagen 1–29.
- Bennike, O., 1999. Colonisation of Greenland by plants and animals after the last ice age: A review. *Polar Rec.* (Gr. Brit.) 35, 323–336. <https://doi.org/10.1017/S0032247400015679>
- Bennike, O., Björck, S., Böcher, J., Hansen, L., Heinemeier, J., Wohlfarth, B., 1999. Early Holocene plant and animal remains from North-east Greenland. *J. Biogeogr.* 26, 667–677. <https://doi.org/10.1046/j.1365-2699.1999.t01-1-00315.x>
- Bennike, O., Sørensen, M., Fredskild, B., Jacobsen, B.H., Böcher, J., Amsinck, S.L., Jeppesen, E., Andreasen, C., Christiansen, H.H., Humlum, O., 2008. Late Quaternary Environmental and Cultural Changes in the Wollaston Forland Region, Northeast Greenland, in: *Advances in Ecological Research*. pp. 45–79. [https://doi.org/10.1016/S0065-2504\(07\)00003-7](https://doi.org/10.1016/S0065-2504(07)00003-7)

- Bennike, O., Wagner, B., 2012. Deglaciation chronology, sea-level changes and environmental changes from Holocene lake sediments of Germania Havn Sø, Sabine Ø, northeast Greenland. *Quat. Res.* (United States) 78, 103–109. <https://doi.org/10.1016/j.yqres.2012.03.004>
- Birks, H.H., Birks, H.J.B., 2006. Multi-proxy studies in palaeolimnology. *Veg. Hist. Archaeobot.* 15, 235–251. <https://doi.org/10.1007/s00334-006-0066-6>
- Birks, H.J.B., Hieri, O., Seppä, H., Bjune, A., 2010. Strengths & Weaknesses of Quantitative Climate Reconstructions Based on Late-Quaternary Biological Proxies. *Open Ecol. J.* 68–110.
- Birks, H.J.B., Lotter, A. e F., Juggins, S., Smol, J.P., 2012a. Tracking Environmental Change Using Lake Sediments Developments in Paleoenvironmental Research.
- Birks, H.J.B., Lotter, A.F., Smol, J.P., Juggins, S., 2012b. *Tracking Environmental Change Using Lake Sediments Volume 5: Data Handling and Numerical Techniques*. Kluwer Academic Publishers, Dordrecht, Holanda.
- Birks, H.J.B., Seppä, H., 2004. Pollen-based reconstructions of late-Quaternary climate in Europe - Progress, problems, and pitfalls. *Acta Palaeobot.* 44, 317–334.
- BJÖRCK, S., WOHLFARTH, B., BENNIKE, O., HJORT, C., PERSSON, T., 1994. Revision of the early Holocene lake sediment based chronology and event stratigraphy on Hochstetter Forland, NE Greenland. *Boreas* 23, 513–523. <https://doi.org/10.1111/j.1502-3885.1994.tb00619.x>
- Blaauw, M., 2010. Methods and code for “classical” age-modelling of radiocarbon sequences. *Quat. Geochronol.* 5, 512–518. <https://doi.org/10.1016/j.quageo.2010.01.002>
- Blaschek, M., Renssen, H., Kissel, C., Thornalley, D., 2015. Holocene North Atlantic Overturning in an atmosphere-ocean-sea ice model compared to proxy-based reconstructions. *Paleoceanography* 30, 1503–1524. <https://doi.org/10.1002/2015PA002828>
- Bouchard, F., Fortier, D., Paquette, M., Boucher, V., Pienitz, R., Laurion, I., 2020. Thermokarst lake inception and development in syngenetic ice-wedge polygon terrain during a cooling climatic trend, Bylot Island (Nunavut), eastern Canadian Arctic. *Cryosph.* 14, 2607–2627.

- Brewer, S., Guiot, J., Barboni, D., Elias, S.A., 2007. Pollen methods and studies: Use of pollen as climate proxies, in: Encyclopedia of Quaternary Science. pp. 2231–2235.
- Briner, J.P., McKay, N.P., Axford, Y., Bennike, O., Bradley, R.S., de Vernal, A., Fisher, D., Francus, P., Fréchette, B., Gajewski, K., Jennings, A., Kaufman, D.S., Miller, G., Rouston, C., Wagner, B., 2016. Holocene climate change in Arctic Canada and Greenland. *Quat. Sci. Rev.* 147, 340–364. <https://doi.org/10.1016/j.quascirev.2016.02.010>
- Buckley, M.W., Marshall, J., 2016. Observations, inferences, and mechanisms of the Atlantic Meridional Overturning Circulation: A review. *Rev. Geophys.* 54, 5–63. <https://doi.org/10.1002/2015RG000493>
- Buizert, C., Keisling, B.A., Box, J.E., He, F., Carlson, A.E., Sinclair, G., DeConto, R.M., 2018. Greenland-Wide Seasonal Temperatures During the Last Deglaciation. *Geophys. Res. Lett.* 45, 1905–1914. <https://doi.org/10.1002/2017GL075601>
- Büntgen, U., Hellmann, L., Tegel, W., Normand, S., Myers-Smith, I., Kirdyanov, A. V., Nievergelt, D., Schweingruber, F.H., 2015. Temperature-induced recruitment pulses of Arctic dwarf shrub communities. *J. Ecol.* 103, 489–501. <https://doi.org/10.1111/1365-2745.12361>
- Cable, S., Christiansen, H.H., Westergaard-Nielsen, A., Kroon, A., Elberling, B., 2018. Geomorphological and cryostratigraphical analyses of the Zackenberg Valley, NE Greenland and significance of Holocene alluvial fans. *Geomorphology* 303, 504–523. <https://doi.org/10.1016/j.geomorph.2017.11.003>
- Cao, X., Tian, F., Telford, R.J., Ni, J., Xu, Q., Chen, F., Liu, X., Stebich, M., Zhao, Y., Herzschuh, U., 2017. Impacts of the spatial extent of pollen-climate calibration-set on the absolute values, range & trends of reconstructed Holocene precipitation. *Quat. Sci. Rev.* 37–53.
- Chevalier, M., Davis, B.A.S., Heiri, O., Seppä, H., Chase, B.M., Gajewski, K., Lacourse, T., Telford, R.J., Finsinger, W., Guiot, J., Kühl, N., Maezumi, S.Y., Tipton, J.R., Carter, V.A., Brussel, T., Phelps, L.N., Dawson, A., Zanon, M., Vallé, F., Nolan, C., Mauri, A., de Vernal, A., Izumi, K., Holmström, L., Marsicek, J., Goring, S., Sommer, P.S., Chaput, M., Kupriyanov, D., 2020.

- Pollen-based climate reconstruction techniques for late Quaternary studies. *Earth-Science Rev.* 210, 103384. <https://doi.org/10.1016/j.earscirev.2020.103384>
- Christensen, T.R., Lund, M., Skov, K., Abermann, J., López-Blanco, E., Scheller, J., Scheel, M., Jackowicz-Korczynski, M., Langley, K., Murphy, M.J., Mastepanov, M., 2021. Multiple Ecosystem Effects of Extreme Weather Events in the Arctic. *Ecosystems* 24, 122–136. <https://doi.org/10.1007/s10021-020-00507-6>
- Christiansen, H.H., 1998. “Little Ice Age” nivation activity in northeast Greenland. *Holocene* 8, 719–728. <https://doi.org/10.1191/095968398666994797>
- Christiansen, H.H., Bennike, O., Böcher, J., Elberling, B., Humlum, O., Jakobsen, B.H., 2002. Holocene environmental reconstruction from deltaic deposits in Northeast Greenland. *J. Quat. Sci.* 17, 145–160. <https://doi.org/10.1002/jqs.665>
- Christiansen, H.H., Sigsgaard, C., Humlum, O., Rasch, M., Hansen, B.U., 2008. Permafrost and Periglacial Geomorphology at Zackenberg, in: Advances in Ecological Research. pp. 151–174. [https://doi.org/10.1016/S0065-2504\(07\)00007-4](https://doi.org/10.1016/S0065-2504(07)00007-4)
- Christoffersen, K.S., Amsinck, S.L., Landkildehus, F., Lauridsen, T.L., Jeppesen, E., 2008. Lake Flora and Fauna in Relation to Ice-Melt, Water Temperature and Chemistry at Zackenberg. *Adv. Ecol. Res.* 40, 371–389. [https://doi.org/10.1016/S0065-2504\(07\)00016-5](https://doi.org/10.1016/S0065-2504(07)00016-5)
- Chung, F.H., 1974. Quantitative interpretation of X-ray diffraction patterns of mixtures. I. Matrix-flushing method for quantitative multicomponent analysis. *J. Appl. Crystallogr.* 7, 519–525. <https://doi.org/10.1107/s0021889874010375>
- Clark, J.P., Feldstein, S.B., 2020. What drives the North Atlantic oscillation’s temperature anomaly pattern? Part I: The growth and decay of the surface air temperature anomalies. *J. Atmos. Sci.* 77, 185–198. <https://doi.org/10.1175/JAS-D-19-0027.1>
- Clarke, G., Leverington, D., Teller, J., Dyke, A., 2003. Superlakes, megafloods, and abrupt climate change. *Science* (80-. ). 301, 922–923. <https://doi.org/10.1126/science.1085921>
- Cohen, K.M., Finney, S.C., Gibbard, P.L., Fan, J.-X., 2013. The ICS international chronostratigraphic chart. *Episodes J. Int. Geosci.* 36, 199–204.
- Correa-Metrio, A., Dechnik, Y., Lozano-García, S., Caballero, M., 2014. Detrended

- correspondence analysis: A useful tool to quantify ecological changes from fossil data sets. *Bol. la Soc. Geol. Mex.* 66, 135–143. <https://doi.org/10.18268/BSGM2014v66n1a10>
- Coyne, P.I., Kelley, J.J., 1974. Variations in carbon dioxide across an Arctic snowpack during spring. *J. Geophys. Res.* 79, 799–802. <https://doi.org/10.1029/jc079i006p00799>
- Cremer, H., Wagner, B., Melles, M., Hubberten, H.W., 2001. The postglacial environmental development of Raffles Sø, East Greenland: Inferences from a 10,000 year diatom record. *J. Paleolimnol.* 26, 67–87. <https://doi.org/10.1023/A:1011179321529>
- Danesh, D.C., Gushulak, C.A.C., Moos, M.T., Karmakar, M., Cumming, B.F., 2022. Changes in the prairie-forest ecotone in northwest Ontario (Canada) across the Holocene. *Quat. Res. (United States)* 106, 44–55. <https://doi.org/10.1017/qua.2021.52>
- de Klerk, P., Teltewskoi, A., Theuerkauf, M., Joosten, H., 2014. Vegetation patterns, pollen deposition and distribution of non-pollen palynomorphs in an ice-wedge polygon near Kytalyk (NE Siberia), with some remarks on Arctic pollen morphology. *Polar Biol.* 37, 1393–1412. <https://doi.org/10.1007/s00300-014-1529-3>
- Djamali, M., Cilleros, K., 2020. Statistically significant minimum pollen count in Quaternary pollen analysis; the case of pollen-rich lake sediments. *Rev. Palaeobot. Palynol.* 275, 104156. <https://doi.org/10.1016/j.revpalbo.2019.104156>
- Easterbrook, D.J., 2016. Temperature fluctuations in Greenland and the Arctic. Evidence-Based Clim. Sci. Data Opposing CO<sub>2</sub> Emiss. as Prim. Source Glob. Warm. Second Ed. 137–160. <https://doi.org/10.1016/B978-0-12-804588-6.00008-2>
- Elberling, B., Nordstrøm, C., Grøndahl, L., Søgaard, H., Friberg, T., Christensen, T.R., Ström, L., Marchand, F., Nijs, I., 2008a. High-Arctic Soil CO<sub>2</sub> and CH<sub>4</sub> Production Controlled by Temperature, Water, Freezing and Snow. *Adv. Ecol. Res.* 40, 441–472. [https://doi.org/10.1016/S0065-2504\(07\)00019-0](https://doi.org/10.1016/S0065-2504(07)00019-0)
- Elberling, B., Tamstorf, M.P., Michelsen, A., Arndal, M.F., Sigsgaard, C., Illeris, L., Bay, C., Hansen, B.U., Christensen, T.R., Hansen, E.S., Jakobsen, B.H., Beyens,

- L., 2008b. Soil and Plant Community-Characteristics and Dynamics at Zackenberg, in: Advances in Ecological Research. pp. 223–248. [https://doi.org/10.1016/S0065-2504\(07\)00010-4](https://doi.org/10.1016/S0065-2504(07)00010-4)
- Engels, S., Helmens, K., 2010. Holocene environmental changes and climate development in Greenland and climate development in Greenland. *Waste Manag.*
- Faegri, K., Iversen, J., 1989. Textbook of pollen analysis. John Wiley & Sons, London.
- Forchhammer, M.C., Christensen, T.R., Hansen, B.U., Tamstorf, M.P., Schmidt, N.M., Høye, T.T., Nabe-Nielsen, J., Rasch, M., Meltofte, H., Elberling, B., Post, E., 2008. Zackenberg in a Circumpolar Context, in: Advances in Ecological Research. pp. 499–544. [https://doi.org/10.1016/S0065-2504\(07\)00021-9](https://doi.org/10.1016/S0065-2504(07)00021-9)
- Fredskild, B., 2000. The Holocene vegetational changes on Qeqertarsuatsiaq, a West Greenland island. *Geogr. Tidsskr.* 100, 7–14. <https://doi.org/10.1080/00167223.2000.10649434>
- Fredskild, B., 1998. The vegetation types of Northeast Greenland. A phytosociological study based mainly on material left by Th. Sørensen from the 1931-35 expeditionsNo Title. *Meddelelser om Groenland, Biosci.* 1–84.
- Fredskild, B., 1995. Palynology and sediment slumping in a high arctic Greenland lake. *Boreas* 24, 345–354. <https://doi.org/10.1111/j.1502-3885.1995.tb00784.x>
- Fredskild, B., 1967. Postglacial plant succession and climatic changes in a west Greenland bog. *Rev. Palaeobot. Palynol.* 4, 113–127. [https://doi.org/10.1016/0034-6667\(67\)90178-9](https://doi.org/10.1016/0034-6667(67)90178-9)
- Fredskild, B., Mogensen, G.S., 1997. ZERO LINE Final Report: A description of the plant communities along the ZERO line from Young Sund to the top of Aucellabjerg and the common plant communities in the Zackenberg valley, Northeast Greenland. Copenhagen, Denmark.
- Funder, S., 1978. Holocene stratigraphy and vegetation history in the Scoresby Sund area, East Greenland. *Bull. Grønlands Geol. Undersøgelse* 129, 1–66. <https://doi.org/10.34194/bullggu.v129.6671>
- Gajewski, K., 2015a. Quantitative reconstruction of Holocene temperatures across the Canadian Arctic and Greenland. *Glob. Planet. Change* 128, 14–23. <https://doi.org/10.1016/j.gloplacha.2015.02.003>

- Gajewski, K., 2015b. Impact of Holocene climate variability on Arctic vegetation. *Glob. Planet. Change* 133, 272–287. <https://doi.org/10.1016/j.gloplacha.2015.09.006>
- Gajewski, K., 2006. Is Arctic Palynology a “blunt instrument”? *Géographie physique et Quat.* 60, 95–102.
- Garcia-Oteyza, J., Giralt, S., Pla-Rabes, S., Antoniades, D., Oliva, M., Ghanbari, H., Osorio-Serrano, R., Palacios, D., 2024. A ~5000 year multiproxy record of summer climate in NE Greenland. *Sci. Total Environ.* 906, 167713. <https://doi.org/10.1016/j.scitotenv.2023.167713>
- Gilbert, G.L., Cable, S., Thiel, C., Christiansen, H.H., Elberling, B., 2017. Cryostratigraphy, sedimentology, and the late Quaternary evolution of the Zackenberg River delta, northeast Greenland. *Cryosphere* 11, 1265–1282. <https://doi.org/10.5194/tc-11-1265-2017>
- Gillet, N.P., Graf, H.F., Osborn, T.J., 2003. Climate change and the North Atlantic oscillation. *Geophys. Monogr. Ser.* 134, 193–209. <https://doi.org/10.1029/134GM09>
- Gong, X., Zhang, Xiangdong, Lohmann, G., Wei, W., Zhang, Xu, Pfeiffer, M., 2015. Higher Laurentide and Greenland ice sheets strengthen the North Atlantic ocean circulation. *Clim. Dyn.* 45, 139–150. <https://doi.org/10.1007/s00382-015-2502-8>
- Gosling, W.D., Julier, A.C.M., Adu-Bredu, S., Djagbletey, G.D., Fraser, W.T., Jardine, P.E., Lomax, B.H., Malhi, Y., Manu, E.A., Mayle, F.E., Moore, S., 2018. Pollen-vegetation richness and diversity relationships in the tropics. *Veg. Hist. Archaeobot.* 27, 411–418. <https://doi.org/10.1007/s00334-017-0642-y>
- Grau, O., Ninot, J.M., Pérez-Haase, A., Callaghan, T. V., 2014. Plant co-existence patterns and high-arctic vegetation composition in three common plant communities in north-east Greenland. *Polar Res.* 33. <https://doi.org/10.3402/polar.v33.19235>
- Grimm, E.C., 2015. *Tilia*.
- Grogan, P., Chapin, I.S., 2000. Initial effects of experimental warming on above- and belowground components of net ecosystem CO<sub>2</sub> exchange in Arctic tundra. *Oecologia* 125, 512–520. <https://doi.org/10.1007/s004420000490>
- Grootes, P.M., Stuiver, M., 1997. Oxygen 18/16 variability in Greenland snow and ice

- with 10 -3- to 105-year time resolutio. *J. Geophys. Res.* 102, 26455–26470.
- Hansen, B.U., Sigsgaard, C., Rasmussen, L., Cappelen, J., Hinkler, J., Mernild, S.H., Petersen, D., Tamstorf, M.P., Rasch, M., Hasholt, B., 2008a. Present-Day Climate at Zackenberg. *Adv. Ecol. Res.* 40, 111–149. [https://doi.org/10.1016/S0065-2504\(07\)00006-2](https://doi.org/10.1016/S0065-2504(07)00006-2)
- Hansen, B.U., Sigsgaard, C., Rasmussen, L., Cappelen, J., Hinkler, J., Mernild, S.H., Petersen, D., Tamstorf, M.P., Rasch, M., Hasholt, B., 2008b. Climate, river discharge and suspended sediment transport in the Zackenberg River drainage basin and Young Sound/Tyrolerfjord, Northeast Greenland, 1995–2003. *Adv. Ecol. Res.* 40, 111–149. [https://doi.org/10.1016/S0065-2504\(07\)00006-2](https://doi.org/10.1016/S0065-2504(07)00006-2)
- Hebbeln, D., Henrich, R., Baumann, K.H., 1998. Paleoceanography of the last interglacial/glacial cycle in the Polar North Atlantic. *Quat. Sci. Rev.* 17, 125–153. [https://doi.org/10.1016/S0277-3791\(97\)00067-X](https://doi.org/10.1016/S0277-3791(97)00067-X)
- Hewitt, H.T., Ridley, J.K., Keen, A.B., West, A.E., Peterson, K.A., Rae, J.G.L., Milton, S.F., Bacon, S., 2015. A seamless approach to understanding and predicting Arctic sea ice in Met Office modelling systems. *Philos. Trans. R. Soc. A Math. Phys. Eng. Sci.* 373. <https://doi.org/10.1098/rsta.2014.0161>
- Hinkler, J., Hansen, B.U., Tamstorf, M.P., Sigsgaard, C., Petersen, D., 2008. Snow and Snow-Cover in Central Northeast Greenland, in: Advances in Ecological Research. pp. 175–195. [https://doi.org/10.1016/S0065-2504\(07\)00008-6](https://doi.org/10.1016/S0065-2504(07)00008-6)
- Hurrell, J.W., Kushnir, Y., Ottersen, G., Visbeck, M., 2003. An overview of the North Atlantic Oscillation. *Geophys. Monogr. Ser.* 134, 1–35. <https://doi.org/10.1029/134GM01>
- IPCC, 2023. Climate Change 2023: Synthesis Report. Contribution of Working Groups I, II and III to the Sixth Assessment Report of the Intergovernmental Panel on Climate Change. Geneva, Switzerland. <https://doi.org/10.59327/IPCC/AR6-9789291691647>
- Iversen, J., 1953. Origin of the Flora of Western Greenland in the Light of Pollen Analysis. *Oikos* 4, 85–103.
- Jakobsen, B.H., Fredskild, B., Pedersen, J.B.T., 2008. Holocene changes in climate and vegetation in the Ammassalik area, East Greenland, recorded in lake sediments and soil profiles. *Geogr. Tidsskr.* 108, 21–50.

<https://doi.org/10.1080/00167223.2008.10649573>

- Johannessen, O.M., Bengtsson, L., Miles, M.W., Kuzmina, S.I., Semenov, V.A., Alekseev, G. V., Nagurnyi, A.P., Zakharov, V.F., Bobylev, L.P., Pettersson, L.H., Hasselmann, K., Cattle, H.P., 2004. Arctic climate change: Observed and modelled temperature and sea-ice variability. *Tellus, Ser. A Dyn. Meteorol. Oceanogr.* 56, 559–560. <https://doi.org/10.1111/j.1600-0870.2004.00092.x>
- Johnsen, S.J., Dahl-Jensen, D., Dansgaard, W., Gundestrup, N., 1995. Greenland palaeotemperatures derived from GRIP bore hole temperature and ice core isotope profiles. *Tellus, Ser. B* 47 B, 624–629. <https://doi.org/10.3402/tellusb.v47i5.16077>
- Jomelli, V., Lane, T., Favier, V., Masson-Delmotte, V., Swingedouw, D., Rinterknecht, V., Schimmelpfennig, I., Brunstein, D., Verfaillie, D., Adamson, K., Leanni, L., Mokadem, F., Aumaître, G., Bourlès, D.L., Keddadouche, K., 2016. Paradoxical cold conditions during the medieval climate anomaly in the Western Arctic. *Sci. Rep.* 6, 1–9. <https://doi.org/10.1038/srep32984>
- Juggins, S., 2018. rioja: Analysis of Quaternary Science data.
- Juggins, S., 2013. Quantitative reconstructions in palaeolimnology: New paradigm or sick science? *Quat. Sci. Rev.* 64, 20–32. <https://doi.org/10.1016/j.quascirev.2012.12.014>
- Karlsen, S.R., Elvebakk, A., 2003. A method using indicator plants to map local climatic variation in the Kangerlussuaq/Scoresby Sund area, East Greenland. *J. Biogeogr.* 30, 1469–1491. <https://doi.org/10.1046/j.1365-2699.2003.00942.x>
- Kaufman, D., McKay, N., Routson, C., Erb, M., Davis, B., Heiri, O., Jaccard, S., Tierney, J., Dätwyler, C., Axford, Y., Brussel, T., Cartapanis, O., Chase, B., Dawson, A., de Vernal, A., Engels, S., Jonkers, L., Marsicek, J., Moffa-Sánchez, P., Morrill, C., Orsi, A., Rehfeld, K., Saunders, K., Sommer, P.S., Thomas, E., Tonello, M., Tóth, M., Vachula, R., Andreev, A., Bertrand, S., Biskaborn, B., Bringué, M., Brooks, S., Caniupán, M., Chevalier, M., Cwynar, L., Emile-Geay, J., Fegyveresi, J., Feurdean, A., Finsinger, W., Fortin, M.C., Foster, L., Fox, M., Gajewski, K., Grosjean, M., Hausmann, S., Heinrichs, M., Holmes, N., Ilyashuk, B., Ilyashuk, E., Juggins, S., Khider, D., Koinig, K., Langdon, P., Larocque-Tobler, I., Li, J., Lotter, A., Luoto, T., Mackay, A., Magyari, E., Malevich, S.,

- Mark, B., Massaferro, J., Montade, V., Nazarova, L., Novenko, E., Pařil, P., Pearson, E., Peros, M., Pienitz, R., Płociennik, M., Porinchu, D., Potito, A., Rees, A., Reinemann, S., Roberts, S., Rolland, N., Salonen, S., Self, A., Seppä, H., Shala, S., St-Jacques, J.M., Stenni, B., Syrykh, L., Tarrats, P., Taylor, K., van den Bos, V., Velle, G., Wahl, E., Walker, I., Wilmshurst, J., Zhang, E., Zhilich, S., 2020. A global database of Holocene paleotemperature records. *Sci. Data* 7, 1–34. <https://doi.org/10.1038/s41597-020-0445-3>
- Klein, D.R., Bruun, H.H., Lundgren, R., Philipp, M., 2008. Climate Change Influences on Species Interrelationships and Distributions in High-Arctic Greenland, in: Advances in Ecological Research. pp. 81–100. [https://doi.org/10.1016/S0065-2504\(07\)00004-9](https://doi.org/10.1016/S0065-2504(07)00004-9)
- Klemm, J., Herzschuh, U., Pisaric, M.F.J., Telford, R.J., Heim, B., Pestryakova, L.A., 2013. A pollen-climate transfer function from the tundra and taiga vegetation in Arctic Siberia and its applicability to a Holocene record. *Palaeogeogr. Palaeoclimatol. Palaeoecol.* 386, 702–713. <https://doi.org/10.1016/j.palaeo.2013.06.033>
- Klug, M., Schmidt, S., Melles, M., Wagner, B., Bennike, O., Heiri, O., 2009. Lake sediments from Store Koldewey, Northeast Greenland, as archive of Late Pleistocene and Holocene climatic and environmental changes. *Boreas* 38, 59–71. <https://doi.org/10.1111/j.1502-3885.2008.00038.x>
- Kobashi, T., Shindell, D.T., Kodera, K., Box, J.E., Nakaegawa, T., Kawamura, K., 2013. On the origin of multidecadal to centennial Greenland temperature anomalies over the past 800 yr. *Clim. Past* 9, 583–596. <https://doi.org/10.5194/cp-9-583-2013>
- Koç, N., Jansen, E., Haflidason, H., 1993. Paleoceanographic reconstructions of surface ocean conditions in the Greenland, Iceland and Norwegian seas through the last 14 ka based on diatoms. *Quat. Sci. Rev.* 12, 115–140. [https://doi.org/https://doi.org/10.1016/0277-3791\(93\)90012-B](https://doi.org/https://doi.org/10.1016/0277-3791(93)90012-B)
- Koch, L., Haller, J., 1971. Geological map of East Greenland 72°-76° N. lat.: de Danske ekspeditioner til Østgrønland 1947-58. Meddelelser om Grønl. 183, 26 pp.
- Kolling, H.M., Stein, R., Fahl, K., Perner, K., Moros, M., 2017. Short-term variability

- in late Holocene sea ice cover on the East Greenland Shelf and its driving mechanisms. *Palaeogeogr. Palaeoclimatol. Palaeoecol.* 485, 336–350. <https://doi.org/10.1016/j.palaeo.2017.06.024>
- Krammer, K., 1991a. Bacillariophyceae 3 Teil; Centralis Fragilariaeae, Eunotiaceae. *Süsswasserflora von Mitteleuropa* 2, 1–576.
- Krammer, K., 1991b. Bacillariophyceae 4. Teil: Achnanthaceae, Kritische Ergänzungen zu Navicula (Lineolatae) und Gomphonema. *Subwasserflora von Mitteleuropa* 2.
- Krammer, K., 1988. Bacillariophyceae 2 Teil; Bacillaricaceae, Epithemiaceae, Surirellaceae. *Süsswasserflora von Mitteleuropa* 2, 1–539.
- Krammer, K., 1986. Bacillariophyceae 1. Teil: Naviculaceae. *Süßwasserflora von Mitteleuropa*.
- Larocca, L.J., Axford, Y., Bjørk, A.A., Lasher, G.E., Brooks, J.P., 2020. Local glaciers record delayed peak Holocene warmth in south Greenland. *Quat. Sci. Rev.* 241, 106421. <https://doi.org/10.1016/J.QUASCIREV.2020.106421>
- Laskar, J., Robutel, P., Joutel, F., Gastineau, M., Correia, A.C.M., Levrard, B., 2004. A long-term numerical solution for the insolation quantities of the Earth. *Astron. Astrophys.* 428, 261–285. <https://doi.org/10.1051/0004-6361:20041335>
- Lebreton, V., Messager, E., Marquer, L., Renault-Miskovsky, J., 2010. A neotaphonomic experiment in pollen oxidation and its implications for archaeopalynology. *Rev. Palaeobot. Palynol.* 162, 29–38. <https://doi.org/10.1016/j.revpalbo.2010.05.002>
- Legendre, P., Gallagher, E.D., 2001. Ecologically meaningful transformations for ordination of species data. *Oecologia* 129, 271–280. <https://doi.org/10.1007/s004420100716>
- Legendre, P., Legendre, L., 2012. Chapter 1 - Complex ecological data sets, in: Legendre, P., Legendre, L.B.T.-D. in E.M. (Eds.), *Numerical Ecology*. Elsevier, pp. 1–57. <https://doi.org/https://doi.org/10.1016/B978-0-444-53868-0.50001-0>
- Li, J., Zhao, Y., Xu, Q., Zheng, Z., Lu, H., Luo, Y., Li, Y., Li, C., Seppä, H., 2014. Human influence as a potential source of bias in pollen-based quantitative climate reconstructions. *Quat. Sci. Rev.* 99, 112–121. <https://doi.org/10.1016/j.quascirev.2014.06.005>

- Lloyd, J.M., Ribeiro, S., Weckström, K., Callard, L., Ó Cofaigh, C., Leng, M.J., Gulliver, P., Roberts, D.H., 2023. Ice-ocean interactions at the Northeast Greenland Ice stream (NEGIS) over the past 11,000 years. *Quat. Sci. Rev.* 308. <https://doi.org/10.1016/j.quascirev.2023.108068>
- Lozano García, S., Correa Metrio, A., Luna, L., 2014. Análisis de la lluvia de polen moderna de la cuenca de México: una herramienta para la interpretación del registro fósil. *Boletín la Soc. Geológica Mex.* 66, 1–10. <https://doi.org/10.18268/bsgm2014v66n1a1>
- Marienfeld, P., 1992. Recent sedimentary processes in Scoresby Sund, East Greenland. *Boreas* 21, 169–186. <https://doi.org/10.1111/j.1502-3885.1992.tb00024.x>
- McKay, D.I.A., Staal, A., Abrams, J.F., Winkelmann, R., Sakschewski, B., Loriani, S., Fetzer, I., Cornell, S.E., Rockström, J., Lenton, T.M., 2022. Exceeding 1.5°C global warming could trigger multiple climate tipping points. *Science* (80-. ). 377. <https://doi.org/10.1126/science.abn7950>
- McKay, N.P., Kaufman, D.S., Routson, C.C., Erb, M.P., Zander, P.D., 2018. The Onset and Rate of Holocene Neoglacial Cooling in the Arctic. *Geophys. Res. Lett.* 45, 12,487–12,496. <https://doi.org/10.1029/2018GL079773>
- Meltofte, H., Christensen, T.R., Elberling, B., Forchhammer, M.C., Rasch, M., 2008. Introduction, in: *Advances in Ecological Research*. pp. 1–12. [https://doi.org/10.1016/S0065-2504\(07\)00001-3](https://doi.org/10.1016/S0065-2504(07)00001-3)
- Meltofte, H., Rasch, M., 2008. The Study Area at Zackenberg, in: *Advances in Ecological Research*. pp. 101–110. [https://doi.org/10.1016/S0065-2504\(07\)00005-0](https://doi.org/10.1016/S0065-2504(07)00005-0)
- Moore, P.D., Webb, J.A., Collinson, M.E., 1991. Pollen analysis, 2nd ed. Blackwell Scientific Publications, Oxford, UK.
- Myers-Smith, I.H., Kerby, J.T., Phoenix, G.K., Bjerke, J.W., Epstein, H.E., Assmann, J.J., John, C., Andreu-Hayles, L., Angers-Blondin, S., Beck, P.S.A., Berner, L.T., Bhatt, U.S., Bjorkman, A.D., Blok, D., Bryn, A., Christiansen, C.T., Cornelissen, J.H.C., Cunliffe, A.M., Elmendorf, S.C., Forbes, B.C., Goetz, S.J., Hollister, R.D., de Jong, R., Loranty, M.M., Macias-Fauria, M., Maseyk, K., Normand, S., Olofsson, J., Parker, T.C., Parmentier, F.J.W., Post, E., Schaeffer-Strub, G.,

- Stordal, F., Sullivan, P.F., Thomas, H.J.D., Tømmervik, H., Treharne, R., Tweedie, C.E., Walker, D.A., Wilmking, M., Wipf, S., 2020. Complexity revealed in the greening of the Arctic. *Nat. Clim. Chang.* 10, 106–117. <https://doi.org/10.1038/s41558-019-0688-1>
- Nabe-Nielsen, J., Normand, S., Hui, F.K.C., Stewart, L., Bay, C., Nabe-Nielsen, L.I., Schmidt, N.M., 2017. Plant community composition and species richness in the High Arctic tundra: From the present to the future. *Ecol. Evol.* 7, 10233–10242. <https://doi.org/10.1002/ece3.3496>
- NOAA, 2009. Climate Variability: North Atlantic Oscillation [WWW Document]. URL <https://www.climate.gov/news-features/understanding-climate/climate-variability-north-atlantic-oscillation> (accessed 1.26.24).
- Oberbauer, S.F., Gillespie, C.T., Cheng, W., Sala, A., Gebauer, R., Tenhunen, J.D., Oberbauer, S.F., Gillespie, C.T., Cheng, W., Gebauer, R., Tenhunen, J.D., Carolina, N., 1996. Diurnal and Seasonal Patterns of Ecosystem CO<sub>2</sub> Efflux from Upland Tundra in the Foothills in Efflux from Tundra of Ecosystem Patterns and Seasonal Diurnal CO<sub>2</sub> Efflux from Upland Tundra of the Brooks Range Alaska, Arct. Alp. Res. 28, 328–338. <https://doi.org/10.1109/ICPEN.2012.6492337>
- Oksanen, J., Blanchet, F.G., Friendly, M., Kindt, R., Legendre, P., McGlinn, D., Minchin, P.R., O’hara, R.B., Simpson, G.L., Solymos, P., 2019. Package ‘vegan.’ Community Ecol. Packag. version 2.
- Olsen, J., Anderson, N.J., Knudsen, M.F., 2012. Variability of the North Atlantic Oscillation over the past 5,200 years. *Nat. Geosci.* 5, 808–812. <https://doi.org/10.1038/ngeo1589>
- Ortega, P., Lehner, F., Swingedouw, D., Masson-Delmotte, V., Raible, C.C., Casado, M., Yiou, P., 2015. A model-tested North Atlantic Oscillation reconstruction for the past millennium. *Nature* 523, 71–74. <https://doi.org/10.1038/nature14518>
- Overeem, I., Nienhuis, J.H., Piliouras, A., 2022. Ice-dominated Arctic deltas. *Nat. Rev. Earth Environ.* 3, 225–240. <https://doi.org/10.1038/s43017-022-00268-x>
- Pados-Dibattista, T., Pearce, C., Detlef, H., Bendtsen, J., Seidenkrantz, M.S., 2022. Holocene palaeoceanography of the Northeast Greenland shelf. *Clim. Past* 18, 103–127. <https://doi.org/10.5194/cp-18-103-2022>
- Parisy, B., Schmidt, N.M., Wirta, H., Stewart, L., Pellissier, L., Holben, W.E.,

- Pannoni, S., Somervuo, P., Jones, M.M., Siren, J., Vesterinen, E., Ovaskainen, O., Roslin, T., 2023. Ecological signals of arctic plant-microbe associations are consistent across eDNA and vegetation surveys. *Metabarcoding and Metagenomics* 7, 155–197. <https://doi.org/10.3897/mbmg.7.99979>
- Perner, K., Moros, M., Lloyd, J.M., Jansen, E., Stein, R., 2015. Mid to late Holocene strengthening of the East Greenland Current linked to warm subsurface Atlantic water. *Quat. Sci. Rev.* 129, 296–307. <https://doi.org/10.1016/j.quascirev.2015.10.007>
- Peros, M.C., Gajewski, K., 2008. Holocene climate and vegetation change on Victoria Island, western Canadian Arctic. *Quat. Sci. Rev.* 27, 235–249. <https://doi.org/10.1016/j.quascirev.2007.09.002>
- R Core Team, 2013. R: a language and environment for statistical computing.
- Rahmstorf, S., 1995. Bifurcations of the Atlantic thermohaline circulation in response to changes in the hydrological cycle. *Nature* 378, 145–149. <https://doi.org/10.1038/378145a0>
- Raynolds, M.K., Walker, D.A., Balser, A., Bay, C., Campbell, M., Cherosov, M.M., Daniëls, F.J.A., Eidesen, P.B., Ermokhina, K.A., Frost, G. V., Jedrzejek, B., Jorgenson, M.T., Kennedy, B.E., Kholod, S.S., Lavrinenko, I.A., Lavrinenko, O. V., Magnússon, B., Matveyeva, N. V., Metúsalemsson, S., Nilsen, L., Olthof, I., Pospelov, I.N., Pospelova, E.B., Pouliot, D., Razzhivin, V., Schaepman-Strub, G., Šibík, J., Telyatnikov, M.Y., Troeva, E., 2019. A raster version of the Circumpolar Arctic Vegetation Map (CAVM). *Remote Sens. Environ.* 232. <https://doi.org/10.1016/j.rse.2019.111297>
- Robinson, C.H., Michelsen, A., Lee, J.A., Whitehead, S.J., Callaghan, T. V, Press, M.C., Jonasson, S., 1997. Elevated atmospheric CO<sub>2</sub> affects decomposition of *Festuca vivipara* (L.) Sm. litter and roots in experiments simulating environmental change in two contrasting arctic ecosystems. *Glob. Chang. Biol.* 3, 37–49.
- Rochardson, A.D., Friedland, A.J., 2007. A review of the theories to explain Arctic and alpine treelines around the world. *J. Sustain. For.* 25.
- Rogers, J., McHugh, M., 2002. On the separability of the North Atlantic oscillation and Arctic oscillation. *Clim. Dyn.* 19, 599–608. <https://doi.org/10.1007/s00382-002-0240-0>

- Rozema, J., Boelen, P., Doorenbosch, M., Bohncke, S., Blokker, P., Boekel, C., Broekman, R.A., Konert, M., 2006. A vegetation, climate and environment reconstruction based on palynological analyses of high arctic tundra peat cores (5000-6000 years BP) from Svalbard. *Plant Ecol.* 182, 155–173. <https://doi.org/10.1007/s11258-005-9024-0>
- Rudd, D.A., Karami, M., Fensholt, R., 2021. Towards high-resolution land-cover classification of greenland: A case study covering Kobbefjord, Disko and Zackenberg. *Remote Sens.* 13. <https://doi.org/10.3390/rs13183559>
- Salonen, J.S., Ilvonen, L., Seppä, H., Holmström, L., Telford, R.J., Gaidamavičius, A., Stančikaite, M., Subetto, D., 2012. Comparing different calibration methods (WA/WA-PLS regression and Bayesian modelling) and different-sized calibration sets in pollen-based quantitative climate reconstruction. *Holocene* 22, 413–424. <https://doi.org/10.1177/0959683611425548>
- Schmidt, S., Wagner, B., Heiri, O., Klug, M., Bennike, O., Melles, M., 2011. Chironomids as indicators of the Holocene climatic and environmental history of two lakes in Northeast Greenland. *Boreas* 40, 116–130. <https://doi.org/10.1111/j.1502-3885.2010.00173.x>
- Schnurrenberger, D., Russell, J., Kelts, K., 2003. Classification of lacustrine sediments based on sedimentary components. *J. Paleolimnol.* 29, 141–154. <https://doi.org/10.1023/A:1023270324800>
- Seppä, H., Birks, H.J.B., 2001. July mean temperature and annual precipitation trends during the Holocene in the Fennoscandian tree-line area: Pollen-based climate reconstructions. *Holocene* 11, 527–539. <https://doi.org/10.1191/095968301680223486>
- Seppä, H., Birks, H.J.B., Odland, A., Poska, A., Veski, S., 2004. A modern pollen-climate calibration set from northern Europe: Developing and testing a tool for palaeoclimatological reconstructions. *J. Biogeogr.* 31, 251–267. <https://doi.org/10.1111/j.1365-2699.2004.00923.x>
- Serreze, M.C., Barry, R.G., 2011. Processes and impacts of Arctic amplification: A research synthesis. *Glob. Planet. Change* 77, 85–96. <https://doi.org/10.1016/j.gloplacha.2011.03.004>

- Serreze, M.C., Francis, J.A., 2006. The arctic amplification debate. *Clim. Change* 76, 241–264. <https://doi.org/10.1007/s10584-005-9017-y>
- Sha, L., Knudsen, K.L., Eiríksson, J., Björck, S., Jiang, H., Yang, X., Yu, X., Li, D., 2022. Diatom-reconstructed summer sea-surface temperatures and climatic events off North Iceland during the last deglaciation and Holocene. *Palaeogeogr. Palaeoclimatol. Palaeoecol.* 602, 111154. <https://doi.org/https://doi.org/10.1016/j.palaeo.2022.111154>
- Shahi, S., Abermann, J., Silva, T., Langley, K., Larsen, S.H., Mastepanov, M., Schöner, W., 2023. The importance of regional sea-ice variability for the coastal climate and near-surface temperature gradients in Northeast Greenland. *Weather Clim. Dyn.* 4, 747–771. <https://doi.org/10.5194/wcd-4-747-2023>
- Smith, J.A., Callard, L., Bentley, M.J., Jamieson, S.S.R., Sánchez-Montes, M.L., Lane, T.P., Lloyd, J.M., McClymont, E.L., Darvill, C.M., Rea, B.R., O’Cofaigh, C., Gulliver, P., Ehrmann, W., Jones, R.S., Roberts, D.H., 2023. Holocene history of the 79°N ice shelf reconstructed from epishelf lake and uplifted glaciomarine sediments. *Cryosph.* 17, 1247–1270. <https://doi.org/10.5194/tc-17-1247-2023>
- Solignac, S., Giraudeau, J., de Vernal, A., 2006. Holocene sea surface conditions in the western North Atlantic: Spatial and temporal heterogeneities. *Paleoceanography* 21, 1–16. <https://doi.org/10.1029/2005PA001175>
- Sørensen, P., Jonasson, S., Michelsen, A., 2006. Nitrogen Fixation, Denitrification, and Ecosystem Nitrogen Pools in Relation to Vegetation Development in the Subarctic. *Arct. Antarct. Alp. Res. - ARCT ANTARCT ALP RES* 38, 263–272. [https://doi.org/10.1657/1523-0430\(2006\)38\[263:NFDAEN\]2.0.CO;2](https://doi.org/10.1657/1523-0430(2006)38[263:NFDAEN]2.0.CO;2)
- Stendel, M., Christensen, J.H., Petersen, D., 2008. Arctic Climate and Climate Change with a Focus on Greenland, in: *Advances in Ecological Research*. pp. 13–43. [https://doi.org/10.1016/S0065-2504\(07\)00002-5](https://doi.org/10.1016/S0065-2504(07)00002-5)
- Stenseth, N.C., Ottersen, G., Hurrell, J.W., Mysterud, A., Lima, M., Chan, K.S., Yoccoz, N.G., Ådlandsvik, B., 2003. Studying climate effects on ecology through the use of climate indices: The North Atlantic Oscillation, El Niño Southern Oscillation and beyond. *Proc. R. Soc. B Biol. Sci.* 270, 2087–2096. <https://doi.org/10.1098/rspb.2003.2415>
- Stewart, L., Alsos, I.G., Bay, C., Breen, A.L., Brochmann, C., Boulanger-Lapointe,

- N., Broennimann, O., Bültmann, H., Bøcher, P.K., Damgaard, C., Daniëls, F.J.A., Ehrich, D., Eidesen, P.B., Guisan, A., Jónsdóttir, I.S., Lenoir, J., le Roux, P.C., Lévesque, E., Luoto, M., Nabe-Nielsen, J., Schönswetter, P., Tribsch, A., Tveraabak, L.U., Virtanen, R., Walker, D.A., Westergaard, K.B., Yoccoz, N.G., Svenning, J.C., Wisz, M., Schmidt, N.M., Pellissier, L., 2016. The regional species richness and genetic diversity of Arctic vegetation reflect both past glaciations and current climate. *Glob. Ecol. Biogeogr.* 25, 430–442. <https://doi.org/10.1111/geb.12424>
- Stockmar, J.A., 1971. Tablets with spores used in absolute pollen analysis. *Pollen et spores* 13, 615–621.
- Stranne, C., Jakobsson, M., Björk, G., 2014. Arctic Ocean perennial sea ice breakdown during the Early Holocene Insolation Maximum. *Quat. Sci. Rev.* 92, 123–132. <https://doi.org/10.1016/j.quascirev.2013.10.022>
- Stuiver, M., Grootes, P.M., Braziunas, T.F., 1995. The GISP2  $\delta^{18}\text{O}$  climate record of the past 16,500 years and the role of the sun, ocean, and volcanoes. *Quat. Res.* <https://doi.org/10.1006/qres.1995.1079>
- Telford, R.J., Birks, H.J.B., 2009. Evaluation of transfer functions in spatially structured environments. *Quat. Sci. Rev.* 28, 1309–1316. <https://doi.org/10.1016/j.quascirev.2008.12.020>
- ter Braak, C.J.F., Juggins, S., 1993. Weighted averaging partial least squares regression (WA-PLS): an improved method for reconstructing environmental variables from species assemblages. *Hydrobiologia* 269/270, 269.
- Thompson, D.W.J., Wallace, J.M., 1998. The Arctic oscillation signature in the wintertime geopotential height and temperature fields. *Geophys. Res. Lett.* 25, 1297–1300. <https://doi.org/10.1029/98GL00950>
- Traverse, A., 2007. Paleopalynology, 2nd ed. Springer US, Dordrecht, Holanda.
- Urrego, D.H., Bush, M.B., Silman, M.R., Correa-Metrio, A.Y., Ledru, M.-P., Mayle, F.E., Paduano, G., Valencia, B.G., 2009. Millennial-scale ecological changes in tropical South America since the Last Glacial Maximum, in: Sylvestre, F., Vimeux, F., Khodri, M. (Eds.), *Past Climate Variability in South America and Surrounding Regions: From the Last Glacial Maximum to the Holocene, Developments in Paleoenvironmental Research*. Springer, New York, pp. 283–

300.

- Vasskog, K., Langebroek, P.M., Andrews, J.T., Nilsen, J.E.Ø., Nesje, A., 2015. The Greenland Ice Sheet during the last glacial cycle: Current ice loss and contribution to sea-level rise from a palaeoclimatic perspective. *Earth-Science Rev.* 150, 45–67. <https://doi.org/10.1016/j.earscirev.2015.07.006>
- Vermassen, F., 2019. Warming waters and melting glaciers: reconstructing ice-ocean interactions from marine sediments in Greenland. <https://doi.org/10.13140/RG.2.2.30473.19045>
- Vincent, W., Hobbie, J., 2000. Ecology of Arctic Lakes and Rivers, in: *The Arctic*. London, pp. 197–232. <https://doi.org/10.4324/9780429340475-8>
- Vinther, B.M., Buchardt, S.L., Clausen, H.B., Dahl-Jensen, D., Johnsen, S.J., Fisher, D.A., Koerner, R.M., Raynaud, D., Lipenkov, V., Andersen, K.K., Blunier, T., Rasmussen, S.O., Steffensen, J.P., Svensson, A.M., 2009. Holocene thinning of the Greenland ice sheet. *Nature* 461, 385–388. <https://doi.org/10.1038/nature08355>
- Wagner, B., 2000. Holocene environmental history of East Greenland - evidence from lake sediments, Reports on Polar Research. <https://doi.org/10.1017/CBO9781107415324.004>
- Wagner, B., Bennike, O., Bos, J.A.A., Cremer, H., Lotter, A.F., Melles, M., 2008. A multidisciplinary study of Holocene sediment records from Hjort Sø on Store Koldewey, Northeast Greenland. *J. Paleolimnol.* 39, 381–398. <https://doi.org/10.1007/s10933-007-9120-3>
- Wagner, B., Heiri, O., Hoyer, D., 2005. Chironomids as proxies for palaeoenvironmental changes in East Greenland: a Holocene record from Geographical Society Ø. *Zeitschrift der Dtsch. Gesellschaft für Geowissenschaften* 156, 543–556. <https://doi.org/10.1127/1860-1804/2005/0156-0543>
- Wagner, B., Melles, M., 2002. Holocene environmental history of western Ymer , East Greenland, inferred from lake sediments. *Quat. Int.* 89, 165–176. [https://doi.org/10.1016/S1040-6182\(01\)00087-8](https://doi.org/10.1016/S1040-6182(01)00087-8)
- Wagner, B., Melles, M., 2001. A Holocene seabird record from Raffles Sø sediments, East Greenland, in response to climatic and oceanic changes. *Boreas* 30, 228–

239. <https://doi.org/10.1080/030094801750424148>
- Wanamaker, A.D., Butler, P.G., Scourse, J.D., Heinemeier, J., Eiríksson, J., Knudsen, K.L., Richardson, C.A., 2012. Surface changes in the North Atlantic meridional overturning circulation during the last millennium. *Nat. Commun.* 3, 899. <https://doi.org/10.1038/ncomms1901>
- Wang, S., Liu, J., Li, X., Ye, Y., Greatbatch, R.J., Chen, Z., Cheng, X., 2022. New insight into the influence of the Greenland high on summer Arctic sea ice. *Environ. Res. Lett.* 17. <https://doi.org/10.1088/1748-9326/ac7ac6>
- Werner, K., Spielhagen, R.F., Bauch, D., Hass, H.C., Kandiano, E., 2013. Atlantic Water advection versus sea-ice advances in the eastern Fram Strait during the last 9 ka: Multiproxy evidence for a two-phase Holocene. *Paleoceanography* 28, 283–295. <https://doi.org/10.1002/palo.20028>
- Westermann, S., Elberling, B., Højlund Pedersen, S., Stendel, M., Hansen, B.U., Liston, G.E., 2015. Future permafrost conditions along environmental gradients in Zackenberg, Greenland. *Cryosphere* 9, 719–735. <https://doi.org/10.5194/tc-9-719-2015>
- Willemse, N.W., Törnqvist, T.E., 1999. Holocene century-scale temperature variability from West Greenland lake records. *Geology* 27, 580–584. [https://doi.org/10.1130/0091-7613\(1999\)027<0580:HCSTVF>2.3.CO;2](https://doi.org/10.1130/0091-7613(1999)027<0580:HCSTVF>2.3.CO;2)
- YAO, Y., Subir, B., Kay, F.D., LI, C., 2014. Pollen morphology in *Saxifraga* (*Saxifragaceae*) from Ny-Ålesund, Svalbard, Arctic, and its taxonomic significance. *Adv. Polar Sci.* 25, 105–112. <https://doi.org/10.13679/j.advps.2014.2.00105>
- YAO, Y., ZHAO, Q., BERA, S., LI, X., LI, C., 2013. Pollen morphology of selected tundra plants from the high Arctic of Ny-Ålesund, Svalbard. *Adv. Polar Sci.* 23, 103–115. <https://doi.org/10.3724/sp.j.1085.2012.00103>
- Zabenskie, S., Gajewski, K., 2007. Post-Glacial climatic change on Boothia Peninsula, Nunavut, Canada. *Quat. Res.* 68, 261–270. <https://doi.org/10.1016/j.yqres.2007.04.003>
- Zhang, R., Sutton, R., Danabasoglu, G., Kwon, Y.O., Marsh, R., Yeager, S.G., Amrhein, D.E., Little, C.M., 2019. A Review of the Role of the Atlantic Meridional Overturning Circulation in Atlantic Multidecadal Variability and

Associated Climate Impacts. Rev. Geophys. 57, 316–375.  
<https://doi.org/10.1029/2019RG000644>

## 7. Appendix

### Appendix 1. Pollen key (in Spanish)

1a	Granos unidos en grupos	2
1b	Granos simples	3
2a	Grupos de dos granos	DIADA
2b	Grupo de cuatro granos	TETRADA
2c	Más de cuatro granos	POLIADA
3a	Granos sin apertura	4
3b	Granos con aperturas o cicatriz	6
4a	Con bolsas que se proyectan desde el grano	SACADO
4b	Sin dichas bolsas	5
5a	Con la forma del grano oscurecida por una gruesa y alta red de crestas o surcos separados por áreas hundidas	CRESTADO
5b	Sin dichas crestas o surcos	INAPERTURADO
6a	Con cicatriz de tres “brazos”, forma de Y	TRILETE
6b	Con aperturas con forma circular o elongada	7
7a	Aperturas tipo poro (circular)	8
7b	Aperturas tipo colpo (surcos) o una combinación de poro y colpo	12
8a	Con un poro	MONOPORADO
8b	Con más de un poro	9
9a	Poros ordenados en la zona ecuatorial	10
9b	Poros distribuidos sobre toda la superficie del grano sin patrón	11
10a	Dos poros	DIZONOPORADO
10b	Tres poros	TRIZONOPORADO

10c	Cuatro poros	TETRAZONOPORADO
10d	Cinco poros	PENTAZONOPORADO
10e	Seis poros	HEXAZONOPORADO
11a	Cuatro poros	TETRAPANTOPORADO
11b	Cinco poros	PENTAPANTOPORADO
11c	Seis poros	HEXAPANTOPORADO
11d	Más de seis poros	POLIPANTOPORADO
12a	Solo colpo	13
12b	Combinación de poro y colpo (colporo)	18
13a	Con un solo colpo	MONOCOLPADO
13b	Con más de un colpo	14
14a	Colpo fusionado, recto o con intersecciones	SINCOLPADO
14b	Colpo con extremos (fin)	15
15a	Colpos ordenados en la zona ecuatorial	16
15b	Colpos distribuidos a lo largo de todo el grano	17
16a	Dos colpos	DIZONOCOLPADO
16b	Tres colpos	TRIZONOCOLPADO
16c	Cuatro colpos	TETRAZONOCOLPADO
16d	Cinco colpos	PENTAZONOCOLPADO
16e	Seis colpos	HEXAZONOCOLPADO
16f	Más de seis colpos	POLIZONOCOLPADO
17a	Cuatro colpos	TETRAPANTOCOLPADO
17b	Cinco colpos	PENTAPANTOCOLPADO
17c	Seis colpos	HEXAPANTOCOLPADO
17d	Más de seis colpos	POLIPANTOCOLPADO
18a	Algunas aperturas tipo colpo y otras tipo colporo	HETEROCOLPADO
18b	Con todas las aperturas tipo colporo	19
19a	Colporo ordenado en la zona ecuatorial	20

19b	Colporo distribuidos en toda la superficie del grano	21
20a	Tres colporos	TRIZONOCOLPORADO
20b	Cuatro colporos	TETRAZONOCOLPORAD O
20c	Cinco colporos	PENTAZONOCOLPORAD O
20d	Seis colporos	HEXAZONOCOLPORADO
20e	Más de seis colporos	POLYZONOCOLPORADO
21a	Cuatro colporos	TETRAPANTOCOLPORAD O
21b	Cinco colporos	PENTAPANTOCOLPORAD O
21c	Seis colporos	HEXAPANTOCOLPORAD O

## TÉTRADA

1a Tétrada con granos psilados, granulados, escabradados o 2  
verrucados.

---

1 Tétrada con granos equinados. Espinas largas ( $> 6 \mu\text{m}$ ) *Selaginella*  
b y escasas.

---

2a Cada grano trizonoporado, con grandes poros *Epilobium* type  
vestibulados.

---

2 Cada grano trizonocolpado o trizonocolporado. 3  
b

---

3a Tétrada lobulada, globular o triangular-obtusa sin una 4  
separación entre los granos. Colpos uniformemente  
espaciados, con o sin costae, cortos, bien definidos o

como grietas, difusos, sinuosos y pueden o no pueden estar oscurecidos por gránulos. Los poros pueden o no ser visibles. Ornamentación psilada, escabrada o verrucada, pero no tan gruesa y sin gemae.

---

3 Tétrada lobulada a globular o triangular-obtusa. Colpos 5

b más largos, angostos como hendiduras o ensanchándose hacia el ecuador, sin gránulos. En vista polar, cada grano individual luce más o menos circular, nunca marcadamente triangular-obtuso. Paredes internas de pueden ser finas y tenues, pero sin perforaciones (o muy pocas).

---

4a Tétrada usualmente triangular-obtusa, nunca lobulada, < *Empetrum* type

40 µm. Paredes internas de la tétrada bastante fuertes, se tiñen más oscuras y tienen un grosor igual o mayor al de las paredes externas. Colpos no granulados, contorno claro. Costae puede o no ser claro, puede o no estar bordeado por endofisuras. Colpos usualmente angostos. Ornamentación de psilada a granulada.

---

4 Colpos granulados, bordes y posiciones oscuros. Costae *Phyllodoce* type

b detectable junto al colpo en vista superficial.  
Ornamentación de psilada a escabrada-verrucada.

---

5a Tétrada lobulada a globular de aprox. 50 µm con colpos *Vaccinium* type

usualmente ensanchándose hacia el ecuador, donde se puede apreciar un claro poro. Costae del colpo insignificante o indetectable en vista superficial. Si está presente se va angostando hacia los extremos de cada colpo. Ornamentación psilada, escabrada o verrucada.

- 5 Tétrada de~24  $\mu\text{m}$ . Colpos largos, estrechos y hundidos. *Cassiope* type
- b Poro usualmente no es claro. Aparente costae en los colpos en vista superficial, aunque no se angosta hacia los extremos del colpo. Ornamentación escabrada/granulada, exina ~1.5  $\mu\text{m}$ , sexina y nexina del mismo grosor. Tétradas lobulares, globuladas o triangular-obtusa.

## SACADO

- 1a Sacci no constreñido en el punto de encuentro con el 2 cuerpo principal, por lo que se la parte más amplia está en la zona de encuentro. Porción distal del cuerpo (entre ambos sacci) es psilada, granulada o microverrucada, a diferencia de la porción proximal (lejos de los sacci) no es, o es levemente ondulada.

- 
- 1 Sacci constreñido en el punto de encuentro con el 3 cuerpo principal, por lo que se presenta más amplio sobre el área de encuentro. Largo del cuerpo principal aproximadamente entre 40-60  $\mu\text{m}$ . La porción proximal del cuerpo puede mostrar una capa exterior levemente ondulada, a veces desarrollando una cresta marginal tipo “vuelo” entre los sacci.

- 
- 2a Verrugas conspicuas en la parte interior de la pared del *Pinus* sub. *strobus* área distal entre los sacci. type

- 
- 2 Pared de la porción distal del cuerpo psilada, granulada *Picea*  
b o microverrucada.

- 
- 3a Verrugas conspicuas en la parte interior de la pared del *Pinus* sub. *strobus* área distal entre los sacci. type

- 
- 3 Sin verrugas conspicuas en la parte interna de la pared *Pinus* sub. *pinus* type  
b de la porción distal, en cambio el área está completamente psilada o levemente granulada.

## CRESTADO

- 1 Grano con más de tres hileras de crestas. Juntas estas forman una gruesa red sobre la superficie del grano, separando áreas deprimidas (lacunae) las cuales están ordenadas en un patrón geométrico. Grano triangular-obtuso a hexangular (rara vez cuadrangular-obtuso a octangular) en vista polar. Columela usualmente detectable bajo las crestas.
- 

## INAPERTURADO

- 1a Grano con forma de frijol, D o elíptica de 25-40 µm. *Blechnum*-type  
Psilado, sin membrana externa, totalmente desprovista de cualquier patrón de ornamentación.

- 
- 1b Grano con una membrana externa de aspecto arrugado. 2

- 
- 1c Sin equinae o capa externa arrugada. Puede ser 3  
baculado, gemado, clavado o con columellas bajo el tectum, pero no psilado.

- 
- 2a Forma relativamente circular (al menos de la capa *Equisetum* interna). Membrana externa extremadamente delgada, totalmente suelta de la membrana interna, sin verrucae, pero con varios dobleces y arrugas.

- 
- 2b Forma de frijol (capa interna). La capa externa Polypodiaceae

evidentemente doblada, arrugada o crestada. Se podría observar una cicatriz monolete.

- 
- 3a Forma de pera o isodiamétricos, a veces colapsados o Cyperaceae  
estropeados Mayor parte de la superficie tectada-perforada, pero con áreas circulares o elípticas donde la superficie es semitectada, verrucada (con “islas” de sexina”).
- 
- 3b Grano circular tamaño menor a 50 µm. Sin tectum, Cupressaceae  
ornamentación microgemada, aunque dicho patrón puede ser poco visible en algunos granos.

### **ESPORA TRILETE**

- 1a Espora reticulada, foveolada, fosulada o con pliegues 2  
irregulares.

- 
- 1 Espora granulada, equinada, microgemada, gemada, 5  
b baculada, verrucada o verrucada-rugulada.

- 
- 2a Foveolas o fusulas presentes, al menos en la superficie *Huperzia selago*  
proximal. Sin equina entre foveolas. Espora triangular con los angulos truncados, Foveolas conspicuas sobre la superficie distal y proximal. Cicatriz trilete con ‘brazos’ largos alcanzando casi el borde de la espora.

- 
- 2 Foveolas o fusulas ausentes, esporas reticuladas o con 3  
b pliegues irregulares. Con retículo en la superficie distal y la superficie proximal con estructura variable. Sin equinae en el muri. Muri todos de la misma altura y aproximadamente el mismo grosor, apenas rectangular en sección cruzada. Superficie proximal reticulada,

psilada o una combinación de ambas. Espora usualmente triangular-obtusa. Tamaño < 50 µm.

---

3a La mayoría de la superficie proximal psilada, retículo *Lycopodium annotinum* type visible solo en los bordes de la cara.

---

3 El reticulado se extiende en la superficie proximal (más 4 de la mitad reticulado).

---

4a Cara proximal casi completamente reticulada. Retículo *Lycopodium clavatum* con esquinas engrosadas en las intersecciones de muri.

---

4 Cara proximal poco reticulada. Se aprecia un área *Diphasiastrum* type b psilada entre los ‘brazos’ del trilete. Retículo sin dichas esquinas gruesas.

---

5a Espora granulada o microgemada. Forma triangular-*Sphagnum* obtusa con lados convexos. Exina más gruesa en los angulos de la forma triangular en vista ecuatorial. Trilete con ‘brazos’ cortos. La ornamentación varía de densamente granulada-microgemada a escasamente, dependiendo del grado de pérdida de la membrana externa.

---

5 Escultura verrucada o verrucada-rugulada. Espora 6 b triangular-obtusa con lados cóncavos, más o menos 50 µm. Verrugas usualmente del mismo tamaño en la superficie distal y proximal con grandes pliegues. Sin grandes pliegues suaves, en cambio, la superficie proximal tiene verrugas de tamaño similar a las de la cara distal.

6a La pared de la espora se engrosa en las esquinas del triángulo en vista ecuatorial, verrugas bajas y sutiles, no elongadas. Trilete con ‘brazos’ cortos más o menos la mitad del radio de la espora. Tamaño 25 – 40 µm.

---

6 Grosor de la pared prácticamente el mismo en toda la *Botrychium* type  
b espora. Verrugas usualmente prominentes, a veces levemente elongadas. Brazos del trilete usualmente sobrepasan la mitad del radio del grano. Diámetro usualmente > 40 µm.

## ESPORA MONOLETE

1a Grano con forma de frijol. La superficie no es del todo psilada. Presenta una membrana externa (perina) totalmente despegada del cuerpo principal con aspecto sacado o crestado.

---

1b Grano con forma de frijol. Presenta una perina *Cystopteris* estrechamente atada al cuerpo principal, excepto en las zonas donde es levantada por papilas o equinae.

---

2a Perina aparentemente despegada del cuerpo interno, *Dryopteris dilatata* usualmente no abultada. Superficie densamente cubierta type de pequeñas equinae (1.5 – 12 µm) que se proyectan desde arrugas pequeñas.

---

2b Superficie de la perina suave o con unos pocos gránulos, *Dryopteris filix-maxima* toda la superficie siendo levantada por pequeñas crestas type torcidas o sacci abultados que raramente se intersectan o anastomosan.

## MONOPORADO

1a Grano subprolado a irregular con apertura ulcerada de *Luzula/Juncus* (2) tamaño variable. Apertura a veces prominente. Exina bastante deteriorada debido a la acetólisis, mostrándose psilada o granulada.

---

1b Grano esferoidal circular tanto en vista polar como Poaceae (3) ecuatorial. Poro prominente con ánulo bien definido. Ornamentación psilada.

---

2 Grano irregular (48x40  $\mu\text{m}$ ) elíptico en vista ecuatorial *Luzula confusa* y circular en vista polar. Apertura ulcerada, a veces prominente o perdida. Exina 1.2  $\mu\text{m}$  de grosor, sexina más gruesa que nexina.

---

3 ~26  $\mu\text{m}$  de diámetro, poro de ~2.8  $\mu\text{m}$  de diámetro. *Deschampsia alpina* Exina ~2  $\mu\text{m}$  de grosor, sexina el doble de grosor que nexina.

## TRIZONOPORADO

1a Grano isopolar < 25  $\mu\text{m}$ . Psilado. Con poros *Betula* (2) prominentes y vestibulados. Vestíbulos con forma cónica y ánulo

---

1b Grano circular en vista polar 30 – 55  $\mu\text{m}$ . Densamente *Campanula* equinado con equinae de base angosta. Poro hundido, grande en relación con el tamaño total del grano. Columelas claras.

---

2a Grano con diámetro <22  $\mu\text{m}$ , poro <2.5  $\mu\text{m}$  de *Betula nana*-type profundidad y relación diámetro/poro 9.95

---

2b Grano con diámetro > 22  $\mu\text{m}$ , poro > 2.5  $\mu\text{m}$  y relación *Betula pubescens*-type diámetro/poro de 8.85

## **TETRAZONOPORADO**

- 1a Grano psilado, escabrado, verrucado, microequinado o *Alnus* microrugulado. Poro vestibulado. Cada poro se conecta con los poros vecinos por arcos o bandas se ensanchamiento de la nexina.
- 
- 1b Grano psilado o escabrado. Poros asimétricamente *Myriophyllum* distribuidos en torno a la circunferencia del grano. Con ánulo grueso. La nexina no se disuelve en la base del poro, sino que llega hasta la punta.

## **PENTAPANTOPORADO/HEXAPANTOPORADO**

- 1a Grano verrucado (a veces no se aprecia bien). Poros *Plantago maritima* pequeños con ánulo o costae, circulares con bordes bien definidos, levemente prominentes. Membrana del poro granulada. Nexina se engrosa hacia el poro en vez de disolverse. Columelas densas.
- 
- 1b Grano < 30 µm. Superficie microequinada a escabrada. *Thalictrum* Poro < 6 µm de diámetro, sin anulo. Columelas muy finas ubicadas bajo el arreglo de microequinae. Gránulos de los poros más gruesos que los de la superficie.

## **POLIPANTOPORADO**

- 1a Grano con superficie psilada-escabrada, tectada- 2 perforada o microequinada sin ninguna verruga.
- 
- 1b Grano con superficie equinada, vaculada, verrucada, 3 foveolada, eureticulada, rugulada-estriada o

microequinada.

---

2a Grano generalmente > 40 poros. Cada poro con bordes bien definidos (ej. anulo). Exina tectada.

---

2b Grano < 70  $\mu\text{m}$ . Exina tectado-perforada, con microequinae, hasta 40 poros. Poro con pequeño anulo, no prominente. Exina se adelgaza hacia el poro. Membrana granulada usualmente presente en el poro.

---

3a Grano equinado, baculado, micro-equinado tamaño < 60 – 4  $\mu\text{m}$ . Equinae < 6  $\mu\text{m}$ .

---

3b Grano tectado-perforado a eureticulado. < 50 poros con bordes bien definidos tipo ánulo y diámetro mucho mayor a la lumina (broqui) interrumpiendo el patrón reticulado.

---

4a Grano tectado-perforado, ornamentación microequinada. Poros circulares y bien definidos, con un ánulo claro que se aprecia como un angostamiento de la sexina y la presencia de una banda ordenada en torno a cada poro. Equinae < 0.5  $\mu\text{m}$ .

---

4b Grano esferoidal entre 18 – 25  $\mu\text{m}$  de diámetro. 9 – 15 poros con borde poco definido e irregular, sin ánulo ni banda alrededor y sin opérculo. Equinae prominente, > 1  $\mu\text{m}$  cónicas, pero no tan gruesas en la base.

---

5a Grano foveolado o eureticulado en el mesoporium, *Silene/Minuartia* (8) foveola o lumina más amplia que el ancho de una columella. Columella en un patrón reticulado bajo el

muri dupli o simplicolumelado. Usualmente > 20 poros.

---

5b Grano tectado-perforado, perforaciones de tamaño 6 menor o igual que el ancho de la columella en sección cruzada. Columella puede o no presentar un patrón reticulado.

---

6a Perforaciones tienden a estar más ordenadas que la 7 columella y son más frecuentes que estas en el mesoporium. Poro sin depresión, por lo que no parece haber crestas. Borde no del todo obtusamente angular, sino que pareciera tener 5 – 6 lados. ~ 15 poros.

---

6b Grano usualmente < 55  $\mu\text{m}$ . Perforaciones tienen la *Silene/Minuartia* (8) misma o menor frecuencia que las columellas, que parecen más densas, en el mesoporium. Columellas gruesas y escasas pueden o no estar ordenadas en un patrón reticulado a bajo foco en el mesoporium. ~16 poros.

$\mu\text{m}$

---

7a Grano de tamaño < 35  $\mu\text{m}$  con > 15 poros pequeños y *Sagina* poco definidos. Columellas irregularmente distribuidas, con poca variación en el grosor. Si el opérculo está presente, está bien definido.

---

7b Grano con poros definidos y grandes en relación con el *Cerastium/Stellaria* tamaño del grano. Columellas irregularmente (9) distribuidas usualmente angostándose hacia su base, variando en tamaño. Las más gruesas y esparcidas se encuentran en el mesoporium mientras que las más delgadas y densas se ordenan en la región cercana al

poro.

- 
- 8a Grano esferoidal ~25 µm. 18 – 24 poros circulares de ~3 *Silene acaulis* µm de diámetro cubiertos por una membrana microequinada. Exina ~2.5 µm de grosor. Ornamentación granulada.
- 8b Grano esferoidal con tamaño ~27 µm. 18 – 20 poros circulares de ~2.5 µm de diámetro cubiertos por una membrana microequinada. Exina ~1.8 µm de grosor. Ornamentación granulada.
- 
- 9 Grano esferoidal, ~40 µm. 18 – 28 poros circulares de *Cerastium arcticum* ~4.5 µm de diámetro cubiertos por una membrana granulada. Exina 3.7 µm de grosor. Ornamentación granulada.

## SINCOLPADO

- 1 Grano subprolado (23x19 µm) bilateralmente simétrico. *Pedicularis* Los fines de cada colpo se anamostosan en los polos, dividiendo el grano en dos partes iguales. Exina ~2 µm de grosor. Sexina casi del mismo grosor que nexina. Ornamentación psilada.
- 

## DIZONOCOLPADO

- 1 Grano reticulado de tamaño < 25 µm con las luminas *Tofieldia* que están cerca del poro levemente más pequeñas que aquellas que se ubican lejos del poro. Columella poco visible, exina < 1 µm.
-

## TRIZONOCOLPADO

1a Psilado.	2
1b Rugulado-estriado.	4
1c Reticulado.	8
1d Equinado o microequinado.	11
1e Escabrado o verrucado a microequinado.	12
2a Grano elíptico a circular en vista ecuatorial, con exina <i>Polygonum</i> evidentemente más gruesa en los polos. La superficie <i>viviparum</i> -type puede ser perforada, con cada perforación dispuesta directamente sobre una columella ramificada, especialmente en la apocolpia engrosada. Colpos relativamente cortos ( $\frac{2}{3}$ a $\frac{3}{4}$ de la distancia entre los polos), estrechos con forma de hendidura, sin membrana granulada.	
2b Grano microrreticulado, con forma circular a lobulada <i>Saxifraga stellaris</i> - en vista polar usualmente $> 18 \mu\text{m}$ . Relación P/E $> 1$ . type (3) Colpos largos y relativamente anchos con membrana granulada. Exina del mismo grosor en todo el grano ( $< 4 \mu\text{m}$ ). Sexina relativamente delgada, apenas más gruesa que la nexina. Apocolpia reticulada, muri amplio y profundo (igual al largo de la columella).	
3a Grano subprolado ( $20 \times 16 \mu\text{m}$ ) elíptico en vista ecuatorial y circular en vista polar. Colpos largos, extendiéndose hasta los polos, anchos, hundidos, con bordes bien definidos y membrana suave. Sin opérculo.	

Exina 2  $\mu\text{m}$  de grosor, grosor de sexina y nexina relativamente igual. Ornamentación granulada-reticulada.

- 
- 3b Grano subprolado ( $18 \times 15 \mu\text{m}$ ) elíptico en vista *Saxifraga nivalis* ecuatorial y circular en vista polar. Colpos muy largos, extendiéndose hasta los polos, angostos, hundidos, con fines agudos, bordes bien definidos y membrana suave.

Sin opérculo. Exina 1.9  $\mu\text{m}$  de grosor, sexina con mayor grosor que nexina. Ornamentación granulada-reticulada.

- 
- 4a Grano de  $\sim 25 \mu\text{m}$  elíptico con ornamentación 6

predominantemente estriada en la mesocolpia. Muri tan anchos o más ancho que la lumina recorren el poro en forma paralela o en un patrón tipo “huella digital”. Tectado o aparentemente tectado.

- 
- 4b Grano  $<50 \mu\text{m}$  con una estructura más “rugulada” en la *Dryas* (5)

mesocolpia (muri más pequeño, no paralelo con mucho anamostasado y entrelazamiento). Colpos largos. Muri a veces paralelos unos a otros, sin embargo, usualmente se presenta curvado o ramificado con cambios repentinos en el ancho, nunca completamente rectos.

- 
- 5 Grano subprolado ( $23 \times 20 \mu\text{m}$ ) elíptico en vista *Dryas octopetala*

ecuatorial y semi-triangular en vista polar. Colpos largos, amplios, hundidos con margen irregular. Exina  $\sim 2.1 \mu\text{m}$  de grosor. Sexina el doble de grosor que la nexina. Ornamentación estriada, muri más amplios que surcos, anastomosados u ondulados.

- 
- 6a Sin gránulos o scabrae sobre el muri. Muri *Saxifraga*

evidentemente más grueso que la lumina, *oppositifolia-type* (7)

anastomosándose o entrelazándose, recorren usualmente en dirección ecuatorial al medio de la mesocolpia y meridional cerca de los márgenes del colpo, formando un patrón tipo “huella digital”.

---

6b Grano subprolado ( $27 \times 22$   $\mu\text{m}$ ) elíptico en vista *Saxifraga cernua*-type ecuatorial y circular en vista polar, borde a veces ondulado. Colpos largos, extendiéndose hasta los polos, angostos, hundidos, fines agudos, con margen irregular y membrana finamente granulada. Sin opérculo. Exina  $2.3 \mu\text{m}$  de grosor, sexina con mayor grosor que nexina. Ornamentación gruesamente granulada. Con evidentes gránulos o scabrae sobre el muri. Estrías sutiles, no del todo claras, con una fila de lo que pareciera ser columellas gruesas bajo cada muri.

---

7a Grano subprolado ( $24 \times 19$   $\mu\text{m}$ ) elíptico en vista *Saxifraga* ecuatorial y circular en vista polar. Colpos largos y *oppositifolia* anchos que llegan hasta los polos, fines obtusos y margen de regular a irregular. Opérculo y membrana del colpo a veces ausente. Exina  $\sim 1.8 \mu\text{m}$  de grosor, sexina más gruesa que nexina. Ornamentación estriada, muri tan o más grueso que los surcos, anastomosando.

---

7b Grano subprolado ( $20 \times 17$   $\mu\text{m}$ ) elíptico en vista *Saxifraga aizoides* ecuatorial y circular en vista polar, borde bisimétrico con un lado obtuso y otro lado convexo. Colpos largos, extendiéndose hasta los polos, angostos, hundidos profundamente, fines agudos, con margen regular. Opérculo usualmente ausente. Exina  $2.3 \mu\text{m}$  de grosor, sexina doble de grosor que nexina. Ornamentación estriada.

- 
- 8a Grano de  $> 40 \mu\text{m}$  eureticulado (muri del retículo son 10 paredes ubicadas junto al techo de las columellas) con lumina  $< 1 \mu\text{m}$  de ancho, exina  $> 4 \mu\text{m}$  de grosor. Colpo largo. Muri apoyado sobre una fila de columellas no ramificadas.
- 
- 8b Grano subprolado de  $\sim 20 \mu\text{m}$  de diámetro (ecuador) *Draba* elíptico en vista ecuatorial y circular (a veces lobulado) en vista polar. Colpos grandes y anchos con membrana granulada. Exina  $\sim 3 \mu\text{m}$  de grosor. Ornamentación reticulada, heterobrocado. Puede presentar cuatro colpos.
- 
- 8c Grano eureticulado de tamaño  $< 40 \mu\text{m}$ , circular a *Salix*-type (9) elíptico en vista ecuatorial. Exina  $< 4 \mu\text{m}$ . Colpos largos y anchos, a veces con membrana granulada, con bordes enrolados. Tamaño de la lumina y grosor de la exina marcadamente disminuye hacia el borde de los colpos, formando un claro *margo*, por lo que el borde del colpo parece ser tectado sin lumina.
- 
- 9 Grano esferoidal de  $\sim 20 \mu\text{m}$  de diámetro. Elíptico en *Salix polaris* vista ecuatorial y circular en vista polar. Colpos anchos y muy largos casi llegando al polo, con membrana finamente granulada. Exina  $\sim 2.8 \mu\text{m}$  de grosor, sexina más gruesa que nexina. Ornamentación reticulada-granulada.
- 
- 10a Grano de  $> 60 \mu\text{m}$ . Reticulo muy grueso, muri mucho *Armeria maritima* tipo más estrecho que la lumina con una fila de equinae de  $> 2 \mu\text{m}$  en la punta. Exina  $> 9 \mu\text{m}$ . Columella elíptica en

sección cruzada.

---

10t Retículo no tan grueso, muri tan ancho como la lumina, *Armeria maritima* tipo sin equinae o microequinae en el muri. Columella B circular en sección cruzada.

---

11a Grano de tamaño < 30 µm, circular a lobulado en vista polar. Sin costae. Equinae < 2 µm. Sin columella. Pequeñas “varillas” que parecen ser columellas atraviesan el tectum y la base de las equinas. Colpos parecen un poro elíptico.

---

11t Grano circular a lobulado en vista polar. Sin costae. Con columella. Exina y columellas uniformes en todo el grano. Equinae < 1 µm cubren densamente la superficie del grano. Infraretículo sutil se junta con la base de las equinas.

---

12a Grano tectado con verrugas, scabras o microequinas 13 regularmente espaciadas en el tectum. Estas están dispuestas sobre columellas.

---

12t Grano tectado con características irregulares en 14 distribución y a veces en forma. Tectum microequinado o con scabrae y verrugas redondeadas, nunca elongadas.

---

13a Columelas uniformes en grosor y conectadas por un *Papaver* (17) sutil Infraretículo bajo el tectum y las microequinas. Las microequinas se ubican sobre las intersecciones del retículo.

---

13t Columelas con gran variación en grosor y altura. Las *Artemisia*

más gruesas ocupan el centro de la mesocolpia mientras que las más finas se encuentran hacia el borde del colpo.

---

14a Columelas de grosor variable: más dispersas y gruesas Ranunculaceae (16)

irregularmente dispersas entre columelas finas más numerosas. El tectum puede parecer más o menos ondulado, elevándose sobre las columelas gruesas y sumergiéndose entre ellas. Microechinae a veces detectable en la superficie, sobre las columelas gruesas. Colpo generalmente ancho y granulado grueso, exina a veces más gruesa a lo largo del margen del colpo.

---

14t Columelas monomórficas, menos gruesas y mucho más Saxifraga cespitosa-

pequeñas con relación al tamaño del grano. Superficie type (15)  
tectada-perforada con pequeñas verrugas o escabras dispersas sobre el tectum. Colpo estrecho con extremos agudos, usualmente hundido, a veces puede conservar el opérculo que no es granulado, sino que posee el mismo patrón de ornamentación que el resto del grano. Exina igual de gruesa en todo el grano.

---

15a Grano prolado ( $26 \times 19 \mu\text{m}$ ) elíptico en vista ecuatorial y Saxifraga hirculus

circular en vista polar. Colpos largos (llegan hasta los polos), anchos, hundidos, con margen regular. Opérculo ausente. Exina  $\sim 2.2 \mu\text{m}$  de grosor. Sexina más gruesa que nexina. Ornamentación estriada.

---

15t Grano subprolado ( $26 \times 21 \mu\text{m}$ ) elíptico en vista Saxifraga rivularis

ecuatorial y circular en vista polar. Colpos largos, extendiéndose hasta los polos, anchos, hundidos, con margen regular. Sin opérculo. Exina  $2.1 \mu\text{m}$  de grosor, sexina con mayor grosor que nexina. Ornamentación

estriada.

- 
- 15c Grano subprolado ( $26 \times 21$   $\mu\text{m}$ ) elíptico en vista ecuatorial y circular en vista polar, borde a veces ondulado. Colpos largos, extendiéndose hasta los polos, anchos, hundidos a veces con mayor profundidad, fines agudos, con margen regular y membrana microequinada. Opérculo presente. Exina  $1.5$   $\mu\text{m}$  de grosor, sexina con mayor grosor que nexina. Ornamentación granulada.

- 
- 16a Grano esferoidal de  $\sim 32$   $\mu\text{m}$  de diámetro, elíptico en *Ranunculus nivalis* vista ecuatorial y circular en vista polar. Membrana del colpo con pequeños gránulos. Exina  $\sim 2.8$   $\mu\text{m}$  de grosor. Ornamentación granulada.

- 
- 16t Grano esferoidal de  $\sim 24$   $\mu\text{m}$  de diámetro, elíptico en *Ranunculus pygmaeus* vista ecuatorial y circular en vista polar. Membrana del colpo con pequeños gránulos. Exina  $\sim 2.6$   $\mu\text{m}$  de grosor. Ornamentación granulada.

- 
- 17 Grano subprolado ( $31 \times 28$   $\mu\text{m}$ ) elíptico en vista *Papaver dahlianum* ecuatorial y circular en vista polar. Colpos anchos y muy largos que se extienden hasta los polos, margen regular y presencia de membrana finamente granulada. Exina  $\sim 2.3$   $\mu\text{m}$  de grosor. Sexina el doble de grosor que nexina. Ornamentación granulada.

#### TETRAZONOCOLPADO/PENTAZONOCOLPADO

- 1 Grano psilado o escabrado-verrucado. Colpos anchos, *Hippuris vulgaris* con extremos obtusos y bordes poco definidos/difusos. Membrana granulada del colpo usualmente está
-

presente, por lo que se puede confundir el colpo de la mesocolpia (en esta última región la exina es más gruesa).

---

### **HEXAZONOCOLPADO/POLIZONOCOLPADO**

- 1 Grano psilado-escabrado con tectum perforado o Rubiaceae microrreticulado. Colpos hundidos. Mesocolpia marcadamente convexa. Nexina gruesa,  $\frac{1}{2}$  el grosor de la sexina.
- 

### **TRIZONOCOLPORADO**

- 1a Psilado a escabrado-verrucado. 2

- 
- 1b Eureticulado. 7

- 
- 1c Suprareticulado a Foveolado. 10

- 
- 1d Equinado a Equinado-verrucado. 11

- 
- 1e Rugulado a Estriado. 12

- 
- 2a Grano aproximadamente tan largo como ancho o más *Oxyria/Rumex* (9) ancho que largo ( $P/E > 1.2$ ). Tectado-perforado (aunque también puede lucir levemente rugulado-estriado). En vista polar posee una forma de circular a levemente globulada y se puede apreciar que la exina no se adelgaza desde el mesocolpio al borde del colpo en sección óptica. En vista ecuatorial tiene forma circular a elíptica, con una sexina cuyo tamaño no varía alrededor del grano, y si es que lo hace es levemente más gruesa

en el polo que en el resto del poro. Colpos largos curvados alrededor del grano, cuya longitud completa no es visible en vista ecuatorial. Endoporo circular-elíptico, sin fastigia (cámara entre sexina y nexina), costae claro. Poro puede o no estar fuertemente anillado por costae.

---

2b Forma prolada.

3

---

3a Vista polar lobulada. Sexina más delgada en los polos, *Artemisia* engrosando hacia el centro de cada mesocolpio. Endoporo claro, circular a ecuatorialmente elíptico. A 1000x se pueden observar microequinas esparcidas por el tectum. Columellas pueden ser finas, densas y cilíndricas o con forma irregular y espaciadas.

---

3b Elíptico a rectangular-obtuso, rectangular-obtuso o con forma de hueso (cóncavo en el ecuador).

---

4a El grosor de la exina varía sobre la superficie del grano (5 excepto en la zona del costae). Los poros o endocolpos transversales nunca se fusionan, aunque puede haber un costae en torno al ecuador.

---

4b Exina con grosor uniforme en todo el grano. Sin forma de hueso. Ectocolpo corto. Poro circular o elíptico bien definido. Con costae evidente.

---

5a Grano con forma de hueso. P/E usualmente > 1.5. Las columellas pueden o no ser más largas en los polos. Poro elíptico, rectangular o representado por un amplio o delgado endocolpo transversal, nunca poro circular.

- 
- 5b Forma elíptica a rectangular-obtusa. Columellas largas. 6
- Sexina más gruesa en los polos. Poro circular o elíptico elongado ecuatorialmente.
- 
- 6a Columelas finas, nunca ramificadas. Endoporo *Polygonum aviculare* transversalmente elíptico-agudo con bordes bien definidos. Superficie tectada, nunca perforada.
- 
- 6b Columelas finas, excepto en los polos donde se puede *Polygonum viviparum* incluso apreciar un patrón ramificado. Endoporo circular a transversalmente elíptico. La superficie puede ser tectada-perforada, las perforaciones se ubican directamente sobre las columelas ramificadas.
- 
- 7a Grano circular, elíptico o rómbico-obtuso en vista *Oxyria/Rumex* (9) ecuatorial. Microrreticulado. Columellas visibles, cortas y finas. Colpos delgados como hendiduras, no se ve toda su extensión en vista ecuatorial. Endoporo circular, elíptico o elíptico-agudo. Exina no se angosta hacia los márgenes del colpo.
- 
- 7b Ornamentación reticulada. 8
- 
- 8a Colpos largos, longitud no es del todo visible en vista ecuatorial, se ensanchan hacia el ecuador, con membrana psilada. Cada poro representado por un mero puente, constricción o ruptura del colpo. Tamaño de la lumina no va reduciéndose hacia el polo. Retículo grueso o fino, sin gránulos ni báculas. Tanto el tamaño de la exina como de las luminas disminuye conforme se acercan hacia el colpo, aunque en el mesocolpio el

tamaño de las luminas no cambia.

- 
- 8b Forma circular en vista ecuatorial y de circular a *Oxyria/Rumex* (9) ligeramente lobulado en vista polar, debido al poro levemente hundido. Colpos estrechos, con margen reticulado o tectado no enrolado. Costae angosto junto a los márgenes del colpo. Endoporo elíptico o circular, bien definido. La exina y luminas pueden o no disminuir de tamaño hacia el colpo. Mesocolpia convexa. Muri sinuoso con ancho variable y usualmente duplicolumelado.
- 
- 9 Grano esferoidal de ~20 µm de diámetro, elíptico en vista ecuatorial y circular en vista polar. Colpo poco profundo, exina ~1.8 µm de grosor, nexina el doble de grosor que la sexina. Ornamentación granulada.
- 
- 10a Grano elíptico. Exina marcadamente más gruesa en los polos. Columelas ramificadas más largas y gruesas en el polo. Foveolas presentes en los polos, cada perforación está ubicada sobre una columella ramificada. Colpos estrechos, márgenes no enrolados.
- 
- 10t Grano elíptico, rectangular-obtuso o rómbico-obtuso. Fabaceae Sin cambios evidentes en el tamaño de la exina en el grano. Columellas finas y cortas ( $\frac{1}{2}$  tamaño de la exina), a veces son visibles solo en el polo. Colpos pueden o no ser estrechos, no enrolados. Endoporo circular o elíptico, muy bien definido debido a que están rodeados por un anillo. Costae muy grueso junto a los márgenes del colpo. El retículo desaparece en los polos. Muri amplio, usualmente <15 luminas por mesocolpio.

---

11a Grano circular o lobulado en vista polar. Poro pequeño *Artemisia*  
sin elongación ecuatorial. Columelas visibles y  
claramente más largas al centro de cada mesocolpio,  
gradualmente disminuyendo el largo hacia los polos y  
colpos. Tectum cubierto de microequinas regularmente  
espaciadas.

---

11t Grano circular o lobulado en vista polar. Equinado, *Asteraceae*  
equinae cónicas > 1.5  $\mu\text{m}$  de largo, más anchas en la base. Poro circular o representado por un endocolpo  
transverso estrecho.

---

12a Grano elíptico o rómbico-obtuso en vista ecuatorial, *Potentilla*  
tamaño < 35  $\mu\text{m}$ . Con colpo operculado. Los márgenes  
del colpo pueden o no ser prominentes en el ecuador.  
Opérculo largo y prominente. Estrías fuertes, largas,  
rectas y paralelas que recorren el grano  
meridionalmente.

---

12t Grano rómbico-obtuso, elíptico o rectangular-obtuso. *Rosaceae* (13)  
Sin opérculo. En el ecuador hay estrías paralelas o  
arrugas irregulares/sinuosas. Muri simplicolumelado o  
duplicolumelado a veces se anastomosa, cubre o se  
hunde bajo otro. Endoporo representado por una mera  
constricción o ruptura en el colpo. Grosor de la exina  
uniforme. Mesocolpio plano o convexo.

---

13a Grano circular o rómbico-obtuso con un característico *Dryas* (14)  
patrón curvado y ramificado de las estrías o de arrugas  
con granos.

13t Colpos con margen muy irregular y membrana *Rubus* granulada, anchos con fines obtusos, con una constricción insignificante (poro). Ornamentación finamente rugulada-estriada. Apocolpia grande en relación con el grano.

- 
- 14 Grano subprolado (23x20  $\mu\text{m}$ ) elíptico en vista *Dryas octopetala* ecuatorial y semi-triangular en vista polar. Colpos largos, amplios, hundidos con margen irregular. Exina ~2.1  $\mu\text{m}$  de grosor. Sexina el doble de grosor que la nexina. Ornamentación estriada, muri más amplios que surcos, anastomosados u ondulados.

**Appendix 2.** Pollen types included for the statistical analysis

<b>Code</b>	<b>Pollen taxa</b>
BETU	<i>Betula</i>
CASS	<i>Cassiope</i>
CYPX	<i>Cyperaceae</i>
DRAB	<i>Draba</i>
DRYA	<i>Dryas</i>
EMPE	<i>Empetrum</i>
ERIX	Ericaceae
HUPE	<i>Huperzia selago</i>
LUZU	<i>Luzula/Juncus</i>
LYCO	<i>Lycopodium</i>
OXRU	<i>Oxyria/Rumex</i>
PAPA	<i>Papaver</i>
POAX	Poaceae
POLX	Polypodiaceae
RANX	Ranunculaceae
SACE	<i>Saxifraga cespitosa</i>
SALI	<i>Salix</i>
SAOP	<i>Saxifraga oppositifolia</i>
SAXX	Saxifragaceae
SCRX	Scrophulariaceae
SIMI	<i>Silene/Minuartia</i>

### **Appendix 3.** Pollen grain taxonomic descriptions

#### **Brassicaceae**

*Draba arctica* J. Vahl (fig. 8, top row).

Pollen grains spheroidal. P/E ratio 1.08. Elliptical in equatorial view: 27.46 (22.6 – 31.15)  $\mu\text{m}$   $\times$  25.31 (18.22 – 29.12)  $\mu\text{m}$ , and circular in polar view 26.59 (22.56 – 28.97)  $\mu\text{m}$   $\times$  25.96 (21.75 – 27.94)  $\mu\text{m}$ . Apertures 3(4)-colporate. Exine ca. 2.52  $\mu\text{m}$  thick, with sexine being twice as thick as nexine. Ornamentation reticulate in both LM and SEM, heterobrochate with brochi ca 0.87  $\mu\text{m}$  diameter and muri ca. 0.55  $\mu\text{m}$  thick.

#### **Polygonaceae**

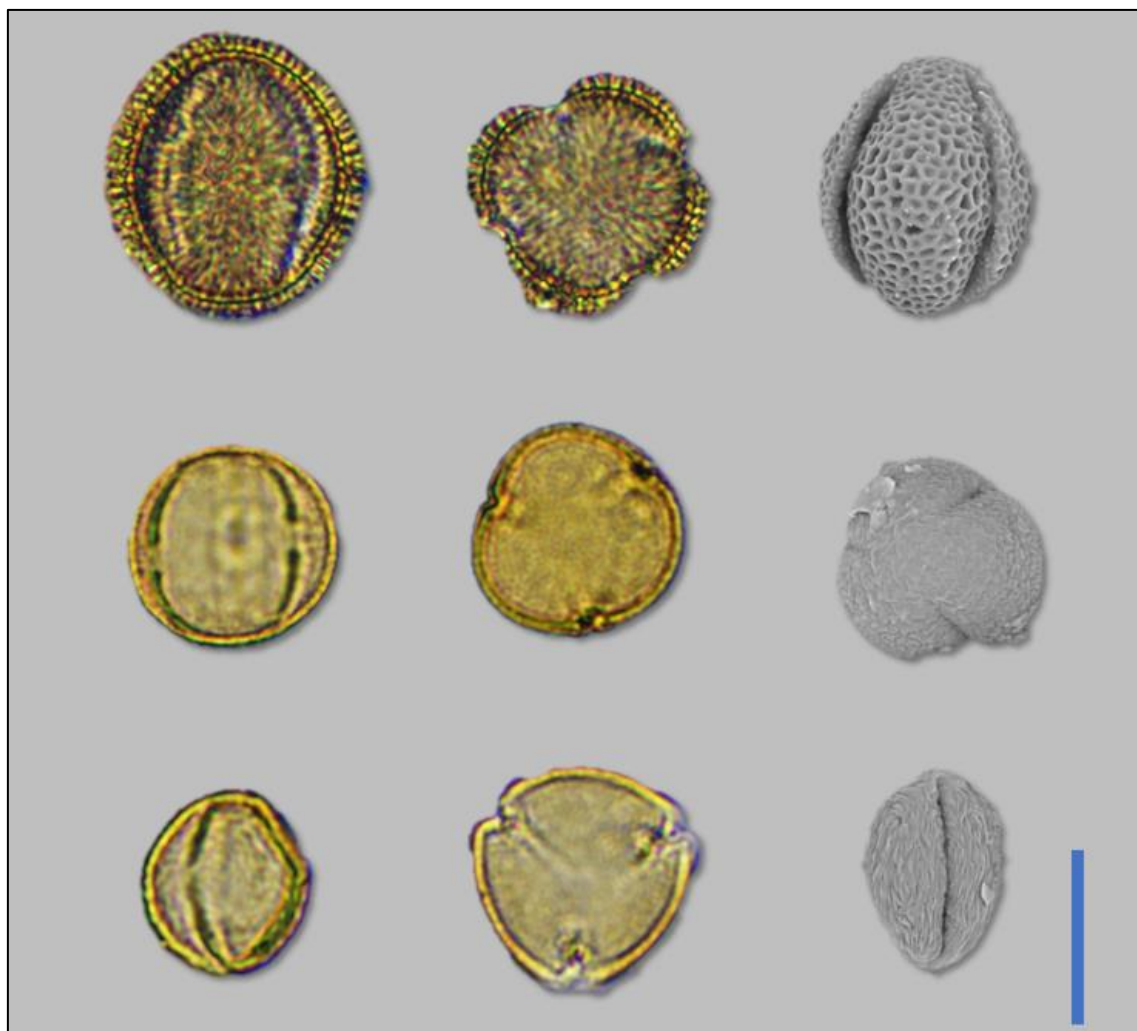
*Oxyria digina* (L.) Hill (fig. 8, middle row).

Pollen grains spheroidal. P/E ratio 0.96. Circular 21.65 (19.19 – 23.51)  $\mu\text{m}$   $\times$  22.62 (20.04 – 26.06)  $\mu\text{m}$  in equatorial view and circular 22.06 (20.02 – 24.9)  $\mu\text{m}$   $\times$  21.84 (19.65 – 24.17)  $\mu\text{m}$  in polar view. Apertures 3-colporate, colpus going from pole to pole with average 0.81  $\mu\text{m}$  width, pore ca 2.24  $\mu\text{m}$  diameter in equatorial view and 1.79  $\mu\text{m}$  in polar view. Exine ca. 1.41  $\mu\text{m}$  thick. Ornamentation granulate in LM and verrucate-perforate in SEM.

#### **Rosaceae**

*Dryas octopetala* L. (fig. 8, bottom row).

Pollen grains spheroidal to subprolate. P/E ratio 1.12. Elliptical 21.75 (19.66 – 26.13)  $\mu\text{m}$   $\times$  19.41 (14.76 – 22.22)  $\mu\text{m}$  in equatorial view and semi-triangular 21.25 (17.11 – 26.65)  $\mu\text{m}$   $\times$  21.21 (16.70 – 29.05)  $\mu\text{m}$  in polar view. Apertures 3-colporate, colpus ca 1  $\mu\text{m}$  width, sunken and with irregular borders, pore ca 1.86  $\mu\text{m}$  diameter. Exine ca. 1.59  $\mu\text{m}$  thick, thicker in the poles. Ornamentation striate in LM and striate-perforate in SEM.



**Appendix 3. Figure 1.** LM equatorial, polar and SEM pictures of *Draba arctica* (top row), *Oxyria digina* (middle row) and *Dryas octopetala* (bottom row).

*Potentilla rubricaulis* Lehm. (fig. 9, top row).

Pollen grains spheroidal to subprolate, sometimes rhomboidal if operculum is present. P/E ratio 1.06. Elliptical 23.99 (20.53 – 28.34)  $\mu\text{m}$   $\times$  22.57 (19.21 – 25.14)  $\mu\text{m}$  in equatorial view and semi-triangular 22.69 (17 – 26.21)  $\mu\text{m}$   $\times$  22.48 (18.34 – 26.67)  $\mu\text{m}$  in polar view. Apertures 3-colporate, colpus going from pole to pole, operculum ca 2.58  $\mu\text{m}$  long. Exine ca. 1.4  $\mu\text{m}$  thick. Ornamentation striate in LM and SEM.

Key to the species:

- i. Grains spheroidal to subprolate, elliptical in equatorial view and semi-triangular in polar view,  $>19 \mu\text{m}$ , 3-colporate, exine ca. 1.86  $\mu\text{m}$ , striate in LM

- and striate-perforate in SEM .....  
*Dryas octopetala*.
- ii. Grains spheroidal to subprolate, even rhomboidal, elliptical in equatorial view and semi-triangular in polar view, >22 µm, 3-colpate, operculum sometimes present, exine ca. 1.4 µm thick, striate ..... *Potentilla rubricaulis*.

### **Salicaceae**

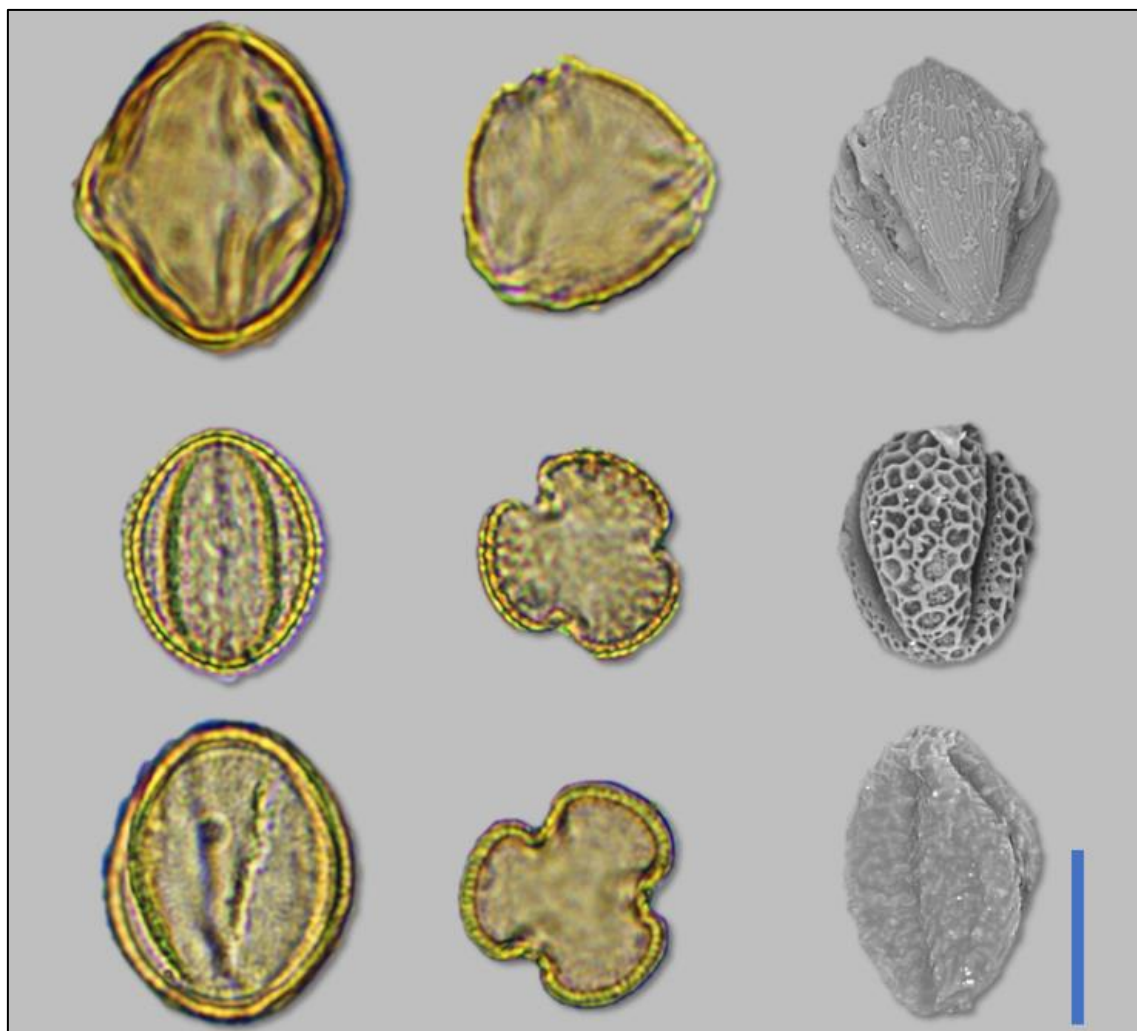
*Salix arctica* Pall. (fig. 9, middle row)

Pollen grains subprolate. P/E ratio 1.18. Elliptical 25.64 (23.41 – 31.83) µm × 21.67 (19.32 – 22.82) µm in equatorial view and circular 23.36 (21.29 – 26.55) µm × 22.04 (19.95 – 23.37) µm in polar view. Apertures 3-colpate, colpus almost reaching the poles, sometimes very broad. Exine ca. 1.58 µm thick. Ornamentation reticulated in LM and SEM. Heterobrochate, broqui diameter ca. 1.01 µm and muri width ca. 0.56 µm in the equatorial area.

### **Saxifragaceae**

*Saxifraga cernua* L. (fig. 9, bottom row)

Pollen grains subprolate. P/E ratio 1.16. Elliptical 29.42 (26.60 – 32.45) µm × 25.35 (23.33 – 28.85) µm in equatorial view and circular 27.42 (24.66 – 29.61) µm × 26.17 (23.44 – 29.29) µm in polar view. Apertures 3-colpate, colpus almost reaching the poles, sometimes irregular in shape and border. Exine ca. 1.48 µm thick, columella very visible. Ornamentation granulated in LM and striate-scabrate in SEM.



**Appendix 3. Figure 2.** LM equatorial, polar and SEM pictures of *Potentilla rubricaulis* (top row), *Salix arctica* (middle row) and *Saxifraga cernua* (bottom row).

### Poaceae

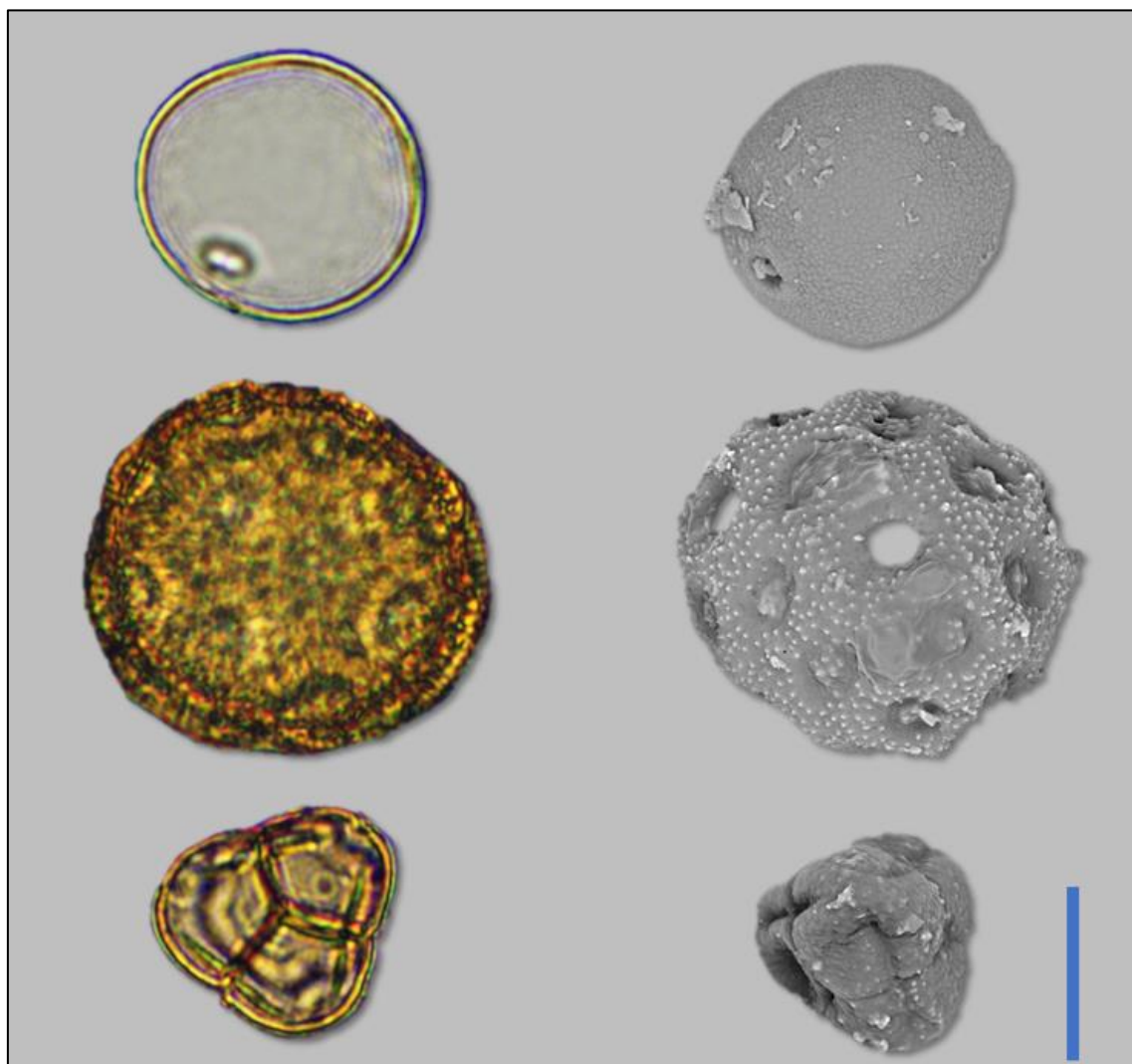
*Poa glauca* Vahl (fig. 10, top row)

Pollen grains spheroidal.  $30.39\ (27.14 - 34.34)\ \mu\text{m} \times 30.91\ (28.52 - 34.80)\ \mu\text{m}$ . P/E ratio 0.98. Apertures monoporate, pore ca.  $2.52\ \mu\text{m}$  diameter, annulus ca  $1.59\ \mu\text{m}$  width. Exine ca.  $1.54\ \mu\text{m}$  thick. Ornamentation psilate in LM and granulate-perforated in SEM.

### Caryophyllaceae

*Cerastium arcticum* Lange (fig. 10, middle row)

Pollen grains spheroidal. P/E ratio 1.11. 43.47 (29.20 – 47.56)  $\mu\text{m}$   $\times$  39.13 (25.39 – 42.87)  $\mu\text{m}$ . Apertures polipantoporate, 18 – 28 pores ca. 3.73  $\mu\text{m}$  diameter, fairly distributed throughout the grain surface. Exine ca. 2.53  $\mu\text{m}$  thick. Ornamentation granulated in LM and microechinate in SEM.



**Appendix 3. Figure 3.** LM and SEM pictures of *Poa glauca* (top row), *Cerastium arcticum* (middle row) and *Cassiope tetragona* (bottom row).

**Ericaceae**

*Cassiope tetragona* (L.) D. Don (fig. 10, bottom row)

Pollen grains circular arranged in a tetrahedral tetrad. 26.93 (22.72 – 30.28)  $\mu\text{m}$   $\times$  25.12 (21.56 – 28.35)  $\mu\text{m}$ . P/E ratio 1.07. Each grain of the tetrad 18.20 (16.29 – 20.87)  $\mu\text{m}$   $\times$  13.43 (11.1 – 15.61)  $\mu\text{m}$ . Apertures 3-colporate. Exine ca. 1.24  $\mu\text{m}$  thick. Septum 1.53  $\mu\text{m}$  thick. Ornamentation psilate in LM and scabrate in SEM.

*Rhododendron lapponicum* (L.) Wahlenb. (fig. 11, top row)

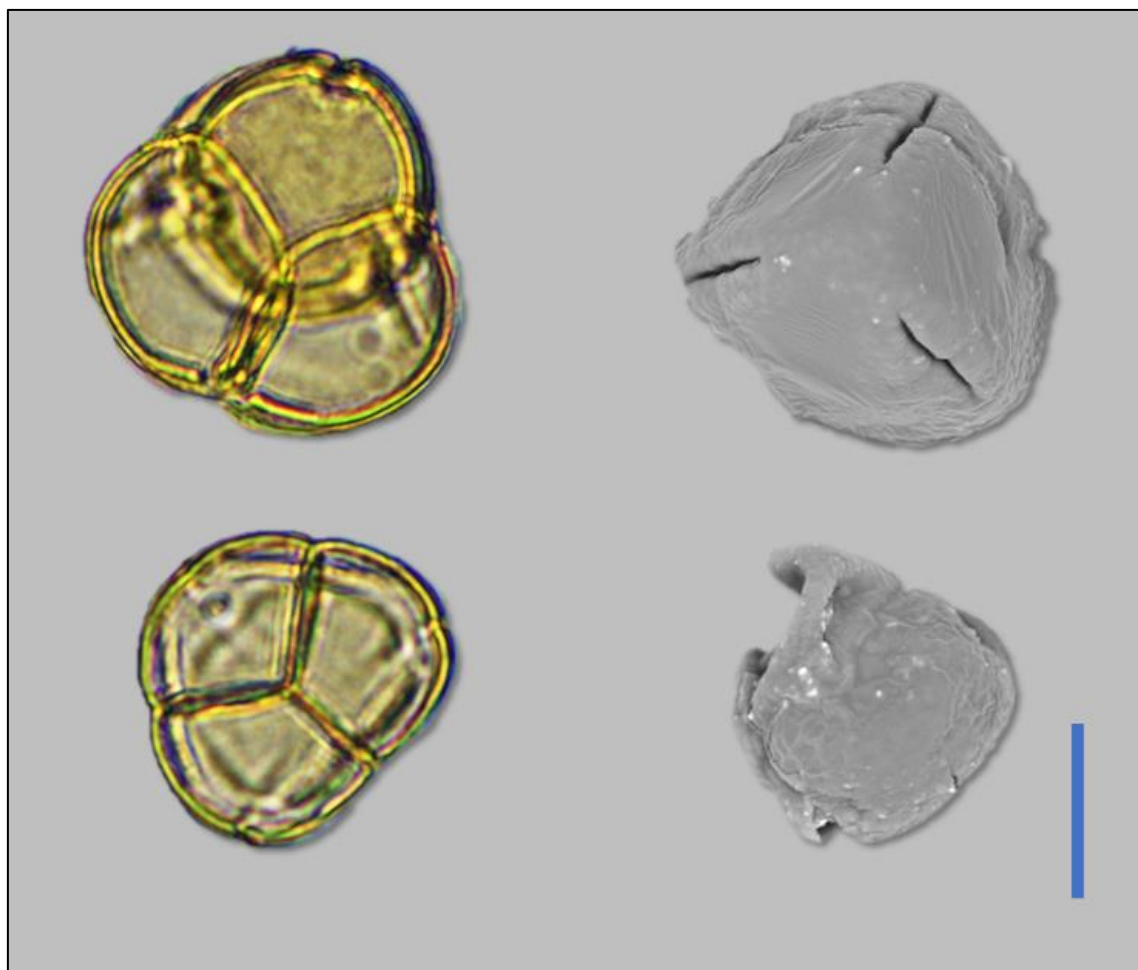
Pollen grains circular arranged in a tetrahedral tetrad. 41.1 (33.38 – 50.66)  $\mu\text{m}$   $\times$  38.78 (31.54 – 50.98)  $\mu\text{m}$ . P/E ratio 1.06. Each grain of the tetrad 28.18 (21.79 – 33.82)  $\mu\text{m}$   $\times$  20.42 (14.56 – 26.46)  $\mu\text{m}$ . Apertures 3-colporate. Exine ca. 1.85  $\mu\text{m}$  thick. Septum 4.05  $\mu\text{m}$  thick. Ornamentation psilate in LM and slightly striate in SEM.

*Vaccinium uliginosum* L. (fig. 11, bottom row)

Pollen grains circular arranged in a tetrahedral tetrad. 32.11 (26.98 – 36.45)  $\mu\text{m}$   $\times$  31.59 (25.15 – 38.54)  $\mu\text{m}$ . P/E ratio 1.02. Each grain of the tetrad 23.46 (19.94 – 25.08)  $\mu\text{m}$   $\times$  16.57 (12.74 – 18.86)  $\mu\text{m}$ . Apertures 3-colporate. Exine ca. 1.52  $\mu\text{m}$  thick. Septum 2.06  $\mu\text{m}$  thick. Ornamentation psilate in LM and rugulate-scabrate in SEM.

Key to the species:

- i. Tetrahedral tetrad ca. 25  $\mu\text{m}$ , 3-colporate, exine ca. 1.24  $\mu\text{m}$ , septum ca. 1.53  $\mu\text{m}$ , psilate in LM and scabrate in SEM ..... *Cassiope tetragona*.
- ii. Tetrahedral tetrad ca. 40  $\mu\text{m}$ , 3-colporate, exine ca. 1.85  $\mu\text{m}$ , septum ca. 4.05  $\mu\text{m}$ , psilate in LM and slightly striate in SEM.....*Rhododendron lapponicum*.
- iii. Tetrahedral tetrad ca. 30  $\mu\text{m}$ , 3-colporate, exine ca. 1.52  $\mu\text{m}$ , septum ca. 2.06  $\mu\text{m}$ , psilate in LM and scabrate-rugulate in SEM ..... *Vaccinium uliginosum*.

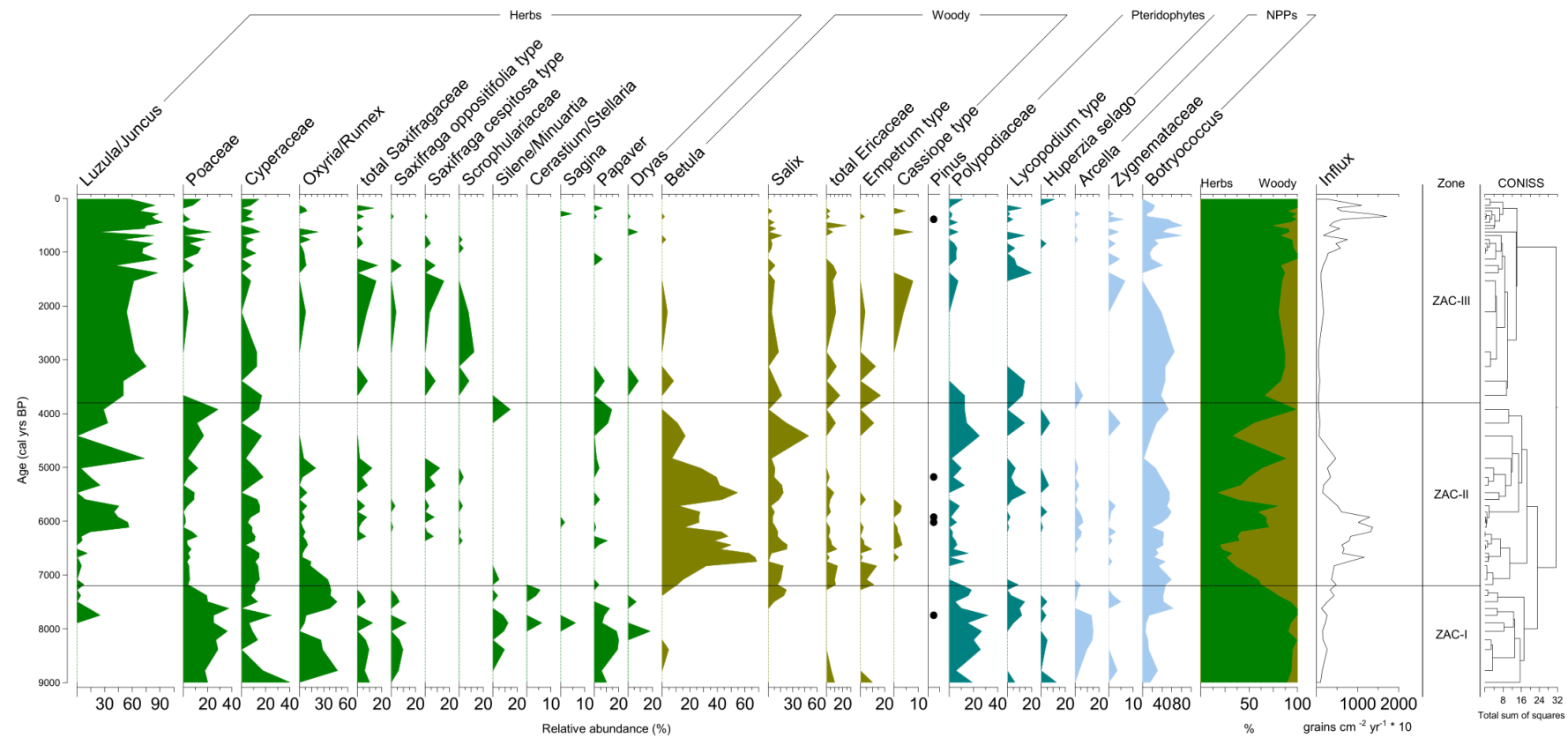


**Appendix 3. Figure 4.** LM and SEM pictures of *Rhododendron lapponicum* (top row) and *Vaccinium uliginosum* (bottom row).

#### **Appendix 4.** ZAC19\_06\_02 pollen abundance data

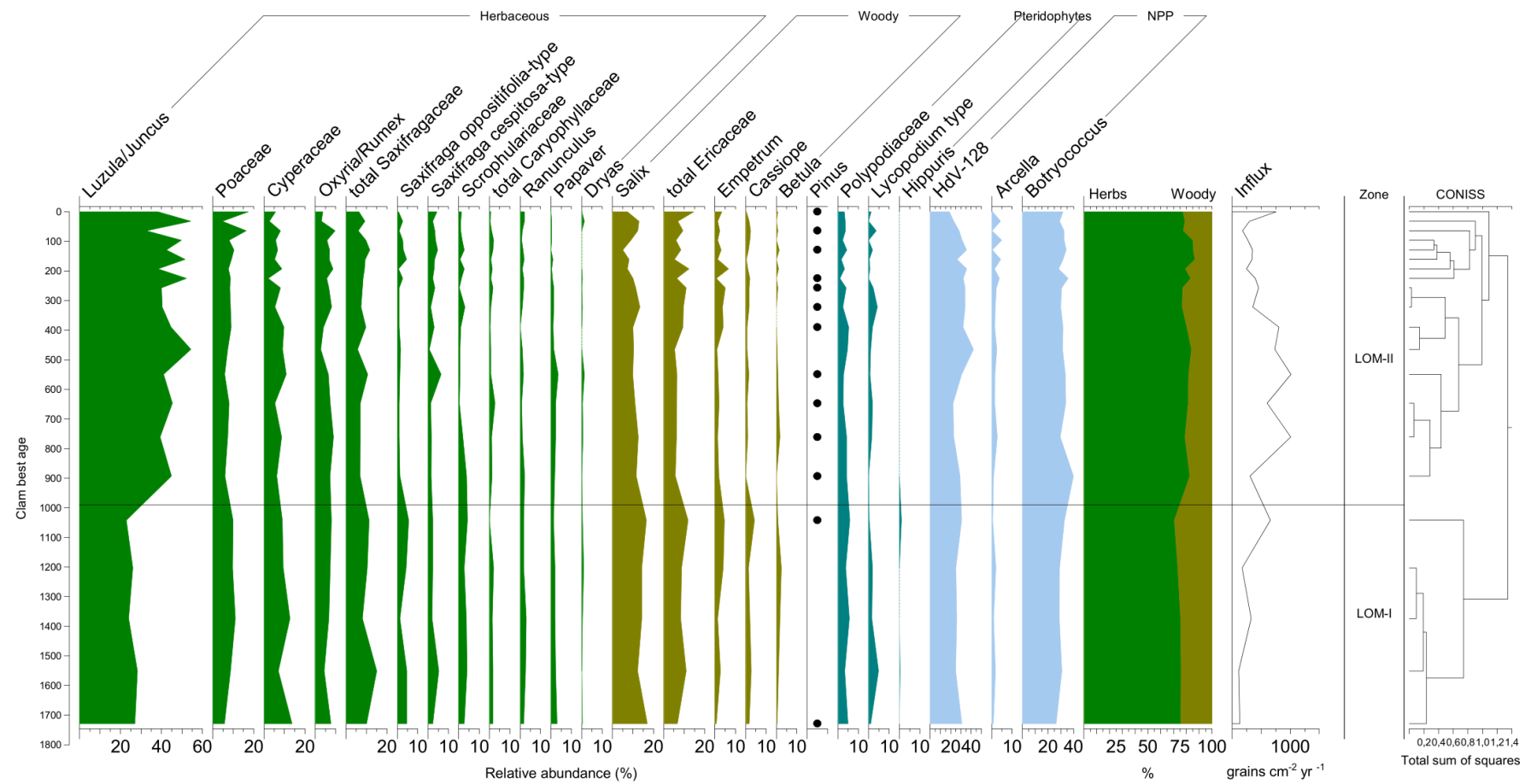
31	33,3	11,1	0	22	0	11	0	0	11	0	0	0	0	0	0	0	0	0	0	0	0	0	0	0	0	0	0	0	14	14	7,1	0	0	0					
32	0	16,7	16,7	50	0	0	0	0	17	0	0	0	0	0	0	0	0	0	0	0	0	0	0	0	0	0	0	0	25	0	0	0	0	0					
34	73,2	3,6	3,6	3,6	0	0	0	0	7,1	5,4	0	0	0	2	0	0	0	0	0	0	0	1,8	0	0	0	0	0	0	0	1,8	0	0	0	0	0				
35	4	12	12	8	0	0	0	0	28	20	0	0	0	0	12	0	0	0	0	0	4	0	0	0	0	0	0	0	10	6,7	0	0	0	0					
36	14,3	3,6	17,9	7,1	4	0	0	0	39	3,6	0	4	0	0	0	3,6	0	3,6	0	0	0	0	0	0	0	0	0	0	3,1	3,1	3,1	3,1	0	0	0				
37	25	0	8,3	17	0	0	0	0	42	0	0	0	0	0	0	8,3	0	0	0	0	0	0	0	0	0	0	0	0	0	13	6,3	6,3	0	0	0	0			
38	0	9,1	0	18	9	0	0	0	55	9,1	0	0	0	0	0	0	0	0	0	0	0	0	0	0	0	0	0	0	0	0	15	0	0	0	0	0	0		
39	8,7	8,7	13	13	0	4,3	0	0	44	0	0	4	0	0	0	0	0	0	0	0	4,3	0	0	0	0	0	0	0	0	0	0	4	0	4	0	0	0	0	
40	45,5	3	15,2	3	0	0	3	0	12	9,1	0	0	0	0	3	3	0	3	0	0	0	0	0	0	0	0	0	0	0	0	8,3	0	0	0	0	0	0		
41	40	0	15	7,5	3	0	2,5	0	28	2,5	0	3	0	0	0	0	0	0	0	0	0	0	0	0	0	0	0	0	0	4,5	0	4,5	0	0	0	0			
42	44,3	1,3	7,6	5,1	0	0	0	0	27	6,3	0	0	0	0	0	7,6	0	0	0	0	0	0	0	0	0	0	0	0	1	0	0	1,2	1,2	2,4	0	0	0	0	
43	55	1,7	5	5	0	0	0	0	27	1,7	0	0	0	3	0	0	0	0	0	0	1,7	0	0	0	0	0	0	0	0	0	1,5	6,2	0	0	0	0	0	0	
44	56,3	0	8,8	8,8	0	2,5	1,3	0	16	3,8	0	0	0	0	1	0	0	0	0	0	1,3	0	0	0	0	0	0	0	0	0	0	1,2	1,2	0	0	0	0	0	
45	14,3	7,1	8,6	11	1	1,4	1,4	0	43	7,1	0	0	0	0	0	1,4	0	1,4	0	0	0	0	0	0	0	0	0	0	0	0	0	2,8	0	0	0	0	0	0	
46	4,5	11,4	11,4	11	0	0	2,3	0	48	4,5	0	0	0	0	0	6,8	0	0	0	0	0	0	0	0	0	0	0	0	0	0	2,2	0	0	0	0	0	0		
47	5,4	2,7	10,8	16	0	2,7	2,7	0	38	8,1	0	0	0	0	0	0	0	2,7	0	0	0	11	0	0	0	0	0	0	0	0	5	0	0	0	3	0	0		
48	0	3,3	3,3	23	0	3,3	3,3	0	50	10	0	0	0	0	0	0	0	0	0	0	0	3,3	0	0	0	0	0	0	0	0	6,3	0	0	0	0	0	0		
49	0	6,5	9,7	23	3	9,7	0	0	42	6,5	0	0	0	0	0	0	0	0	0	0	0	0	0	0	0	0	0	0	0	3,1	0	0	0	0	0	0			
50	11,1	3,7	14,8	3,7	0	0	0	0	63	3,7	0	0	0	0	0	0	0	0	0	0	0	0	0	0	0	0	0	0	0	0	16	0	0	0	0	0	0		
51	0	5,5	14,5	1,8	0	1,8	1,8	0	67	3,6	0	2	0	0	0	0	0	0	0	0	0	0	0	0	0	0	0	0	1,8	0	0	0	0	0	0				
52	2,9	2,9	11,4	0	0	0	0	0	69	14	0	0	0	0	0	0	0	0	0	0	0	0	0	0	0	0	0	0	0	0	0	0	0	0	0	0	0	0	
53	4,5	4,5	13,6	18	0	14	0	0	32	14	0	0	0	0	0	0	0	0	0	0	0	0	0	0	0	0	0	0	0	0	0	0	0	0	0	0	0	0	
56	0	5	15	15	5	5	0	0	15	35	0	0	0	0	0	0	0	5	0	0	0	0	0	0	0	0	0	0	0	0	0	0	0	0	0	0	0	0	0
57	7,4	3,7	11,1	11	0	11	0	3,7	11	37	0	0	0	0	0	0	0	0	0	0	3,7	0	0	0	0	0	0	0	0	0	9,1	9,1	0	0	0	0	0	0	
58	0	11,1	11,1	22	0	0	0	0	5,6	39	6	0	0	0	0	0	0	0	6	0	0	0	0	0	0	0	0	0	0	0	18	0	0	0	0	0	0		
59	3,8	19,2	7,7	19	0	0	0	0	0	39	0	0	0	0	4	0	0	0	3,8	4	0	0	0	0	0	0	0	0	0	16	3,1	0	0	0	0	0	0		
60	0	20	13,3	6,7	0	0	0	0	0	47	0	0	0	0	7	0	0	0	0	0	0	6,7	0	0	0	0	0	0	0	0	4,8	14	4,8	0	0	5	0		
61	12,5	37,5	0	0	0	0	0	0	0	38	0	0	0	0	0	0	0	0	0	0	0	13	0	0	0	0	0	0	0	0	10	10	0	0	0	0	0	0	
62	25	25	25	0	0	0	0	0	0	8,3	0	0	0	0	0	0	0	8,3	0	0	8,3	0	0	0	0	0	0	0	0	4	32	12	4	0	0	0	0		
63	0	25	6,3	0	0	0	0	6,3	0	6,3	0	13	0	0	13	0	0	0	13	6	6,3	6,3	0	0	0	0	0	0	0	0	15	5	0	0	0	0	0	0	
64	0	36,4	9,1	0	0	0	0	9,1	0	0	0	0	0	0	0	0	0	9,1	0	0	18	18	0	0	0	0	0	0	0	0	27	0	0	0	0	0	0		
65	0	26,7	13,3	0	0	0	0	0	0	27	0	0	0	0	7	0	0	0	0	0	20	0	0	0	0	6,7	0	0	0	20	0	5	0	0	0	0	0		
66	0	28,6	0	0	0	0	0	4,8	29	0	0	0	0	10	0	0	0	9,5	0	0	19	0	0	0	0	0	0	0	0	26	0	3,2	0	3	0	0	0		
68	0	17,6	17,6	0	6	0	0	0	0	47	0	0	0	0	6	0	0	0	0	0	0	5,9	0	0	0	0	0	0	0	0	5,6	0	0	0	0	0	0	0	
69	0	20	40	0	0	10	0	0	0	0	0	0	0	0	10	0	0	0	0	0	0	10	0	10	0	0	0	0	0	0	19	6,3	13	0	0	0	0	0	0

## Appendix 5. ZAC19\_06\_02 pollen diagram per age



## **Appendix 6. LOM18\_02 pollen abundance data**

**Appendix 7. LOM18\_02 pollen abundance diagram per age**



**Appendix 8.** Pollen taxa included in the calibration set.

Code	Pollen taxa
ALCRISPA	<i>Alnus crispa</i>
ALRUGOSA	<i>Alnus rugosa</i>
ALNUSX	<i>Alnus</i>
AMBROSIA	<i>Ambrosia</i>
ARTEMISIA	<i>Artemisia</i>
ASTERX	Asteraceae
BETULA	<i>Betula</i>
BOTRYCHIUM	<i>Botrychium</i>
BRASSICACEAE	Brassicaceae
CARYOPHYLL	Caryophyllaceae
CHENOAMX	Chenopodiaceae/Amaranthaceae
CORYLUS	<i>Corylus</i>
CUPRESSA	Cupressaceae
CYPERACE	Cyperaceae
DRYAS	<i>Dryas</i>
ELAEAGNX	Elaeagnaceae
EQUISETU	<i>Equisetum</i>
ERIVACCI	<i>Vaccinium</i>
ERICACEX	Ericaceae
ERICALES	Ericales
FABACEAE	Fabaceae
KOENISLD	<i>Koenigia Islandica</i>
LARIXPSEU	<i>Larix/Pseudotsuga</i>
LYCOANNO	<i>Lycopodium annotinum</i>
LYCOSELA	<i>Lycopodium selago</i>
LYCOPODX	<i>Lycopodium</i>
MYRICACX	Myricaceae
ONAGRACEAE	Onagraceae
OXYRIA	<i>Oxyria</i>
PAPAVERX	Papaveraceae
PICEAX	<i>Picea</i>
PINDIPLO	<i>Pinus diploxyylon</i>
PINUSX	<i>Pinus</i>

POACEAE	Poaceae
POLEMONI	Polemoniaceae
POLYGBIS	<i>Polygonum bistortoides</i>
POLYPOD	Polypodiaceae
POPULUS	<i>Populus</i>
POTENTILLA	<i>Potentilla</i>
RANUNCUL	Ranunculaceae
ROSACEAX	Rosaceae
RUBUS	<i>Rubus</i>
RUMEOXYR	<i>Oxyria/Rumex</i>
SALIX	<i>Salix</i>
SXFRAOPP	<i>Saxifraga oppositifolia</i>
SXFRAGAX	Saxifragaceae
SCROPHUL	Scrophulariaceae
SELAGINE	<i>Selaginella</i>
SPHAGNUM	<i>Sphagnum</i>
THALICTRUM	<i>Thalictrum</i>
TILIA	<i>Tilia</i>

## **Appendix 9.** Calibration set pollen abundance data



























## Appendix 10. WA-PLS quantitative reconstruction R script

```
#abrir paquetes de datos necesarios
library(analogue)
library(rioja)
library(vegan)
#cargar datos de polen actual
polen <- read.csv("polenarctic.csv", header=T, dec=",", sep = ";",
row.names = 1)
#transformar datos porcentuales de pollen a hellinger
polen2<-decostand(polen, "hellinger")
#eliminar outliers (sitios con datos 99999999)
##outliers <- c(filas que no cuentan)
##polen3<- polen2[-outliers, ] #matriz de polen con la que
trabajaremos

#dca matriz polinica, para evaluar la distribucion de los datos
biológicos
dca.polen <- decorana(polen2, iweigh = 1)
summary(dca.polen) #fijarse en longitud del eje. >2 = CCA, <2=RDA

#DCA1 axis lenght = 2.3 -> RDA!!!

#rda matriz polinica
rda.polen<-rda(polen2)
plot(rda.polen)
summary(rda.polen) # asi se distribuyen nuestros sitios en base a los
datos polínicos
#
#ahora clima

clima <- read.csv("climaarctic.csv", header=TRUE, dec=",", sep = ";",
row.names = 1)
summary(clima)
clima2<- clima[-outliers, ]

#prueba de normalidad
#valores de p<0.05 no tienen normalidad por lo que hay que
transformar a log10. Valores de p >0.05 son normales y no hay q
transforar
#shapiro wilks con datos brutos
shapiro.test(clima$Ta) #anormal
shapiro.test(clima$Tmax) #anormal
shapiro.test(clima$Tmin) #anormal
shapiro.test(clima$Ths) #anormal
shapiro.test(clima$Tcs) #anormal
```

```

shapiro.test(clima$Pa) #anormal
shapiro.test(clima$Pmax) #anormal
shapiro.test(clima$Pmin) #anormal
shapiro.test(clima$Pws) #anormal
shapiro.test(clima$Pds) #anormal

#transformacion se hace seleccionando los no normales
anorclim <- subset(clima, select=c(6,7,8,9,10)) #datos de pp
positivos anormales
anormclimlog<-log10(anorclim)
str(anormclimlog)

anorclimneg <- subset(clima, select=c(1, 2, 3,4,5)) #datos de t? que
tienen valores negativos
anormclimlogneg <- log10((anorclimneg+42.11)) #para solucionar el
problema con los datos negativos

##unen los tres subset para estandarizacion
env2w<-cbind(anormclimlog, anormclimlogneg) #juntar los tres subsets
str(env2w)
#estandarizar tod el dataframe recien unido
env_standw<-decostand(env2w,"standardize")
summary(env_standw) #-> nuestra matriz clim?tica estandarizada!

# RDA, significativas:
rdax <- rda(downweight(polen2)~Ths, data=env_standw)
summary(rdax)
set.seed(65)
anova(rdax) #significancia del modelo
#se obtiene:
#Variable      Single Proportion Explained (RDA1)
#Relative explanatory power (eigenvalues RDA1/PC1      )
#p-value (set.seed (65)           <- anova

#regresion multiple para las variables significativas### leer manual
juggins PLEASE

modell1<-lm(Ta~+Ths+Tcs+Pds, data=env_standw)
summary(modell1)
anova(modell1)

#rda general con variables significativas: cuanto porcentaje explica
mis vars sign

```

```

BIG.rda<-rda(downweight(polen2)~Ta+Ths+Tcs, data=env_standw) # obtener
eigenvalue de RDA1 dividido por PC1: poder explicativo de la variable
BIG.rda
plot(BIG.rda, scaling = 2) #tesis

rda
vif.cca(BIG.rda)

### RDA parcial, cada variable con respecto al resto
pRDA<-rda(downweight(polen2)~Pds+Condition(Pws), data=env_standw)
summary(pRDA) #la varianza explicada despues de tomar en cuenta las
otras variables como covariables
set.seed(65)
anova(pRDA)

#conclusi?n: usar ThS (Temperatura de verano)
#ahora crear funciones de transferencia
mod <- WAPLS (polen2, clima$Ths)
mod
plot(mod)

#validaci?n cruzada
cv.mod <- crossval(mod, cv.method="boot", nboot=1000)
cv.mod
rand.t.test(cv.mod)
plot(cv.mod) #tesis
coef(cv.mod) #seleccionamos funci?n de dos componentes

#abrir planilla de fosil (en este caso de Lomso)
fosillom <- read.csv("lomfosilmarzo.csv", header=T, dec=",", sep =
";", row.names = 1)
#aplicar funci?n de transferencia
lomso <- predict(cv.mod, fosillom)
lomso$fit

#ahora ZAC
fosilzac <- read.csv("zacfosilmarzo.csv", header=T, dec=",", sep =
";", row.names = 1)
#aplicar funci?n de transferencia
zac <- predict(cv.mod, fosilzac)
zac$fit

```

**Appendix 11.** Statistic parameters of each climatic variable considering others as co-variables.

Variable	Co-variable	% Explained	$\lambda_1/\lambda_2$	p-value
Ta	-	18.58	0.92	0.001
	Tmax	4.78	0.22	0.001
	Tmin	15.53	0.77	0.001
	Ths	2.99	0.14	0.001
	Tcs	8.29	0.39	0.001
	Pa	14.9	0.69	0.001
	Pmax	13.43	0.62	0.001
	Pmin	15.3	0.73	0.001
	Pws	13.98	0.64	0.001
	Pds	14.07	0.66	0.001
Tmax	-	17.51	0.87	0.001
	Ta	3.52	0.16	0.001
	Tmin	15.3	0.77	0.001
	Ths	2.13	0.09	0.001
	Tcs	9.16	0.44	0.001
	Pa	14.34	0.71	0.001
	Pmax	13.53	0.67	0.001
	Pmin	14.44	0.7	0.001
	Pws	13.84	0.69	0.001
	Pds	13.3	0.64	0.001
Tmin	-	5.79	0.18	0.001
	Ta	2.26	0.09	0.001
	Tmax	3.27	0.14	0.001
	Ths	2.33	0.1	0.001
	Tcs	3.8	0.15	0.001
	Pa	3.58	0.11	0.001
	Pmax	2.99	0.1	0.001
	Pmin	3.13	0.1	0.001
	Pws	3.38	0.11	0.001
	Pds	2.4	0.08	0.001
Ths	-	18.93	1.01	0.001
	Ta	3.4	0.16	0.001

	Tmax	3.81	0.17	0.001
	Tmin	15.95	0.83	0.001
	Tcs	9.3	0.45	0.001
	Pa	15.52	0.81	0.001
	Pmax	14.64	0.76	0.001
	Pmin	15.63	0.8	0.001
	Pws	15.02	0.78	0.001
	Pds	14.39	0.73	0.001
Tcs	-	13.72	0.55	0.001
	Ta	2.81	0.12	0.001
	Tmax	4.99	0.23	0.001
	Tmin	11.89	0.5	0.001
	Ths	3.46	0.16	0.001
	Pa	10.04	0.38	0.001
	Pmax	8.43	0.32	0.001
	Pmin	10.45	0.4	0.001
	Pws	9.15	0.35	0.001
	Pds	9.09	0.34	0.001
Pa	-	6.17	0.2	0.001
	Ta	1.93	0.01	0.001
	Tmax	2.57	0.11	0.001
	Tmin	3.97	0.13	0.001
	Ths	2.22	0.1	0.001
	Tcs	2.17	0.08	0.001
	Pmax	2.04	0.06	0.001
	Pmin	2.95	0.09	0.001
	Pws	1.53	0.05	0.001
	Pds	2.85	0.09	0.001
Pmax	-	7.68	0.26	0.001
	Ta	1.84	0.07	0.001
	Tmax	3.23	0.14	0.001
	Tmin	4.93	0.16	0.001
	Ths	2.8	0.13	0.001
	Tcs	2.02	0.07	0.001
	Pa	3.62	0.11	0.001

	Pmin	4.35	0.14	0.001
	Pws	2.37	0.07	0.001
	Pds	3.44	0.11	0.001
Pmin	-	4.73	0.15	0.001
	Ta	0.89	0.04	0.001
	Tmax	1.19	0.05	0.001
	Tmin	2.03	0.06	0.001
	Ths	0.85	0.04	0.001
	Tcs	1.12	0.04	0.001
	Pa	1.45	0.04	0.001
	Pmax	1.29	0.04	0.001
	Pws	1.23	0.04	0.001
	Pds	1.12	0.04	0.001
Pws	-	7.31	0.24	0.001
	Ta	2.07	0.08	0.001
	Tmax	3.18	0.14	0.001
	Tmin	4.94	0.16	0.001
	Ths	2.84	0.13	0.001
	Tcs	2.72	0.09	0.001
	Pa	2.4	0.08	0.001
	Pmax	1.97	0.06	0.001
	Pmin	3.9	0.12	0.001
	Pds	3.17	0.1	0.001
Pds	-	6.17	0.2	0.001
	Ta	0.97	0.04	0.001
	Tmax	1.39	0.06	0.001
	Tmin	2.79	0.09	0.001
	Ths	0.91	0.04	0.001
	Tcs	1.13	0.04	0.001
	Pa	2.85	0.09	0.001
	Pmax	1.86	0.06	0.001
	Pmin	2.62	0.08	0.001
	Pws	1.98	0.06	0.001

**Appendix 12.** ZAC reconstructed *Ths* values

Age (cal yrs BP)	<i>Ths</i> (°C)
0	-2,224
128	2,8662
181	-1,0497
234	0,3515
286	1,6691
338	-0,7543
391	7,7933
446	-0,5817
503	6,886
562	2,7955
625	0,1932
692	7,4075
763	2,4301
840	-0,0737
925	3,7498
1020	0,0545
1127	-3,0394
1246	0,632
1382	8,7343
1534	-0,8793
2111	3,1764
2854	8,0883
3122	6,886
3392	4,0571
3660	3,8452
3922	-1,1603
4174	3,2484
4412	3,0879
4830	2,5777

5013	2,5581
5179	8,0663
5331	6,0509
5470	8,7902
5598	8,5792
5715	1,7262
5824	7,6784
5925	6,1135
6021	6,9038
6111	6,7104
6198	8,0729
6281	7,8996
6362	5,2231
6440	6,7706
6517	7,7824
6594	7,7099
6671	5,2231
6748	7,3234
6828	6,7368
7083	7,7099
7176	0,578
7276	1,1483
7382	-1,2047
7495	3,2113
7617	-0,5566
7748	-1,2061
7889	-2,2016
8041	-2,6413
8205	-3,0255
8381	-3,2619
8774	-0,6649
8993	0,0949

**Appendix 13.** Lomsø reconstructed *Ths* values

Age (cal yrs BP)	<i>Ths</i> (°C)
0	3,3861
32	1,2118
64	2,6266
96	1,2232
129	1,5099
161	0,7687
193	2,5495
225	1,3332
257	2,049
322	2,6247
390	2,1477
465	1,9256
549	0,9253
647	1,3528
761	1,7673
893	1,5
1042	1,7617
1203	1,9745
1374	2,4409
1551	1,9628
1729	1,2152

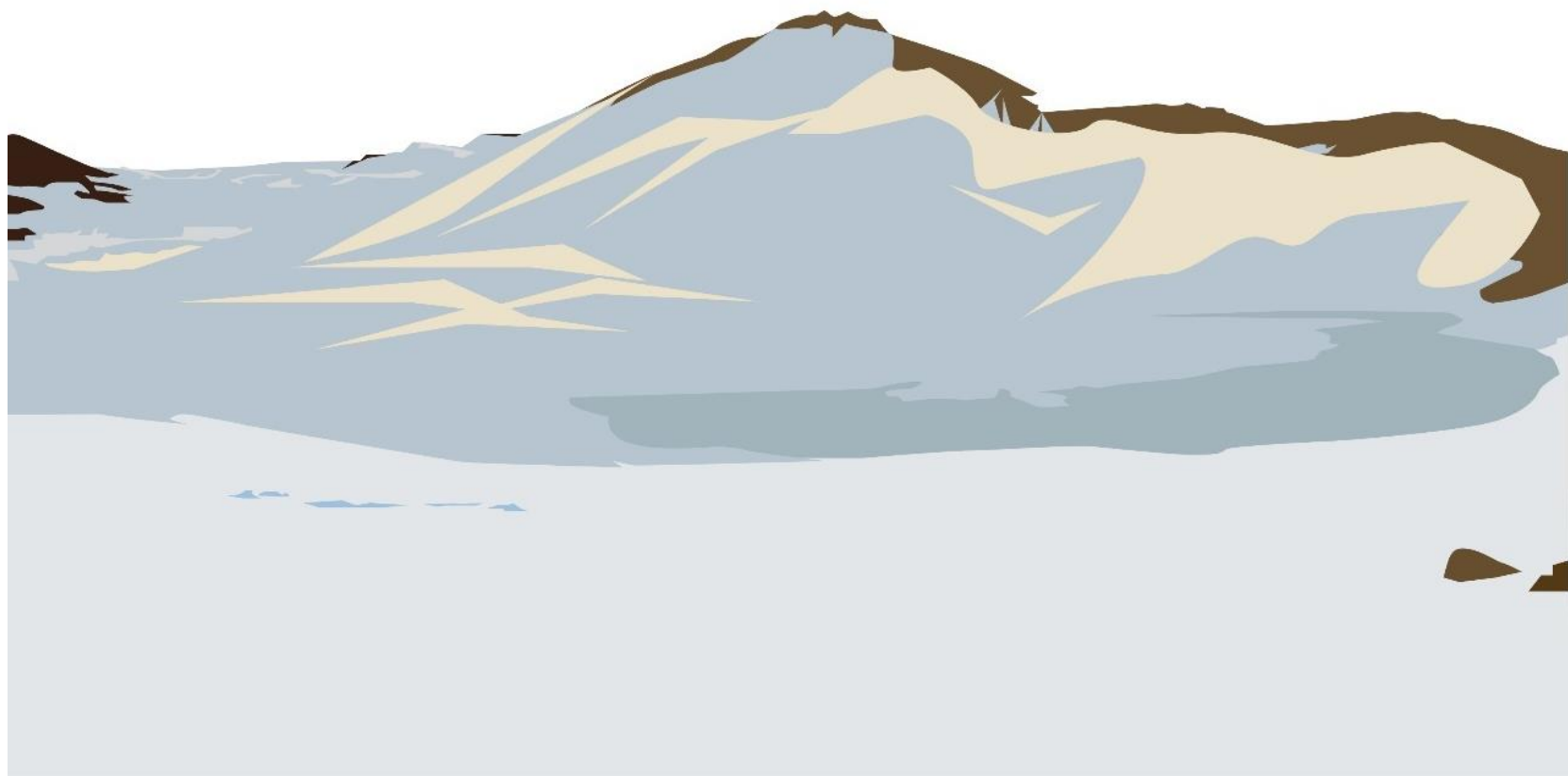
**Appendix 14.** Detailed landscape reconstruction of Lomsø and its surroundings (9,000 – 7,200 cal yrs BP)



**Appendix 15.** Detailed landscape reconstruction of ZAC and its surroundings (9,000 – 7,200 cal yrs BP)



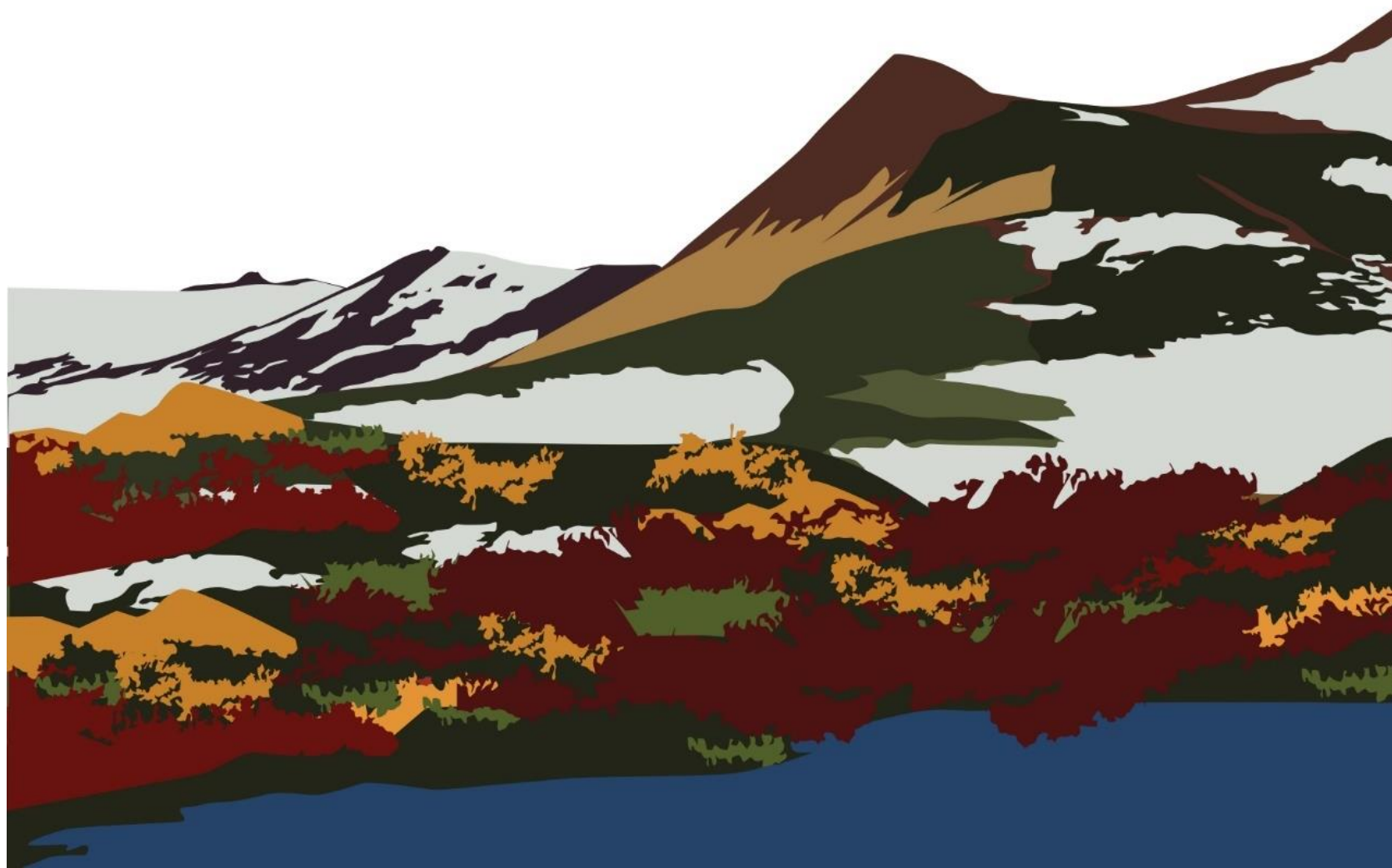
**Appendix 16.** Detailed landscape reconstruction of Aucella and its surroundings (9,000 – 7,200 cal yrs BP)



**Appendix 17.** Detailed landscape reconstruction of Lomsø and its surroundings (7,200 – 3,800 cal yrs BP)



**Appendix 18.** Detailed landscape reconstruction of ZAC and its surroundings (7,200 – 3,800 cal yrs BP)



**Appendix 19.** Detailed landscape reconstruction of Aucella and its surroundings (7,200 – 3,800 cal yrs BP)



**Appendix 20.** Detailed landscape reconstruction of Lomsø and its surroundings (3,800 cal yrs BP – present)



**Appendix 21.** Detailed landscape reconstruction of ZAC and its surroundings (3,800 cal yrs BP – present)



**Appendix 22.** Detailed landscape reconstruction of Aucella and its surroundings (3,800 cal yrs BP – present)



**Appendix 23.** Evolution model of sedimentary processes in Aucella Lake since 5,000 cal yrs BP. Source: García-Oteyza et al. (2024).

